Characterization and Informed Design of Downregulating Anti-Epidermal Growth Factor Receptor Antibodies

by

Jamie Berta Spangler

B.S. Biomedical Engineering
The Johns Hopkins University, 2006

SUBMITTED TO THE DEPARTMENT OF BIOLOGICAL ENGINEERING IN PARTIAL FULFILLMENT OF THE REQUIREMENTS FOR THE DEGREE OF

DOCTOR OF PHILOSOPHY IN BIOLOGICAL ENGINEERING
at the
MASSACHUSETTS INSTITUTE OF TECHNOLOGY

September 2011

Jamie Spangler
Department of Biological Engineering
June 16, 2011

K. Dane Wittrup
C. P. Dubbs Professor of Chemical & Biological Engineering
Thesis Supervisor

Forest M. White
Associate Professor of Biological Engineering
Chairman, Committee for Graduate Students

Committee Members

Douglas A. Lauffenburger (Chairman)
Ford Professor of Biological Engineering, Chemical Engineering, & Biology

Forest M. White
Associate Professor of Biological Engineering

K. Dane Wittrup
C. P. Dubbs Professor of Chemical & Biological Engineering

Characterization and Informed Design of Downregulating Anti-Epidermal Growth Factor Receptor Antibodies

by

Jamie Berta Spangler

Submitted to the Department of Biological Engineering on June 16, 2011
in partial fulfillment of the requirements for the degree of
Doctor of Philosophy in Biological Engineering

ABSTRACT

Due to its common dysregulation in epithelial-based cancers and the extensive characterization of its role in tumor growth, epidermal growth factor receptor (EGFR) has long been an attractive target for monoclonal antibodies. Intense research has culminated in the approval of two antibody-based drugs against EGFR for cancer treatment, with numerous others in clinical trials. However, therapeutic efficacy of these drugs has been disappointingly low due to autocrine signaling, receptor mutation, and transport limitations, necessitating novel antibody designs and mechanisms of action. Recently, it was reported that treatment with combinations of antibodies can induce receptor clustering, leading to synergistic receptor downregulation and anti-tumor activity. The aim of this thesis is to elucidate the details of this phenomenon and to exploit this mechanism to design more effective therapeutic antibodies targeting EGFR.

We first illuminate several key aspects of combination antibody-induced clustering. By screening a panel of pairwise combinations, we show that the most potently downregulating pairs consist of two non-competitive antibodies that target EGFR extracellular domain 3. We further find the mechanism underlying downregulation to be consistent with recycling inhibition. Lastly, in contrast to the agonism associated with ligand-induced downregulation, we demonstrate that combination mAb-induced downregulation does not activate EGFR or its downstream effectors and it leads to synergistic reduction in migration and proliferation of cells that secrete autocrine ligand.

To enhance antibody binding and induced receptor clustering, we design multispecific antibody-based constructs that engage up to four distinct epitopes on EGFR. We engineer two classes of constructs: one consisting of a full EGFR-specific antibody fused to the variable domain of a second anti-EGFR antibody and the other consisting of a full EGFR-specific antibody fused to one or more EGFR-targeted tenth type three domains of human fibronectin. Both classes of constructs induce robust receptor clustering and downregulation in the absence of signal activation. *In vitro* downregulation correlates well with *in vivo* inhibition of tumor growth in several mouse xenograft tumor models and mutational analysis demonstrates that the efficacy of our fusions is attributable to both signaling effects and antibody-dependent cell-mediated cytotoxicity. Our multi-epitopic strategy may be readily applied to other receptor systems to form the basis for a new category of antibody-based therapeutics.

Thesis Supervisor: K. Dane Wittrup
Title: C.P. Dubbs Professor of Chemical & Biological Engineering

Jamie B. Spangler

ACADEMIC BACKGROUND

Massachusetts Institute of Technology, Cambridge, MA (September, 2006 – present)

- PhD Candidate in Department of Biological Engineering, Bioengineering Track
- Thesis Project: Characterization and informed design of downregulating anti-EGFR antibodies

The Johns Hopkins University, Baltimore, MD (September, 2002 – January, 2006)

- B.S. in Biomedical Engineering, Chemical Engineering Concentration, French Minor
- Graduated in 2006 with General and Departmental Honors

RESEARCH EXPERIENCE

K. Dane Wittrup Laboratory, Massachusetts Institute of Technology, Cambridge, MA

Graduate Research Fellow (January, 2007 – present)

- Characterized the dynamics and structural dependence of epidermal growth factor receptor (EGFR) trafficking and signaling in response to treatment with combination antibody therapeutics that induce receptor clustering and down-regulation
- Elucidated the kinetic mechanism of steady-state surface EGFR downregulation using an abstracted model of receptor trafficking
- Designing novel multispecific antibodies targeting multiple epitopes of EGFR incorporating scFv and human tenth type III fibronectin domains to cluster and down-regulate receptor as a potential therapeutic strategy
- Quantifying receptor down-regulation and signaling as well as inhibition of cancer cell migration and proliferation following treatment with engineered and pre-existing anti-EGFR antibodies
- Validating results of kinetic and *in vitro* assays with spheroid models and mouse tumor xenografts
- Developing fibronectin clones targeting other receptor tyrosine kinases implicated in anti-EGFR therapy resistance for use in multispecific constructs

National Institute of Allergy and Infectious Disease, Lab of Molecular Microbiology, Bethesda, MD

Supervisor: Dr. Jonathan Silver, Head of Biophysical Virology Section

Post-Baccalaureate Research Fellow (January – August, 2006)

- Probed biophysical mechanism of HIV-1 viral-mediated membrane fusion and entry into cells using molecular biology techniques in tandem with high-sensitivity imaging
- Studied antibody neutralization kinetics of vesicular stomatitis virus (VSV) using sensitive luciferase-based infectivity assay
- Constructed device for imaging bilayer lipid membranes and quantum dot-labeled retroviral particles

Kalina Hristova Laboratory, The Johns Hopkins University, Baltimore, MD

Undergraduate Research Assistant (January, 2003 – December, 2005)

- Investigated consequences of cysteine mutations and disulfide bond stability on fibroblast growth factor receptor 3 (FGFR3) dimerization and cell signaling
- Performed unprecedented measurements of dimerization free energy changes due to pathogenic mutations in receptor protein via FRET experiments in detergents and liposomes
- Conducted solid-phase peptide synthesis and peptide analysis for FGFR3 characterization
- Examined effects of achondroplasia mutation in rat DNA on protein expression

PUBLICATIONS

1. Spangler JB, Neil JR, Abramovitch S, Yarden Y, White FM, Lauffenburger DA, & Wittrup KD. Combination antibody treatment down-regulates epidermal growth factor receptor by inhibiting endosomal recycling. *Proc Natl Acad Sci U S A.* 2010. 107(30):13252-7.
2. You M, Spangler J, Li E, Han X, Ghosh P, & Hristova K. Effect of pathosgenic cysteine mutations on FGFR3 transmembrane domain dimerization in detergents and lipid bilayers. *Biochemistry.* 2007. 4(39):11039-46.
3. Iwamoto T, You M, Li E, Spangler J, Tomich JM, & Hristova K. Synthesis and initial characterization of FGFR3 transmembrane domain: Consequences of sequence modifications. *Biochim Biophys Acta.* 2005. 1668(2):240-7.

ORAL PRESENTATIONS

MIT Koch Institute Retreat (October, 2010)
Spangler J & Wittrup KD. Informed design and therapeutic evaluation of epidermal growth factor receptor antibodies.

Biomedical Engineering Society Annual Meeting (October, 2010)
Spangler J & Wittrup KD. Characterization and informed design of down-regulating epidermal growth factor receptor antibodies.

MIT Koch Institute Seminar (April, 2010)
Spangler J & Wittrup KD. Design and evaluation of epidermal growth factor receptor antibodies that induce clustering and consequent down-regulation.

MIT Cell Decision Processes Seminar (March, 2010)
Spangler J & Wittrup KD. Characterization of down-regulating epidermal growth factor receptor antibodies.

POSTER PRESENTATIONS

International Conference on Biomolecular Engineering (January, 2011)
Spangler J, Epstein B, Ross B, & Wittrup KD. Design and preclinical evaluation of novel multispecific antibody-based constructs targeting EGFR.

Protein Society Annual Meeting (August, 2010)
Spangler J, Epstein B, Ross B, Murray M, & Wittrup KD. Characterization and informed design of down-regulating EGFR antibodies.

Cambridge Health Institute Protein Engineering Summit (May, 2010)
Spangler J, Neil J, & Wittrup KD. Characterization of downregulating EGFR antibodies.

IBC Antibody Engineering Conference (December, 2009)
Spangler J, Neil J, & Wittrup KD. Synergistic down-regulation of EGFR induced by combination and multispecific antibody treatment.

IBC Drug Discovery Conference (August, 2009)
Spangler J, Hackel B, & Wittrup KD. Synergistic down-regulation and antagonism of EGFR induced by combination antibody treatment.

IBC Antibody Engineering Conference (December, 2008)
Spangler J, Manzari M, & Wittrup KD. Characterization of EGFR down-regulation induced by combination antibody treatment.

Biophysical Society Annual Meeting (February, 2006)
Spangler J, You M, Li E, & Hristova K. SDS-PAGE analysis of disulfide bonding in pathogenic FGFR3 cysteine mutations.

Howard Hughes Poster Presentation (August, 2005)
Spangler J, You M, Li E, & Hristova K. Measurements of the comparative dimerization of pathogenic FGFR3 transmembrane domain mutants using SDS-PAGE analysis.

PATENTS

Wittrup KD, Epstein B, Ross B, & Spangler J. Bispecific antibodies directed against tyrosine kinase receptors. 2010. Patent Application # 61/375765 *(Provisional)*.

Wittrup KD, Hackel B, & Spangler J. Engineered proteins including mutant fibronectin domains. 2010. PCT/US10/45490.

TEACHING AND SUPERVISORY EXPERIENCE

Teaching Assistant, Massachusetts Institute of Technology

Biomolecular Kinetics and Cellular Dynamics (September – December, 2008)

An in-depth study of kinetic and equilibrium mathematical models of biomolecular interactions, as well as the application of these quantitative analyses to biological problems across a wide range of levels of organization, from individual molecular interactions to populations of cells

- Held tutorials, recitations, and office hours with a particular emphasis on MATLAB applications
- Assisted with the formulation, administration, and evaluation of homework assignments and examinations

Supervision of Undergraduate Student Projects

Elizabeth Rosalia (December, 2010 – present)

Evaluating cell proliferation in autocrine EGFR ligand-driven models of cancer.

Fangdi Sun (December, 2010 – present)

Therapeutic analysis of multispecific EGFR-targeted antibodies in tumor xenograft models.

Mandana Manzari (September, 2010 – present)

Engineering antibody-fibronectin fusion constructs with increased valency, specificity, and therapeutic potency.

Mariah Murray (June, 2010 – present)

Analysis of cellular growth and migration in response to multispecific antibody-fibronectin fusion treatment.

Brian Ross (April, 2010 – present)

In vitro characterization and in vivo evaluation of a bispecific antibody targeting multiple epitopes of EGFR.

Alexandra Doolittle (December, 2009 – March, 2010)

High-resolution imaging of antibody-induced EGFR clusters via deconvolution microscopy.

Benjamin Epstein (September, 2009 – May, 2010)

Design and mechanistic characterization of a bispecific antibody targeting multiple epitopes of EGFR.

PROFESSIONAL SKILLS

- Programming experience in MATLAB and Java
- Expertise in protein synthesis, characterization, and analysis
- Extensive experience with molecular biology, cell biology, and yeast surface display
- Proficiency in flow cytometry and bead-based immunoassays
- Familiarity with confocal and deconvolution microscopy
- Experience with mouse xenograft models

HONORS AND AWARDS

• International Conference on Biomolecular Engineering Top Poster Award	2011
• Repligen Koch Institute for Integrative Cancer Research Fellowship	2010
• IBC Antibody Engineering Student Poster Scholarship	2008, 2009
• National Defense Science and Engineering Graduate Fellowship	2007
• MIT Graduate Presidential Fellowship	2006
• Howard Hughes Undergraduate Research Fellowship	2005
• Alpha Eta Mu Beta Biomedical Engineering Honor Society	2005
• Tau Beta Pi Engineering Honor Society	2004
• William R. Roberts Leadership Award	2004
• National Society of Collegiate Scholars Honor Society	2003
• National Merit Scholarship	2002

SOCIETY MEMBERSHIPS

• Biomedical Engineering Society	2010
• Protein Society	2010

ACKNOWLEDGMENTS

This thesis is the culmination of the efforts of many individuals who made invaluable contributions to both the vision and execution of this project.

I would first and foremost like to thank my advisor, Dane, for his incredible guidance, insight, and inspiration from start to finish. His ability to balance excitement with patience, direction with independence, and encouragement with constructive feedback has been a driving force behind this project. Dane never ceases to amaze me by keeping scientific contact rolling at all hours of the day and with the seemingly inexhaustible reservoir of ideas and directions he provides. It has been a privilege to learn from the best in terms of both my scientific and professional development.

I would also like to thank my thesis committee members, Doug and Forest, for offering their unique perspectives and experience throughout the course this project. It was an early suggestion from Doug and Forest to explore alternative model systems that originally got my project off the ground. This token of advice and others like it were instrumental in galvanizing and advancing the work described in this thesis.

One of the most cherished aspects of my graduate school experience has been the interactions I have shared with my colleagues in the Wittrup Lab. It has been an honor to work with such a brilliant, creative, and passionate group of scientists who are always willing to make time for a rich scientific discussion or to offer experimental or technical guidance. Drs. Ginger Chao, Shanshan Howland, Greg Thurber, Stephen Sazinsky, Mike Schmidt, Kelly Orcutt, and Margie Ackerman provided excellent technical assistance and expertise with protein production and characterization. In addition to spearheading the Fn3 work and isolating the three EGFR-binding clones used in our Ab-Fn3 fusions, Ben Hackel offered exceptional scientific and technical guidance. John Rhoden and Xiaosai Yao offered extensive assistance with animal studies and Tiffany Chen contributed insight and experimental assistance with effector function analysis. Chris Pirie and Jordi Mata-Fink participated in valuable scientific discussions and offered constructive advice. Seymour de Picciotto has provided helpful insight into the ErbB network and Nicole Yang, Cary Opel, Alice Tzeng, Byron Kwon, and Michael Santos have provided useful input for experimental and project directions.

Throughout this project, we were the beneficiaries of extremely helpful and dedicated collaborators. Sivan Abramovitch in Yosef Yarden's lab generously provided us with antibodies and Steven Wiley kindly provided us with autocrine ligand-expressing cell lines. Jason Neil in Forest White's lab performed a global phosphotyrosine mass spectrometry screen on one of our downregulating antibody cominations. Justin Pritchard of Doug Lauffenburger's lab and Mike Lee of Mike Yaffe's lab provided instruction and reagents for high-throughput signaling assays.

The incredibly talented undergraduates that I have had the opportunity to supervise over the past five years have contributed a great deal to the work presented in this thesis and, perhaps unwittingly, have played a formative role in the development of my mentorship skills. Mandana Manzari, Mariah Murray, and Elizabeth Rosalia assisted with Ab-Fn3 fusion development; Benjamin Epstein, Brian Ross, and Fangdi Sun contributed to the BS28 work; and Alexandra Doolittle assisted with live cell imaging.

Finally, I would like to thank my family and friends for the unwavering support and encouragement they have provided me throughout my graduate school career. In particular, I would like to thank my parents, Bonnie and David, for instilling in me from a young age the value of hard work and dedication. I thank my brothers, Ben and Joey, for being constant sources of support and inspiration. Last, but certainly not least, I would like to thank my fiancé Brett for being there for me in every way that I have needed him and for always believing in me and encouraging me to pursue my dreams.

TABLE OF CONTENTS

LIST OF ABBREVIATIONS

EGFR Epidermal growth factor receptor
EGF Epidermal growth factor
RTK Receptor tyrosine kinase
TGFα Transforming growth factor Alpha
MAPK Mitogen-activated protein kinase
PI3K Phosphoinositide 3-kinase
mAb Monoclonal antibody
Ab Antibody
SD Standard deviation
PE Phycoerythrin
PBS Phosphate buffered saline
BSA Bovine serum albumin
PBSA Phosphate buffered saline containing 0.1% BSA
K_d Equilibrium dissociation constant
FBS Fetal bovine serum
CHO Chinese hamster ovary
HMEC Human Mammary Epithelial Cells
DMEM Dulbecco's modified Eagle medium
EDTA Ethylenediaminetetraacetic acid
IgG Immunoglobulin G
HEK Human embryonic kidney
SDS-PAGE Sodium dodecyl sulfate polyacrylamide gel electrophoresis
Fn3 Tenth type 3 domain of human fibronectin
Ab-Fn3 Fusion Antibody-Fibronectin domain fusion
PMSF Phenylmethanesulfonylfluoride
CDC Complement-dependent cytotoxicity
ADCC Antibody-dependent cell-mediated cytotoxicity
SEM Standard error of the mean
ANOVA Analysis of variance

1. Background

Epidermal Growth Factor Receptor Structure and Signaling

The epidermal growth factor receptor (EGFR, also known as ErbB1), is one of four members of the ErbB family of transmembrane proteins, which is responsible for mediating the effects of growth factors such as epidermal growth factor (EGF), transforming growth factor-α (TGF-α), amphiregulin, and neuregulins (1-3). The four ErbB receptors (EGFR, ErbB2, ErbB3, and ErbB4) are prototypical receptor tyrosine kinases that homo- and heterodimerize in the presence of ligand to form ten functional signaling complexes. Receptor interaction results in trans-phosphorylation of tyrosine residues in the constituent receptors' intracellular domains, recruiting phosphotyrosine-binding adaptor proteins which in turn activate downstream pathways. Each ErbB receptor has distinct ligand-binding and dimerization propensities; For instance ErbB2 does not bind to any known ligand and ErbB3 has an inactive kinase domain, making both of these receptors dependent upon heterodimerization for signaling. Notably, ErbB2 is the favored heterodimeric partner of the other ErbB family receptors and its preferred interaction partner is ErbB3, resulting in a potently signaling heterodimer (4).

The interplay between ErbB family members creates a horizontal and vertical signaling network that leads to activation of a variety of pathways, including the mitogen-activated protein kinase (MAPK) pathway, the protein kinase C (PKC) pathway, and the phosphoinositide 3-kinase (PI3K) pathway. Activation of these pathways ultimately converges on transcription factors, whose modulation leads to an array of cellular responses including growth, adhesion, migration, differentiation, and apoptosis. The ErbB family signaling network as it is currently understood is summarized in Figure 1.1 (2). This diagram encapsulates the complexity of the network, yet eloquently abstracts ErbB family signaling into an input layer of ligand binding, a signal processing layer of adaptor protein recruitment and transcription factor regulation, and an output layer of cell behaviors.

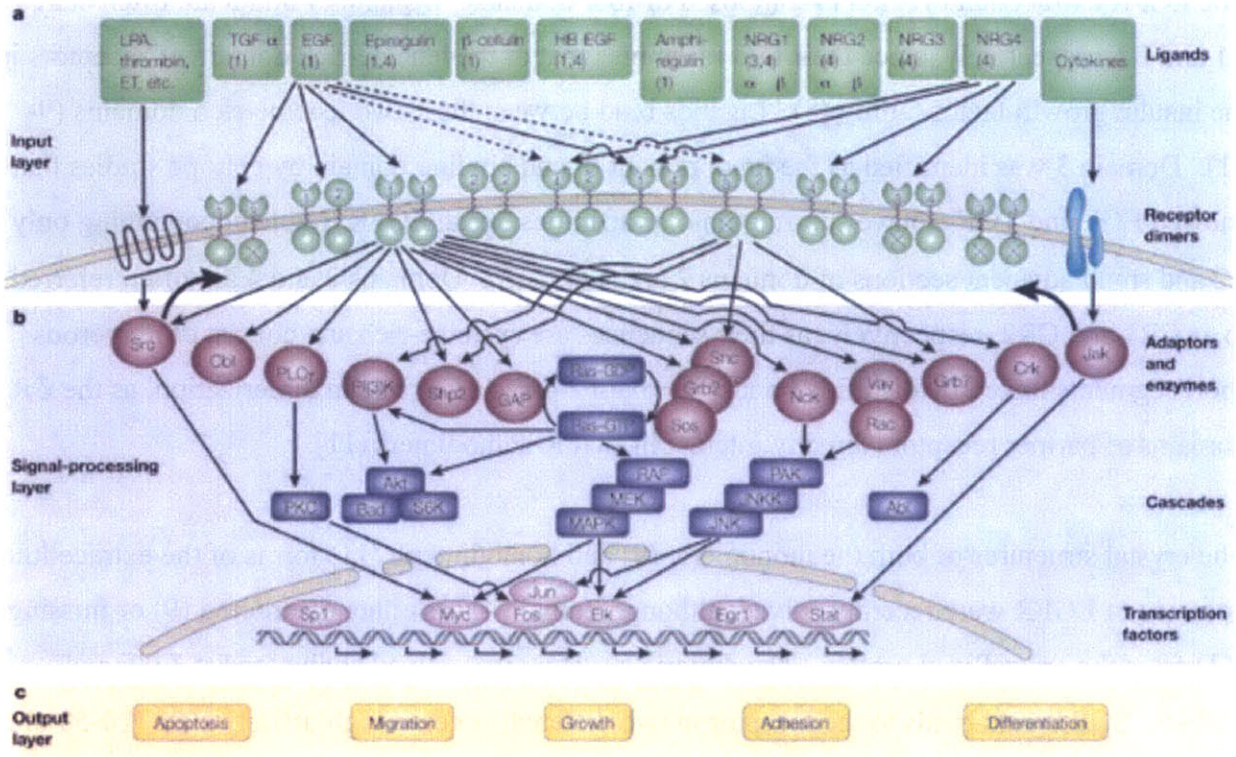

Figure 1.1. Schematic of the ErbB signaling pathway including stimulating ligands, ErbB family receptors, effector proteins, and downstream transcription factors regulated by the indicated signaling cascades, from (2), reproduced with permission. Note that the diagram is abstracted into input signal, signal processing network, and output response layers.

Among the members of the ErbB family, EGFR is by far the best characterized. EGFR is a 170-kDa protein that is 1186 amino acids in length. Over 20% of the receptor mass is contributed by N-linked glycosylation, which is requisite for both localization and function (5). Like the other ErbB family receptors, EGFR consists of an extracellular region (domains I-IV), a transmembrane (TM) domain, a juxtamembrane (6) domain, a tyrosine kinase domain (TK), and a carboxyl-terminal region (CT), as shown in Figure 1.2. ErbB family members share 37%-49% sequence identity and the three-dimensional folds of ErbB receptors are similar, except for possible divergence in the C-terminal domains (7).

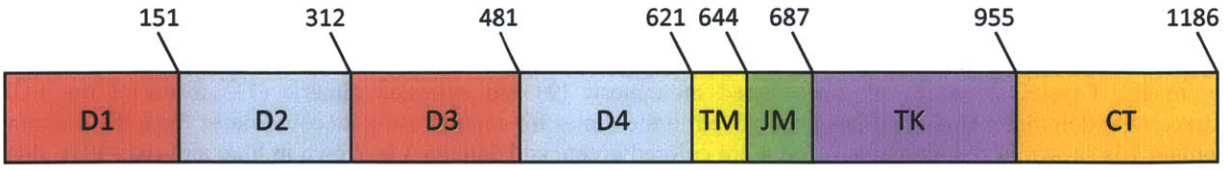

Figure 1.2: Schematic of the four extracellular domains, the transmembrane domain, and the intracellular domains (tyrosine kinase and c-terminal domain) of EGFR. Numbers represent amino acid positions along the receptor.

The EGFR extracellular region is composed of four domains. Domains 1 and 3 are often called L1 and L2, respectively, since their fold resembles that of the leucine-rich domain of receptors in the insulin growth factor family (8). Ligands bind between these two leucine-rich domains (9-11). Domain 3 was identified as the predominant ligand binding domain by epitope studies that showed EGF and TGF-α have sub-micromolar affinities for an EGFR fragment containing only L2 and small adjacent sections of domains 2 and 4 (12, 13). Domains 2 and 4 are often referred to as CR1 and CR2, respectively, as their sequences are cysteine-rich and consist of numerous short segments linked by disulfide bonds. Domain 2 plays a key role in dimerization, as the CR1 domains of partner receptors directly interact in EGFR homodimers (11).

The crystal structures of both the monomeric (9) and homodimeric (11) forms of the extracellular domains of EGFR were recently solved, although domain 4 was either disordered (9) or missing (11) from the crystallized protein. The dimeric structure was solved conjugated to EGF and TGF-α. EGF ligand binds to the receptor in two different states: a high-affinity state (10-50 pM) and a low-affinity state (1-2 nM), possibly differing in dimeric conformations or activity (14). EGF ligand interacts with domains 1 and 3 of the tethered receptor monomer, distal from the dimerization interface. It is believed that binding of a growth factor induces a 130° rigid body rotation that transitions EGFR into the dimeric conformation, as shown in Figure 1.3 (15).

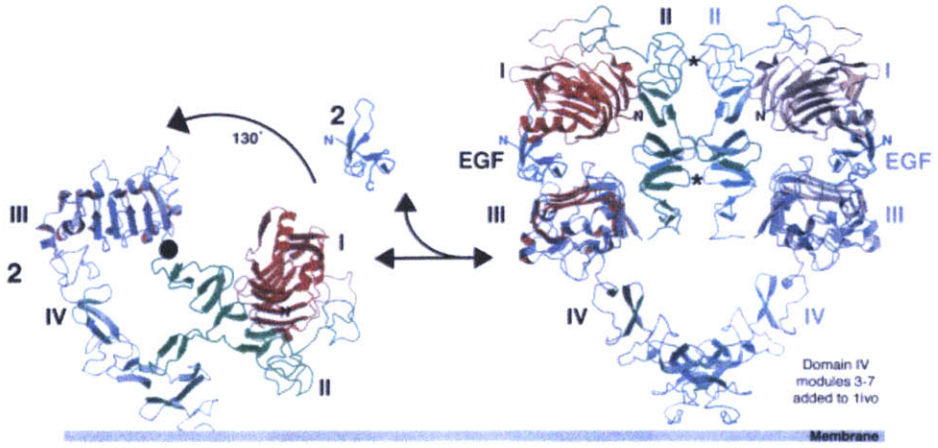

Figure 1.3: Crystal structures of the tethered monomeric (9) and extended dimeric (11) forms of the EGFR extracellular domains. Domain 4 has been added to the dimer for context using its coordinates from the monomer. Domain 1 is shown in red, domains 2 and 4 are colored green, and domain 3 is shown in blue and red. EGF ligand is shown in teal. The domain 2 dimerization contacts between interacting receptors are marked with asterisks. Figure reproduced with permission from reference (15).

EGFR dimers exist in 2:2 receptor:ligand complexes, although dimerization is entirely receptor-mediated. The dimerization interface is localized to domain 2, as shown in Figure 1.3. Residues 242-259 of each EGFR molecule contact and interact with domain 2 residues of the partner receptor (15). Additional domain 2 contacts occur between residues 193-195, 204-205, and 279-280 of partner receptors (11). Domain 4 may play a role in the dimerization interface as it has been reported that peptides that mimic modules 6 and 7 of this extracellular domain can disrupt EGFR homo- and heterodimerization (16). Also, domain 4 mutations have been shown to obstruct ligand binding and tyrosine phosphorylation, but the role of domain 4 in dimerization has yet to be fully elucidated due to the inability to crystallize this region (17). The orientation and interacting residues in the EGFR dimer are depicted in Figure 1.3.

Although the structure of the extracellular domain and its rearrangement upon ligand-mediated dimerization are now well understood, the mechanism of kinase activation was, until recently, poorly defined. Conflicting structural data showed the active kinase domain crystallized in both symmetric and asymmetric formats (18, 19). Further mutational and biochemical analysis by Zhang and colleagues demonstrated that dimerization of the extracellular domain relieves the autoinhibition of the intracellular kinase domain through formation of an asymmetric kinase dimer in which the C-terminal lobe of one kinase domain interacts with the N-terminal lobe of its partner receptor in an analogous manner to the interaction between cyclin and cyclin-dependent kinases. This interaction exposes the active site on one receptor, allowing for kinase activity. The two receptors can dynamically switch positions to enable trans-phosphorylation of both receptors, as shown in Figure 1.4 (19).

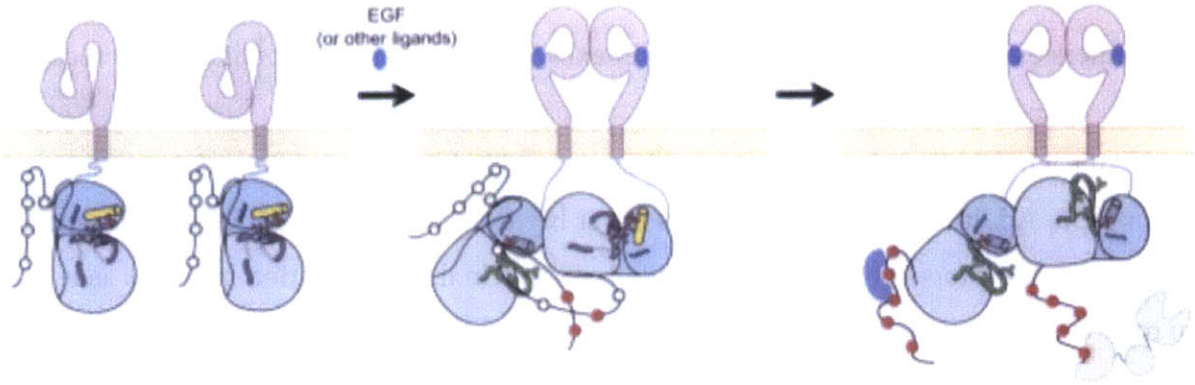

Figure 1.4. Schematic of EGFR kinase domain activation following EGF activation. Ligand-induced symmetric extracellular dimerization (pink) effects the rearrangement of intracellular tyrosine kinase domains to relieve autoinhibition and enable activation in a structurally similar manner to the cyclin/cyclin-dependent kinase interaction. The active kinase domain then trans-phosphorylates its partner receptor. The two receptors may switch positions to allow for activation of both molecules. Figure reproduced with permission from (19).

EGFR signaling is critical for epithelial cell development and its knockout in mice results in death either in mid-gestation, at birth, or postnatal day 20, depending on the genetics of the particular mouse strain (20-23). In contrast, mice show much less sensitivity to the absence of EGFR ligands, suggesting extensive redundancy in their function. Knockout of EGF and amphiregulin have no palpable effects on mouse phenotype (24) and knockout of TGF-α results only in slight abnormalities in the eye and in hair follicles (25). Even simultaneous knockout of EGF, amphiregulin, and TGF-α results in relatively mild defects including slight growth retardation and irregularities in the small intestine (26).

EGFR Trafficking

The structural and signaling properties of EGFR are intimately linked to its trafficking kinetics. In the absence of ligand, the vast majority of EGFR is localized to the cell surface (80-90%), but it is constantly shuttled in and out of the cell with an internalization halftime of 30 minutes and a rapid rate of recycling (27). Since the metabolic half-life of EGFR is 10-14 hours in fibroblasts and epithelial cells and 20-48 hours in transformed cells, receptors cycle through the endocytic pathway dozens of times with little risk of degradation (Figure 1.5) (1, 28, 29).

Once a ligand binds to and activates EGFR, the rate of internalization increases 5-10 fold and the degradation fraction is augmented at the expense of recycling (27, 30). This phenomenon,

known as receptor downregulation, is thought to be a negative feedback mechanism to attenuate growth factor signaling.

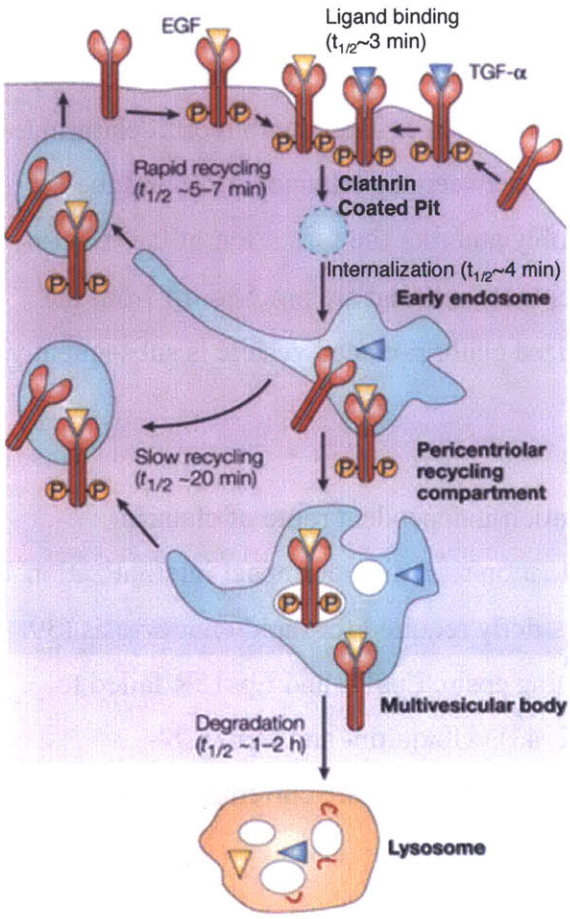

Figure 1.5. Schematic of EGFR trafficking with known time constants labeled. EGFR is constitutively shuttled in and out of the cell with an internalization halftime of 30' and a high probability of rapid recycling. Upon ligand stimulation, internalization is accelerated five- to tenfold and recycled fraction is dramatically reduced, shunting receptors to late endosomes and, ultimately, degradation in the lysosome. This figure is reproduced with permission from (1).

Acceleration of endocytosis rate is a direct consequence of recruitment to the clathrin-mediated endocytosis pathway compared to basal internalization routes. Clathrin-mediated endocytosis is by far the fastest means of receptor internalization and is the predominant endocytic route for activated receptor under physiological conditions (31). However, additional modes of internalization involving lipid rafts, caveolae, membrane ruffling, and pinocytosis have also been described (32-36). Unlike clathrin-mediated internalization, though, these alternative mechanisms do not accelerate EGFR endocytosis compared to constitutive kinetics. Also, accumulating evidence shows that these pathways are active only in the presence of extremely high concentrations of EGF, well above those observed physiologically (37-39).

Immediately following activation of EGFR, Cbl proteins bind to the EGFR phosphotyrosine domain through complexation with the adapter protein Grb2 or a presently uncharacterized protein (referred to as "X" in Figure 1.6), both of which interact with the receptor. Cbl family proteins, which have E3 ubiquitin ligase activity, monoubiquitinate EGFR with the assistance of E2 ubiquitin conjugating enzymes (31). These proteins are in turn phosphorylated by Src, increasing their interaction with the Cbl-interacting protein CIN85. CIN85 is constitutively associated with endophilins, which regulate clathrin-

mediated endocytosis, suggesting a role for this protein in internalization. However, the role of CIN85 in trafficking of membrane-bound EGFR remains undefined as its presence has not yet been detected in coated pits.

Ubiquitinated EGFR is recognized by ubiquitin binding domains (UBDs) of the EGFR pathway substrates 15 (EPS15) and 15R (Eps15R) as well as epsin, which collaborate to recruit clathrin to the cell surface and facilitate the formation of a complex between the tetramer AP-2 and the receptor to be internalized. AP-2 drives clathrin assembly and thus the formation of the 0.2-μm vesicles known as clathrin-coated pits. Receptors enter these pits and are pinched off from the membrane with the aid of dynamin (40). The internalized clathrin-coated vesicle is subsequently uncoated and fuses with an early endosome.

It should be noted that there is evidence of a ubiquitination-independent route of clathrin-mediated endocytosis. Mutation of the EGFR ubiquitination sites did not impact internalization rate, implying that Cbl-mediated ubiquitination is not strictly required for rapid endocytosis (39, 41, 42). Also, siRNA knockdown of the UBD-containing epsin, Eps15, and Eps15R failed to inhibit clathrin-dependent internalization of EGFR (32, 43). Ubiquitin- and Grb2/Cbl-independent mechanisms of EGFR recruitment to clathrin-coated pits are currently being investigated.

In contrast with ubiquitination, kinase domain activity is requisite for clathrin-mediated endocytosis. Mutation of the kinase domain's catalytic lysine and competitive inhibition of kinase activation result in significant reductions in endocytosis rate in the presence of ligand (on the order of basal endocytosis) and inefficient recruitment to clathrin-coated pits (44-48). Thus, accelerated endocytosis through clathrin-coated pits requires intact kinase activity.

From the early endosome, a receptor may be sorted for recycling back to the surface (known as quick recycling). Unbound receptors are typically shunted to this pathway whereas active EGF-bound receptors are rarely recycled and remain in the endosome as it matures into the late endosome, also known as a multi-vesicular body (MVB). Within the MVB, activated ubiquitinated EGFR forms a complex with ESCRT-0 (consisting of STAM, signal transduction

adaptor molecule, and HRS, hepatocyte-growth-factor-regulated tyrosine-kinase substrate) through its UBDs. The receptor is then encapsulated into the intraluminal vesicles of MVBs, which subsequently fuse with lysosomes, where protein degradation is carried out by hydrolases (49). Small amounts of recycling (known as late recycling) also occur from MVBs. The EGFR internalization pathway and approximate timescales for relevant events are summarized in Figure 1.5 and a more detailed depiction of the endocytic pathway is provided in Figure 1.6.

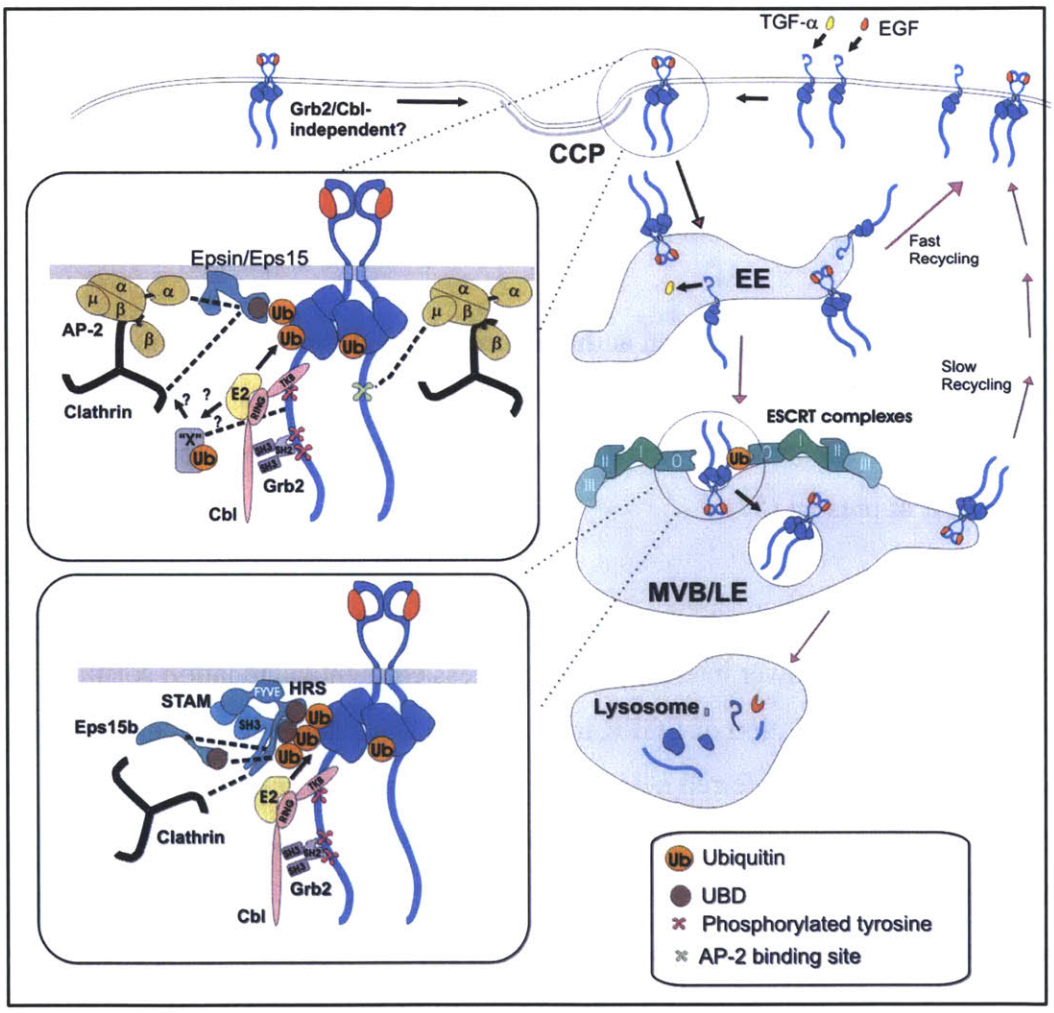

Figure 1.6. Model of EGFR endocytosis and intracellular trafficking following ligand stimulation. Briefly, EGF or TGF-α binding to EGFR (blue) induces dimerization and phosphorylation. The Grb2-Cbl adaptor protein complex is then recruited to phosphotyrosine sites in the C-terminal domain of the receptor. The RING domain of Cbl in turn recruits E2 enzymes to ubiquitinate the receptor. Ubiquitinated receptor is recognized by ubiquitin binding domains (UBDs) of epsin, Eps15, and Eps15R, which are associated with AP-2 and clathrin heavy chain, the principle constituent of clathrin-coated pits (CCPs). Note that there may also be Grb2-Cbl complex-independent modes of CCP recruitment. CCPs containing EGFR fuse with early endosomes (EEs) and receptor may either be rapidly recycled or remain encapsulated in endosomes as they mature into multivesicular bodies (MVBs). Ubiquitinated EGFR that remains in MVBs interacts with the UBDs of the ESCRT-0 complex (consisting of HRS and STAM) as well as Eps15b, resulting in its localization to internal MVB vesicles. MVB then fuses with primary lysosomes, where vesicle-bound EGFR-EGF complexes are degraded. Figure reproduced with permission from (31).

Internalization has historically been viewed exclusively as a mechanism for quenching receptor signaling, but it is now known that most if not all EGFR in endosomes is capable of signal transduction (50, 51). However, the signaling pathways that are activated and the duration of activation differ for internalized receptors compared with their surface-bound counterparts (52). While PLC-γ and PI3K pathway activation are reported to be restricted to surface-bound receptors, the *ras*-dependent MAPK can be activated from both surface-bound and intracellular receptors (53, 54). Endosomal signaling has also been linked to tumor development. For instance, nuclear localization of EGFR has been observed following endocytosis and this localization is enhanced in cancer cells, but the role that nuclear EGFR plays in signal transduction or cancer development has yet to be established (55).

Aside from receptor internalization, an additional mechanism for signal attenuation is dephosphorylation of internalized EGFR at the endoplasmic reticulum by protein tyrosine phosphatase-1B (PTP1B) (56). However, the relationship between receptor deactivation and sorting is unclear at present (57).

EGFR trafficking and internalization are also affected by heterodimerization. All other ErbB family members exhibit slower internalization and less efficient degradation sorting than EGFR (58-61), resulting in modulation of EGFR trafficking kinetics depending on dimer distribution. In particular, ErbB2 is the preferred heterodimerization partner of EGFR and the formation of a complex between these two ErbB family members results in enhanced affinity for EGF, but reduced internalization and degradation (20, 27). Consequently, EGFR downregulation is decreased and EGFR signaling persists for longer time periods in the presence of excess ErbB2.

Linking EGFR to Cancer

For the past three decades, EGFR has been under intensive study due to its common overexpression in epithelial-based tumors. EGFR expression is found at increased levels in many head, neck, breast, bladder, prostate, kidney, non-small-cell lung cancers, and gliomas (57). Between 33 and 50% of human epithelial tumors overexpress EGFR and this aberrant

expression has been linked to poor clinical outcome, making EGFR a particularly attractive target for anti-cancer therapeutics (62, 63).

In addition to aberrant expression, mutations of the EGFR gene that dysregulate receptor signaling are often detected in cancer cells. Heterozygous somatic mutations including deletions, insertions, and point mutations have been observed in the EGFR kinase domain, particularly in lung cancer patients (64-66). These mutations strengthen receptor interactions with ATP, amplifying autophosphorylation and boosting cell survival (67, 68).

Numerous non-kinase domain EGFR mutants have also been observed, particularly in tumors with EGFR gene amplification. Mutants with deletions, sequence duplications, and defective kinase regulatory signals have been reported. As many as 20% of glioblastomas express EGFR variants (69, 70), the most common of which is EGFRvIII (71), a splice mutant that deletes residues 6-273 of the receptor (most of extracellular domains 1 and 2). Due to the absence of domain 1-mediated tetheringin EGFRvIII, it is locked in the extended dimeric conformation. The TK domain is thus constitutively active, independent of ligand binding (57). Other non-kinase rearrangements within the ErbB1 gene such as large deletions, point mutants, and insertions are also common, particularly in gliomas (72).

Finally, ErbB receptors have been linked to cancer in the context of autocrine signaling. Expression of an ErbB receptor in conjunction with an excess of its ligand can lead to unregulated cell growth. Autocrine production of TGF-α and EGF in cancer patients is correlated with increased mortality (73, 74). Also, autocrine signaling by neuregulin has been shown to induce uncontrolled proliferation of human vestibular schwannoma cells (75). Thus, anti-cancer therapeutics must often compete with high concentrations of endogenous ligands *in vivo*.

Anti-EGFR Therapeutics

Extensive overexpression and dysregulation of EGFR in a wide variety of cancer forms make this receptor an attractive therapeutic target. The two main compounds that have been used for

targeting EGFR are small-molecule tyrosine kinase inhibitors (TKIs) and anti-EGFR monoclonal antibodies (mAbs).

TKIs block activation of the EGFR TK domain by binding to the intracellular Mg-ATP binding site, obstructing ATP binding and subsequent autophosphorylation. The best-characterized TKIs are gefitinib and erlotinib, both of which are synthetic anilinoquinazolines that inhibit EGFR TK activity with nanomolar IC_{50} values. Complementing its primary action of blocking ATP binding, gefitinib has also been shown to indirectly reduce angiogenesis (76). Treatment with gefitinib or erlotinib inhibits tumor cell proliferation, probably through induction of cell cycle arrest or apoptosis, and both drugs were recently approved by the FDA in the treatment of non-small-cell lung cancer (77, 78). There are several other TKIs in clinical trials, including canertinib, lapatinib, AG-1478, and HKI-272 (57).

mAbs are Y-shaped homodimeric proteins that consist of two identical heavy and two identical light chains. The structure of a standard immunoglobulin G (IgG) is shown in Figure 1.7. The heavy and light chains contain an N-terminal variable fragments (VH and VL, respectively). Each variable fragment has a beta barrel structure with conserved beta sheets (the framework regions) separated by three hypervariable loops known as the complementarity determining regions that confer specificity to a target antigen (79, 80). In addition to variable domains, antibody heavy chains consist of three constant domains (CH1, CH2, and CH3) and the light chains include one constant domain (CL), all of which are uniform for a particular antibody isotype. The heavy chain CH2 and CH3 constant domains are collectively termed the Fc region, and interact with complement or Fcγ receptors found on several types of leukocytes, including natural killer cells, macrophages, and neutrophils, to elicit an immune response (81).

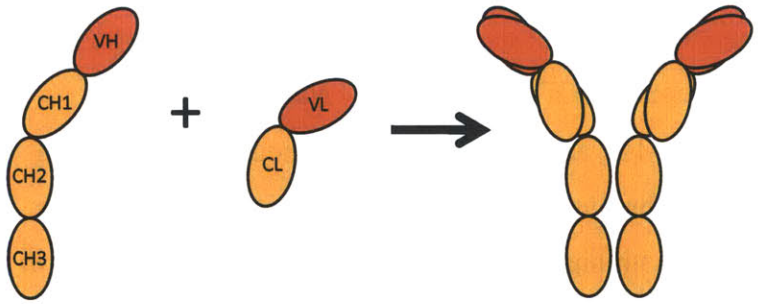

Figure 1.7. Schematic of the assembly and structure of IgG antibody. The structure of the heavy (left) and light (midde) chains are presented. These chains assemble via four disulfide bridges to form the symmetric 2:2 dimer shown at right. Note that the heavy chain consists of an N-terminal variable domain and three constant domains whereas the light chain consists of an N-terminal variable domain and one constant domain.

Antibodies assemble into 2:2 heavy:light chain complexes, linked by four disulfide bonds: One between CH1 and CL of each arm and two in the hinge region (N-terminal end of the CH2 domain). Crystallization of a full, intact human IgG revealed substantial asymmetry emanating from the extensive flexibility in antibody structure (82). Their ability to specifically target an antigen of interest and to foment an immune response have made mAbs attractive therapeutic molecules. In cancer treatment alone, there are ten clinically approved antibody-based drugs, with 165 others currently undergoing clinical trials (6).

mAbs specific for EGFR function both by recruiting cytotoxic lymphocytes or other white blood cells to enhance the immune response to cancer in a process known as antibody-dependent cell-mediated cytotoxicity (ADCC) (81) and by directly inhibiting EGFR signaling. The first antibody-based EGFR therapeutic to receive clinical approval was cetuximab (humanized form of murine mAb 225) (83). Originally isolated from immunized mice, mAb 225 was reconstructed as a chimeric human Immunoglobulin G1 (IgG1) for clinical use. With a 100-fold greater affinity for EGFR than the native EGF ligand, mAb 225 directly competes with ligand binding to domain III, blocking dimerization and autophosphorylation (84, 85). Its binding has been shown to enhance EGFR internalization and degradation in some cell lines (86, 87). mAb 225 treatment has been shown to induce G1-phase cell-cycle arrest and enhanced apoptosis in a range of human tumor cell lines (88, 89). Incidentally, mAb 225 also inhibits vascular endothelial growth factor (VEGF), further enhancing its anti-tumor activity (90).

Following successful phase III clinical trials, mAb 225 was recently approved to treat metastatic colorectal cancer (91) and squamous cell carcinoma of the head and neck (92, 93). Other monoclonal antibodies targeting the EGFR ligand-binding domain include the FDA-approved panitumumab and several compounds undergoing clinical trials, including matuzumab and hR-3 (94, 95).

A monoclonal antibody (mAb 806) that specifically targets EGFRvIII was recently discovered (96). mAb 806 binds to a cysteine loop at the end of EGFR extracellular domain II, a conformational epitope that is exposed only when the receptor transitions into the open conformation upon dimerization (97-99). Since this antibody is not competitive with compounds

targeting the ligand-binding domain, it is undergoing clinical testing for both monotherapy and combination therapy. A recent phase I clinical trial of mAb 806 demonstrated specific targeting of the mutant receptor and no significant toxicity (100).

Despite recent advances in the development of monoclonal antibody therapeutics against EGFR, large deficiencies remain in the efficacy of these drugs. For instance, mAb 225 showed an 11% response rate as a monotherapy and a 23% response rate in combination with chemotherapy in metastatic colorectal cancer and showed a response rate of 13% in squamous cell carcinoma of the head and neck (Erbitux® prescribing information). The other clinically approved anti-EGFR antibody, panitumumab, had only an 8% response rate in metastatic colorectal cancer (Vectibix® prescribing information). It should also be noted that these antibodies are ineffective against EGFRvIII and tumor cells that secrete high levels of autocrine EGFR ligands due to their reliance on ligand competition for efficacy. In addition, poor tumor penetration, autocrine signaling, acquired resistance, and receptor mutation hinder drug performance (101). It is therefore of interest to develop complementary therapeutic strategies to enhance mAb efficacy.

Antibody-Induced Clustering

It was recently established that particular combinations of non-competitive anti-EGFR mAbs synergistically reduce surface receptor levels both *in vitro* and *in vivo*. This downregulation of receptor is independent of tyrosine kinase activity and leads to enhanced tumor cell killing and prolonged survival in mouse xenograft models of cancer (102-105). Consistency between downregulation levels and combination efficacy in mouse models was also reported for ErbB2 (106). Friedman *et al* proposed that antibody synergism results from the formation of large clusters of crosslinked receptors on the cell surface following combination mAb treatment (102). Biochemical evidence for the formation of higher-order clusters of EGFR was presented by Zhu *et a*l using the tyrosine kinase inhibitor decorin (107).

In particular, inclusion of the 806 monoclonal antibody in combination antibody treatments could be of significant utility in targeting EGFR. Due to its selectivity for mutant or overactive receptors and its neutralizing activity, it may be able to evade some of the shortcomings of mAbs that compete with ligand binding (96, 98). In a recent study, it was demonstrated that EGFR

undergoes synergistic downregulation in the presence of mAb 806 and mAb 528, an antibody with similar specificity and binding affinity to mAb 225 (103). This study points again to the possibility of receptor crosslinking and clustering, which can impact both trafficking and downstream signaling.

We hypothesized that receptor clustering could lead to downregulation through internalization enhancement or degradation fraction augmentation. We note that the endocytic machinery is saturable (37), thus improving the efficiency of internalization via simultaneous entry of multiple clustered receptors could enhance the rate of receptor internalization compared to that of untreated cells. Additionally, whereas unoccupied single receptors are rapidly recycled back to the membrane following internalization, oligomeric receptors are preferentially retained in endosomes through maturation and lysosomal fusion (31, 108), which could potentially result in enhancement of EGFR degradation.

Receptor clustering could be advantageous in that it would complement existing therapeutic mechanisms by downregulation of EGFR and its signaling. Also, a clustering strategy would be independent of ligand binding, allowing for efficacy in constitutively active systems involving mutated receptor or dysregulated ligand, which resist treatment by currently approved therapeutics. The characterization and, ultimately, the exploitation of antibody-mediated clustering holds promise as a novel strategy for therapeutic EGFR targeting in cancer.

Thesis Contributions

At the outset of this thesis work, the idea of antibody-induced clustering was just beginning to be explored. The objective of our project was to characterize the reproducibility and scope of this phenomenon and to isolate its mechanistic basis to gain insights that would inform design of EGFR-downregulating compounds for therapeutic applications. In the work described herein, we identify the requirements for antibody-induced downregulation, elucidate its kinetic mechanism, and evaluate its efficacy in a simulated tumor environment. We then apply our insights to the design of two novel classes of multispecific antibodies that show therapeutic promise in both *in vitro* and *in vivo* models of cancer.

In Chapter 2, we illuminate several crucial properties of combination antibody-induced clustering. By screening a panel of pairwise antibody combinations, we show that co-treatment with non-competitive mAbs targeting distinct epitopes on EGFR elicits up to 80% receptor downregulation. Receptor downregulation induced by mAb combinations is found to be inversely proportional to receptor density and requires bivalency of both constituent antibodies. We further find that mAb pairs consisting of two non-competitive antibodies that target EGFR domain 3 show the highest downregulation activity. The mechanism underlying downregulation is found to be consistent with recycling inhibition. Importantly, in contrast to the agonism associated with ligand-induced downregulation, we find that combination mAb-induced downregulation does not activate EGFR or downstream signaling pathways and that it leads to synergistic reduction in migration and proliferation of autocrine ligand-secreting cells.

After establishing the parameters for combination mAb-induced downregulation, we attempt to enhance antibody binding and induced receptor clustering through avidity effects. We employ two novel design approaches for our multispecific antibodies: (1) Fusion of the a full anti-EGFR antibody with the variable domain fragment of a second EGFR-targeted antibody (described in Chapter 3) and (2) Fusion of a full EGFR-specific antibody fused to one or more EGFR-binding variants of the tenth type three domain of human fibronectin (detailed in Chapter 4). We demonstrate that both classes of constructs induce robust receptor clustering and reproducible downregulation on a range of cancerous cell lines. We also establish that these multispecific fusions downregulate both through blockade of receptor recycling and via acceleration of endocytosis and that downregulation is independent of receptor surface density. To motivate therapeutic application, we show that multispecific compounds do not agonize EGFR signaling and that they inhibit motility and growth of cells that aberrantly express autocrine ligand.

We present evidence in Chapter 5 that both of our multispecific strategies effectively curtail growth in tumor xenograft models that resist treatment with standard of care antibodies and that *in vivo* inhibition of tumor growth channels *in vitro* receptor downregulation. In particular, we show dramatic control of tumors that contain genetic mutations in effector proteins downstream of EGFR (*raf* and *ras*). Through mutational analysis, we demonstrate that ligand inhibition, receptor inhibition, and effector function all contribute to therapeutic efficacy.

In summary, we have rigorously characterized and defined requirements for antibody-induced downregulation and applied this information to the design of novel classes of EGFR-targeted antibody-based therapeutics. The modularity of our constructs and the generality of our system suggests extensibility of the multi-epitopic strategy to other ErbB family members and, more generally, to receptor proteins of therapeutic interest.

References

1. Sorkin A & Von Zastrow M (2002) Signal transduction and endocytosis: close encounters of many kinds. *Nat Rev Mol Cell Biol* 3(8):600-614.
2. Yarden Y & Sliwkowski MX (2001) Untangling the ErbB signalling network. *Nat Rev Mol Cell Biol* 2(2):127-137.
3. Hynes NE & Lane HA (2005) ERBB receptors and cancer: the complexity of targeted inhibitors. *Nat Rev Cancer* 5(5):341-354.
4. Tzahar E, *et al.* (1996) A hierarchical network of interreceptor interactions determines signal transduction by Neu differentiation factor/neuregulin and epidermal growth factor. *Mol Cell Biol* 16(10):5276-5287.
5. Slieker LJ, Martensen TM, & Lane MD (1986) Synthesis of epidermal growth factor receptor in human A431 cells. Glycosylation-dependent acquisition of ligand binding activity occurs post-translationally in the endoplasmic reticulum. *J Biol Chem* 261(32):15233-15241.
6. Reichert J (2011) Antibodies for cancer: Past, present, and future. *Seventh Annual Protein Engineering Summit.*
7. Jorissen RN, *et al.* (2003) Epidermal growth factor receptor: mechanisms of activation and signalling. *Exp Cell Res* 284(1):31-53.
8. Garrett TP, *et al.* (1998) Crystal structure of the first three domains of the type-1 insulin-like growth factor receptor. *Nature* 394(6691):395-399.
9. Ogiso H, *et al.* (2002) Crystal structure of the complex of human epidermal growth factor and receptor extracellular domains. *Cell* 110(6):775-787.

10. Garrett TP, *et al.* (2002) Crystal structure of a truncated epidermal growth factor receptor extracellular domain bound to transforming growth factor alpha. *Cell* 110(6):763-773.
11. Ferguson KM, *et al.* (2003) EGF activates its receptor by removing interactions that autoinhibit ectodomain dimerization. *Mol Cell* 11(2):507-517.
12. Kohda D, *et al.* (1993) A 40-kDa epidermal growth factor/transforming growth factor alpha-binding domain produced by limited proteolysis of the extracellular domain of the epidermal growth factor receptor. *J Biol Chem* 268(3):1976-1981.
13. Lemmon MA, *et al.* (1997) Two EGF molecules contribute additively to stabilization of the EGFR dimer. *EMBO J* 16(2):281-294.
14. Lin CR, *et al.* (1986) Protein kinase C phosphorylation at Thr 654 of the unoccupied EGF receptor and EGF binding regulate functional receptor loss by independent mechanisms. *Cell* 44(6):839-848.
15. Burgess AW, *et al.* (2003) An open-and-shut case? Recent insights into the activation of EGF/ErbB receptors. *Mol Cell* 12(3):541-552.
16. Berezov A, *et al.* (2002) Disabling receptor ensembles with rationally designed interface peptidomimetics. *J Biol Chem* 277(31):28330-28339.
17. Saxon ML & Lee DC (1999) Mutagenesis reveals a role for epidermal growth factor receptor extracellular subdomain IV in ligand binding. *J Biol Chem* 274(40):28356-28362.
18. Stamos J, Sliwkowski MX, & Eigenbrot C (2002) Structure of the epidermal growth factor receptor kinase domain alone and in complex with a 4-anilinoquinazoline inhibitor. *J Biol Chem* 277(48):46265-46272.
19. Zhang X, Gureasko J, Shen K, Cole PA, & Kuriyan J (2006) An allosteric mechanism for activation of the kinase domain of epidermal growth factor receptor. *Cell* 125(6):1137-1149.
20. Citri A & Yarden Y (2006) EGF-ERBB signalling: towards the systems level. *Nat Rev Mol Cell Biol* 7(7):505-516.
21. Miettinen PJ, *et al.* (1995) Epithelial immaturity and multiorgan failure in mice lacking epidermal growth factor receptor. *Nature* 376(6538):337-341.
22. Threadgill DW, *et al.* (1995) Targeted disruption of mouse EGF receptor: effect of genetic background on mutant phenotype. *Science* 269(5221):230-234.

23. Sibilia M & Wagner EF (1995) Strain-dependent epithelial defects in mice lacking the EGF receptor. *Science* 269(5221):234-238.
24. Luetteke NC, *et al.* (1999) Targeted inactivation of the EGF and amphiregulin genes reveals distinct roles for EGF receptor ligands in mouse mammary gland development. *Development* 126(12):2739-2750.
25. Mann GB, *et al.* (1993) Mice with a null mutation of the TGF alpha gene have abnormal skin architecture, wavy hair, and curly whiskers and often develop corneal inflammation. *Cell* 73(2):249-261.
26. Troyer KL, *et al.* (2001) Growth retardation, duodenal lesions, and aberrant ileum architecture in triple null mice lacking EGF, amphiregulin, and TGF-alpha. *Gastroenterology* 121(1):68-78.
27. Wiley HS (2003) Trafficking of the ErbB receptors and its influence on signaling. *Exp Cell Res* 284(1):78-88.
28. Stoscheck CM & Carpenter G (1984) Characterization of the metabolic turnover of epidermal growth factor receptor protein in A-431 cells. *J Cell Physiol* 120(3):296-302.
29. Burke PM & Wiley HS (1999) Human mammary epithelial cells rapidly exchange empty EGFR between surface and intracellular pools. *J Cell Physiol* 180(3):448-460.
30. Worthylake R, Opresko LK, & Wiley HS (1999) ErbB-2 amplification inhibits down-regulation and induces constitutive activation of both ErbB-2 and epidermal growth factor receptors. *J Biol Chem* 274(13):8865-8874.
31. Sorkin A & Goh LK (2009) Endocytosis and intracellular trafficking of ErbBs. *Exp Cell Res* 315(4):683-696.
32. Sigismund S, *et al.* (2005) Clathrin-independent endocytosis of ubiquitinated cargos. *Proc Natl Acad Sci U S A* 102(8):2760-2765.
33. Chinkers M, McKanna JA, & Cohen S (1979) Rapid induction of morphological changes in human carcinoma cells A-431 by epidermal growth factors. *J Cell Biol* 83(1):260-265.
34. Haigler HT, McKanna JA, & Cohen S (1979) Direct visualization of the binding and internalization of a ferritin conjugate of epidermal growth factor in human carcinoma cells A-431. *J Cell Biol* 81(2):382-395.
35. Yamazaki T, *et al.* (2002) Role of Grb2 in EGF-stimulated EGFR internalization. *J Cell Sci* 115(Pt 9):1791-1802.

36. Orth JD, Krueger EW, Weller SG, & McNiven MA (2006) A novel endocytic mechanism of epidermal growth factor receptor sequestration and internalization. *Cancer Res* 66(7):3603-3610.

37. Wiley HS (1988) Anomalous binding of epidermal growth factor to A431 cells is due to the effect of high receptor densities and a saturable endocytic system. *J Cell Biol* 107(2):801-810.

38. Lund KA, Opresko LK, Starbuck C, Walsh BJ, & Wiley HS (1990) Quantitative analysis of the endocytic system involved in hormone-induced receptor internalization. *J Biol Chem* 265(26):15713-15723.

39. Jiang X & Sorkin A (2003) Epidermal growth factor receptor internalization through clathrin-coated pits requires Cbl RING finger and proline-rich domains but not receptor polyubiquitylation. *Traffic* 4(8):529-543.

40. Waterman H & Yarden Y (2001) Molecular mechanisms underlying endocytosis and sorting of ErbB receptor tyrosine kinases. *FEBS Lett* 490(3):142-152.

41. Huang F, Kirkpatrick D, Jiang X, Gygi S, & Sorkin A (2006) Differential regulation of EGF receptor internalization and degradation by multiubiquitination within the kinase domain. *Mol Cell* 21(6):737-748.

42. Huang F, Goh LK, & Sorkin A (2007) EGF receptor ubiquitination is not necessary for its internalization. *Proc Natl Acad Sci U S A* 104(43):16904-16909.

43. Huang F, Khvorova A, Marshall W, & Sorkin A (2004) Analysis of clathrin-mediated endocytosis of epidermal growth factor receptor by RNA interference. *J Biol Chem* 279(16):16657-16661.

44. Chen WS, *et al.* (1989) Functional independence of the epidermal growth factor receptor from a domain required for ligand-induced internalization and calcium regulation. *Cell* 59(1):33-43.

45. Wiley HS, *et al.* (1991) The role of tyrosine kinase activity in endocytosis, compartmentation, and down-regulation of the epidermal growth factor receptor. *J Biol Chem* 266(17):11083-11094.

46. Sorkina T, Huang F, Beguinot L, & Sorkin A (2002) Effect of tyrosine kinase inhibitors on clathrin-coated pit recruitment and internalization of epidermal growth factor receptor. *J Biol Chem* 277(30):27433-27441.

47. Sorkin A, Waters C, Overholser KA, & Carpenter G (1991) Multiple autophosphorylation site mutations of the epidermal growth factor receptor. Analysis of kinase activity and endocytosis. *J Biol Chem* 266(13):8355-8362.

48. Lamaze C & Schmid SL (1995) Recruitment of epidermal growth factor receptors into coated pits requires their activated tyrosine kinase. *J Cell Biol* 129(1):47-54.

49. Bache KG, Raiborg C, Mehlum A, & Stenmark H (2003) STAM and Hrs are subunits of a multivalent ubiquitin-binding complex on early endosomes. *J Biol Chem* 278(14):12513-12521.

50. Wang Y, Pennock S, Chen X, & Wang Z (2002) Endosomal signaling of epidermal growth factor receptor stimulates signal transduction pathways leading to cell survival. *Mol Cell Biol* 22(20):7279-7290.

51. Pennock S & Wang Z (2003) Stimulation of cell proliferation by endosomal epidermal growth factor receptor as revealed through two distinct phases of signaling. *Mol Cell Biol* 23(16):5803-5815.

52. Schmidt MH, Furnari FB, Cavenee WK, & Bogler O (2003) Epidermal growth factor receptor signaling intensity determines intracellular protein interactions, ubiquitination, and internalization. *Proc Natl Acad Sci U S A* 100(11):6505-6510.

53. Haugh JM, Huang AC, Wiley HS, Wells A, & Lauffenburger DA (1999) Internalized epidermal growth factor receptors participate in the activation of p21(ras) in fibroblasts. *J Biol Chem* 274(48):34350-34360.

54. Haugh JM & Meyer T (2002) Active EGF receptors have limited access to PtdIns(4,5)P(2) in endosomes: implications for phospholipase C and PI 3-kinase signaling. *J Cell Sci* 115(Pt 2):303-310.

55. Lo HW, *et al.* (2005) Novel prognostic value of nuclear epidermal growth factor receptor in breast cancer. *Cancer Res* 65(1):338-348.

56. Haj FG, Verveer PJ, Squire A, Neel BG, & Bastiaens PI (2002) Imaging sites of receptor dephosphorylation by PTP1B on the surface of the endoplasmic reticulum. *Science* 295(5560):1708-1711.

57. Sebastian S, *et al.* (2006) The complexity of targeting EGFR signalling in cancer: from expression to turnover. *Biochim Biophys Acta* 1766(1):120-139.

58. Waterman H, Sabanai I, Geiger B, & Yarden Y (1998) Alternative intracellular routing of ErbB receptors may determine signaling potency. *J Biol Chem* 273(22):13819-13827.

59. Baulida J, Kraus MH, Alimandi M, Di Fiore PP, & Carpenter G (1996) All ErbB receptors other than the epidermal growth factor receptor are endocytosis impaired. *J Biol Chem* 271(9):5251-5257.

60. Baulida J & Carpenter G (1997) Heregulin degradation in the absence of rapid receptor-mediated internalization. *Exp Cell Res* 232(1):167-172.

61. Waterman H, Alroy I, Strano S, Seger R, & Yarden Y (1999) The C-terminus of the kinase-defective neuregulin receptor ErbB-3 confers mitogenic superiority and dictates endocytic routing. *EMBO J* 18(12):3348-3358.

62. Nicholson RI, Gee JM, & Harper ME (2001) EGFR and cancer prognosis. *Eur J Cancer* 37 Suppl 4:S9-15.

63. Earp HS, 3rd, Calvo BF, & Sartor CI (2003) The EGF receptor family--multiple roles in proliferation, differentiation, and neoplasia with an emphasis on HER4. *Trans Am Clin Climatol Assoc* 114:315-333; discussion 333-314.

64. Lynch TJ, *et al.* (2004) Activating mutations in the epidermal growth factor receptor underlying responsiveness of non-small-cell lung cancer to gefitinib. *N Engl J Med* 350(21):2129-2139.

65. Paez JG, *et al.* (2004) EGFR mutations in lung cancer: correlation with clinical response to gefitinib therapy. *Science* 304(5676):1497-1500.

66. Pao W, *et al.* (2004) EGF receptor gene mutations are common in lung cancers from "never smokers" and are associated with sensitivity of tumors to gefitinib and erlotinib. *Proc Natl Acad Sci U S A* 101(36):13306-13311.

67. Tracy S, *et al.* (2004) Gefitinib induces apoptosis in the EGFRL858R non-small-cell lung cancer cell line H3255. *Cancer Res* 64(20):7241-7244.

68. Sordella R, Bell DW, Haber DA, & Settleman J (2004) Gefitinib-sensitizing EGFR mutations in lung cancer activate anti-apoptotic pathways. *Science* 305(5687):1163-1167.

69. Ekstrand AJ, *et al.* (1991) Genes for epidermal growth factor receptor, transforming growth factor alpha, and epidermal growth factor and their expression in human gliomas in vivo. *Cancer Res* 51(8):2164-2172.

70. Liu L, *et al.* (2005) Clinical significance of EGFR amplification and the aberrant EGFRvIII transcript in conventionally treated astrocytic gliomas. *J Mol Med* 83(11):917-926.

71. Wong AJ, *et al.* (1992) Structural alterations of the epidermal growth factor receptor gene in human gliomas. *Proc Natl Acad Sci U S A* 89(7):2965-2969.

72. Ekstrand AJ, Sugawa N, James CD, & Collins VP (1992) Amplified and rearranged epidermal growth factor receptor genes in human glioblastomas reveal deletions of sequences encoding portions of the N- and/or C-terminal tails. *Proc Natl Acad Sci U S A* 89(10):4309-4313.

73. Hirai T, *et al.* (1998) Clinical results of transhiatal esophagectomy for carcinoma of the lower thoracic esophagus according to biological markers. *Dis Esophagus* 11(4):221-225.

74. Tateishi M, Ishida T, Mitsudomi T, Kaneko S, & Sugimachi K (1990) Immunohistochemical evidence of autocrine growth factors in adenocarcinoma of the human lung. *Cancer Res* 50(21):7077-7080.

75. Hansen MR, Roehm PC, Chatterjee P, & Green SH (2006) Constitutive neuregulin-1/ErbB signaling contributes to human vestibular schwannoma proliferation. *Glia* 53(6):593-600.

76. Arteaga CL & Baselga J (2003) Clinical trial design and end points for epidermal growth factor receptor-targeted therapies: implications for drug development and practice. *Clin Cancer Res* 9(5):1579-1589.

77. Lichtner RB, Menrad A, Sommer A, Klar U, & Schneider MR (2001) Signaling-inactive epidermal growth factor receptor/ligand complexes in intact carcinoma cells by quinazoline tyrosine kinase inhibitors. *Cancer Res* 61(15):5790-5795.

78. Azemar M, *et al.* (2000) Recombinant antibody toxins specific for ErbB2 and EGF receptor inhibit the in vitro growth of human head and neck cancer cells and cause rapid tumor regression in vivo. *Int J Cancer* 86(2):269-275.

79. Wu TT & Kabat EA (1970) An analysis of the sequences of the variable regions of Bence Jones proteins and myeloma light chains and their implications for antibody complementarity. *J Exp Med* 132(2):211-250.

80. Al-Lazikani B, Lesk AM, & Chothia C (1997) Standard conformations for the canonical structures of immunoglobulins. *J Mol Biol* 273(4):927-948.

81. Clynes RA, Towers TL, Presta LG, & Ravetch JV (2000) Inhibitory Fc receptors modulate in vivo cytoxicity against tumor targets. *Nat Med* 6(4):443-446.

82. Saphire EO, *et al.* (2002) Contrasting IgG structures reveal extreme asymmetry and flexibility. *J Mol Biol* 319(1):9-18.

83. Di Gennaro E, *et al.* (2003) Critical role of both p27KIP1 and p21CIP1/WAF1 in the antiproliferative effect of ZD1839 ('Iressa'), an epidermal growth factor receptor tyrosine kinase inhibitor, in head and neck squamous carcinoma cells. *J Cell Physiol* 195(1):139-150.

84. Grunwald V & Hidalgo M (2003) Developing inhibitors of the epidermal growth factor receptor for cancer treatment. *J Natl Cancer Inst* 95(12):851-867.

85. Li S, *et al.* (2005) Structural basis for inhibition of the epidermal growth factor receptor by cetuximab. *Cancer Cell* 7(4):301-311.

86. de Bono JS & Rowinsky EK (2002) Therapeutics targeting signal transduction for patients with colorectal carcinoma. *Br Med Bull* 64:227-254.

87. Ennis BW, Lippman ME, & Dickson RB (1991) The EGF receptor system as a target for antitumor therapy. *Cancer Invest* 9(5):553-562.

88. Ciardiello F, *et al.* (1999) Antitumor activity of sequential treatment with topotecan and anti-epidermal growth factor receptor monoclonal antibody C225. *Clin Cancer Res* 5(4):909-916.

89. Prewett MC, *et al.* (2002) Enhanced antitumor activity of anti-epidermal growth factor receptor monoclonal antibody IMC-C225 in combination with irinotecan (CPT-11) against human colorectal tumor xenografts. *Clin Cancer Res* 8(5):994-1003.

90. Mendelsohn J (2001) The epidermal growth factor receptor as a target for cancer therapy. *Endocr Relat Cancer* 8(1):3-9.

91. Cunningham D, *et al.* (2004) Cetuximab monotherapy and cetuximab plus irinotecan in irinotecan-refractory metastatic colorectal cancer. *N Engl J Med* 351(4):337-345.

92. Bonner JA, *et al.* (2004) Anti-EGFR-mediated radiosensitization as a result of augmented EGFR expression. *Int J Radiat Oncol Biol Phys* 59(2 Suppl):2-10.

93. Bonner JA, *et al.* (2006) Radiotherapy plus cetuximab for squamous-cell carcinoma of the head and neck. *N Engl J Med* 354(6):567-578.

94. Mateo C, *et al.* (1997) Humanization of a mouse monoclonal antibody that blocks the epidermal growth factor receptor: recovery of antagonistic activity. *Immunotechnology* 3(1):71-81.

95. Spicer J (2005) Technology evaluation: nimotuzumab, the Center of Molecular Immunology/YM BioSciences/Oncoscience. *Curr Opin Mol Ther* 7(2):182-191.

96. Johns TG, *et al.* (2002) Novel monoclonal antibody specific for the de2-7 epidermal growth factor receptor (EGFR) that also recognizes the EGFR expressed in cells containing amplification of the EGFR gene. *Int J Cancer* 98(3):398-408.

97. Chao G, Cochran JR, & Wittrup KD (2004) Fine epitope mapping of anti-epidermal growth factor receptor antibodies through random mutagenesis and yeast surface display. *J Mol Biol* 342(2):539-550.

98. Johns TG, *et al.* (2004) Identification of the epitope for the epidermal growth factor receptor-specific monoclonal antibody 806 reveals that it preferentially recognizes an untethered form of the receptor. *J Biol Chem* 279(29):30375-30384.

99. Garrett TP, *et al.* (2009) Antibodies specifically targeting a locally misfolded region of tumor associated EGFR. *Proc Natl Acad Sci U S A* 106(13):5082-5087.

100. Scott AM, *et al.* (2007) A phase I clinical trial with monoclonal antibody ch806 targeting transitional state and mutant epidermal growth factor receptors. *Proc Natl Acad Sci U S A* 104(10):4071-4076.

101. Martinelli E, De Palma R, Orditura M, De Vita F, & Ciardiello F (2009) Anti-epidermal growth factor receptor monoclonal antibodies in cancer therapy. *Clin Exp Immunol* 158(1):1-9.

102. Friedman LM, *et al.* (2005) Synergistic down-regulation of receptor tyrosine kinases by combinations of mAbs: implications for cancer immunotherapy. *Proc Natl Acad Sci U S A* 102(6):1915-1920.

103. Perera RM, *et al.* (2005) Treatment of human tumor xenografts with monoclonal antibody 806 in combination with a prototypical epidermal growth factor receptor-specific antibody generates enhanced antitumor activity. *Clin Cancer Res* 11(17):6390-6399.

104. Pedersen MW, *et al.* (2010) Sym004: a novel synergistic anti-epidermal growth factor receptor antibody mixture with superior anticancer efficacy. *Cancer Res* 70(2):588-597.

105. Kamat V, *et al.* (2008) Enhanced EGFR inhibition and distinct epitope recognition by EGFR antagonistic mAbs C225 and 425. *Cancer Biol Ther* 7(5):726-733.

106. Ben-Kasus T, Schechter B, Lavi S, Yarden Y, & Sela M (2009) Persistent elimination of ErbB-2/HER2-overexpressing tumors using combinations of monoclonal antibodies: relevance of receptor endocytosis. *Proc Natl Acad Sci U S A* 106(9):3294-3299.

107. Zhu JX, *et al.* (2005) Decorin evokes protracted internalization and degradation of the epidermal growth factor receptor via caveolar endocytosis. *J Biol Chem* 280(37):32468-32479.

108. French AR & Lauffenburger DA (1996) Intracellular receptor/ligand sorting based on endosomal retention components. *Biotechnol Bioeng* 51(3):281-297.

2. Characterization of Receptor Clustering and Downregulation Induced by Combination Antibody Treatment

Introduction

As discussed in Chapter 1, epidermal growth factor receptor (EGFR) is a member of the ErbB family of single-pass transmembrane receptor tyrosine kinases (RTKs). Under normal conditions, EGFR activation is tightly regulated by its native ligands, epidermal growth factor (EGF) and transforming growth factor α (TGFα), which bind to the receptor extracellular domain (1). Ligand binding induces conformational changes in EGFR that stabilize homo- or hetero-dimerization, leading to autophosphorylation of its intracellular domain. Phosphorylation of selected tyrosine residues activates signaling effectors in downstream pathways, including the MAPK and PI3K pathways, eliciting responses such as growth, migration, differentiation, and apoptosis (2). The primary mechanisms of signal attenuation are receptor deactivation via phosphatase activity and receptor degradation following endocytosis (3). Ligand activation accelerates receptor endocytosis and simultaneously decreases the recycling to degradation ratio to terminate EGFR signaling (4).

Dysregulation of EGFR leading to unregulated growth has been observed in a variety of cancers. Means of dysregulation include receptor overexpression, which occurs in one-third of all epithelial-based tumors (5), mutation, aberrant localization, autocrine ligand secretion, and obstruction of endocytosis (3). Due to its prevalence and altered expression in cancer patients, several therapeutic strategies have been employed to target EGFR, one of which involves the use of monoclonal antibodies (mAbs) that bind the receptor ectodomain. mAbs act through multiple mechanisms including immune cell recruitment, toxin delivery, and direct inhibition of receptor signaling via ligand competition, obstruction of dimerization, or modulation of trafficking (6). Both clinically approved mAbs targeting EGFR (cetuximab and panitumumab) bind domain 3 of the EGFR ectodomain, directly competing with ligand and thereby preventing dimerization and activation (7-9). Unfortunately, the monotherapy objective response rates of cetuximab and panitumumab are tepid: 11% (10) and 8% (9, 11) respectively in the treatment of metastatic colorectal cancer. Although these rates improve when mAbs are used in combination with chemotherapy, poor tumor penetration, autocrine signaling, acquired resistance, and receptor

mutation hinder drug performance (12). It is therefore of interest to develop complementary therapeutic strategies to enhance mAb efficacy.

It was recently established that particular combinations of non-competitive anti-EGFR mAbs synergistically reduce surface receptor levels both *in vitro* and *in vivo*. This downregulation of receptor leads to enhanced tumor cell killing and prolonged survival in mouse xenograft models of cancer (13-16). Consistency between downregulation levels and combination efficacy in mouse models was also reported for ErbB2 (17). Friedman *et al* proposed that synergism results from clustering of receptors on the cell surface following combination mAb treatment (13). Preliminary evidence for the formation of such clusters was presented by Zhu *et al* using the tyrosine kinase inhibitor decorin (18).

In order to gain deeper mechanistic insights motivated by these exciting results and to inform the development of more potent antibody-based therapeutics, we investigated binding and trafficking processes underlying combination mAb-induced downregulation. Our findings establish a connection between binding epitopes and downregulatory activity of mAb pairs and show that synergistic downregulation results from receptor recycling inhibition. We further demonstrate that unlike EGF-induced downregulation, mAb-induced downregulation is not agonistic and it coincides with reduced migration and proliferation of autocrine ligand-secreting cells.

Results

Combinations of anti-EGFR mAbs reproducibly downregulate surface receptor in both normal and transformed human cell lines

Using a panel of six anti-EGFR mouse mAbs, we compared the ability of pairwise combinations to downregulate receptor on seven normal or transformed cell lines, whose origins and receptor densities are detailed in Table 2.1. Note that the surface EGFR levels span more than an order of magnitude, ranging from 1.0×10^5 to 2.8×10^6 receptors per cell.

Cell Line	Origin	EGFR per Cell
HT-29	Colorectal adenocarcinoma	1.0×10^5
Hela	Cervical adenocarcinoma	1.7×10^5
U87	Glioblastoma	1.9×10^5
HMEC	Human mammary epithelial tissue	4.5×10^5
CHO-EG	Chinese hamster ovary (EGFR-GFP transfected)	1.6×10^6
U87-SH	Glioblastoma (mutant EGFRvIII transfected)	1.6×10^6
A431	Epidermoid carcinoma	2.8×10^6

Table 2.1. Cell line origins and surface receptor densities. The source and EGFR expression levels are provided for the seven normal and transformed cell lines assessed in our pairwise antibody downregulation screen. Note that U87-SH contains 1.4×10^6 transfected copies of the EGFRvIII mutant and 1.9×10^5 endogenous wild type EGFR per cell (19, 20). Also, CHO-EG cells express 1.6×10^6 transfected GFP-fused EGFR per cell (21).

The steady state (13 h) surface receptor levels following treatment with each pairwise mAb combination are displayed in Figure 2.1A. In general, mAb pairs downregulate more effectively than does single mAb treatment and the relative performance of each combination is fairly consistent across cell lines. Also, downregulation extent decreases as receptor density increases. This trend parallels that for ligand-induced downregulation (Figure 2.1B) and is suggestive of endocytic machinery saturability (22).

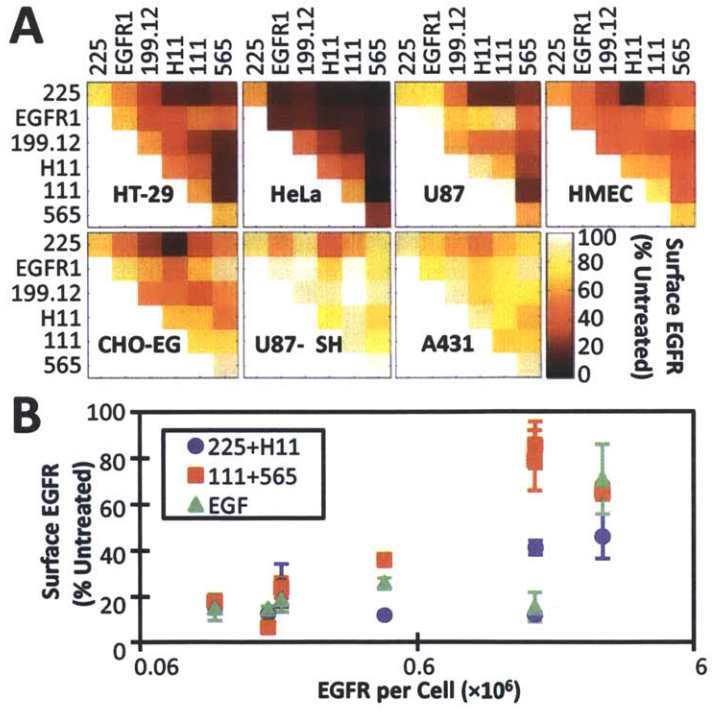

Figure 2.1. EGFR surface downregulation across seven cell lines following pairwise mAb treatment. (A) The indicated cell lines were treated with the denoted antibody pairs for 13 h at 37°C. Cells were then detached with trypsin, acid stripped to remove bound antibody, washed, and relabeled with murine 225 and an anti-mouse fluorescent secondary antibody to detect surface EGFR. Receptor levels relative to those of untreated cells were analyzed via flow cytometry. Values presented on the heat map represent the averages of three independent experiments. (B) Comparison of the 13 h surface EGFR levels following treatment with either 225+H11 (●), 111+565 (■), or EGF (▲) plotted against receptor density for each of the seven cell lines analyzed (±SD, n=3).

To confirm that differential downregulation extent between cell lines resulted from divergence in receptor abundance and not coincidental genetic variability, these assays were reproduced in a series U87 cell lines transfected with varying numbers of receptor (Table 2.2) (19, 20). As shown in Figure 2.2, the trend of decreasing downregulation efficiency with increasing receptor abundance was recapitulated in the U87 system. EGF was not included in this panel since it does not downregulate the EGFRvIII mutant receptor (19).

Cell Line	wtEGFR/cell	EGFRvIII/cell	Total EGFR/cell
U87	1.9×10^5	-	1.9×10^5
U87-M	1.9×10^5	5.0×10^5	6.9×10^5
U87-DK	1.9×10^5	8.1×10^5	1.0×10^6
U87-H	1.9×10^5	1.1×10^6	1.3×10^6
U87-SH	1.9×10^5	1.4×10^6	1.6×10^6
U87-WT	1.9×10^6	-	1.9×10^6

Table 2.2. U87 cell line surface EGFR (wild type and mutant) densities. Wild type (wt) and transfected mutant (vIII) surface EGFR expression levels as determined by flow cytometry. M = medium, DK = dead kinase (Inactive kinase domain due to K721M mutation in transfected EGFRvIII), H = high, SH = super high, WT = wild type overexpressing.

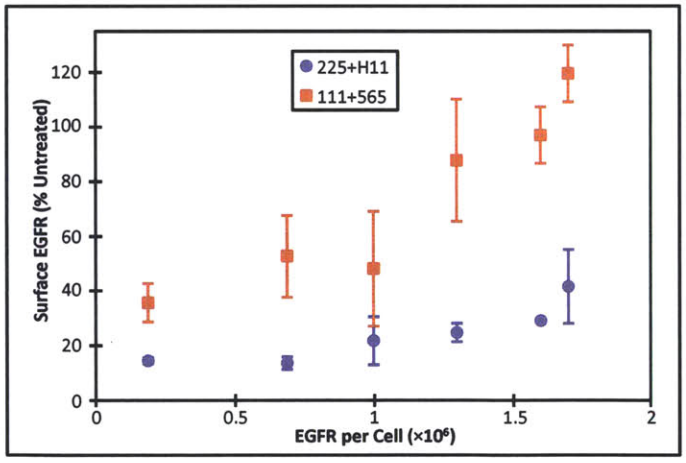

Figure 2.2. Receptor density versus downregulation extent in U87-derived cell lines. U87 cell lines transfected with varying numbers of mutant EGFRvIII receptors were subjected to combination mAb treatment (either 225+H11, blue circles, or 111+565, red squares) for 13 h at 37°C. Surface receptor levels were then measured by flow cytometry. Remaining surface EGFR signal (relative to that of untreated cells) is plotted as a function of total receptor number per cell (±SD; n=3).

Intriguingly, downregulation does not require kinase activity, as the transfected kinase defective mutant form of EGFRvIII in U87-DK cells is downregulated as effectively as transfected EGFRvIII with an intact kinase region (Figure 2.2). This distinguishes antibody-mediated downregulation from EGF-induced downregulation and hints at an alternative mechanism of action.

From our pairwise screen, we note that one specific mAb combination, that of 225 (the murine version of cetuximab) and H11, downregulates significantly better than other pairs, particularly in cell lines with high EGFR expression levels. Downregulation by the combination of the domain 3-directed 225 and H11 mAbs also exhibits less sensitivity to receptor density than do other combinations (Figures 2.1, 2.2).

To determine whether or not surface EGFR downregulation coincides with total receptor downregulation, we examined the abundance of a transfected EGFR-GFP fusion on CHO-EG cells following combination antibody treatment. As shown in Figure 2.3, the observed reduction in surface EGFR directly corresponds to a reduction in total EGFR, albeit on a delayed timescale due to the additional requirements for endosomal maturation, lysosomal fusion, and protein degradation. EGF-induced downregulation parallels this trend, although with much more rapid kinetics ($t_{1/2,\,EGF}$ = 0.35 h versus $t_{1/2,\,225+H11}$ = 1.5 h for surface EGFR and $t_{1/2,\,EGF}$ = 0.51 h versus $t_{1/2,\,225+H11}$ = 2.4 h for total EGFR).

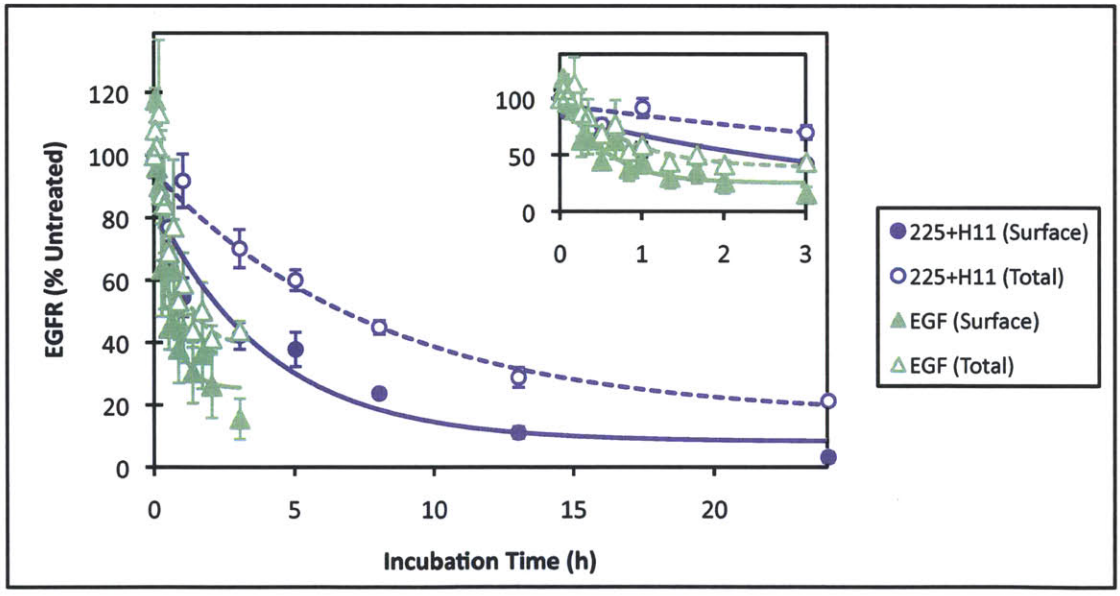

Figure 2.3. Surface vs. total EGFR downregulation kinetics. CHO cells stably transfected with an EGFR-GFP fusion (denoted CHO-EG) (23) were treated with the 225+H11 mAb combination (blue circles) or EGF (green triangles) for the indicated time periods at 37°C. Cells were then acid stripped and relabeled with 225 to detect surface EGFR; GFP signal was used as a readout for total EGFR expression. Cells were analyzed via flow cytometry and the relative surface (closed symbols) and total (open symbols) EGFR levels compared to those of untreated cells are plotted over the 24 h time course (±SD; n=3). The extrapolated curves show nonlinear least squares regression fits to single exponential functions. The inset enlarges the first 3 hours post-treatment to resolve EGF behavior at early time points.

Combinations of domain 3 binders downregulate receptor most efficiently

To examine the correlation between downregulation and epitope, we mapped the binding domains of the tested mAbs. By sorting a randomized EGFR ectodomain library displayed on the surface of yeast, we identified residues that were critical for the binding of each mAb (Table 2.3) with the exception of 225, for which a crystal structure was available (8) and which our lab had previously mapped by this method (24).

mAb	Mapped Residues	Domain(s)
199.12	S137, K165	1/2
EGFR1	R141, Q193	1/2
225	Q384, Q408, H409, K443, K465, I467, N473*	3
H11	S356, H359	3
111	R353, S356, H359	3
565	K322, N328, N331	3

Table 2.3. Binding epitopes of anti-EGFR mAbs. The epitopes for the antibodies characterized in our pairwise downregulation screen (Figure 2.1) were determined via yeast surface display-based technique (24). *Epitope obtained from published crystal structure (8).

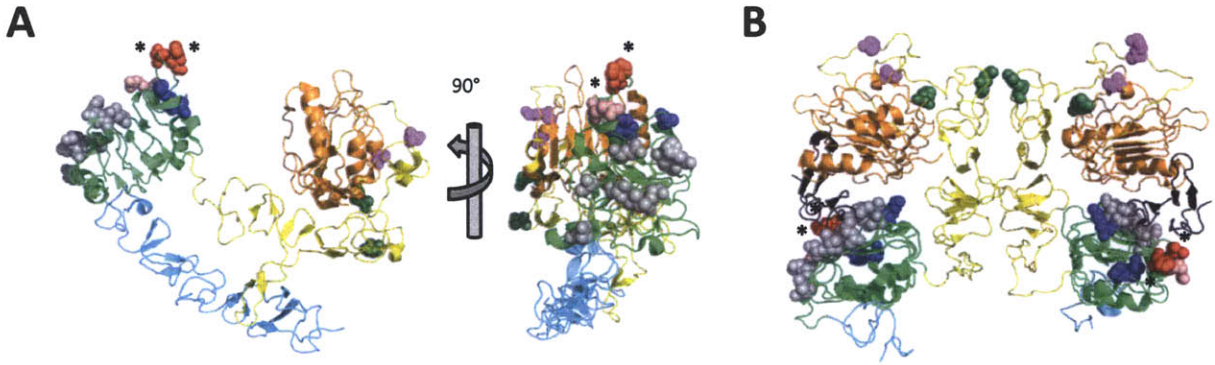

Figure 2.4. Mapped epitopes of anti-EGFR mAbs. Using a yeast library of EGFR ectodomain mutants, the binding domains of five mAbs were determined. Domains 1 (orange), 2 (yellow), 3 (green), and 4 (cyan) are displayed in the monomeric (A) and dimeric (B) forms of the receptor. EGF ligand is shown in black in the dimeric structure. Epitopes for EGFR1 (dark green), 199.12 (magenta), H11 (25), 111 (pink), and 565 (blue) are shown as spheres. Starred residues are part of both the H11 and 111 epitopes. The 225 epitope identified in the published crystal structure is shown in gray (8). The monomeric and dimeric structures are adapted from 1nql (1) and 1ivo (26), respectively.

Figure 2.4 depicts the locations of the mAb epitopes on EGFR in its monomeric (1) and dimeric (26) forms. Consistent with the structural data, 111 and H11 crossblock, as do 199.12 and EGFR1. Also, 225, H11, 111, and 565 compete with EGF ligand. The most active combination

of downregulating mAbs identified from Figure 2.1 (225+H11) consists of two constructs that bind to extracellular domain 3, the ligand-binding domain, but are non-competitive (Figure 2.5).

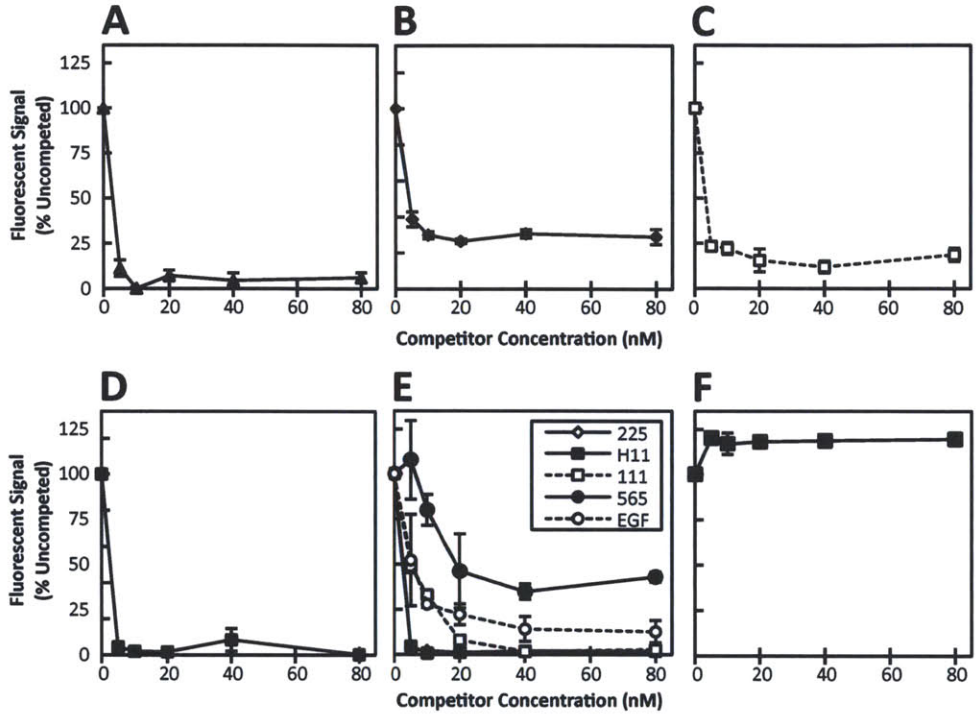

Figure 2.5. mAb and EGF competition assays. HMEC cells were pre-blocked for 1 h at 4°C with the indicated concentration of unlabeled competitor: 199.12 (▲) (A), EGFR1 (◆) (B), 111 (□) (C), H11 (■) (D) and (F), or 225 (◇), H11 (■), 111 (□), 565 (●), and EGF (○) (E). Fluorescently-labeled mAb or EGF (20 nM) was then added: EGFR1 (A), 199.12 (B), 111 (C), H11 (D), EGF (E), or 225 (F) and incubation proceeded at 4°C for 30 min. Fluorescence was analyzed via flow cytometry and signal intensity (relative to that in uncompeted cells) is plotted as a function of competitor concentration (±SD; n=3).

Amongst the antibodies tested, combinations consisting of two non-competitive domain 3 binders downregulate receptor more effectively than both competitive combinations and combinations with one domain 3 binder and one domain 1/2 binder (Figure 2.6), implicating stereospecific dependence of downregulation. The downregulation activity of each antibody combination the seven cell lines we examined is ranked in Table 2.4. Preference for antibodies targeting non-overlapping epitopes is consistent with receptor clustering, as competitive mAbs cannot form chains of crosslinked receptor.

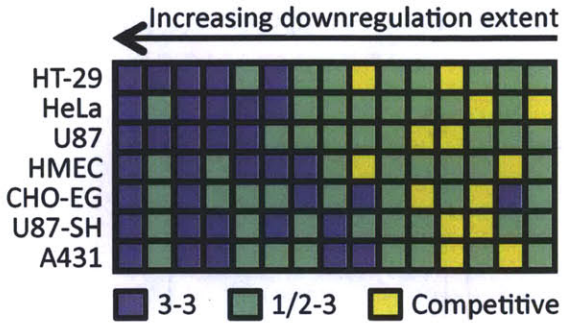

Figure 2.6. Epitope dependence of combination mAb-induced surface EGFR downregulation. The 15 pairwise mAb combinations in our six by six panel were ranked in order of EGFR downregulation extent for each of the seven indicated cell lines. Pairs consisting of two non-competitive domain 3 binders (blue), pairs consisting of one domain 1/2 and one domain 3 binder (green), and competitive pairs (yellow) are denoted.

HT-29	HeLa	U87-MG	HMEC	CHO-EG	U87-MGSH	A431
225+111	111+565	225+111	225+H11	225+H11	225+H11	225+H11
H11+565	199.12+565	225+H11	225+199.12	225+199.12	225+EGFR1	225+199.12
111+565	225+565	111+565	225+111	225+111	225+111	H11+565
225+H11	H11+565	225+565	199.12+565	199.12+111	H11+565	225+111
199.12+565	225+111	H11+565	H11+565	EGFR1+H11	EGFR1+H11	225+EGFR1
225+565	225+H11	199.12+565	111+565	225+EGFR1	111+565	199.12+H11
199.12+111	EGFR1+565	EGFR1+565	225+565	H11+565	EGFR1+565	EGFR1+H11
225+199.12	EGFR1+H11	199.12+111	199.12+111	199.12+H11	225+565	111+565
EGFR1+199.12	225+EGFR1	225+199.12	EGFR1+199.12	225+565	225+199.12	225+565
199.12+H11	EGFR1+111	199.12+H11	EGFR1+H11	199.12+565	199.12+H11	199.12+111
EGFR1+H11	199.12+111	H11+111	199.12+H11	EGFR1+199.12	199.12+565	199.12+565
H11+111	225+199.12	EGFR1+199.12	225+EGFR1	EGFR1+111	H11+111	H11+111
EGFR1+565	EGFR1+199.12	EGFR1+H11	EGFR1+111	H11+111	EGFR1+199.12	EGFR1+111
EGFR1+111	199.12+H11	225+EGFR1	H11+111	111+565	EGFR1+111	EGFR1+199.12
225+EGFR1	H11+111	EGFR1+111	EGFR1+565	EGFR1+565	199.12+111	EGFR1+565

	Domain 3-Domain 3
	Domain 1/2-Domain 3
	Competitive

Table 2.4. Comparison of mAb combination performance in seven EGFR-expressing cell lines. The fifteen pairwise mAb combinations are ranked in descending order of downregulation potency for each cell line examined in our pairwise downregulation screen. Pairs consisting of two non-competitive domain 3 binders (blue), pairs consisting of one domain 1/2 and one domain 3 binder (green), and competitive pairs (yellow) are indicated.

Receptor downregulation requires two bivalent antibodies

In an effort to determine whether or not hypothesized antibody-mediated clustering plays a role in the observed receptor downregulation, we digested the full IgG constructs from our most actively downregulating combination of antibodies (225+H11) into Fab fragments. Fab fragments consist of a single variable and constant domain of each chain and are consequently monovalent binders. As shown in Figure 2.7, Fabs by themselves or in combination do not substantively reduce surface EGFR levels. Also, single mAb treatment or combination of a Fab and a mAb do not elicit downregulation. However, the combination of two full IgGs markedly reduces surface EGFR levels on all seven cell lines examined, indicating the requirement for bivalency to effect receptor downregulation, suggestive of a clustering mechanism.

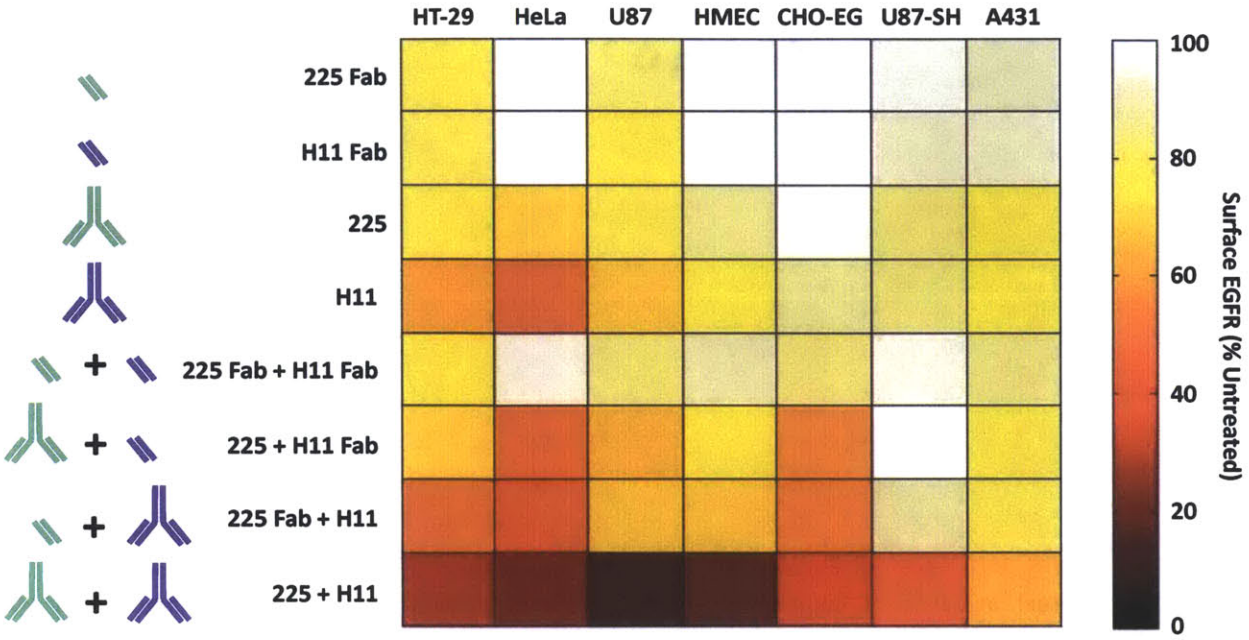

Figure 2.7. Two bivalent IgG molecules required to achieve receptor downregulation. The 225 and H11 antibodies were digested into their respective monovalent Fab fragments using the enzyme ficin. The indicated Fabs, full IgGs, and combinations thereof were incubated with the seven cell lines shown for 13 h at 37°C. Cells were then detached, stripped of antibody, and relabeled for surface EGFR via flow cytometry. Surface EGFR levels normalized by those of untreated cells are presented for each condition.

Antibody treatment results in punctate clustered distribution of EGFR

We visualized receptor distribution on A431 cells following single versus combination antibody treatment via deconvolution fluorescence microscopy. As evidenced in Figure 2.8, the receptor distribution (tracked by fluorescent 225) changes dramatically upon the addition of H11. Compared to the diffuse surface-staining pattern we observe following 225 monotherapy, treatment with 225 and H11 results in a punctate EGFR distribution both intracellularly and extracellularly, indicative of receptor clustering. Clustering is observed as early as 1 h post-antibody administration and endures throughout the 6 h timecourse.

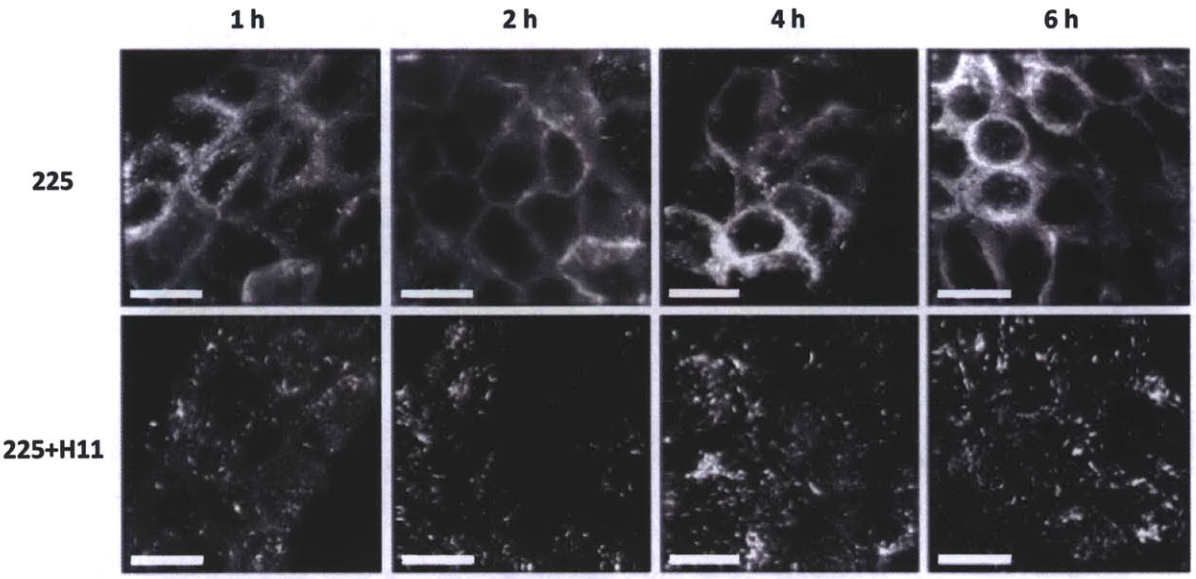

Figure 2.8. Visual evidence of combination antibody-induced clustering. A431 cells were treated with fluorescently-labeled 225 in the presence or absence of H11 for the indicated time periods at 37°C. Cells were washed to remove free antibody and imaged on a DeltaVision deconvolution microscope. Images reflect projections of deconvolved 0.15 μm thick z-sections through the cell monolayer. Scale bars = 30 μm.

mAb-induced downregulation is significantly slower than EGF-induced downregulation

The kinetics of antibody-induced EGFR downregulation treatment were compared to those of EGF-induced downregulation. Both combination mAb treatment and EGF treatment ultimately result in a maximum of 80% downregulation, although EGF reduces surface receptor expression much more rapidly (Figure 2.9).

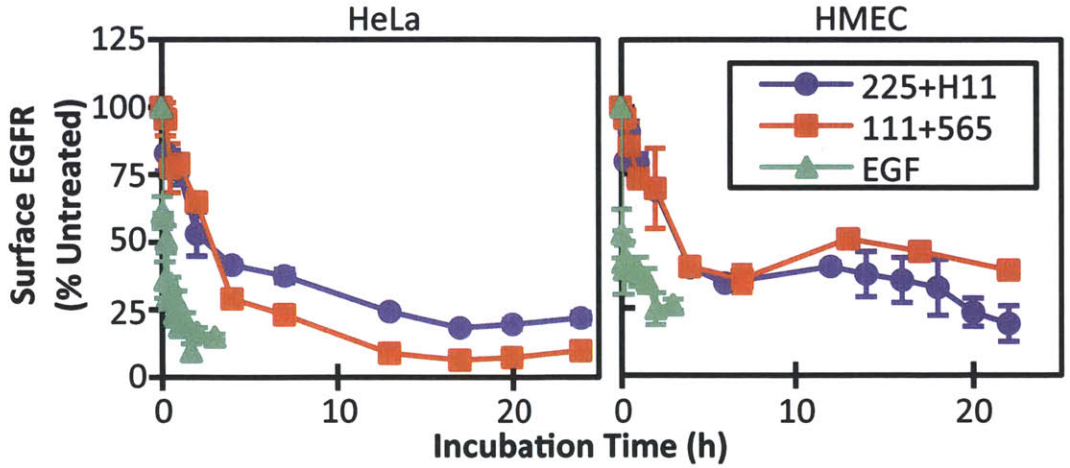

Figure 2.9. Surface EGFR downregulation kinetics. HeLa (left) and HMEC (right) cells were incubated at 37°C in the presence of 225+H11 (●), 111+565 (■), or EGF (▲). At the specified time points, surface receptor was quantified via flow cytometry. Surface EGFR levels relative to those of untreated cells are plotted as a function of time (±SD; n=3).

Downregulation halftimes for the potent 225+H11 pair, the moderately effective 111+565 pair, and EGF are provided in Table 2.5. Note that the mAb-induced downregulation timescales are independent of receptor density and consistent across cell lines, typically ranging from 0.5-2.5 h.

Cell Line	225+H11 $t_{1/2}$ (h)	111+565 $t_{1/2}$ (h)	EGF $t_{1/2}$ (h)
HT-29	4.88	2.15	0.02
HeLa	2.12	2.39	0.13
U87	1.84	0.81	0.14
HMEC	1.86	1.22	0.02
CHO-EG	1.50	0.55	0.35
A431	1.40	*	0.02

Table 2.5. Surface EGFR downregulation rates. Receptor downregulation halftimes were measured on the six cell lines shown. Kinetic downregulation data were fit to a single exponential using non-linear least squares regression. *111+565 did not reduce A431 surface EGFR levels.

Combination mAb treatment downregulates surface receptor by abrogating recycling

We next sought to elucidate the kinetic rate processes underlying EGFR downregulation. To this end, we considered a simple material balance for receptor trafficking (Figure 2.10). A full derivation for our trafficking model is provided in Appendix A.

Solving for the steady state surface (R_S) and internal (R_I) receptor levels, we find that:

$$R_S = \frac{P_{syn}}{k_e}\left(1+\frac{k_{rec}}{k_{deg}}\right) \text{ and } R_I = \frac{P_{syn}}{k_{deg}} \qquad \text{Equation 2.1}$$

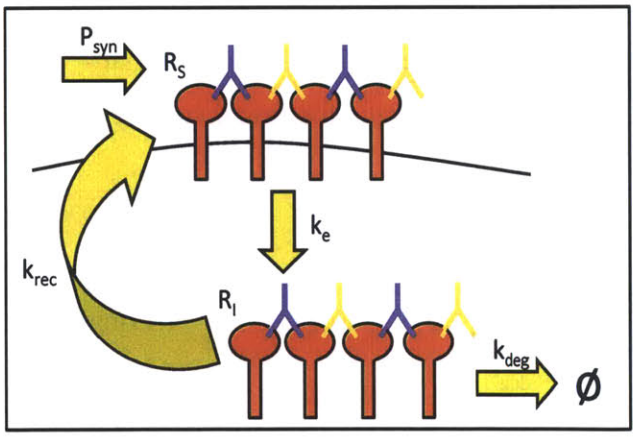

Figure 2.10. Modulation of EGFR trafficking via combination mAb treatment. A basic model of receptor clustering and trafficking following treatment with non-competitive EGFR-targeted mAbs is shown. Note that two bivalent antibodies are required to cluster surface EGFR via crosslinked chains. Relevant rate parameters and species are labeled. EGFR can be surface-bound (R_S) or internal (R_I). Receptor is synthesized with a rate P_{syn}, internalized with rate k_e, recycled back to the surface with rate k_{rec}, and degraded with rate k_{deg}.

Surface receptor levels can thus be lowered by (1) decreasing synthesis, (2) increasing the endocytosis rate constant, (3) decreasing the recycling to degradation ratio, or by a combination of these factors.

Cells treated with and without the protein synthesis inhibitor cycloheximide (27) exhibit similar downregulation kinetics (Figure 2.11), implying that altered receptor synthesis is not responsible for the observed drop in surface EGFR. Furthermore, the relatively slow downregulation rate (on the order of the constitutive endocytosis rate) indicates that first-pass endocytosis is certainly not accelerated in treated cells (Figure 2.9).

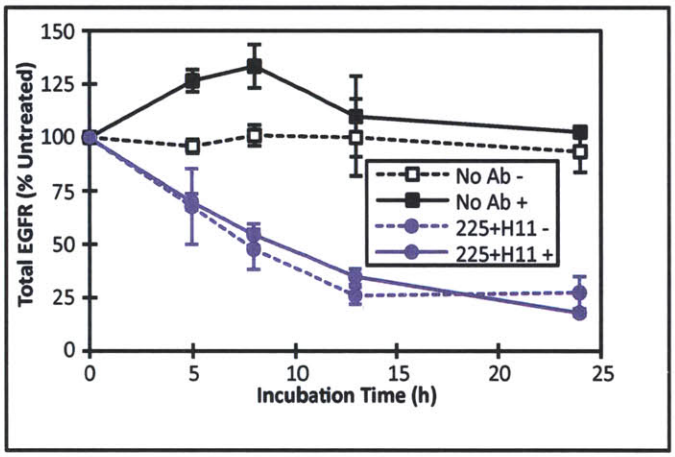

Figure 2.11. Impact of synthesis inhibition on EGFR levels. (A) CHO-EG cells were incubated at 37°C with (blue circles) or without (black squares) 225 and H11 in the absence (open symbols) or presence (closed symbols) of the receptor synthesis inhibitor cycloheximide (40 μM). At each time point, cells were detached and total EGFR content (based on GFP fluorescence) was measured via flow cytometry. GFP signal relative to that of untreated cells is plotted against incubation time (±SD; n=3). "+" = With and "-" = Without cycloheximide.

We then considered the possibility that mAb treatment inhibits recycling. Assuming that synthesis and degradation rates are unchanged, the model predicts the fractional surface receptor remaining after treatment to be:

$$\frac{R_{S,t}}{R_{S,u}} = \left(\frac{k_{e,u}}{k_{e,t}}\right)\left(\frac{1}{1+\frac{k_{rec,u}}{k_{deg}}}\right) \qquad \text{Equation 2.2}$$

where "u" and "t" represent the untreated and treated cases, respectively. Thus, downregulation extent depends on the ratio of the untreated and treated endocytic and recycling rates. Also, there is predicted to be a lower bound on EGFR levels, even if recycling is completely blocked by treatment (i.e. $R_{S,t} \neq 0$ even when $k_{rec,t} = 0$). This is consistent with the 80% downregulation limit observed in our panel and the fact that treatment with 225+H11 plus additional monoclonal and polyclonal antibodies does not drive downregulation further (Figure 2.12).

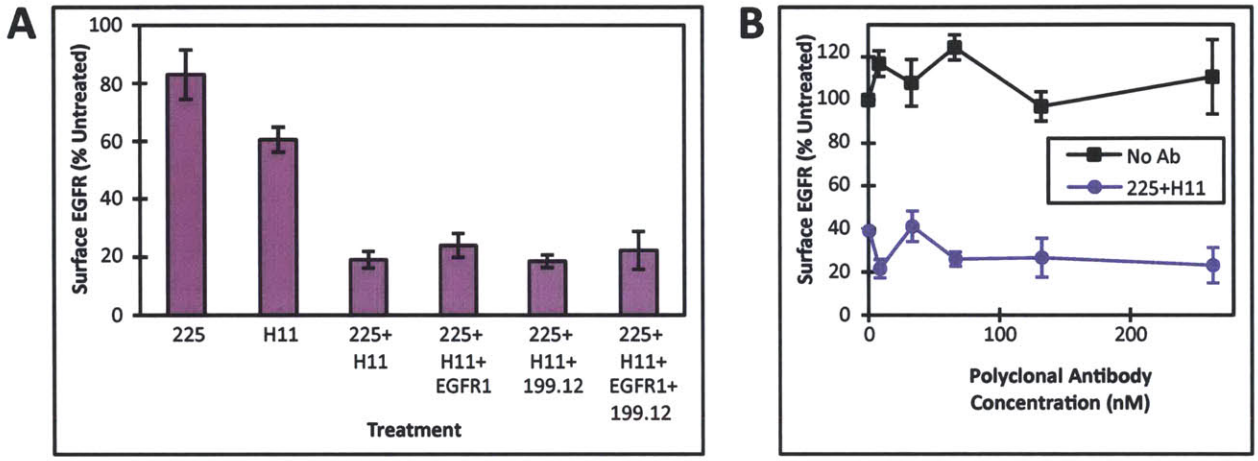

Figure 2.12. Effects of supplementing 225+H11 combination with additional monoclonal and polyclonal antibodies. (A) HT-29 cells were treated with the indicated mAbs (66 nM for single treatments and 33 nM each in combination) for 13 h at 37°C. Surface EGFR levels relative to those of untreated control cells were determined through flow cytometry and are displayed for each treatment condition (±SD; n=6). (B) CHO-EG cells were treated with (●) or without (■) the 225+H11 mAb combination (33 nM each) and incubated at 37°C for 30 min. An anti-mouse polyclonal antibody was then added at the indicated concentration and incubation proceeded for 13 h at 37°C. Surface EGFR was analyzed by flow cytometry and receptor levels relative to those of untreated cells are plotted as a function of polyclonal antibody concentration (±SD; n=3).

To determine whether receptor recycling is hindered by mAb treatment, a pulse-chase quenching assay was performed. Briefly, A431 cells were pulsed with Alexa 488-labeled 225 in the presence or absence of H11. Surface 225 was then quenched by the addition of Alexa 488 quenching antibody. Cells were subsequently chased in the continued presence of quenching antibody so that any incremental drop in signal during this period would result from internal 225 recycling to the cell surface, a surrogate for receptor recycling. As shown in Figure 2.13A, 488 signal drops during the chase period in the absence but not in the presence of H11, implying that combination treatment blocks the recycling that is observed following single mAb treatment. To independently confirm this result, cells were treated with or without the recycling inhibitor

monensin (28) in the absence or presence of the 225+H11 combination. As shown in Figure 2.13B, treatment with monensin alone evokes essentially the same response as 225+H11 treatment with or without monensin, consistent with the hypothesis that combination treatment substantively vitiates receptor recycling.

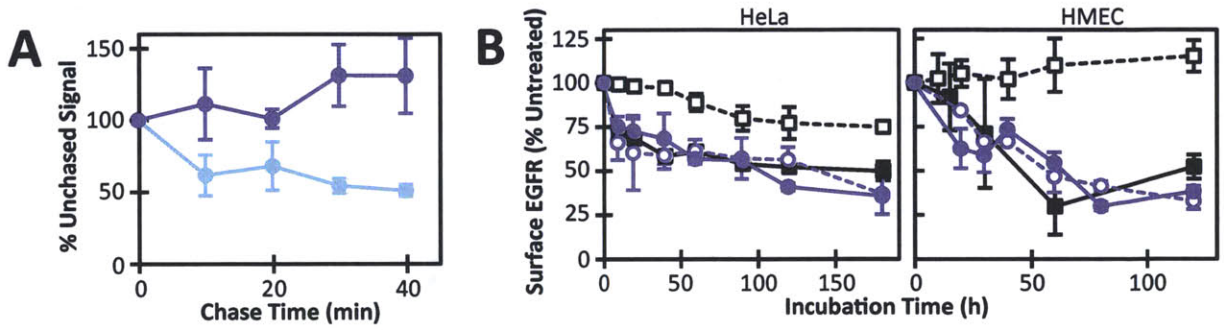

Figure 2.13. Inhibition of EGFR recycling via combination mAb treatment. (A) A431 cells were pulsed with Alexa 488-conjugated 225 for 2 h in the presence (●) or absence (●) of H11. Surface receptor signal was then quenched by adding 25 μg/mL Alexa 488 quenching antibody and cells were chased at 37°C in the continued presence of quenching antibody. Total fluorescence was determined at each time point and signal relative to the unchased control is plotted versus time (±SD; n=3). (B) HT-29 (left) and HMEC (right) cells were incubated at 37°C with (circles) or without (squares) 225 and H11 in the absence (open symbols) or presence (closed symbols) of the recycling inhibitor monensin (200 μM). Surface EGFR levels compared to those of untreated cells are plotted against incubation time (±SD; n=3).

Less potent mAb combinations induced greater receptor downregulation in the presence than in the absence of monensin, indicating that recycling was less dramatically impaired in these treatment conditions compared to the 225+H11 administration (Figure 2.14).

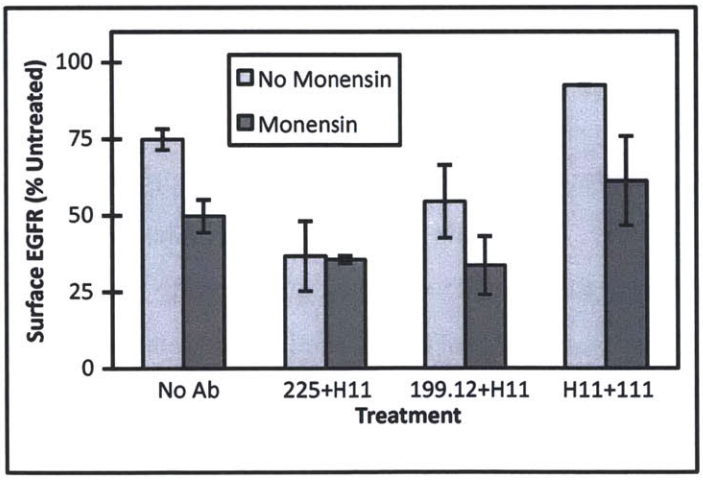

Figure 2.14. Impact of recycling inhibition on EGFR levels of combination antibody-treated cells. (B) HeLa cells were incubated for 13 h at 37°C with the indicated antibody combinations in the absence (light gray) or presence (dark gray) of the recycling inhibitor monensin (200 μM). Cells were detached and analyzed for surface EGFR. Surface receptor levels relative to those of untreated cells from the 0 h time point are plotted against incubation time (±SD; n=3).

mAb treatment does not agonize EGFR or activate downstream signaling effectors

Since EGFR signals actively from endosomes following ligand stimulation (29), we examined whether or not mAb-induced internalization was similarly agonistic. We first evaluated EGFR activation in A431 cells at eight known phosphosites in the intracellular domain using in-cell western assays (Figure 2.15A). None of these phosphosites were stimulated by single or combination mAb treatment, including three major autophosphorylation sites (Y1068, Y1148, and Y1173) (30), one minor autophosphorylation site (Y1086) (31), and targets of Src tyrosine kinase (Y845) (32), Ca-calmodulin-dependent kinase II (S1046) (33), protein kinase C (T654) (34), and MAPK (T669) (35). In contrast, most sites were activated two- to threefold by EGF.

Bead-based immunosorbent assays were also conducted on A431 cells to test for activation of downstream pathway effector MAPK (ERK). As Figure 2.15B demonstrates, incubation with 225 and H11 singly and in combination failed to phosphorylate MAPK above control levels.

To obtain a more global perspective of cell response, we used an iTRAQ-based mass spectrometry screen to assess phosphorylation following treatment with an isotype control mAb, 225, H11, 225+H11, or EGF. Lists of all phosphoproteins identified from the mass spectrometry screen and their relative signals compared to control treatment are provided in Appendix B. Figure 2.15C focuses on the relative phosphorylation of proteins associated with two critical pathways downstream of EGFR: the MAPK and PI3K cascades. In agreement with our phosphotyrosine mass spectrometry screen, neither single nor combination mAb treatment activates any of these signaling effectors based on a cut-off of 1.7-fold background.

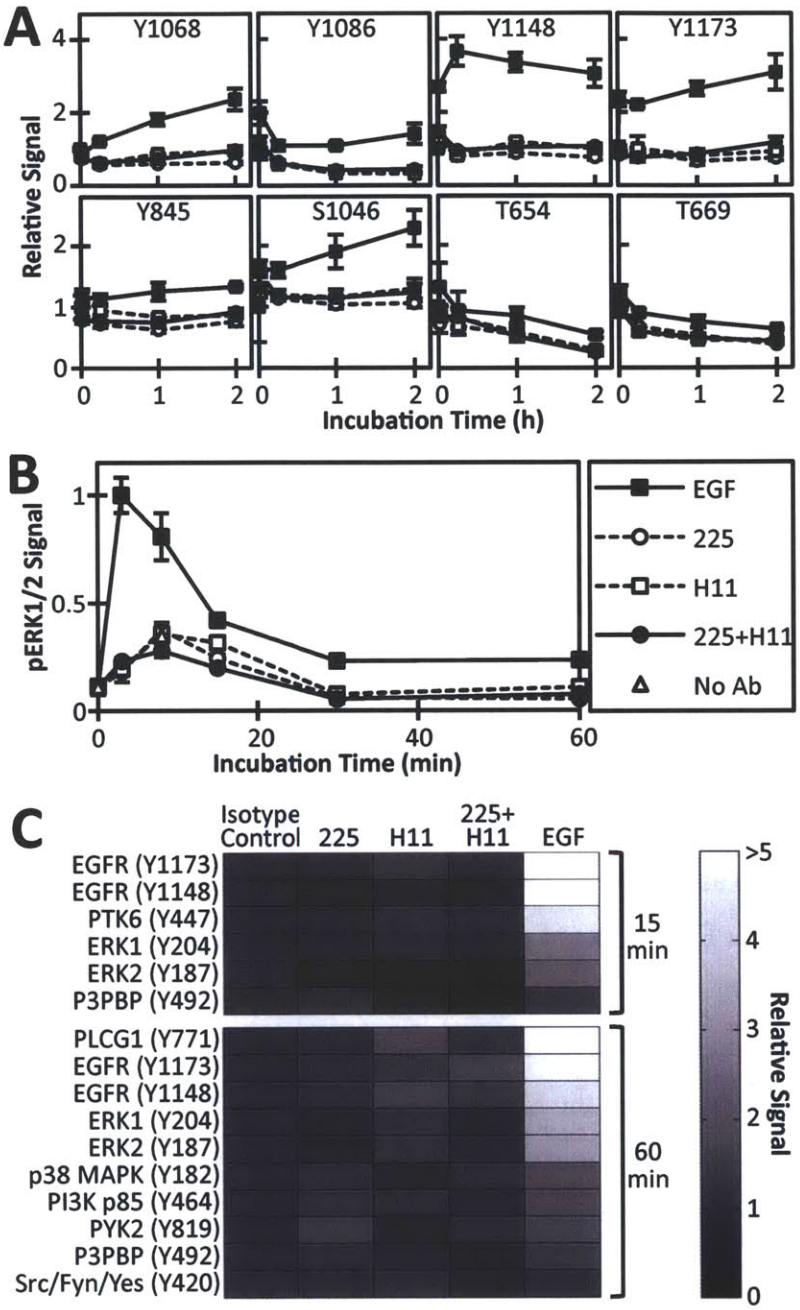

Figure 2.15. Downstream signaling implications of combination mAb treatment. (A) In-cell western assays were performed on A431 cells for eight known EGFR phosphosites. Activation profiles are shown for EGF (■), 225 (○), H11 (□), and 225+H11 (●). Phosphoprotein fluorescence was normalized by DNA fluorescence and signal relative to that of untreated cells is plotted versus time (±SD; n=3). (B) The timecourse of ERK 1/2 activation in A431 cells following mAb or EGF treatment was measured via bead-based immunoassay. Normalized phosphoprotein signal is plotted for cells treated with EGF (■), 225 (○), H11 (□), 225+H11 (●), and an antibody-free control (△) (±SD; n=3). (C) Serum-starved A431 cells were incubated with 225, H11, the 225+H11 combination, and EGF at 37°C for 15 min (36) or 60 min (*bottom*). EGF stimulation was held constant at 15 min for both screens. Cells were then lysed and relative protein phosphorylation was measured using an iTraq-based mass spectrometry screen. Phosphorylation levels were normalized by total protein content and signal strength relative to that in cells treated with an isotype control mAb is presented for MAPK and PI3K pathway components. Repetition of the 60 min screen yielded consistent results for proteins identified in both cohorts.

Downregulating mAb combination impedes cell migration and proliferation

We further explored the therapeutic promise of the most efficacious downregulating combination by examining its effects on migration and proliferation of cultured cells. An artificially constructed autocrine HMEC cell line (denoted ECT) that sheds surface-expressed chimeric EGF chimera at a fractional release rate of 0.3 h^{-1} (23) was tested. This autocrine model simulates a tumor environment in which growth factor expression is dysregulated (37-39). In ECT cells, the 225+H11 combination significantly ($P<0.01$) reduces the extent of cell migration compared to both untreated cells and cells treated with either mAb alone. In contrast, migration is not significantly further inhibited by combination treatment compared to 225 monotherapy in normal HMEC cells (Figure 2.16A). The same trend of selective inhibition of autocrine-expressing cells was observed for cell proliferation in the ECT and HMEC lines (Figure 2.16B), demonstrating that combination treatment is more effective than monotherapy in a system that aberrantly overexpresses EGF ligand.

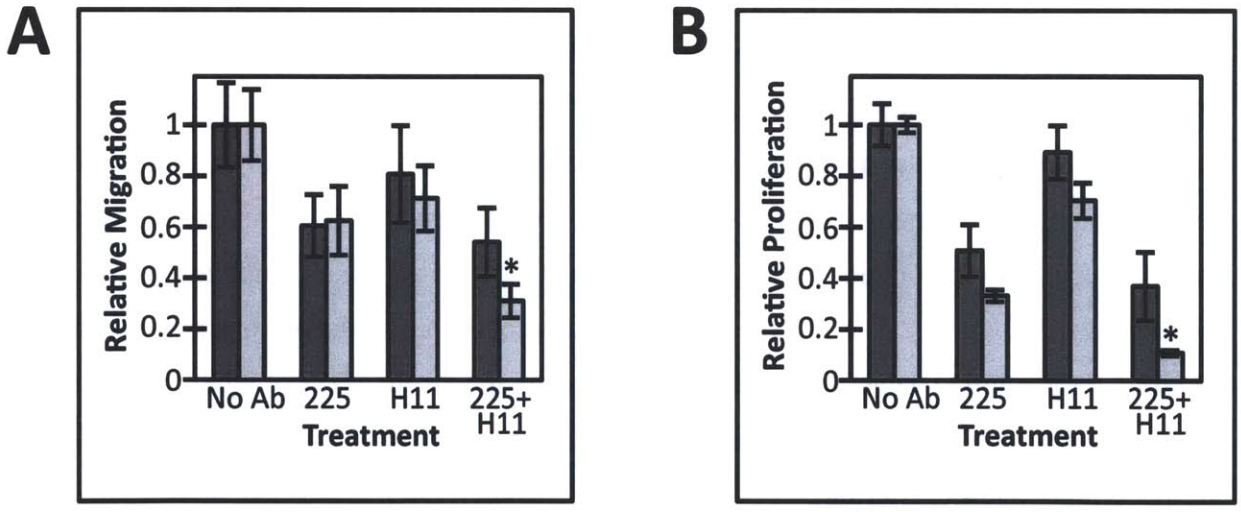

Figure 2.16. Cell migration and proliferation following mAb treatment. (A) Migration of HMEC (dark gray) and HMEC-derived autocrine EGF-secreting ECT (light gray) cells was assessed using a scratch wound healing assay. Confluent monolayers were wounded and subsequently incubated with the indicated mAbs for 24 h at 37°C. Relative migration is shown as fractional wound replenishment compared to that of an untreated control (±SD; n=6). (B) Proliferation of HMEC (dark gray) and ECT (light gray) cells was measured using the MTT assay. Cells were treated with the specified mAbs for 72 h at 37°C. Relative proliferation is presented as viable cell abundance compared to that of untreated cells (±SD; n=6). Asterisks denote $P<0.01$ for the 225+H11 combination relative to treatment with either mAb alone.

Discussion

The use of non-competitive antibody combinations to engage multiple therapeutic mechanisms is an increasingly popular and attractive strategy for enhancing drug efficacy (6). Understanding the biophysical and biochemical bases for antibody synergy will be helpful for designing the next generation of combination and multispecific treatments. The work discussed herein offers insights into the structural dependence and molecular mechanism of synergy.

Despite limited prior physical evidence for formation of receptor clusters, there had been extensive speculation that combination mAb treatment induces clustering, leading to downregulation (13, 15, 18). We show that two bivalent antibodies are required for downregulation (Figure 2.7) and present images of punctate receptor distribution following combination mAb treatment (Figure 2.8). This corroborates recent observations of punctate receptor distributions following treatment with a cocktail of non-competitive EGFR-targeted antibodies developed by Symphogen (15) and supports a clustering-dependent downregulation model.

From our pairwise combination screen, we observed that all mAb pairs that were examined elicit some level of downregulation, although the most effective combinations include two mAbs against EGFR extracellular domain 3, the ligand-binding domain (Figure 2.6). In particular, the combination of one antibody that binds proximal to the EGF epitope (225) and a second antibody that binds upstream in domain 3 (H11) appears to out-perform all other combinations in the cell lines examined (Figures 2.1, 2.4, 2.6). This finding is congruous with previous observations of domain 3-targeted mAb synergism (13, 16). In general, the extent of downregulation induced by a mAb pair may depend on the structure of the bound receptor and the degree to which its orientation facilitates clustering.

Observed saturability of downregulation manifested in downregulation dependence on receptor density is consistent with previous findings in cell lines expressing elevated levels of EGFR (22). The inability to improve upon receptor downregulation by supplementing the 225+H11 combination with additional monoclonal and polyclonal antibodies (Figure 2.12) is consistent

with a mechanism reliant on recycling inhibition, as surface levels are determined by the steady state balance between synthesis and constitutive endocytosis.

Combining our kinetic model with experimental findings (Figs. 2.9 - 2.14), we deduced that synergistic EGFR downregulation is a consequence of a decrease in the ratio of the recycling to degradation rates. Treatment with the most effectively downregulating combination completely blocks recycling in the three *in vitro* systems examined (Figure 2.13), consistent with the formation of internalized clusters incapable of returning to the cell surface through recycling endosomes. Extending this result, less potent combinations may fail to efficiently cluster receptors, thereby only partially obstructing recycling (Figure 2.14).

Our finding that the downregulation mechanism operates intracellularly to reduce endosomal recycling resonates with previous experimental and theoretical analyses of endosomal sorting outcomes (40, 41) and agrees with our further observations that downregulation is antibody-dependent and saturable (Figures 2.1, 2.2). There is no evidence of endocytic rate acceleration, as occurs in clathrin-mediated endocytosis stimulated by EGF (4, 42). We speculate that internalization following combination mAb treatment does not occur through clathrin-coated pits, but rather through basal membrane turnover or via lipid rafts such as caveolae. Indeed, Zhu and colleagues demonstrated that receptor clustering effected by decorin led to caveolin-mediated internalization of EGFR and, ultimately, its degradation.

Encouragingly, contrary to ligand-induced internalization, mAb-induced internalization does not activate EGFR or its downstream effectors (Figure 2.15). Lysosomal targeting of the receptor is expected to require ubiquitinylation (43), but if so we find it to be independent of kinase activity (Figure 2.2). This is consistent with previous work showing that EGFR and its effector pathways are differentially activated by distinct liands and mAbs (16, 44). Our results support a therapeutic strategy that utilizes endogenous trafficking machinery to reduce surface EGFR expression without activating downstream signaling pathways.

While combination therapy did not affect migration and proliferation relative to monotherapy in normal cells, it inhibited both processes in a cell line that exhibits autocrine ligand secretion, a

common means of EGFR dysregulation in cancer (Figure 2.16). This suggests selective sensititvity of transformed cells to combination antibody therapy.

In vivo, others have shown correlation between receptor downregulation and drug efficacy in mouse xenograft models (13, 14, 17), offering promise for the therapeutic potential of synergistically downregulating mAb pairs identified in our screen. Also, the observation of ErbB2 downregulation by mAb combinations (17) suggests that clustering receptor may be an effective approach for targeting other ErbB family receptors and receptor tyrosine kinases in general.

Overall, our work demonstrates that combinations of anti-EGFR mAbs reproducibly reduce surface receptor levels in a structurally-dependent fashion by inhibiting receptor recycling. These mAb combinations show therapeutic promise in that they do not agonize signaling and they hamper the migration and proliferation of cells that secrete autocrine EGF.

Based on the successful application of our combination downregulating strategy to an *in vitro* model of the tumor environment, we engineered novel antibody fusions to encapsulate the multi-epitopic strategy in single therapeutic molecules. The two formats we pursued for these constructs were: (1) Bispecific antibodies containing a full EGFR-specific IgG fused to the scFv of a second non-competitive anti-EGFR antibody and (2) Multispecific antibody-fibronectin domain fusions consisting of a full EGFR-targeted IgG fused to one or more EGFR-binding variants of the tenth type 3 domain of human fibronectin. The design and preliminary characterization of these constructs are detailed in Chapters 3 and 4, respectively and their therapeutic efficacies are evaluated *in vivo* in Chapter 5.

Materials and Methods

Cell lines and antibodies

The transfected CHO-EG (21), U87-MG-derived EGFRvIII-expressing lines (20), and ECT (23) cell lines were established as described previously and all other lines were obtained from ATCC (Manassas, VA). Cells were maintained in their respective growth media (from ATCC unless

otherwise indicated): DMEM for A431, U87-MG, U87-MGSH, and CHO-EG cells, McCoy's Modified 5A media for HT-29 cells, EMEM for HeLa cells, and HuMEC Ready Medium (Invitrogen, Carlsbad, CA) for HMEC and ECT cells. U87-MG, U87-MGSH, and CHO-EG media were supplemented with 1 mM sodium pyruvate (Invitrogen) and 0.1 mM non-essential amino acids (Invitrogen) and transfected lines U87-MGSH and CHO-EG were selected with 0.3 mM Geneticin (Invitrogen). ATCC media was supplemented with 10% fetal bovine serum (FBS). 225 was secreted from the hybridoma cell line (ATCC). EGFR1 (AbCam, Cambridge, MA) and H11 and 199.12 (LabVision, Fremont, CA) were purchased. 111 and 565 were prepared as described previously (13).

Unless otherwise noted, all washes were conducted in PBSA (PBS containing 0.1% BSA) and all mAbs were used at a concentration of 40 nM for single treatment and 20 nM each for combination treatment. EGF (Sigma, St. Louis, MO) was dosed at 20 nM. Trypsin-EDTA (Invitrogen) contains 0.05% trypsin and 0.5 mM EDTA.

Receptor quantification

Cells were serum starved for 12-16 h, washed, digested in trypsin-EDTA (20 min at 37°C), neutralized with complete medium, and labeled with 20 nM 225 for 1 h on ice. They were then washed, labeled with 66 nM phycoerythrin (PE)-conjugated goat anti-mouse antibody (Invitrogen) for 20 min on ice, washed again, and subjected to quantitative flow cytometry on an EPICS XL cytometer (Beckman Coulter, Fullerton, CA). Receptor density was calculated based on extrapolation from a curve of identically labeled anti-mouse IgG-coated beads (Bangs Laboratories, Fishers, IN).

Receptor downregulation assays

Cells were seeded at 5×10^4 per well in 96-well plates, serum starved for 12-16 h, treated with the indicated mAbs in serum-free medium, and incubated at 37°C. At each time point, cells were washed and treated with trypsin-EDTA for 20 min at 37°C. Trypsin was neutralized with medium (10% FBS) and cells were transferred to v-bottom plates on ice. They were then washed, acid stripped (0.2 M acetic acid, 0.5 M NaCl, pH 2.5), and washed again prior to incubation with 20 nM 225 for 1 h on ice to label surface EGFR. Cells were then washed and

labeled with 66 nM PE-conjugated goat anti-mouse antibody (Invitrogen) for 20 min on ice. After a final wash, plates were analyzed on a FACS Calibur cytometer (BD Biosciences, San Jose, CA). Cell pelleting was conducted at 1000×*g*.

Antibody and EGF competition assays

mAbs were labeled using an Alexa 488 microscale labeling kit (Invitrogen). Alexa 488-labeled EGF was purchased from Invitrogen. HMEC cells were seeded in 10 cm culture dishes and grown to confluence. They were then serum starved for 12-16 h, washed in PBS, and incubated with trypsin-EDTA for 20 min at 37°C. The trypsin was then neutralized by the addition of rich medium and cells were transferred to 96-well v-bottom plates (1×10^5 per well) and incubated on ice for 1 h with the specified unlabeled competitor mAb or EGF at the prescribed concentration. The indicated Alexa 488-labeled mAb or EGF was then added to a final concentration of 20 nM and cells were incubated for an additional 30 min on ice. After the cells were washed (PBS, 0.1% BSA), 488 signal was analyzed via flow cytometry, as described for receptor downregulation assays.

Fine epitope mapping of anti-EGFR mAbs

A mutagenized library (average of one mutation per clone) of yeast expressing the EGFR ectodomain followed by a c-myc tag was generated, induced, and sorted as previously described (24). The library was subjected to two rounds of selection: One against the mapped mAb and for c-myc binding and one for simultaneous 225 and c-myc binding to select for properly folded, full-length clones. Selected clones were sequenced to identify residues that interact with the mAb.

Digestion of IgG to form Fab fragments

The 225 and H11 murine IgG1 mAbs were digested into their respective Fab fragments using the immobilized ficin mouse IgG1 Fab preparation kit following the manufacturer's protocol (Thermo Fisher Scientific, Waltham, MA, Product # 44680). Fab was isolated from CH2-CH3 domains using protein A affinity chromatography. Fabs were reconstituted in PBS using Zeba desalting columns and recovery was quantified via 280 nm absorbance (Thermo Fisher Scientific). Purity was confirmed via SDS-PAGE analysis.

Live cell deconvolution microscopy

mAb 225 was labeled with Alexa 488 using a fluorescent labeling kit (Invitrogen). A431 cells were plated at 50,000 per well in 8-well microscopy chambers and allowed to settle overnight. Cells were serum-starved for 8-12 h and incubated with 20 nM fluorescently-labeled 225 in the absence or presence of 20 nM mAb H11 for the indicated time lengths at 37°, 5% CO_2. Cells were immediately washed and reconstituted in phenol red-free medium (Invitrogen) for imaging on a Delta Vision inverted deconvolution microscope at 60X magnification (oil immersion lens). Deconvolution and projection of 0.15 μm z-slices and image analysis were performed using the Softworx software package. All compared images were obtained using identical settings with normalized brightness and contrast levels set.

Cycloheximide synthesis inhibition assays

CHO-EG cells were seeded at 5×10^4 per well in 96-well plates and serum starved for 12-16 h. They were then reconstituted in serum-free medium in the presence or absence of 40 μM cycloheximide (Sigma) to block *de novo* receptor synthesis. After 20 min incubation at 37°C, the indicated mAbs were added to each well and incubation at 37°C proceeded for the specified length of time. Cells were then washed with PBS and the medium was replaced with trypsin-EDTA. After 20 min incubation at 37°C, the trypsin was neutralized by the addition of medium containing 10% FBS. Cells were then transferred to 96-well v-bottom plates, washed (PBS, 0.1% BSA), and analyzed for GFP content via flow cytometry, as detailed for receptor downregulation assays.

Polyclonal antibody treatment downregulation assays

CHO-EG cells were seeded at 5×10^4 per well in 96-well plates and serum starved for 12-16 h. They were then reconstituted in serum-free medium with or without 33 nM each of mAbs 225 and H11. After 30 min incubation at 37°C, goat anti-mouse polyclonal antibody (Invitrogen) was added at the indicated concentration and incubation at 37°C continued for 13 h. Cells were then detached, acid stripped, relabeled for surface EGFR, and analyzed as in receptor downregulation assays.

Alexa 488 quenching pulse-chase assays

225 was labeled using an Alexa 488 microscale labeling kit (Invitrogen). A431 cells were seeded at 5×10^4 per well in 96-well plates and serum starved for 12-16 h. They were then pulsed with Alexa 488-labeled 225 with or without H11 in serum-free medium and incubated at 37°C for 2 h. Cells were subsequently treated with 25 μg/mL anti-Alexa-488 quenching antibody (Invitrogen) for 30 min on ice and chased at 37°C for the indicated length of time in the presence of quenching antibody. Cells were returned to ice, washed, incubated with trypsin-EDTA for 30 min, and neutralized (DMEM, 10% FBS). They were then transferred to v-bottom plates, washed, and analyzed on a FACS Calibur cytometer (BD Biosciences). Percent unchased signal was calculated relative to cells that were not returned to 37°C after quenching (45, 46).

Monensin recycling assays

Cells were seeded at 5×10^4 per well in 96-well plates and serum starved for 12-16 h. They were then treated with or without 200 μM monensin (Sigma) in serum-free medium and incubated at 37°C for 20 min. The indicated mAbs were then added and incubation proceeded at 37°C. At each time point, surface EGFR was analyzed as in receptor downregulation assays.

In-cell western assays

A431 cells were seeded at 4×10^4 per well in 96-well plates and allowed to adhere for 24 h. Following 12-16 h of serum starvation, cells were treated with the designated mAbs in serum-free medium at 37°C for the specified time length. All subsequent incubations were performed at room temperature. Cells were fixed for 20 min (PBS containing 4% formaldehyde), permeabilized via four 5 min incubations (PBS containing 0.1% triton), blocked for 1 h in Odyssey blocking buffer (Licor Biosciences, Lincoln, NE), and labeled for 1 h with 15 nM anti-phosphosite antibodies (Genscript, Piscataway, NJ) in blocking buffer. Cells were then washed three times with PBST (PBS containing 0.1% Tween-20) and labeled with 66 nM 800-conjugated goat anti-rabbit antibody (Rockland Immunochemicals, Gilbertsville, PA) and 400 nM TO-PRO-3 DNA stain (Invitrogen) in blocking buffer for 30 min. After three final PBST washes, wells were aspirated dry for analysis on a Licor Odyssey Scanner (Licor Biosciences). Signal was normalized to cell abundance by dividing 800 (phosphoprotein) by 700 (TO-PRO-3) channel fluorescence.

Luminex (bead-based immunosorbent) phosphoprotein quantification assays

A431 cells seeded in 96-well plates at 3×10^4 per well were allowed to settle for 24 h prior to 12-16 h serum starvation. Cells were then incubated with the specified mAbs in serum-free medium at 37°C. At the indicated times, cells were lysed using the Bio-Plex cell lysis kit (Bio-Rad, Hercules, CA). Phosphorylated ERK1/2 abundance was quantified using the Luminex bead-based immunoassay, performed with the Bio-Plex Phospho-ERK1/2 (T202/Y204, T185/Y187) bead kit and the Bio-Plex Phosphoprotein Detection Reagent kit on the Bio-Plex 200 platform (Bio-Rad).

Global phospho-mass spectrometry screens.

1×10^6 A431 cells per well were seeded in 6-well plates, grown to confluence, and incubated with the appropriate mAbs in serum-free medium at 37°C for 15 or 60 min. Cells were washed once with chilled PBS and lysed at 4°C (8 M urea, 1 mM Na_3VO_4). Protein concentration was measured via bicinchoninic acid assay (Pierce, Rockford, IL). Lysate reduction, alkylation, trypsin digestion, and peptide fractionation were performed as previously described (47). Samples were labeled separately with 8 isotopic iTRAQ reagents (Applied Biosystems, Foster City, CA) for 2 h at room temperature, combined, and concentrated. Immunoprecipitation with pooled anti-phosphotyrosine antibodies (4G10 (Millipore, Billerica, MA), pTyr100 (Cell Signaling, Beverly, MA), and PT-66 (Sigma)) proceeded for 16 h at 4°C using protein G agarose beads (Calbiochem, San Diego, CA) in IP buffer (100 mM Tris, 100 mM NaCl, 1% Nonidet P-40, pH 7.4). Phosphopeptide enrichment by IMAC and analysis and quantification of eluted peptides were conducted via ESI LC/MS/MS on an LTQ-Orbitrap (Thermo Fisher Scientific). Phosphopeptides were identified using Mascot analysis software (48) and spectra were manually validated (49). Signal intensities were normalized by total protein levels and compared to isotype control treatment.

Migration assays

HMEC and ECT cells were seeded at 5×10^4 per well in 96-well plates and grown to confluence. Monolayers were wounded with a pipet tip, washed with PBS, and placed in complete medium with the indicated mAbs. Scratch area was measured immediately and after 24 h incubation at

37°C using Image J software analysis of images from a Nikon confocal microscope (Nikon Instruments, Melville, NY). Percent migration was calculated as the fractional reduction in scratch area in the treated wells divided by that of the untreated wells.

Cell proliferation assays

HMEC and ECT cells were seeded at 5×10^3 per well in 96-well plates and allowed to adhere for 24 h. They were then treated with the indicated mAbs in complete medium and incubated at 37°C for 72 h. Cell viability (relative to an untreated control) was assessed using the [3-(4,5-dimethylthiazol-2-yl)-2,5-diphenyltetrazolium bromide] (MTT) assay (Invitrogen) (50).

Statistical analysis

Heteroscedastic two-tailed student's t tests were performed on migration and proliferation assay results to compare combination and single mAb treatment.

References

1. Ferguson KM, *et al.* (2003) EGF activates its receptor by removing interactions that autoinhibit ectodomain dimerization. *Mol Cell* 11(2):507-517.
2. Yarden Y & Sliwkowski MX (2001) Untangling the ErbB signalling network. *Nat Rev Mol Cell Biol* 2(2):127-137.
3. Abella JV & Park M (2009) Breakdown of endocytosis in the oncogenic activation of receptor tyrosine kinases. *Am J Physiol Endocrinol Metab* 296(5):E973-984.
4. Wiley HS (2003) Trafficking of the ErbB receptors and its influence on signaling. *Exp Cell Res* 284(1):78-88.
5. Mendelsohn J (2001) The epidermal growth factor receptor as a target for cancer therapy. *Endocr Relat Cancer* 8(1):3-9.
6. Carter P (2001) Improving the efficacy of antibody-based cancer therapies. *Nat Rev Cancer* 1(2):118-129.
7. Grunwald V & Hidalgo M (2003) Developing inhibitors of the epidermal growth factor receptor for cancer treatment. *J Natl Cancer Inst* 95(12):851-867.

8. Li S, *et al.* (2005) Structural basis for inhibition of the epidermal growth factor receptor by cetuximab. *Cancer Cell* 7(4):301-311.
9. Cohenuram M & Saif MW (2007) Panitumumab the first fully human monoclonal antibody: from the bench to the clinic. *Anticancer Drugs* 18(1):7-15.
10. Cunningham D, *et al.* (2004) Cetuximab monotherapy and cetuximab plus irinotecan in irinotecan-refractory metastatic colorectal cancer. *N Engl J Med* 351(4):337-345.
11. Van Cutsem E, *et al.* (2007) Open-label phase III trial of panitumumab plus best supportive care compared with best supportive care alone in patients with chemotherapy-refractory metastatic colorectal cancer. *J Clin Oncol* 25(13):1658-1664.
12. Martinelli E, De Palma R, Orditura M, De Vita F, & Ciardiello F (2009) Anti-epidermal growth factor receptor monoclonal antibodies in cancer therapy. *Clin Exp Immunol* 158(1):1-9.
13. Friedman LM, *et al.* (2005) Synergistic down-regulation of receptor tyrosine kinases by combinations of mAbs: implications for cancer immunotherapy. *Proc Natl Acad Sci U S A* 102(6):1915-1920.
14. Perera RM, *et al.* (2005) Treatment of human tumor xenografts with monoclonal antibody 806 in combination with a prototypical epidermal growth factor receptor-specific antibody generates enhanced antitumor activity. *Clin Cancer Res* 11(17):6390-6399.
15. Pedersen MW, *et al.* (2010) Sym004: a novel synergistic anti-epidermal growth factor receptor antibody mixture with superior anticancer efficacy. *Cancer Res* 70(2):588-597.
16. Kamat V, *et al.* (2008) Enhanced EGFR inhibition and distinct epitope recognition by EGFR antagonistic mAbs C225 and 425. *Cancer Biol Ther* 7(5):726-733.
17. Ben-Kasus T, Schechter B, Lavi S, Yarden Y, & Sela M (2009) Persistent elimination of ErbB-2/HER2-overexpressing tumors using combinations of monoclonal antibodies: relevance of receptor endocytosis. *Proc Natl Acad Sci U S A* 106(9):3294-3299.
18. Zhu JX, *et al.* (2005) Decorin evokes protracted internalization and degradation of the epidermal growth factor receptor via caveolar endocytosis. *J Biol Chem* 280(37):32468-32479.

19. Huang HS, *et al.* (1997) The enhanced tumorigenic activity of a mutant epidermal growth factor receptor common in human cancers is mediated by threshold levels of constitutive tyrosine phosphorylation and unattenuated signaling. *J Biol Chem* 272(5):2927-2935.

20. Huang PH, *et al.* (2007) Quantitative analysis of EGFRvIII cellular signaling networks reveals a combinatorial therapeutic strategy for glioblastoma. *Proc Natl Acad Sci U S A* 104(31):12867-12872.

21. Harms BD, Bassi GM, Horwitz AR, & Lauffenburger DA (2005) Directional persistence of EGF-induced cell migration is associated with stabilization of lamellipodial protrusions. *Biophys J* 88(2):1479-1488.

22. Wiley HS (1988) Anomalous binding of epidermal growth factor to A431 cells is due to the effect of high receptor densities and a saturable endocytic system. *J Cell Biol* 107(2):801-810.

23. Joslin EJ, Opresko LK, Wells A, Wiley HS, & Lauffenburger DA (2007) EGF-receptor-mediated mammary epithelial cell migration is driven by sustained ERK signaling from autocrine stimulation. *J Cell Sci* 120(Pt 20):3688-3699.

24. Chao G, Cochran JR, & Wittrup KD (2004) Fine epitope mapping of anti-epidermal growth factor receptor antibodies through random mutagenesis and yeast surface display. *J Mol Biol* 342(2):539-550.

25. Lauffenburger DA, *et al.* (1996) Engineering dynamics of growth factors and other therapeutic ligands. *Biotechnol Bioeng* 52(1):61-80.

26. Ogiso H, *et al.* (2002) Crystal structure of the complex of human epidermal growth factor and receptor extracellular domains. *Cell* 110(6):775-787.

27. Kominek LA (1975) Cycloheximide production by Streptomyces griseus: alleviation of end-product inhibition by dialysis-extraction fermentation. *Antimicrob Agents Chemother* 7(6):861-863.

28. Basu SK, Goldstein JL, Anderson RG, & Brown MS (1981) Monensin interrupts the recycling of low density lipoprotein receptors in human fibroblasts. *Cell* 24(2):493-502.

29. Wang Y, Pennock S, Chen X, & Wang Z (2002) Endosomal signaling of epidermal growth factor receptor stimulates signal transduction pathways leading to cell survival. *Mol Cell Biol* 22(20):7279-7290.

30. Downward J, Waterfield MD, & Parker PJ (1985) Autophosphorylation and protein kinase C phosphorylation of the epidermal growth factor receptor. Effect on tyrosine kinase activity and ligand binding affinity. *J Biol Chem* 260(27):14538-14546.
31. Margolis BL, *et al.* (1989) All autophosphorylation sites of epidermal growth factor (EGF) receptor and HER2/neu are located in their carboxyl-terminal tails. Identification of a novel site in EGF receptor. *J Biol Chem* 264(18):10667-10671.
32. Sato K, Sato A, Aoto M, & Fukami Y (1995) c-Src phosphorylates epidermal growth factor receptor on tyrosine 845. *Biochem Biophys Res Commun* 215(3):1078-1087.
33. Countaway JL, Nairn AC, & Davis RJ (1992) Mechanism of desensitization of the epidermal growth factor receptor protein-tyrosine kinase. *J Biol Chem* 267(2):1129-1140.
34. Takishima K, Griswold-Prenner I, Ingebritsen T, & Rosner MR (1991) Epidermal growth factor (EGF) receptor T669 peptide kinase from 3T3-L1 cells is an EGF-stimulated "MAP" kinase. *Proc Natl Acad Sci U S A* 88(6):2520-2524.
35. Hunter T, Ling N, & Cooper JA (1984) Protein kinase C phosphorylation of the EGF receptor at a threonine residue close to the cytoplasmic face of the plasma membrane. *Nature* 311(5985):480-483.
36. Saphire EO, *et al.* (2003) Crystal structure of an intact human IgG: antibody asymmetry, flexibility, and a guide for HIV-1 vaccine design. *Adv Exp Med Biol* 535:55-66.
37. Hirai T, *et al.* (1998) Clinical results of transhiatal esophagectomy for carcinoma of the lower thoracic esophagus according to biological markers. *Dis Esophagus* 11(4):221-225.
38. Tateishi M, Ishida T, Mitsudomi T, Kaneko S, & Sugimachi K (1990) Immunohistochemical evidence of autocrine growth factors in adenocarcinoma of the human lung. *Cancer Res* 50(21):7077-7080.
39. Hansen MR, Roehm PC, Chatterjee P, & Green SH (2006) Constitutive neuregulin-1/ErbB signaling contributes to human vestibular schwannoma proliferation. *Glia* 53(6):593-600.
40. French AR & Lauffenburger DA (1996) Intracellular receptor/ligand sorting based on endosomal retention components. *Biotechnol Bioeng* 51(3):281-297.
41. French AR & Lauffenburger DA (1997) Controlling receptor/ligand trafficking: effects of cellular and molecular properties on endosomal sorting. *Ann Biomed Eng* 25(4):690-707.

42. Sorkin A & Goh LK (2009) Endocytosis and intracellular trafficking of ErbBs. *Exp Cell Res* 315(4):683-696.

43. Marmor MD & Yarden Y (2004) Role of protein ubiquitylation in regulating endocytosis of receptor tyrosine kinases. *Oncogene* 23(11):2057-2070.

44. Jorissen RN, *et al.* (2003) Epidermal growth factor receptor: mechanisms of activation and signalling. *Exp Cell Res* 284(1):31-53.

45. Austin CD, *et al.* (2004) Endocytosis and sorting of ErbB2 and the site of action of cancer therapeutics trastuzumab and geldanamycin. *Mol Biol Cell* 15(12):5268-5282.

46. Jaramillo ML, *et al.* (2006) Effect of the anti-receptor ligand-blocking 225 monoclonal antibody on EGF receptor endocytosis and sorting. *Exp Cell Res* 312(15):2778-2790.

47. Zhang Y, *et al.* (2005) Time-resolved mass spectrometry of tyrosine phosphorylation sites in the epidermal growth factor receptor signaling network reveals dynamic modules. *Mol Cell Proteomics* 4(9):1240-1250.

48. Perkins DN, Pappin DJ, Creasy DM, & Cottrell JS (1999) Probability-based protein identification by searching sequence databases using mass spectrometry data. *Electrophoresis* 20(18):3551-3567.

49. Nichols AM & White FM (2009) Manual validation of peptide sequence and sites of tyrosine phosphorylation from MS/MS spectra. *Methods Mol Biol* 492:143-160.

50. Mosmann T (1983) Rapid colorimetric assay for cellular growth and survival: application to proliferation and cytotoxicity assays. *J Immunol Methods* 65(1-2):55-63.

3. Design of Multispecific Antibodies Targeting Both Wild Type and Mutant EGFR

Introduction

As discussed in Chapter 1, the first antibody-based EGFR therapeutic to be clinically approved was cetuximab, the chimeric human IgG1 form of the murine mAb 225 (1). With a 100-fold greater affinity for EGFR than the native EGF ligand, mAb 225 directly competes with ligand binding to domain III, blocking dimerization and, consequently, receptor activation (2, 3). Cetuximab can also exert effects via alternative mechanisms including antibody-dependent cellular cytotoxicity (4), induction of receptor internalization and degradation (5), induction of G1-phase cell-cycle arrest, enhanced apoptosis (6, 7), and inhibition of vascular endothelial growth factor (VEGF), although these effects vary between cell lines. Other monoclonal antibodies targeting the EGFR ligand-binding domain include the FDA-approved panitumumab and several compounds undergoing clinical trials, including matuzumab and hR-3 (8, 9).

As discussed in Chapter 1, the approved therapeutic mAbs have not lived up to their promise in the clinic. The monotherapy objective response rates of cetuximab and panitumumab are just 11% and 8%, respectively, in the treatment of metastatic colorectal cancer (10-12). These response rates approximately double when the drugs are used in combination with chemotherapeutics, but there is still much opportunity for the improvement of EGFR-targeted antibody therapeutics. The tepid clinical response of cetuximab and panitumumab can be attributed to delivery limitations, acquired resistance, and receptor mutation (1). Specifically, antibody penetration into solid tumors is limited by transport and catabolism. Also, tumors may develop resistance to mAbs, often through genetic mutation of EGFR. Heterozygous somatic mutations including deletions, insertions, and point mutations have been observed in the EGFR kinase domain in some lung cancer patients (13-15). These mutations strengthen receptor interactions with ATP, amplifying autophosphorylation and boosting cell survival (16, 17). Furthermore, rearrangements within the ErbB1 gene such as large deletions, point mutants, and insertions are also common, particularly in gliomas (18). As many as 20% of glioblastomas express EGFR variants (19, 20), the most common of which is EGFRvIII, a constituitively active truncation mutant that lacks the entire domain I and the majority of domain II of the EGFR extracellular domain to lock the receptor in the active conformation (21). Tumors may also

exhibit antibody resistance through abnormal expression of the ligand, for instance through autocrine production or through increased spatial accessibility as a result of aberrant colocalization of the receptor and ligand (22, 23). Due to their reliance on ligand competition for efficacy, the current clinically approved antibodies targeting EGFR are ineffective against tumor cells that express mutants such as EGFRvIII and those that dysregulate EGFR ligands. Consequently, there is a dire need for effective EGFR-targeted mAbs that operate through complementary mechanisms to inhibit receptor signaling.

Based on our kinetic characterization and *in vitro* proliferation and migration analysis of combination antibody treatment, we established that antibody-induced receptor clustering and downregulation provides a novel and effective therapeutic strategy for targeting EGFR. We demonstrate the ability to modulate trafficking through recycling inhibition by targeting multiple epitopes on the EGFR extracellular domain (24). Encouragingly, this mechanism does not agonize receptor activity or downstream effectors in contrast to EGF-mediated downregulation. Others have shown that synergistic EGFR downregulation leads to inhibition of xenografted tumor growth (24-27). Antibody-induced clustering thus provides an alternative strategy to ligand inhibition that could be of particular utility in systems that resist ligand competition treatment, such as autocrine tumors or constitutively active mutations such as EGFRvIII.

An alternative mechanism to ligand inhibition exploited by approved EGFR-targeted antibodies involves binding to cryptic epitopes that are exposed only in mutant or activated receptor. This strategy offers the advantage of selectively binding to transformed cells, thus minimizing off-target effects. As discussed in Chapter 1, a monoclonal antibody that specifically targets the truncation mutant EGFRvIII, mAb 806, was discovered in 2002 (28). As shown in Figure 3.1, mAb 806 binds to a cysteine loop at the tail end of EGFR extracellular domain II, a conformational epitope that is exposed only when the receptor transitions into the open conformation upon dimerization (29-31). The residues implicated in the 806 epitope are provided in Table 3.1. Since this antibody is not competitive with currently approved anti-EGFR mAbs, it is undergoing both monotherapy and combination therapy clinical trials. A recent phase I clinical trial of mAb 806 demonstrated robust pharmacokinetic properties, effective therapeutic, targeting and no significant toxicity (32).

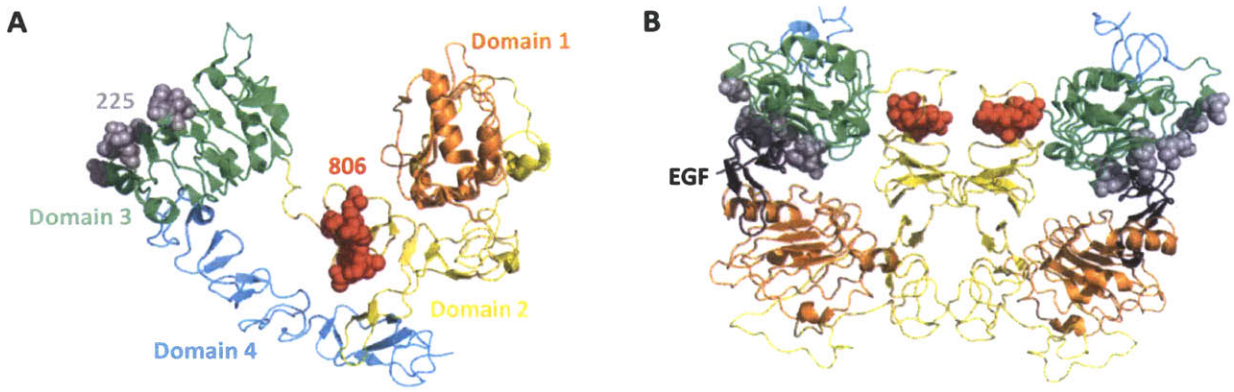

Figure 3.1. Epitopes of mAb 225 and 806 on EGFR ectodomain. The binding epitopes of the two antibodies that comprise BS28 are depicted on the EGFR monomer (A) (3) and dimer (B) (33). The 806 epitope is shown in red spheres (31) and the 225 epitope is shown in gray spheres (3). The EGF ligands are shown in black in the 2:2 ligand:receptor dimeric conformation. Domains 1 (orange), 2 (yellow), 3 (green), and 4 (cyan) of the EGFR ectodomain are depicted. Note that 225 and 806 are noncompetitive and that while 225 competes with ligand, 806 does not. The 806 epitope is exposed only in the active dimeric conformation.

Construct	EGFR Binding Domain	Epitope
mAb 225	3	Q384, Q408, H409, K443, K465, I467, N473
mAb 806	2	C287, E293, D297, G298, V299, R300, K301, C302

Table 3.1. Binding epitopes of 225 and 806. Residues implicated in the 225 and 806 epitopes from the published crystal structure of the bound Fab fragments of the respective antibodies are shown (3). Note that the epitopes are non-overlapping and 225 is competitive with ligand, whereas 806 is not.

mAb 806 could be informative for developing the next generation of antibody-based EGFR drugs. Due to its selectivity for mutant or overactive receptors and its distinct mechanism of action, it may be able to circumvent some of the shortcomings of antibodies that act through ligand inhibition alone. In a recent study, it was demonstrated that EGFR undergoes synergistic downregulation following combination treatment with 806 and mAb 528, an antibody with similar specificity and binding affinity to mAb 225 (25). This study points to the possibility of receptor crosslinking and clustering, which have been shown to impact both trafficking and signaling (24, 26).

To harness the power of both combination antibody-induced clustering and preferential targeting of mutant or activated EGFR, we sought to combine the 225 and 806 mAbs for therapeutic development. In an effort to attain and potentially enhance mAb-induced downregulation and enhance tumor cell selectivity, we created an immunoglobulin-based bispecific antibody that

incorporates the variable domains of both 225 and 806. As shown in Figure 3.2, such an antibody would be capable of crosslinking EGFR in the same manner as does a mixture of two antibodies.

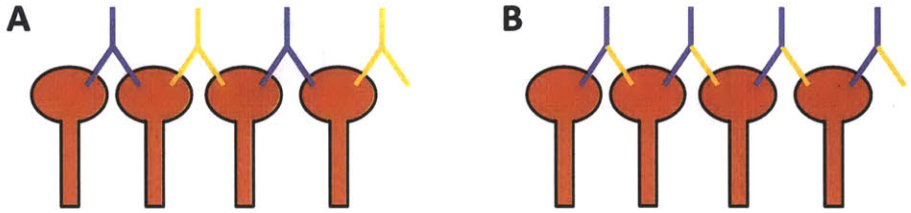

Figure 3.2. Bispecific antibodies induce receptor clustering in analogous manner to mAb combinations. Like combinations of monoclonal antibodies targeted to non-overlapping epitopes on a single receptor (A), bispecific antibodies that engage multiple non-redundant epitopes on a single receptor (B) have the potential to induce clustering.

In addition to promoting crosslinking to complement endogenous mAb effects, the bispecific antibody format enhances clustering through avidity effects. By bringing two EGFR binding sites into proximity of one another and of other receptors, bispecific antibodies increase the local concentration of antibody and augment the likelihood of epitope presentation. This strategy is of particular utility in the case of mAb 806, which recognizes a cryptic epitope on EGFR. Enhanced clustering capacity renders bispecific antibodies superior to existing therapeutic compounds or mAb combinations in terms of targeting EGFR and inhibiting its signaling. Additionally, the presence of the 806 variable region renders this treatment effective on both wild type and mutant versions of the receptor. The modular structure and design of our multi-epitopic compound could also form the basis for a new generation of antibody-based therapeutics against EGFR and other receptor tyrosine kinases that operates through a distinct clustering mechanism.

In general, bispecific antibodies are constructed to target two different antigens to improve selectivity of targeting and binding affinity. Bispecific molecules have also found utility in multi-step targeting strategies involving toxin administration or engagement of immune cells, for instance through T cell receptor specificity (35-37). Our strategy differs from conventional bispecific therapeutic strategies since rather than endeavoring to engage multiple unique proteins with our construct, we aim to target a single receptor at two distinct epitopes to modulate its trafficking and, ultimately, its expression.

There are currently in excess of 35 different bispecific antibody formats in pre-clinical or clinical development. These formats comprise seven classes of constructs: (1) Asymmetric IgG-like antibodies, which contain all constant and variable IgG domains but contain distinct variable regions on either arm to confer dual specificity; (2) Symmetric IgG-like antibodies, which have two specificities within a single variable domain, allowing for molecular symmetry; (38) IgG fusions, which conjugate additional variable domains at one or more termini of the IgG light or heavy chain; (4) Fc fusions, which stabilize single-chain variable fragments (scFv's) or diabodies by linking them to constant domains CH2 and CH3; (5) Fab fusions, which connect two distinct Fabs using a chemical crosslinker or a flexible linker sequence; (6) ScFv- and diabody-based antibodies, which consist of two different variable domain fragments either independently or fused to a stabilizing protein such as human serum albumin; and (7) IgG/Non-IgG fusions, which link antibody constant and variable domains to naturally-occurring or chimeric cytokines or receptor proteins (39).

For our bispecific antibody design, we wished to establish a stable, non-immunogenic construct with built-in flexibility at variable domain joints. Consequently, we chose to mimic the antibody format by engineering an IgG fusion consisting of the full 225 human IgG1 with an 806 scFv (heavy and light chain variable regions linked head-to-tail) fused to the light or heavy chain at the N or C terminus. Flexible $(G_4S)_2$ linkers were used between the scFv and IgG components. This bispecific format had been previously established with a dual-targeted anti-1,4,7,10-tetraazacyclododecane-1,4,7,10-tetraacetic acid (DOTA), anti-carcinoembryoinic antigen antibody (40).

Preliminary work has shown that the bispecific antibody is stably secreted in the scFv fusion format. Also, binding of this bispecific compound is improved over the binding of both constituent antibodies and, in some cases, binding is enabled in cell lines that do not show native interactions with mAb 806. Multi-epitopic binding results in formidable and reproducible downregulation by bispecific antibodies across a panel of eleven cell lines expressing both wild type and mutant EGFR. These promising *in vitro* downregulation results motivated the *in vivo*

characterization of our lead bispecific construct in the treatment of the EGFRvIII-expressing glioblastoma cell line U87-SH (41), the results of which are detailed in Chapter 5.

Results

mAb 806 binds weakly to most wild type EGFR-expressing cell lines

We examined the binding of mAb 806 to a series of EGFR-expressing cell lines that contain 1.0×10^5 to 2.8×10^6 receptors per cell, as described in Chapter 2. We found that mAb 806 showed strong selectivity for EGFRvIII, which was expressed only on U87-SH cells (41) in the panel shown in Figure 3.3. U87-SH cells express 1.7×10^5 wild type and 1.4×10^6 mutant EGFR per cell (24). Binding to all other cells lines was weak or absent, with the exception of A431, which is known to have a maximum of 10% of EGFR in the active dimeric conformation in unstimulated cells due to extensive EGFR overexpression (28).

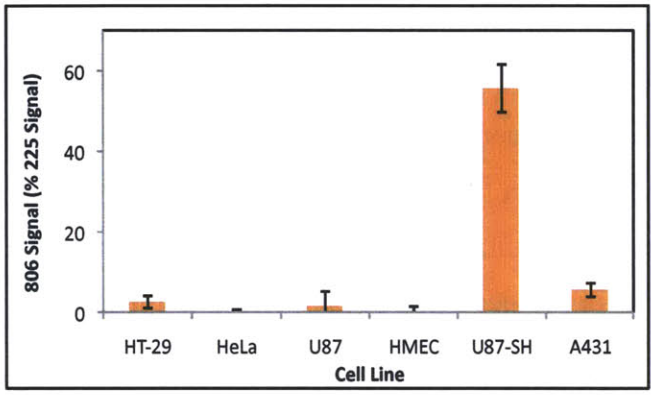

Figure 3.3 Binding of mAb 806. The proportion of 806-binding receptors was determined in six EGFR-expressing cell lines. Saturating concentrations (20 nM) of both 225 or 806 were incubated with the indicated cell lines. Cells were then washed, labeled with fluorophore-conjugated secondary antibody, washed again, and analyzed via flow cytometry. The 806 signal relative to 225 signal is presented for each cell line, representing 806 binding as a fraction of total surface EGFR binding (±SD, n=3). Cell lines are listed in increasing order of receptor density.

Bispecific antibodies consisting of the full 225 IgG and an 806 scFv are stably secreted in HEK 293 mammalian expression system

Antibodies were designed using a modular format that fused the 225 mAb with the 806 scFv. Constructs consist of a full human IgG1 backbone with the 225 variable domains with an 806 scFv conjugated to either the light chain or heavy chain at the N- or C-terminal ends. Due to symmetric assembly of the IgG heavy and light chains, these bispecific constructs are bispecific and tetravalent. 225-806 bispecific antibodies will henceforth be designated BS28 followed by the location of scFv fusion, as depicted in Figure 3.4.

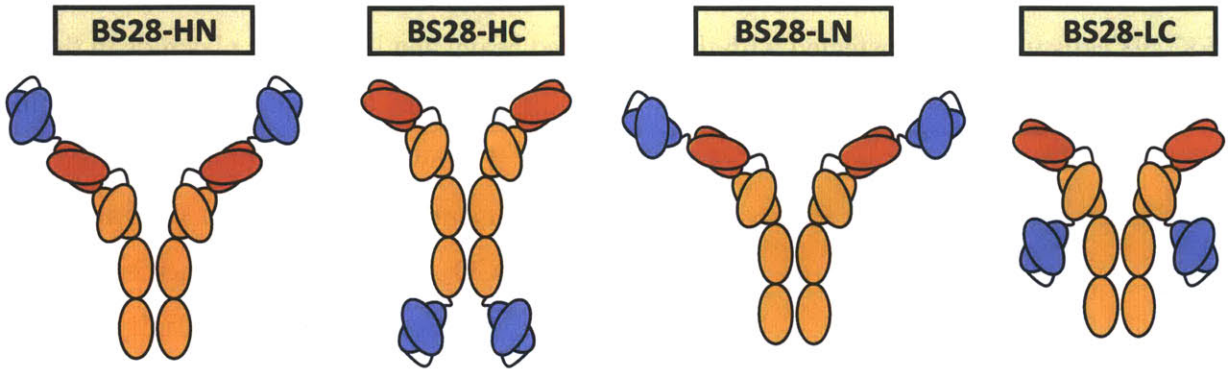

Figure 3.4. BS28 bispecific antibody structure. A human IgG1 isotype backbone is used as a scaffold for engineering BS28 constructs. The heavy chain consists of three constant domains (CH1, CH2, and CH3) and one variable domain (VH), whereas the light chain consists of one constant domain (CL) and one variable domain (VL). Constant domains are shown in orange and variable domains are displayed in red. The 806 scFv (blue) is fused to the heavy or light chain at the N or C terminus with a flexible linker and the fusion constructs are named as indicated. Antibody light and heavy chains are assembled *in vitro* in 2:2 complexes, linked by three disulfide bonds. Full sequences of the four BS28 constructs that were designed are provided in Appendix C.

Bispecific antibodies were secreted from HEK 293F cells co-transfected with the appropriate heavy and light chain expression plasmids derived from the gWiz mammalian expression vector. The sequences for the four bispecific plasmids as well as the unconjugated 225 heavy and light chain plasmids are provided in Appendix C. All constructs include a Kozak consensus sequence immediately upstream of the leader sequence to enhance yield (42). Although not essential, our modular bispecific format allows for the insertion of an epitope tag to facilitate labeling and/or purification. As proof of principle, a cmyc tag was fused to the C-terminal end of BS28-LC. Note that the BS28 constructs are approximately 1.3 times the size of the 225 antibody.

For the preparation of each bispecific construct, one chain was conjugated to an scFv of the 806 antibody and the other chain was identical to that of the unmodified 225 antibody. The molecular weights of each of the constructs are detailed in Table 3.2.

Construct	Heavy Chain MW (g/mol)	Light Chain MW (g/mol)	Full Antibody MW (g/mol)
225	51082	25629	153422
BS28-HN	77218	25629	205640
BS28-HC	77634	25629	206471
BS28-LN	51082	52423	206955
BS28-LC	51082	53510	209129

Table 3.2. Molecular weights of BS28 constructs. The molecular weights (MWs) of the heavy chain, light chain, and fully-assembled antibody are provided for the unmodified 225 mAb and the four secreted BS28 constructs.

HEK 293 cells were co-transfected with the designated heavy and light chain plasmids in the presence of 2 μg/mL polyethylinimine. Following transfection, cells were incubated for 7 days at 37°C and 5% CO_2. Secretions were then harvested, purified via protein A affinity chromatography, and reconstituted in phosphate buffered saline. Purity was evaluated via SDS-PAGE analysis. As displayed in Figure 3.5, the molecular weights of the fully assembled BS28 constructs and their respective heavy and light chains matched expectations and the purity of these antibodies was high, with no visible aggregates or degradation products.

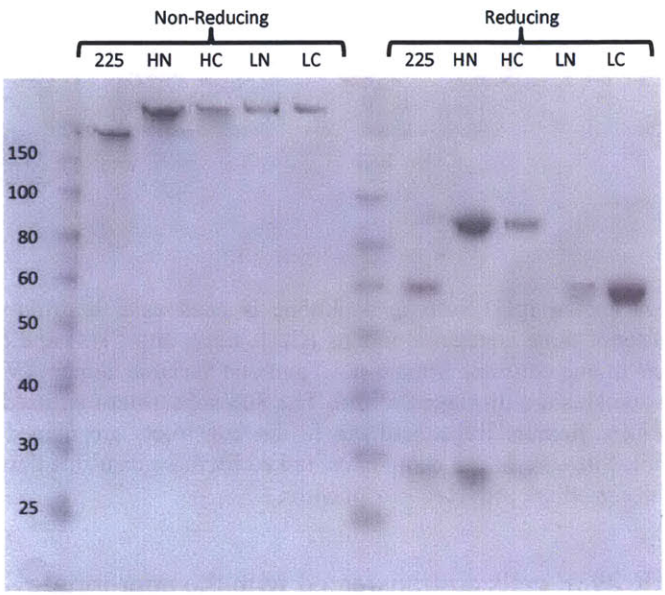

Figure 3.5. SDS-PAGE analysis of secreted BS28 constructs. The four secreted and protein A-purified BS28 constructs (denoted by orientation as shown in Figure 3.4) were characterized by SDS-PAGE analysis under non-reducing (left) and reducing (right) conditions. The unconjugated 225 IgG is shown for reference.

Engineered bispecific antibody yields ranged from 2 to 1383 μg/L depending on scFv orientation. A comparison of the yields for each BS28 format is provided in Figure 3.6. Note that the heavy chain N-terminal fusion secretes the most robustly. Comparison with secretion levels of the 225 IgG shows that BS28-HN secretes with a yield of nearly two-fold that of the base antibody. In contrast, the light chain N-terminal scFv fusion secretes poorly. Due to the low levels of BS28-LN secretion, this construct was omitted in subsequent characterization and analysis.

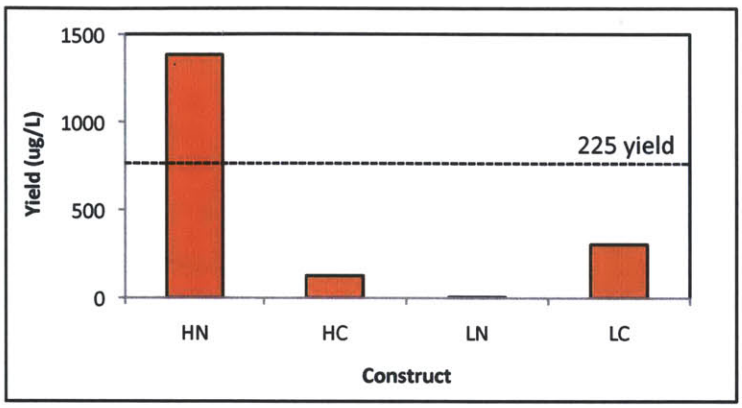

Figure 3.6. Bispecific antibody yield summary. BS28 antibodies were secreted from HEK 293F cells in the four orientations shown in Figure 3.4 and the resulting yields of the protein A-purified products are presented. Note that HN secretes best (1383 μg/L), followed by LC (305 μg/L), HC (125 μg/L), and LN (4 μg/L). Secretion levels of the 225 base antibody (731 μg/L) are indicated by the dashed line.

Bispecific antibodies bind EGFR with higher affinity than constituent monoclonal antibodies

The interaction between the bispecific constructs and their target antigen, EGFR, was characterized on the surface of A431 cells. Since the 806 variable domain only binds to 10% of surface EGFR in the A431 cell line (Figure 3.3), we might not expect to see enhanced binding of the bispecific antibody relative to the unconjugated 225 IgG. However, as shown in Figure 3.7 and Table 3.3, we observe that the affinity of the Ab-Fn3 fusion is 4-6 times greater than that of the unmodified 225 antibody at endosomal pH (6.0) and ten- to twenty-fold greater than that of the unmodified 225 antibody at physiological pH (7.4). This is a direct consequence of avidity effects emanating from the bispecificity of the BS28 construct. Hence, from an interaction standpoint alone, we observe that multispecificity confers binding of 806 to wild type EGFR in cell lines that show little interaction with this antibody in the monoclonal format.

We further observe from Table 3.3 that binding affinity is roughly equivalent between endosomal and physiological pH and that both K_d values are in the tens of picomolar range. The insensitivity of binding to pH reduction indicates that the compound will remain bound to EGFR following internalization, as does the 225 base antibody.

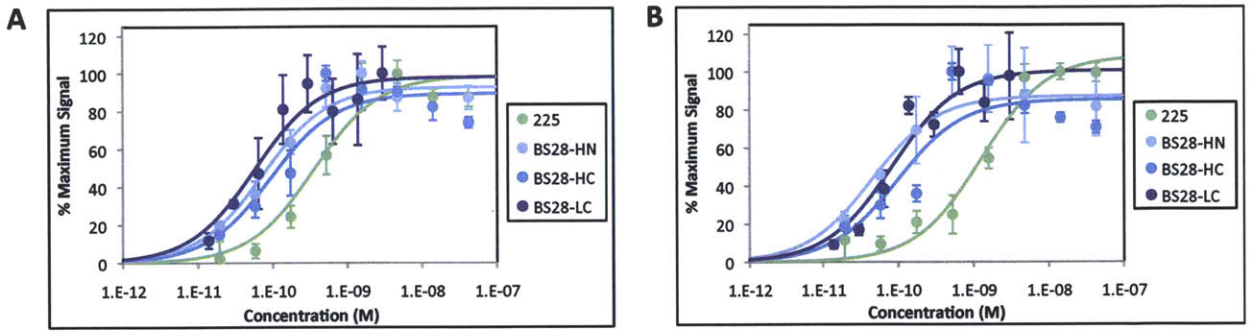

Figure 3.7. BS28 binding kinetics. BS28-HN (light blue), HC (medium blue), and LC (dark blue) were titrated on the surface of A431 cells at pH 6.0 (A) and pH 7.4 (B). Due to avidity effects resulting from the bispecificity of these constructs, all three have a higher affinity for their target antigen, EGFR, than the unmodified 225 antibody (green). Nonlinear least squares regression fits to a 1:1 binding isotherm are shown for 225 and BS28 constructs (solid lines).

Construct	K_d (pH 6.0, pM)	K_d (pH 7.4, pM)
225	370	1284
BS28-HN	76	47
BS28-HC	97	100
BS28-LC	59	86

Table 3.3. Equilibrium dissociation constructs of BS28 constructs. Using nonlinear least squares regression, the titration curves shown in Figure 8 were fitted to binding isotherms (% bound = [L]/([L]+K_d where [L] is antibody concentration and K_d is the apparent equilibrium dissociation constant) and the K_d values were were determined. Compared to unmodified 225 mAb, bispecific constructs have four-to-six-fold tighter interactions with EGFR at pH 6.0 and ten- to twenty-fold tighter interactions with EGFR at pH 7.4.

Bispecific antibodies induce surface downregulation of both EGFRvIII and wild type EGFR

Improved receptor clustering manifests itself through enhanced surface EGFR downregulation. We hypothesized that bispecific antibody-induced clustering would be more efficient than combination antibody-induced clustering based on avidity and effective concentration effects, so we sought to examine clustering efficiency by quantifying surface downregulation following treatment with monoclonal versus bispecific antibodies.

To demonstrate the advantage of using a bispecific, and in particular one that includes 806 to target mutant receptors, we measured surface EGFR downregulation in a series of cell lines derived from the U87 glioblastoma line that express various numbers of EGFRvIII (41, 43). All six cell lines express 1.7×10^5 wild type EGFR and variable amounts of transfected EGFRvIII (24). Note that the U87-DK (dead kinase) cell line is transfected with EGFRvIII possessing the K721M mutation, which is known to inactivate the tyrosine kinase domain (43), and the U87-

WT (wild type) line is transfected with wild type EGFR (41). The receptor densities of each of these cell lines are provided in Chapter 2, Table 2.2.

To quantify surface EGFR downregulation, cells were treated with 20 nM total of either mAb 225, mAb 806, mAbs 225 and 806 combined, BS28-HC, or BS28-LC for 13 h at 37°C. This allows for the receptors to achieve a new steady state in the presence of antibody. Cells were then acid stripped to remove surface antibody, relabeled with an anti-EGFR antibody followed by a fluorophore-conjugated secondary antibody, and quantified via flow cytometry.

The six U87-derived EGFRvIII-expressing cell lines tested were virtually unaffected by mAb 225 and mAb 806 treatment (Figure 3.8), consistent with the results of single antibody treatment in our combination antibody downregulation panel (Chapter 2, Figure 2.1). In particular, 806 had no effect on any of the lines, even though all but U87 and U87-WT express EGFRvIII. Interestingly, the combination of mAbs 225 and 806 did not significantly alter surface EGFR levels. However, all three bispecific constructs tested elicited 50-80% downregulation of surface EGFR on the six cell lines examined.

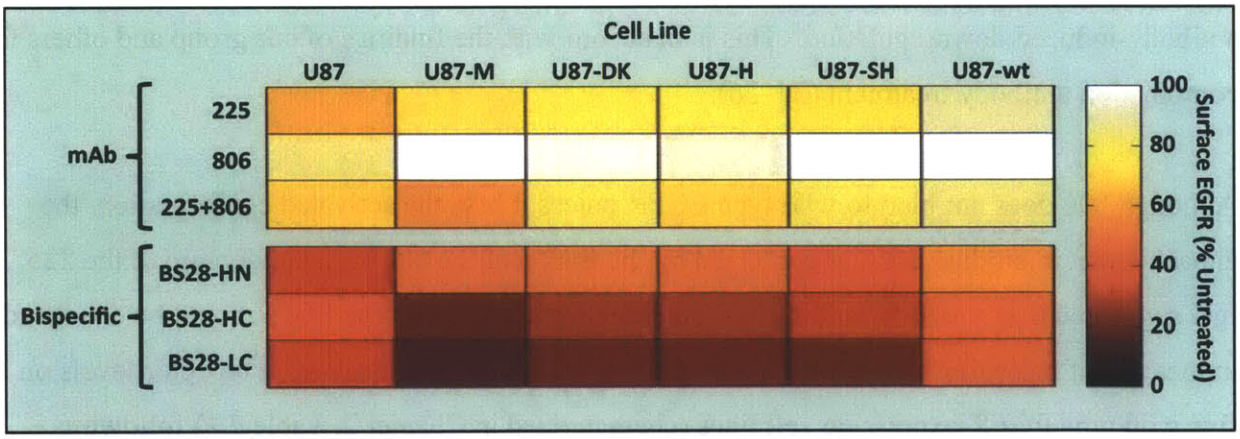

Figure 3.8 Surface EGFR downregulation in U87-derived cells following BS28 treatment. Six U87-derived cell lines (listed in increasing order of EGFR expression level) were treated at a total concentration of 20 nM of the indicated antibodies for 13 h at 37°C. They were then acid stripped, labeled with an anti-EGFR antibody and a fluorescent secondary antibody, and analyzed via flow cytometry to quantify remaining surface receptor relative to that of untreated cells.

Notably, bispecific antibody orientation impacts the extent of downregulation. Specifically, the fusions with a greater spatial separation between the 225 and 806 variable domains (HC and LC) downregulate more potently than the construct with adjacent variable domains (HN).

Additionally, the LC construct performs slightly better (average downregulation = 72%) than the HC construct (average downregulation = 65%), suggesting an optimum spacing between the 225 variable domain and the 806 scFv.

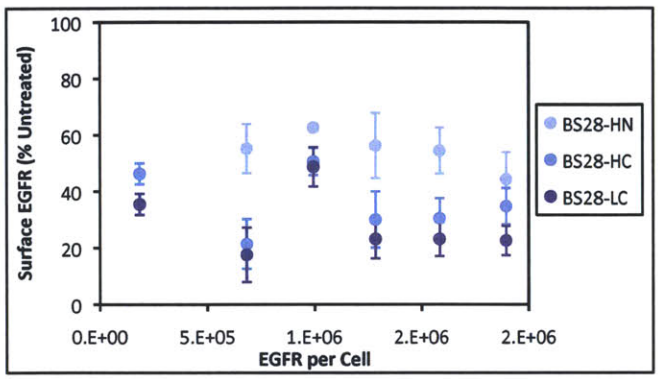

Figure 3.9. Mutant EGFR downregulation extent is independent of initial receptor number. Downregulation data from each cell line shown in Figure 3.8 is plotted against receptor density. Surface receptor remaining is presented as a percentage of the untreated control (±SD, n=3).

Recall from Chapter 2 that pairwise mAb downregulation extent was inversely correlated with EGFR density, particularly in the case of less potently downregulating combinations. In contrast, downregulation extent is uncorrelated with receptor expression levels for BS28 constructs; These antibodies perform consistently well in all six cell lines tested (Figure 3.9).

Finally, we note that downregulation of the U87-DK cell line is as effective as downregulation of other U87-derived cell lines, indicating that kinase activity is not required for bispecific antibody-induced downregulation. This is in accord with the findings of our group and others for combination antibody treatment (24, 26).

Although 806 does not bind to wild type EGFR unless it is in the activated conformation, the enhancement in binding affinity conferred by the fusion of the 806 variable domain to the 225 IgG suggested that antibody binding and downregulation of wild type EGFR could be enhanced in the case of bispecific treatment. Consequently, we examined steady-state receptor levels on five wild type EGFR-expressing cell lines (characterized in Chapter 2, Table 2.1) following single, combination, or bispecific antibody treatment. The U87-SH mutant EGFR-expressing cell line was included with this panel for reference.

As was the case for mutant EGFR-expressing cell lines, single or combination mAbs had minimal effects, whereas BS28-HN, HC, and LC decreased surface receptor levels by 50-80% in the six cell lines that were tested (See Figure 3.10). While all three BS28 constructs

reproducibly effected downregulation, BS28-HN was notably less active than the HC and LC constructs, as was observed for the U87 panel. Also consistent with the U87 data, BS28-LC (average downregulation = 64%) was slightly more potent than BS28-HC (average downregulation = 53%).

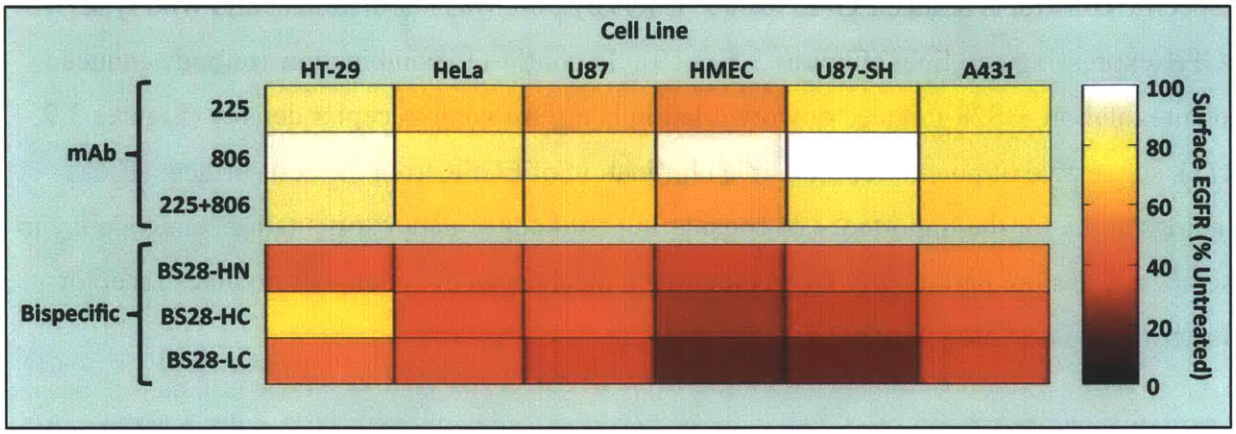

Figure 3.10 Surface EGFR downregulation in U87-derived cells following BS28 treatment. Six U87-derived cell lines (listed in increasing order of EGFR expression level) were treated at a total concentration of 20 nM of the indicated antibodies for 13 h at 37°C. They were then acid stripped, labeled with an anti-EGFR antibody and a fluorescent secondary antibody, and analyzed via flow cytometry to quantify remaining surface receptor relative to that of untreated cells.

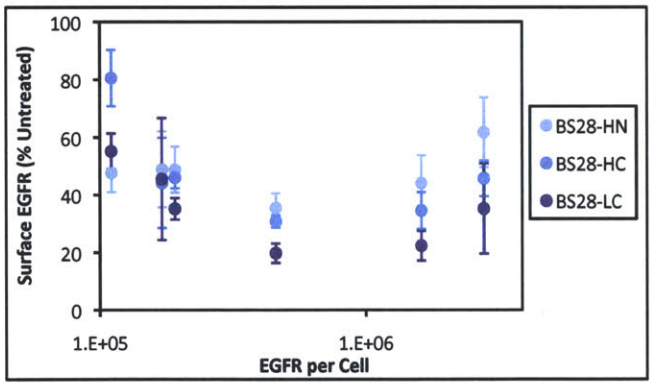

Figure 3.11. Wild type EGFR downregulation extent is independent of initial receptor number. Downregulation data from the cell lines shown in Figure 3.10 is plotted against receptor density. Surface receptor remaining is presented as a percentage of that of untreated cells (±SD, n=3).

As was observed for U87-derived cell lines, BS28 constructs substantively downregulate wild type EGFR-expressing cell lines regardless of receptor expression level (See Figure 3.11). This result reinforces the distinction between mAb combinations and bispecific constructs in terms of downregulation dependence on initial surface EGFR levels.

Taken together, the mutant and wild type EGFR downregulation results are suggestive of greatly enhanced receptor clustering in the presence of the bispecific antibody compared to mAb 225, mAb 806, or the combination thereof.

Discussion

We have demonstrated that use of a bispecific format for administration 225 and 806 results in synergy between these two mAbs in a system where combination monoclonal antibody treatment is insufficient. Although combination treatment does not induce receptor downregulation, bispecific constructs reduce EGFR surface levels by 50-80% in both mutant and wild type EGFR-expressing cell lines (Figures 3.8, 3.10). In contrast to combination antibody-induced downregulation, BS28-induced downregulation is insensitive to receptor density (Figures 3.9, 3.11), suggestive of potent, reproducible elimination of EGFR from the cell surface. These findings argue for the importance of considering antibody structure, orientation, and valency in therapeutic design, particularly when pursuing a mechanism of action that involves receptor clustering and downregulation.

There are clear physical advantages to the administration of bispecific antibodies over mAb combinations in the context of receptor clustering. As described in Chapter 2, receptor clustering can be induced by using a combination of antibodies with non-overlapping epitopes. However, this requires alternating receptor binding, as shown in Figure 3.1. The advantage of the bispecific antibody is that every molecule displays both EGFR-targeted paratopes, reducing transport limitations and facilitating receptor crosslinking, since every antibody molecule is capable of extending the growing receptor-antibody chain.

Bispecific constructs also have enhanced binding compared to monoclonal antibodies, as shown in Figure 3.7 and Table 3.3. This is the result of the cooperativity of binding that stems from avidity effects. The presence of multiple antibody interactions increases the probability of binding and reduces the probability of dissociation since the likelihood of multiple interactions terminating simultaneously is low. Furthermore, if one paratope of the tetravalent antibody dissociates from the receptor while the three other paratopes may remain bound to surface receptors, the local apparent concentration of the free paratope in the vicinity of surface-bound is drastically inflated. In all likelihood, the dissociated paratope will rebind, strengthening the apparent affinity of the antibody for its target receptor.

In the particular case of the 225-806 bispecific construct, binding is not only enhanced, but enabled through avidity effects. Recall that the 806 epitope is only exposed when EGFR is in its active conformation (28-31). However, due to thermodynamic fluctuations of the receptor, the 806 epitope can be exposed even when the receptor is in the tethered monomeric state. If the 225 paratope is already bound to EGFR, the range of the 806 paratope is constrained, increasing the apparent concentration of 806 paratope to which the receptor is exposed and increasing the probability that 806 will bind when its epitope is exposed. Thus, the 806 paratope on the bispecific antibody is much more likely to capture its epitope in the 225-bound constrained state compared to the unconstrained state in free solution. Improved 806 binding in the bispecific state is evidenced by the affinity enhancement of BS28 constructs compared to mAb 225 in A431 cells at physiological and endosomal pH. The 806 monoclonal antibody only binds to approximately 10% of EGFR in A431 cells (the activated fraction), yet in a bispecific with 225, it improves the affinity of the monoclonal 225 antibody at pH 7.4 by more than an order of magnitude (Figure 3.7B and Table 3.3). This improved 806 scFv binding also facilitates crosslinking, thus augmenting receptor clustering.

In addition to the therapeutic advantages of using a bispecific antibody as opposed to a single antibody or a drug cocktail, there are commercial advantages to the development of multispecific compounds. From a logistical standpoint, combining two therapeutics into a single compound facilitates preparation on the production side and administration on the clinical side. Also, clinical testing of a bispecific compound may be expedited compared to a drug cocktail since one would only be required to characterize the properties of a single compound as opposed to multiple compounds (36, 37). Lastly, the presence of multiple antibody variable domains and the recruitment of multiple therapeutic mechanisms within a single compound along with the binding and clustering advantages of a bispecific antibody combine to make multispecific antibodies more potent than their monoclonal counterparts. As a result, drug dosage is reduced for bispecific compounds, potentially reducing off-target effects.

Our comprehensive study of the class of single scFv fusions for 225-806 bispecific design (Figure 3.4) offers insight into the structural bias of antibody-induced downregulation. Specifically, we find that fusion of the scFv in the HN position enhances antibody secretion

(Figure 3.6), but does not optimize downregulation. The HC and LC fusions, which further separate the two variable domains, more effectively reduce surface EGFR levels, with the LC spacing showing a slight advantage over the HC orientation (Figures 3.8, 3.10).

The ability of our BS28 constructs to downregulate both EGFR and EGFRvIII is significant since the two FDA-approved antibody drugs that target EGFR are ineffective against this mutant, as they rely significantly on ligand competition for therapeutic efficacy. The recruitment of a mechanism that is independent of ligand binding implies that BS28 would also have a therapeutic advantage in cases where EGFR ligands are overexpressed or otherwise dysregulated. Clearly, BS28 constructs have the potential to complement the effects and overcome the limitations of currently approved antibodies targeting EGFR.

In our combination mAb studies discussed in Chapter 2, clustering was shown to abrogate EGFR recycling, thereby decreasing surface receptor expression and activation of downstream signaling pathways (24). By altering the trafficking of EGFR using the endogenous endocytic machinery, clustering reduces the steady state surface levels of EGFR, thus reducing the number of receptors available for signal activation. Importantly, receptor clustering was found not to be agonistic, achieving downregulation without activating downstream pathways. We also found combination antibody-mediated downregulation to coincide with inhibition of the migration and growth of transformed cells (24). Based on the similarity in mechanism and downregulatory capacity between mAb combinations and our engineered bispecific antibodies, we predict that our BS28 series would exhibit an analogous correlation between receptor downregulation and efficacy in the absence of agonism.

The therapeutic promise of our BS28 bispecific antibodies has been confirmed *in vitro* through surface EGFR downregulation assays on human cancer cell lines. Previous work has demonstrated tumor inhibition by EGFR downregulating constructs (25-27, 44, 45). Based on these results, we pursued *in vivo* characterization of our most potently downregulating bispecific antibody (BS28-LC) via mouse xenograft studies, as described in Chapter 5.

Use of the bispecific construct we have developed offers numerous therapeutic advantages over current clinically available treatments. The strategy of administering a bispecific antibody with two variable domains targeting non-overlapping epitopes on a single receptor tyrosine kinase can also be generalized as a robust therapeutic option. The modular format of the bispecific constructs we have developed allows for the presentation of any antibody variable domain with engineered specificity for multiple non-overlapping sites on any antigen of interest. This provides a generalized scaffold for eliciting receptor clustering, which could be extended to other members of the ErbB family or to other receptor tyrosine kinases. The IgG backbone will allow for superior retention in the bloodstream via neonatal Fc receptor recycling (46) and the molecular specificity of the two variable domains will minimize off-target toxicity. This novel targeting approach has the potential to complement existing therapeutic mechanisms such as ligand competition, immune recruitment, and angiogenesis inhibition to enhance drug efficacy via clustering, receptor downregulation, increased binding affinity, and selective targeting. Additionally, compared to administration of a cocktail of antibodies, the bispecific approach enhances or, as is the case for 225 and 806, enables synergy between its constituent antibodies.

The primary commercial application we envision for BS28 constructs is use as a targeted therapeutic in multiple forms of epithelial-based cancer. Although 806 specifically targets EGFRvIII, our *in vitro* downregulation data suggests that BS28 may be effective on a wide range of cancer cell lines with varied wild type and mutant receptor densities, even those that do not bind to the 806 monoclonal antibody (Figures 3.3, 3.8, 3.10).

A further application of BS28 constructs could be as delivery agents for multi-step targeting applications. Fusion to toxins, endosomalytic species, siRNA, or other cell disruption agents would direct these molecules to wild type and mutant EGFR-expressing tumors and allow for their rapid internalization. Through formation of large depots of clustered EGFR-antibody complexes in the cytoplasm, bispecific molecules could provide high local concentrations of toxin or to selectively destroy transformed cells. Furthermore, conjugation of BS28 constructs to fusogenic peptides could facilitate disruption of the endosomal membrane and allow for diffusion of conjugated toxins into the cytosol, enhancing therapeutic efficacy.

Finally, aside from their potential as therapeutic agents, BS28 constructs could be developed as research and diagnostic tools. With picomolar affinity for EGFR (Figure 3.7 and Table 3.3) and targeted recognition of the mutant EGFRvIII with the 806 moiety, BS28 antibodies tightly and selectively bind EGFR, providing accurate and highly sensitive detection for tumor diagnosis applications.

Materials and Methods

Cell lines and antibodies

The transfected CHO-EG (47) and U87-derived (41) cell lines were established as described previously and all other lines were obtained from ATCC (Manassas, VA). Cells were maintained in their respective growth media (from ATCC unless otherwise indicated): DMEM for A431, U87-MG, transfected U87-MG, and CHO-EG cells, McCoy's Modified 5A media for HT-29 cells, EMEM for HeLa cells, and HuMEC Ready Medium (Invitrogen, Carlsbad, CA) for HMEC cells. U87-MG, transfected U87-MG, and CHO-EG media were supplemented with 1 mM sodium pyruvate (Invitrogen) and 0.1 mM non-essential amino acids (Invitrogen) and transfected U87-MG lines and CHO-EG were selected with 0.3 mM Geneticin (Invitrogen). ATCC media was supplemented with 10% fetal bovine serum (FBS). Murine 225 was secreted from the hybridoma cell line (ATCC).

Unless otherwise noted, all washes were conducted in PBS containing 0.1% BSA and all mAbs were used at a concentration of 20 nM for single treatment and 10 nM each for combination treatment. EGF (Sigma, St. Louis, MO) was dosed at 20 nM. Trypsin-EDTA (Invitrogen) contains 0.05% trypsin and 0.5 mM EDTA. Cell pelleting was conducted at 1000×g.

225 and 806 mAb binding assays

To characterize mAb 225 and 806 binding to cells, the indicated cell lines were grown to confluence and subsequently serum-starved for 12 h. Cells were then trypsinized, washed in PBSA, and incubated with 20 nM mAb 225 or 806 (human IgG 1) in a 96-well plate on ice for 1 h. Cells were then washed and labeled with 66 nM PE-conjugated goat anti-human antibody (Rockland Immunochemicals, Gilbertsville, PA) for 20 min on ice. After a final wash, plates

were analyzed on a FACS Calibur cytometer (BD Biosciences, San Jose, CA). 806 fluorescence intensity was normalized by 225 fluorescence intensity to determine the fraction of surface EGFR molecules that bind the 806 mAb.

Production of mAb and BS28 constructs via HEK cell transfection

The human IgG1 heavy and light chains of each BS28 construct and the 225 and 806 mAbs were inserted into the gWiz mammalian expression vector (Genlantis). The sequences for all 225, 806, and BS28 plasmids are provided in Appendix C. Constructs were verified by sequence analysis. HEK 293F cells (Invitrogen) were grown to 1.2 million cells per mL and diluted to one million per mL. Miniprepped DNA and polyethyleneimine (Sigma) were independently diluted to 0.05 and 0.1 mg/mL in OptiPro medium and incubated at 22° for 15 min. Equal volumes of DNA and polyethyleneimine were mixed and incubated at 22° for 15 min. 500 mL of cells in FreeStyle media and 20 mL of DNA/polyethyleneimine mixture in OptiPro were added to a 2 L roller bottle and incubated at 37°, 5% CO_2 on a roller bottle adapter for seven days. The cell secretions were then centrifuged for 30 min at 15,000×g and the supernatant was filtered through a 0.22 μm bottle-top filter and purified via affinity column chromatography using protein A resin (Thermo Fisher Scientific, Waltham, MA). The eluted bispecific antibodies were concentrated and transferred to PBS and then characterized by sodium dodecyl sulfate polyacrylamide gel electrophoresis (SDS-PAGE) analysis. For reducing SDS-PAGE, samples were treated with 0.6 M dithiothreitol.

BS28 and mAb cell surface affinity titrations

To characterize bispecific construct binding affinities, A431 cells were grown to confluence and serum-starved for 12 h. Cells were then trypsinized, washed in PBSA and incubated with various concentrations of Ab-Fn3 or mAb 225 in a 96-well plate on ice. The number of cells and sample volumes were selected to ensure at least tenfold excess Ab-Fn3 relative to EGFR. Cells were incubated on ice for sufficient time to ensure that the approach to equilibrium was at least 99% complete. Cells were then washed and labeled with 66 nM PE-conjugated goat anti-human antibody (Rockland Immunochemicals) for 20 min on ice. After a final wash, plates were analyzed on a FACS Calibur cytometer (BD Biosciences). Fluorescence intensities are normalized to the maximum value for a give construct. The minimum and maximum

fluorescence and the K_d value were determined by minimizing the sum of squared errors assuming a 1:1 binding interaction (% Bound = [L]/([L]+K_d) where [L] is bispecific antibody concentration and K_d is the apparent equilibrium dissociation constant of the BS28 construct. Titrations were performed at both pH 6.0 (endosomal pH) and pH 7.4 (physiological pH). All curve fitting was implemented in MATLAB (Mathworks, Natick, MA).

Receptor downregulation assays

Cells were seeded at 5×10^4 per well in 96-well plates and allowed to adhere overnight. They were then serum starved for 12-16 h, treated with the indicated mAbs or BS28 constructs in serum-free medium, and incubated at 37°C for 13 h. Subsequently, cells were washed and treated with trypsin-EDTA for 20 min at 37°C. Trypsin was neutralized with medium (10% FBS) and cells were immediately transferred to v-bottom plates on ice. They were then washed, acid stripped (0.2 M acetic acid, 0.5 M NaCl, pH 2.5), and washed again prior to incubation with 20 nM murine 225 for 1 h on ice to label surface EGFR. Cells were then washed and labeled with 66 nM PE-conjugated goat anti-mouse antibody (Invitrogen) for 20 min on ice. After a final wash, plates were analyzed on a FACS Calibur cytometer (BD Biosciences). Results are presented as fluorescence intensity of treated cells divided by that of untreated control cells. Each value presented in the heat maps and downregulation versus receptor density graphs represents the mean downregulation extent in triplicate wells averaged over three independent experiments.

References

1. Martinelli E, De Palma R, Orditura M, De Vita F, & Ciardiello F (2009) Anti-epidermal growth factor receptor monoclonal antibodies in cancer therapy. *Clin Exp Immunol* 158(1):1-9.
2. Grunwald V & Hidalgo M (2003) Developing inhibitors of the epidermal growth factor receptor for cancer treatment. *J Natl Cancer Inst* 95(12):851-867.
3. Li S, *et al.* (2005) Structural basis for inhibition of the epidermal growth factor receptor by cetuximab. *Cancer Cell* 7(4):301-311.

4. de Bono JS & Rowinsky EK (2002) Therapeutics targeting signal transduction for patients with colorectal carcinoma. *Br Med Bull* 64:227-254.
5. Ennis BW, Lippman ME, & Dickson RB (1991) The EGF receptor system as a target for antitumor therapy. *Cancer Invest* 9(5):553-562.
6. Prewett MC, *et al.* (2002) Enhanced antitumor activity of anti-epidermal growth factor receptor monoclonal antibody IMC-C225 in combination with irinotecan (CPT-11) against human colorectal tumor xenografts. *Clin Cancer Res* 8(5):994-1003.
7. Ciardiello F, *et al.* (1999) Antitumor activity of sequential treatment with topotecan and anti-epidermal growth factor receptor monoclonal antibody C225. *Clin Cancer Res* 5(4):909-916.
8. Mateo C, *et al.* (1997) Humanization of a mouse monoclonal antibody that blocks the epidermal growth factor receptor: recovery of antagonistic activity. *Immunotechnology* 3(1):71-81.
9. Sebastian S, *et al.* (2006) The complexity of targeting EGFR signalling in cancer: from expression to turnover. *Biochim Biophys Acta* 1766(1):120-139.
10. Cunningham D, *et al.* (2004) Cetuximab monotherapy and cetuximab plus irinotecan in irinotecan-refractory metastatic colorectal cancer. *N Engl J Med* 351(4):337-345.
11. Cohenuram M & Saif MW (2007) Panitumumab the first fully human monoclonal antibody: from the bench to the clinic. *Anticancer Drugs* 18(1):7-15.
12. Van Cutsem E, *et al.* (2007) Open-label phase III trial of panitumumab plus best supportive care compared with best supportive care alone in patients with chemotherapy-refractory metastatic colorectal cancer. *J Clin Oncol* 25(13):1658-1664.
13. Lynch TJ, *et al.* (2004) Activating mutations in the epidermal growth factor receptor underlying responsiveness of non-small-cell lung cancer to gefitinib. *N Engl J Med* 350(21):2129-2139.
14. Paez JG, *et al.* (2004) EGFR mutations in lung cancer: correlation with clinical response to gefitinib therapy. *Science* 304(5676):1497-1500.
15. Pao W, *et al.* (2004) EGF receptor gene mutations are common in lung cancers from "never smokers" and are associated with sensitivity of tumors to gefitinib and erlotinib. *Proc Natl Acad Sci U S A* 101(36):13306-13311.

16. Tracy S, *et al.* (2004) Gefitinib induces apoptosis in the EGFRL858R non-small-cell lung cancer cell line H3255. *Cancer Res* 64(20):7241-7244.
17. Sordella R, Bell DW, Haber DA, & Settleman J (2004) Gefitinib-sensitizing EGFR mutations in lung cancer activate anti-apoptotic pathways. *Science* 305(5687):1163-1167.
18. Ekstrand AJ, Sugawa N, James CD, & Collins VP (1992) Amplified and rearranged epidermal growth factor receptor genes in human glioblastomas reveal deletions of sequences encoding portions of the N- and/or C-terminal tails. *Proc Natl Acad Sci U S A* 89(10):4309-4313.
19. Ekstrand AJ, *et al.* (1991) Genes for epidermal growth factor receptor, transforming growth factor alpha, and epidermal growth factor and their expression in human gliomas in vivo. *Cancer Res* 51(8):2164-2172.
20. Liu L, *et al.* (2005) Clinical significance of EGFR amplification and the aberrant EGFRvIII transcript in conventionally treated astrocytic gliomas. *J Mol Med* 83(11):917-926.
21. Wong AJ, *et al.* (1992) Structural alterations of the epidermal growth factor receptor gene in human gliomas. *Proc Natl Acad Sci U S A* 89(7):2965-2969.
22. Tateishi M, Ishida T, Mitsudomi T, Kaneko S, & Sugimachi K (1990) Immunohistochemical evidence of autocrine growth factors in adenocarcinoma of the human lung. *Cancer Res* 50(21):7077-7080.
23. Hirai T, *et al.* (1998) Clinical results of transhiatal esophagectomy for carcinoma of the lower thoracic esophagus according to biological markers. *Dis Esophagus* 11(4):221-225.
24. Spangler JB, *et al.* (2010) Combination antibody treatment down-regulates epidermal growth factor receptor by inhibiting endosomal recycling. *Proc Natl Acad Sci U S A* 107(30):13252-13257.
25. Perera RM, *et al.* (2005) Treatment of human tumor xenografts with monoclonal antibody 806 in combination with a prototypical epidermal growth factor receptor-specific antibody generates enhanced antitumor activity. *Clin Cancer Res* 11(17):6390-6399.
26. Friedman LM, *et al.* (2005) Synergistic down-regulation of receptor tyrosine kinases by combinations of mAbs: implications for cancer immunotherapy. *Proc Natl Acad Sci U S A* 102(6):1915-1920.

27. Pedersen MW, *et al.* (2010) Sym004: a novel synergistic anti-epidermal growth factor receptor antibody mixture with superior anticancer efficacy. *Cancer Res* 70(2):588-597.
28. Johns TG, *et al.* (2002) Novel monoclonal antibody specific for the de2-7 epidermal growth factor receptor (EGFR) that also recognizes the EGFR expressed in cells containing amplification of the EGFR gene. *Int J Cancer* 98(3):398-408.
29. Chao G, Cochran JR, & Wittrup KD (2004) Fine epitope mapping of anti-epidermal growth factor receptor antibodies through random mutagenesis and yeast surface display. *J Mol Biol* 342(2):539-550.
30. Johns TG, *et al.* (2004) Identification of the epitope for the epidermal growth factor receptor-specific monoclonal antibody 806 reveals that it preferentially recognizes an untethered form of the receptor. *J Biol Chem* 279(29):30375-30384.
31. Garrett TP, *et al.* (2009) Antibodies specifically targeting a locally misfolded region of tumor associated EGFR. *Proc Natl Acad Sci U S A* 106(13):5082-5087.
32. Scott AM, *et al.* (2007) A phase I clinical trial with monoclonal antibody ch806 targeting transitional state and mutant epidermal growth factor receptors. *Proc Natl Acad Sci U S A* 104(10):4071-4076.
33. Ogiso H, *et al.* (2002) Crystal structure of the complex of human epidermal growth factor and receptor extracellular domains. *Cell* 110(6):775-787.
34. Ettenberg SA, *et al.* (2010) Inhibition of tumorigenesis driven by different Wnt proteins requires blockade of distinct ligand-binding regions by LRP6 antibodies. *Proc Natl Acad Sci U S A* 107(35):15473-15478.
35. Cochran JR (2010) Engineered proteins pull double duty. *Sci Transl Med* 2(17):17ps15.
36. Muller D & Kontermann RE (2010) Bispecific antibodies for cancer immunotherapy: Current perspectives. *BioDrugs* 24(2):89-98.
37. Muller D & Kontermann RE (2007) Recombinant bispecific antibodies for cellular cancer immunotherapy. *Curr Opin Mol Ther* 9(4):319-326.
38. Khambata-Ford S, *et al.* (2007) Expression of epiregulin and amphiregulin and K-ras mutation status predict disease control in metastatic colorectal cancer patients treated with cetuximab. *J Clin Oncol* 25(22):3230-3237.
39. Baeuerle PA (2011) Constructing bispecifics with improved properties. *Seventh Annual Protein Engineering Summit (PEGS).*

40. Orcutt KD, *et al.* (2011) Engineering an antibody with picomolar affinity to DOTA chelates of multiple radionuclides for pretargeted radioimmunotherapy and imaging. *Nucl Med Biol* 38(2):223-233.

41. Huang PH, *et al.* (2007) Quantitative analysis of EGFRvIII cellular signaling networks reveals a combinatorial therapeutic strategy for glioblastoma. *Proc Natl Acad Sci U S A* 104(31):12867-12872.

42. Kozak M (1977) Nucleotide sequences of 5'-terminal ribosome-protected initiation regions from two reovirus messages. *Nature* 269(5627):391-394.

43. Huang HS, *et al.* (1997) The enhanced tumorigenic activity of a mutant epidermal growth factor receptor common in human cancers is mediated by threshold levels of constitutive tyrosine phosphorylation and unattenuated signaling. *J Biol Chem* 272(5):2927-2935.

44. Ben-Kasus T, Schechter B, Lavi S, Yarden Y, & Sela M (2009) Persistent elimination of ErbB-2/HER2-overexpressing tumors using combinations of monoclonal antibodies: relevance of receptor endocytosis. *Proc Natl Acad Sci U S A* 106(9):3294-3299.

45. Roovers RC, *et al.* (2011) A bi-paratopic anti-EGFR nanobody efficiently inhibits solid tumour growth. *Int J Cancer*.

46. Simister NE & Mostov KE (1989) An Fc receptor structurally related to MHC class I antigens. *Nature* 337(6203):184-187.

47. Harms BD, Bassi GM, Horwitz AR, & Lauffenburger DA (2005) Directional persistence of EGF-induced cell migration is associated with stabilization of lamellipodial protrusions. *Biophys J* 88(2):1479-1488.

4. Design of Downregulating Multispecific Antibody-Fibronectin Fusions

Introduction

Having successfully demonstrated the ability to synergistically downregulate surface EGFR using a combination of antibodies targeting non-overlapping extracellular epitopes on this receptor (1), we wished to enhance this effect by engineering multispecific molecules motivated by our downregulation insights that would be capable of engaging multiple sites on the EGFR extracellular domain. The concept of using bispecific antibodies has been around for the past twenty years, but complications in production, stability, and immunogenicity have hindered their development (2). As detailed in Chapter 3, improved manufacturing strategies and novel recombinant formats have circumvented these obstacles and allowed for the pre-clinical characterization and more recently the clinical development of bispecific therapeutics (3-8).

The canonical model for a bispecific antibody is a molecule with binding sites to two different target antigens. Engaging multiple receptors allows for increased selectivity and specificity of protein therapeutics and permits multi-step targeting strategies in which one site interacts with target antigen and the other site recognizes a toxin, radionuclide, or contrast agent (9). In addition, targeting multiple receptors can improve the affinity of an antibody through avidity effects, improving therapeutic potency and potentially reducing manufacturing costs throughout the drug characterization and commercial development processes.

Accumulating evidence argues for the use of multispecific antibodies targeting distinct epitopes on a single receptor (10-13). In addition to enhancing affinity and specificity, the use of multispecific antibodies against a single target can elicit receptor clustering and downregulation, complementing inherent mechanisms of action of constituent monoclonal antibodies such as ligand inhibition. Clustering is enhanced in the multispecific format compared to combination treatment due to avidity effects. Furthermore, increased valency and functionality of the multispecific format allows for efficient surface clustering with a single agent (See Figure 4.1). An improvement in clustering efficiency may in turn enhance antibody-dependent cell-mediated cytotoxicity (ADCC) and/or complement-dependent cytotoxicity (CDC) through formation of

large antibody-receptor complexes. In support of this hypothesis, enhanced CDC activity function was observed following combination treatment with non-competitive EGFR-targeted antibodies (11).

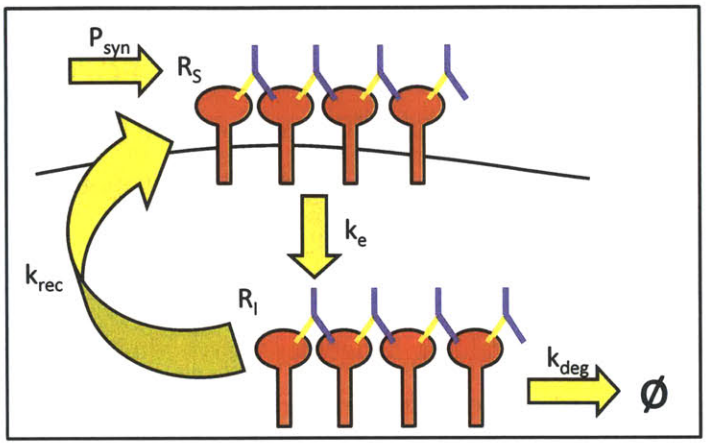

Figure 4.1. Modulation of EGFR trafficking via multispecific antibody treatment. A basic model of receptor clustering and trafficking following treatment with a bispecific antibody targeting two non-overlapping epitopes on EGFR is shown. Note that in contrast to the requirement for two mAbs to propagate crosslinking, a single bispecific antibody can efficiently cluster surface receptor. Trafficking parameters and species are indicated. EGFR can be surface-bound (R_S) or internal (R_I). Receptor is synthesized with a rate P_{syn}, internalized with rate k_e, recycled back to the surface with rate k_{rec}, and degraded with rate k_{deg}.

Numerous formats have been employed in the development of multispecific antibodies, as discussed in Chapter 3. To create compounds with two or more specificities, we chose to use a full human IgG1 with appended single-domain binding moieties to retain the benefits of the antibody format such as stability, lack of immunogenicity, and long serum halflife. Indeed we showed robust secretion of an IgG-scFv fusion in Chapter 3. An alternative approach we pursued involved the design of IgG fusions to fibronectin domain variants. Our results with combinations of EGFR-targeted antibodies suggested that a multispecific strategy that included at least one ligand-competitive antibody would be optimal (1). We consequently fused the clinically approved human mAb 225 (cetuximab) with variants of the tenth type III domain of human fibronectin (Fn3) that recognize EGFR (14). Fn3 is a 94 amino acid (≈10 kDa) soluble beta-sandwich protein with three solvent-exposed variable loops, similar to an scFv. The domain natively functions in molecular recognition and can be engineered to bind a variety of target antigens (15). Head-to-tail fusion of Fn3 domains maintains them in their native conformation (16, 17), allowing fusion to multidomain proteins to design multispecific constructs. We thus fused Fn3 domains to full-length IgG to establish multispecific antibody-fibronectin fusions (hereafter referred to as Ab-Fn3 fusions) that would induce downregulation of EGFR.

In previous work, Hackel *et al* used directed evolution on the yeast surface display platform to isolate three non-competitive variants of the Fn3 domain that bind to EGFR on three different

extracellular domains (See Figure 4.2, Tables 4.1, 4.2) (14). Clone A binds domain 1, clone B binds domain 3, the ligand binding domain, and clone D binds at the domain 3/4 interface. These Fn3 variants bind EGFR with nanomolar or sub-nanomolar affinity, as detailed in Table 4.2. When fused head-to-tail separated by a flexible linker to form heterobivalent constructs, Fn3 clones induce moderate levels of EGFR downregulation in the absence of receptor or downstream agonism. These clones also synergize with 225 to inhibit migration and proliferation of cells that secrete autocrine EGF, simulating the tumor environment (18). In particular, a fusion of clones A and D where A is N-terminal potently inhibits both migration and proliferation (≈80%) in the presence of 225 (14). Fusing these Fn3 constructs to the full 225 IgG would capture this synergy and potentially enhance it via improvement in clustering and, consequently, downregulation. Furthermore, the presence of the antibody Fc domain would aid in the persistence of these fusions in the bloodstream via neonatal Fc receptor recycling (19) and could facilitate immune cell recruitment, rendering Ab-Fn3 fusions superior to heterobivalent fibronectin fusions as therapeutic compounds. The modular structure and design of these constructs could allow for them to form the basis for a new generation of antibody-based therapeutics against EGFR or other receptor targets.

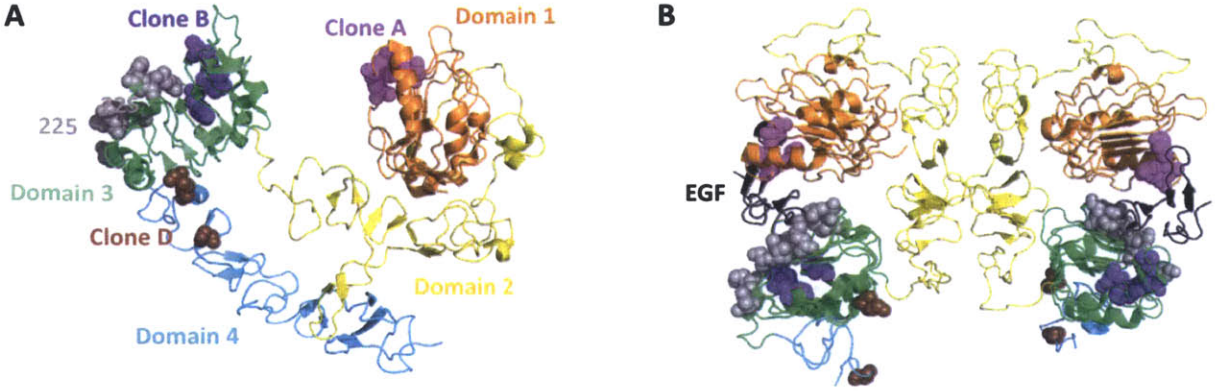

Figure 4.2. EGFR binding epitopes of engineered Fn3 domains. The binding locations of the three non-competitive fibronectin clones were identified using yeast surface display-based fine epitope mapping (20). The epitopes of clone A (magenta), clone B (violet), and clone D (brown) are depicted as spheres on the EGFR ectodomain in the tethered monomeric (A) or active dimeric conformation (B). The 225 antibody epitope is shown in gray (21). Domains 1 (orange), 2 (yellow), 3 (22), and 4 (cyan) of the EGFR extracellular domain are displayed, with the EGF binding site shown in black on the dimeric receptor. The monomeric and dimeric structures are adapted from 1nql (23) and 1ivo (24), respectively. Epitopes were obtained from (14).

Protein	EGFR Binding Domain(s)	Epitope
Fn3 Clone A	I	L14, Q16, Y45, H69
Fn3 Clone B	III	I327, V350M, F352V, W386R
Fn3 Clone D	III/IV	K430, S506
mAb 225	III	Q384, Q408, H409, K443, K465, I467, N473

Table 4.1. Binding epitopes of Fn3 moieties. Residues implicated in the binding of the EGFR targeted fibronectin clones were identified using yeast surface display-based fine epitope mapping (20). The 225 epitope from the published crystal structure of the bound Fab fragment is also listed (21). Data obtained from (14).

	Sequence				K_d [nM]
Fn3 Clone	**BC Loop**	**DE Loop**	**FG Loop**	**Framework**	**A431, pH 7.4**
A	FDYAVTY	GWIST	DNSHWPFRST	I90T	0.26 ± 0.13
B	YGFSLASS	RSPWF	SNDFSNRYSG	-	30 ± 3
D	LHHRSDVRS	GSRSL	WGSYCCSN	E47K	0.25 ± 0.05

Table 4.2. Sequences and binding affinities of engineered Fn3 domains. Sequences of the three variable loops and framework mutations for the three EGFR-targeted Fn3 clones are indicated. The affinity of each clone was determined through titration on the surface of A431 cells at pH 7.4 (20). Data obtained from (14).

Results

Expression of Bispecific Ab-Fn3 Fusions

Bispecific Ab-Fn3 fusions were designed by conjugating a single Fn3 domain (A, B, or D) at the four possible termini of the 225 human IgG1 backbone (heavy chain N or C terminus and light chain N or C terminus), separated by a flexible $(Gly_4Ser)_2$ linker. The design of these modular constructs is depicted in Figure 4.3. Constructs are named according to the position of Fn3 conjugation followed by the designation of the clone used (*e.g.* HN-A).

The 180 kDa Ab-Fn3 fusions were secreted from human embryonic kidney (HEK) 293 cells co-transfected with the appropriate heavy and light chain expression plasmids. Sequences for these plasmids in all four constuct orientations are provided in Appendix C. Antibodies were purified via protein A affinity chromatography and analyzed via SDS-PAGE for purity. A representative SDS-PAGE for Ab-Fn3 fusion constructs in the four bispecific orientations is shown in Figure 4.4A.

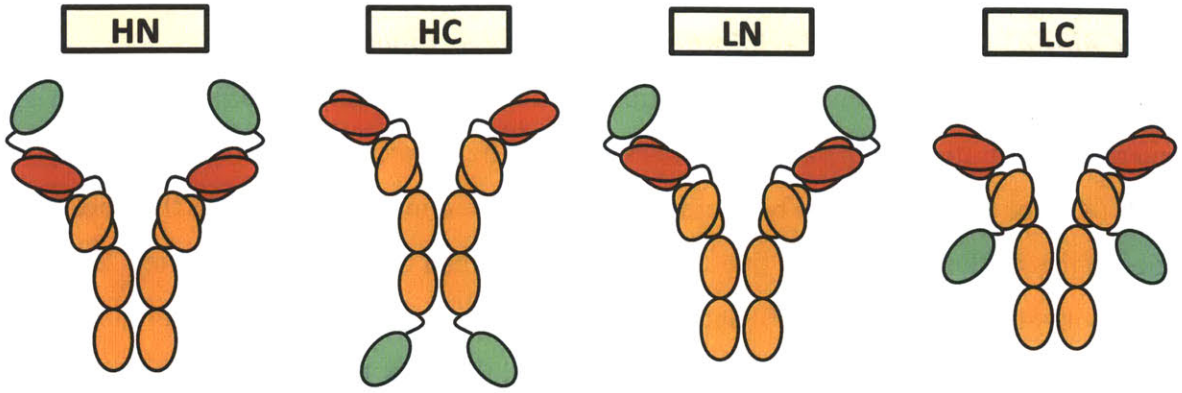

Figure 4.3. Bispecific Ab-Fn3 fusion orientations. The 225 human IgG1 isotype backbone is used as a scaffold for engineering Ab-Fn3 fusions. The heavy chain consists of three constant domains (CH1, CH2, and CH3) and one variable domain (VH), whereas the light chain consists of one constant domain (CL) and one variable domain (VL). The tenth type III domain of human fibronectin (Fn3), shown in green, is fused to the heavy or light chain at the N or C terminus with a flexible linker and the fusion constructs are named as indicated. Antibodies are assembled in vitro in two-to-two complexes of heavy and light chain moieties, linked by three disulfide bonds. The full sequences of the plasmids used to prepare the heavy and light chains of bispecific Ab-Fn3 fusions are provided in Appendix C.

Bispecific Ab-Fn3 yields ranged from 1 - 10,000 μg/L depending on antibody format and the Fn3 clone used. In general, fusions in the HN orientation secreted the most robustly for all three Fn3 moieties and fusions in the LN orientation secreted at the lowest levels. The HC and LC fusions secreted equally well but yields were at least 100-fold less than those of HN fusions (Figure 4.4B). In fact, Fn3 fusion in the HN orientation appeared to rescue secretion as HN constructs secreted at five- to tenfold higher levels than the unconjugated 225 antibody. Consequently, we selected HN fusions for extensive characterization and follow-up.

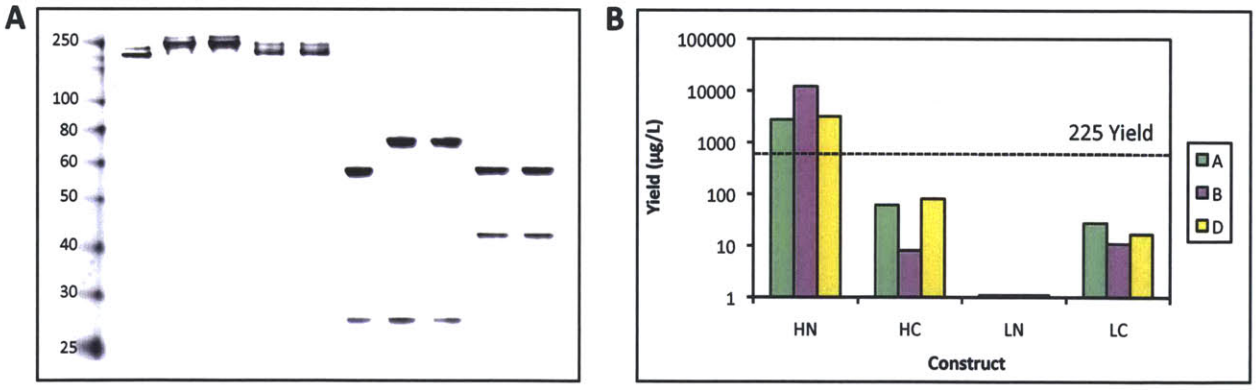

Figure 4.4. Bispecific Ab-Fn3 fusion yields. (A) SDS-PAGE analysis of a representative protein A-purified secreted Ab-Fn3 fusion. The 225 mAb and the HN-D, HC-D, LN-D, and LC-D constructs were visualized in the non-reduced (left) and reduced (right) states. Reference molecular weights in kDa are shown in the left lane. (B) Summary of Ab-Fn3 bispecific fusion yields. The specified Fn3 clones (A, B, or D) were fused in the indicated orientation and yield was quantified based on 280 nm absorbance. Yield of the base 225 IgG is marked with a dashed line.

Bispecific Ab-Fn3 Fusions Bind EGFR with Sub-Nanomolar Affinity

The interaction between Ab-Fn3 fusion constructs and their target antigen, EGFR, was characterized by titration on the surface of A431 cells. The apparent equilibrium dissociation constants (K_d) for all secreted HN bispecific fusions are listed in Table 4.3. Note that the affinities of the Ab-Fn3 fusions are five- to tenfold tighter than that of the unmodified 225 antibody, both at endosomal pH (6.0) and physiological pH (7.4). Insensitivity of binding to pH reduction indicates that the constructs will remain bound to EGFR following internalization. The measured K_d values fall in the tens to hundreds picomolar to hundreds of picomolar range, corresponding with binding half-lives on the order of days.

Construct	K_d, A431 pH 6.0	K_d, A431 pH 7.4
225	3.7×10^{-10} M	1.2×10^{-9} M
HN-A	1.9×10^{-10} M	2.4×10^{-10} M
HN-B	2.4×10^{-11} M	6.1×10^{-11} M
HN-D	4.0×10^{-11} M	7.5×10^{-11} M

Table 4.3. Bispecific Ab-Fn3 fusion binding kinetics. Due to avidity effects that emanate from the dual specificity of the Ab-Fn3 fusion, these novel constructs generally have higher affinity for EGFR. Samples were titrated at the indicated pH on the surface of A431 cells, which express 2.8×10^6 EGFR per cell (1). K_d values from nonlinear least squares regression fits to a 1:1 binding isotherm are listed.

Bispecific Ab-Fn3 Fusions Substantively Downregulate EGFR

To evaluate the ability of bispecific fusions to induce EGFR downregulation, we performed downregulation assays on the seven cell lines used in our combination antibody screen described in Chapter 2. Downregulation levels were compared to those induced by treatment with the most active combination of antibodies, 225+H11.

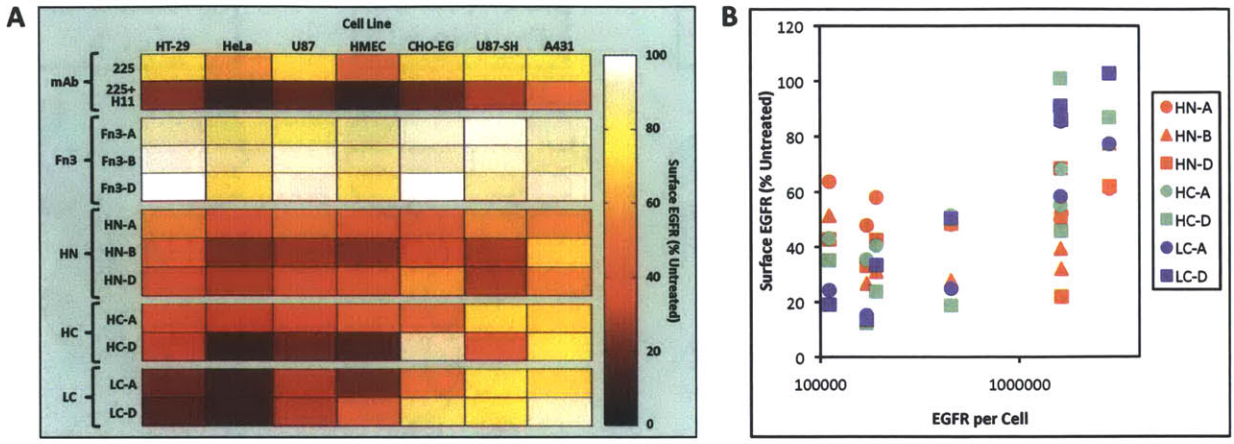

Figure 4.5. Surface EGFR downregulation following bispecific Ab-Fn3 treatment. (A) Seven EGFR expressing cell lines (listed in increasing order of receptor density) were treated with 20 nM of the specified constructs for 13 h at 37°C. Cells were then acid stripped, relabeled for EGFR, and analyzed via flow cytometry. Percent surface receptor remaining relative to an untreated control is shown. (B) Relative surface receptor remaining plotted against receptor density for each Ab-Fn3 fusion.

We found that HN, HC, and LC fusions induced appreciable levels of receptor downregulation, but none were as potent as the 225+H11 combination, particularly on cell lines with high receptor density (Figure 4.5A). In the case of HC and LC fusions, the extent of downregulation was inversely correlated with receptor density, whereas HN fusion downregulation was consistent across the panel of cell lines (Figure 4.5B). As expected, monovalent Fn3 domains did not elicit EGFR downregulation; The multivalent fusion format was required.

Expression of Tri- and Tetraspecific Ab-Fn3 Fusions

To increase the valency and potentially enhance fusion-mediated clustering through avidity effects, we conjugated additional Fn3 domains to the 225 IgG scaffold. Given three non-competitive Fn3 domains plus the 225 variable domain, we have the ability to target four unique epitopes on EGFR. We consequently designed both trispecific and tetraspecific molecules in the four orientations shown in Figure 4.6. Cis-trispecifics fuse two Fn3 domains to the HN position, trans-trispecifics consist of one HN and one LC Fn3 fusion, double HC trispecifics include one HN and one HC Fn3 domain, and tetraspecifics contain one HN, one HC, and one LC Fn3 moiety. LN fusion was avoided due to low secretion levels. As with the bispecifics, tri- and tetraspecific constructs were secreted from HEK 293 cells co-transfected with heavy and light chain plasmids and purified via protein A affinity chromatography.

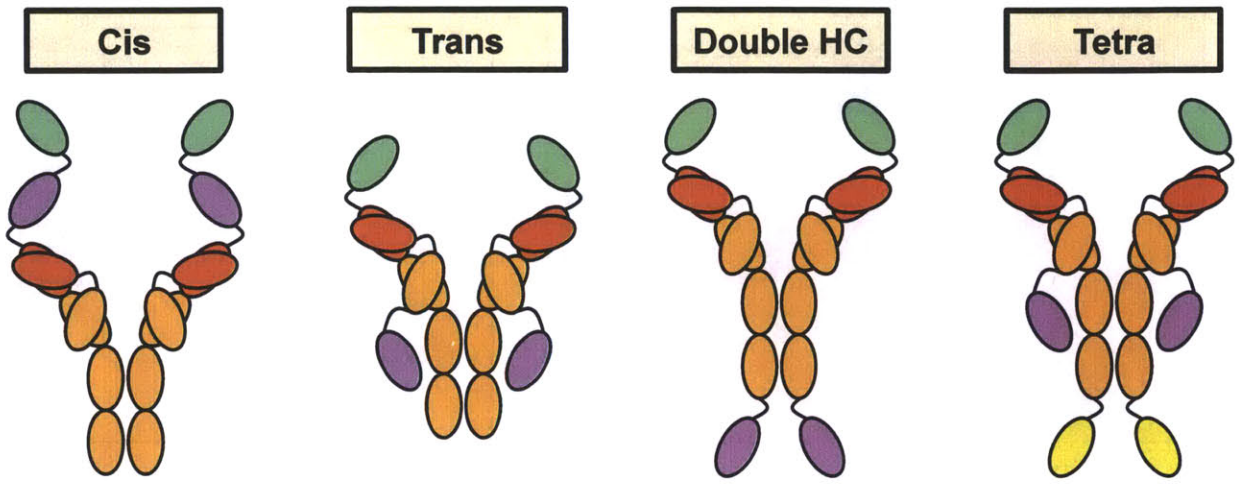

Figure 4.6. Tri- and tetraspecific Ab-Fn3 fusion orientations. The 225 human IgG1 isotype backbone (constant dpmains in orange and variable domains in red) was fused to two or three Fn3 domains (green, magenta, and yellow) at the positions shown. Three trispecific and one tetraspecific constructs were secreted from HEK 293 cells. The full sequences of the plasmids used to prepare the heavy and light chains of these multispecific Ab-Fn3 fusions are provided in Appendix C.

The yields of these 200-225 kDa antibodies varied from 5 to 5000 μg/L depending on both the fusion format and the Fn3 clone position. SDS-PAGE analyses of protein A-purified constructs from each orientation are shown in Figure 4.7A. Note the non-reduced Ab-Fn3 fusion constructs run at higher molecular weights than unconjugated IgG, with heavy and light chain bands at the expected molecular weights in the reduced samples. Based on the robust expression of fusions with Fn3 domains at the heavy chain N terminus, we used HN fusions as a basis for all four formats. The cis- and trans-trispecific fusions secreted best, whereas yields for the double HC-trispecific and the tetraspecific formats were ten- to 100-fold lower. Notably, secretion of the cis- and trans-trispecific fusions was superior to that of the unmodified 225 antibody by three- to six-fold (Figure 4.7B).

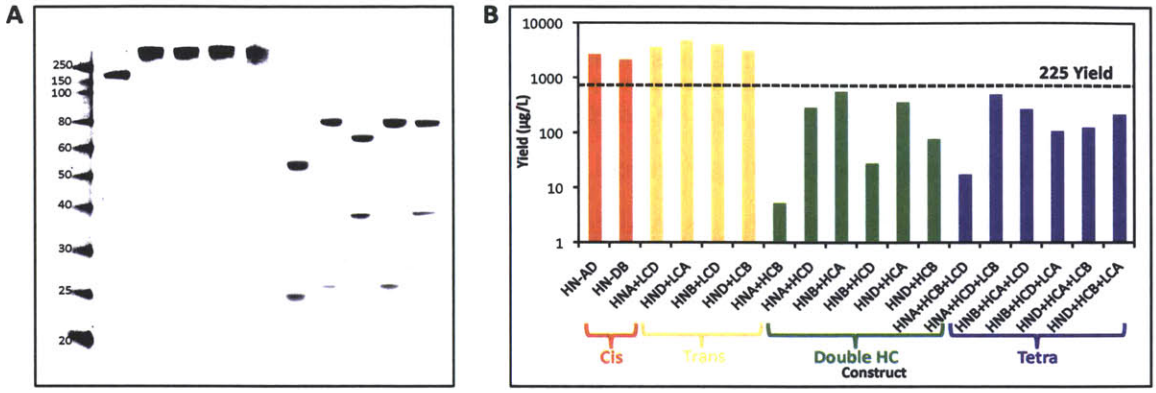

Figure 4.7. Tri- and tetraspecific Ab-Fn3 fusion yields. (A) SDS-PAGE analysis of a representative protein A-purified secreted Ab-Fn3 fusion from each of the four categories: cis-trispecific (HN-AD); trans-trispecific (HNA+LCD); double HC-trispecific (HNB+HCA); and tetraspecific (HNB+HCD+LCA). The 225 mAb is shown for molecular weight comparison and a standards ladder is provided in the left lane. All constructs were visualized under non-reducing (left) and reducing (right) conditions. (B) Summary of multispecific Ab-Fn3 fusion yields. The specified Fn3 clones (A, B, or D) were fused in the indicated orientation and yield from HEK 293 cell secretion was quantified based on 280 nm absorbance. Expression level of the base 225 IgG is marked with a dashed line.

Trans-Trispecific Ab-Fn3 Fusions Bind EGFR with Sub-Nanomolar Affinity

We characterized the binding kinetics of the two well-secreted classes of multispecific fusions, the cis- and trans-trispecifics, on the surface of A431 cells (Table 4.4).

Construct	K_d, A431 pH 6.0	K_d, A431 pH 7.4
225	3.7×10^{-10} M	1.2×10^{-9} M
HN-AD	1.3×10^{-9} M	1.3×10^{-9} M
HN-DB	1.2×10^{-10} M	1.6×10^{-9} M
HNA+LCD	1.7×10^{-10} M	2.8×10^{-10} M
HND+LCA	3.9×10^{-10} M	2.1×10^{-10} M
HNB+LCD	2.1×10^{-10} M	2.0×10^{-10} M
HND+LCB	1.2×10^{-10} M	2.9×10^{-10} M

Table 4.4. Trispecific Ab-Fn3 fusion binding kinetics. The binding kinetics of cis- and trans-trispecific Ab-Fn3 fusions were characterized on the surface of A431 cells. Fusions were titrated at the indicated pH and apparent K_d values computed from a nonlinear least squares regression fit to a 1:1 binding isotherm are presented.

Surprisingly, cis-trispecifics bind EGFR with a slightly weaker affinity than the 225 base antibody, perhaps due to impaired interaction in the presence of three proximal binding moieties. In contrast, the trans-trispecifics had five- to tenfold tighter EGFR affinities than the base 225 antibody, with apparent equilibrium dissociation constant values in the hundreds of picomolar range (half-lives on the order of days). Consistent with the bispecific constructs, the trispecific Ab-Fn3 fusions bind with similar kinetics at physiological and endosomal pH, suggesting robust receptor interaction both on the cell surface and in the cytoplasm. Interestingly, trispecific Ab-Fn3 binding affinity does not depend on fibronectin clone orientation.

Multispecific Ab-Fn3 Fusions Potently Downregulate Surface EGFR

To determine which tri- and tetraspecific constructs most effectively downregulate surface receptor, we compared the performance of all secreted fusions on four different EGFR-expressing cell lines. As demonstrated in Figure 4.8, the most effective fusions are in the trans-trispecific and tetraspecific format. The cis- and double HC-trispecific fusions perform approximately equivalently to the bispecific fusions. Within the trans-trispecific constructs, HNA+LCD, HND+LCA, and HNB+LCD outperform HND+LCB and within the tetraspecific fusions, those with clone B at the HN position elicit the most potent downregulation. The most potent trans-trispecific and tetraspecifc downregulate as efficiently or better than the 225+H11 mAb combination identified from downregulation screens described in Chapter 2.

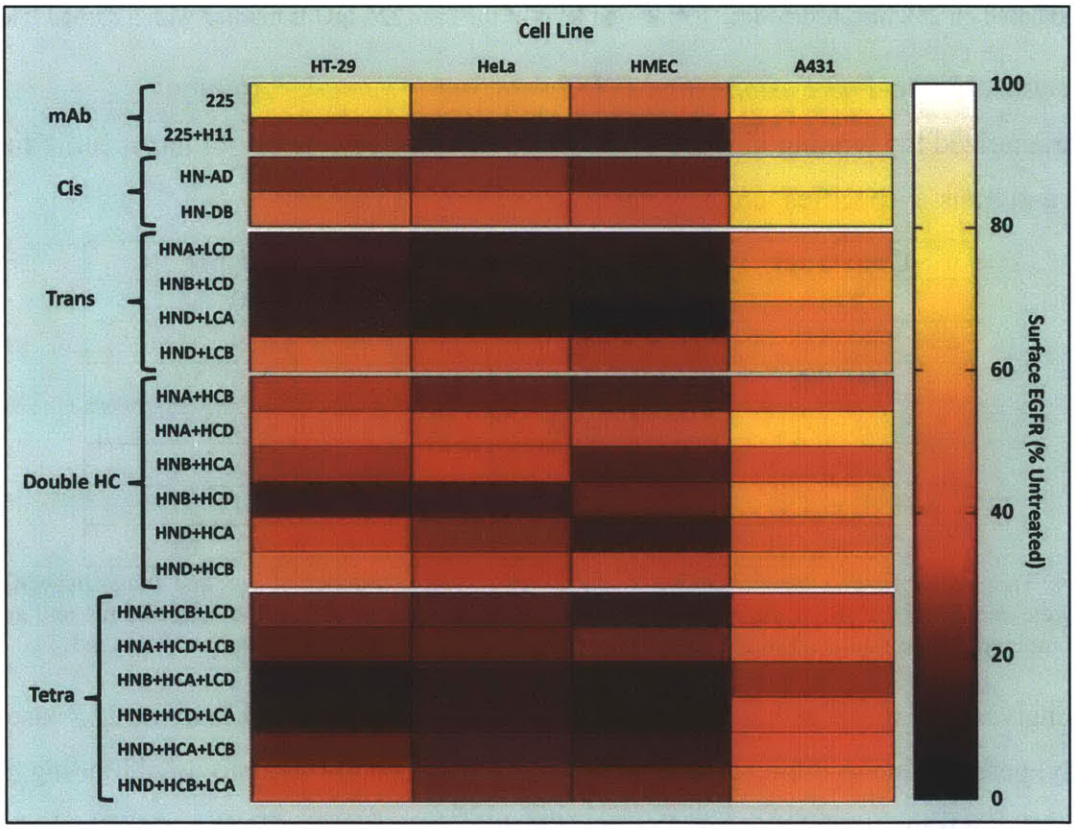

Figure 4.8. Surface EGFR downregulation following tri- and tetraspecific Ab-Fn3 treatment. Four EGFR expressing cell lines (listed in order of increasing receptor density) were treated with 20 nM of the specified constructs from the four engineered tri- and tetraspecific orientations. Incubation proceeded for 13 h at 37°C. Cells were subsequently acid stripped to remove surface-bound Ab-Fn3, re-labeled for EGFR, and analyzed via flow cytometry. Percent surface receptor remaining relative to an untreated control is shown. Surface EGFR levels following incubation with either mAb 225 or the potently downregulating 225+H11 mAb combination are provided for reference.

Based on our multispecific downregulation screen, the two classes of constructs with the highest downregulation capacity are the trans-trispecifics and the tetraspecifics. Due to secretion limitations for tetraspecific compounds, we selected the trans-trispecifics for further characterization and therapeutic evaluation.

The trans-trispecific fusions were comprehensively analyzed on a panel of 13 EGFR-expressing cell lines of varying origins and receptor densities (Table 4.5). As demonstrated in Figure 4.9A, three out of the four trans-trispecific constructs (HNA+LCD, HND+LCA, and HNB+LCD) downregulate surface receptor by 80-90% in all cell lines examined, with the notable exception of the most EGFR-dense cell line, A431, where downregulation stands at only 40-50%. Other than the A431 anomaly, however, receptor density and downregulation are uncorrelated for trans-trispecific treatment (Figure 4.9B). We also note that the HND+LCA construct downregulates most actively and consistently across the examined cell lines while the HND+LCB shows the weakest downregulation amongst the trans-trispecifics examined.

Cell Line	Origin	EGFR/cell
HT-29	Colorectal Carcinoma	1.1E+05
Hela	Cervical Carcinoma	1.7E+05
U87	Glioblastoma	1.9E+05
BT-20	Triple Negative Breast Cancer	2.4E+05
HCT-116	Colorectal Carcinoma	2.4E+05
Hs578T	Triple Negative Breast Cancer	3.0E+05
BT-549	Triple Negative Breast Cancer	4.1E+05
HMEC	Human Mammary Epithelium	4.5E+05
MD-MBA-231	Triple Negative Breast Cancer	5.9E+05
A549	Lung Carcinoma	1.2E+06
CHO-EG	Chinese Hamster Ovary	1.6E+06
U87-SH	Glioblastoma	1.6E+06
A431	Epidermoid Carcinoma	2.8E+06

Table 4.5. EGFR surface expression levels of downregulation panel cell lines. Thirteen EGFR-expressing cell lines of varying mammalian origins (both normal and transformed) were assessed for EGFR expression via quantitative flow cytometry. The calculated number of receptors per cell is indicated for each line.

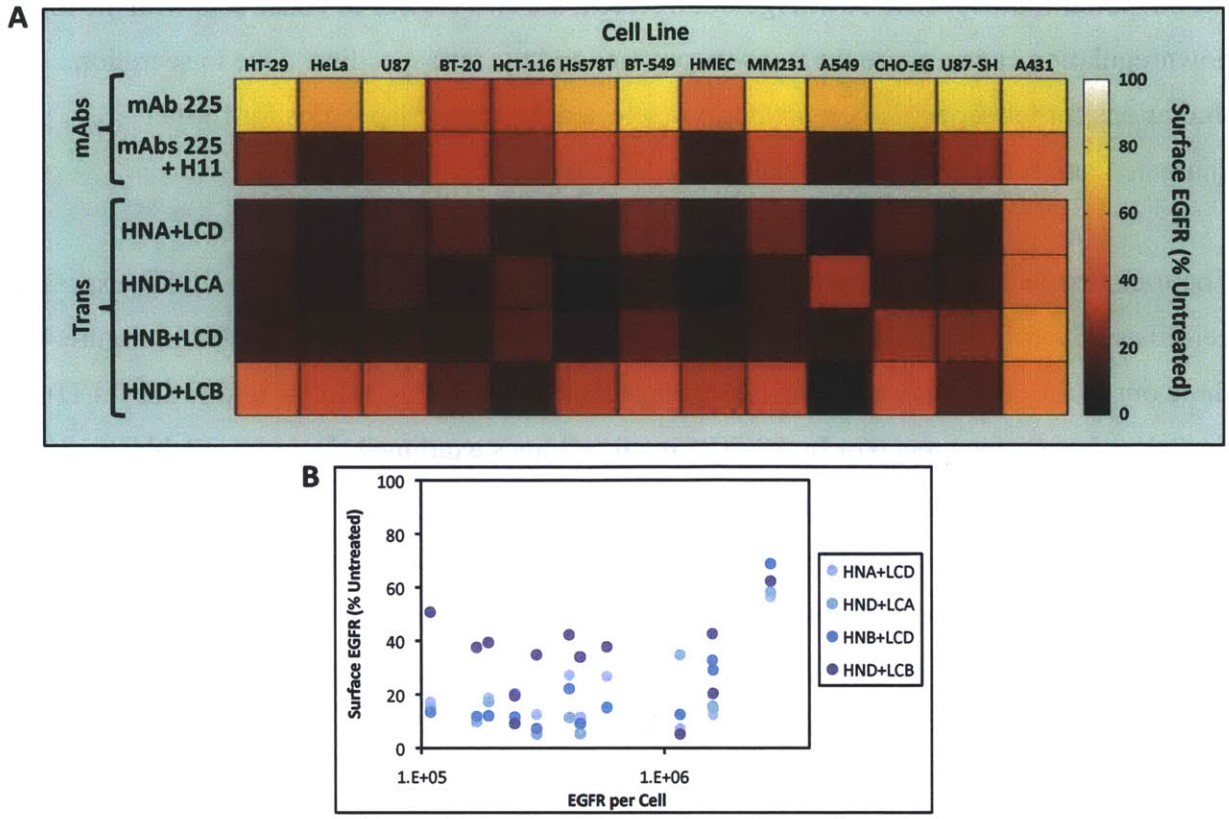

Figure 4.9. Surface EGFR downregulation following trans-trispecific Ab-Fn3 treatment. (A) Thirteen EGFR-expressing cell lines (listed in order of increasing receptor density) were treated with 20 nM of trans-trispecifics or the indicated mAbs for 13 h at 37°C. Cells were then acid stripped, re-labeled for EGFR, and analyzed via flow cytometry. Percent surface receptor remaining relative to an untreated control is shown. (B) Relative surface receptor remaining at steady state from (A) plotted against receptor density for each trans-trispecific Ab-Fn3 fusion.

Multispecific Ab-Fn3 Fusions Rapidly and Efficiently Cluster EGFR

As was done with 225+H11 combination mAb treatment, we examined Ab-Fn3 fusion treated cells for evidence of clustering. Deconvolution microscopy images show a dramatic change in receptor localization following Ab-Fn3 fusion treatment relative to 225 mAb treatment in two EGFR-expressing tumor cell lines, indicative of receptor clustering.

In A431 cells, we find that clusters appear within 1 h of Ab-Fn3 treatment and to persist for at least 6 h (Figure 4.10A). Also, based on isolation of 0.15 μm z-sections through the cell monolayer in HT-29 cells treated with the HND+LCA construct, we observe that receptor-Ab-Fn3 fusion clusters are located both intracellularly and extracellularly (Figure 4.10B). In A549 cells, we monitored the evolution of clusters over a 21-minute timecourse (Figure 4.10C). As early as 9 minutes post-treatment, puncta are visible. These clusters increase in size and quantity over time.

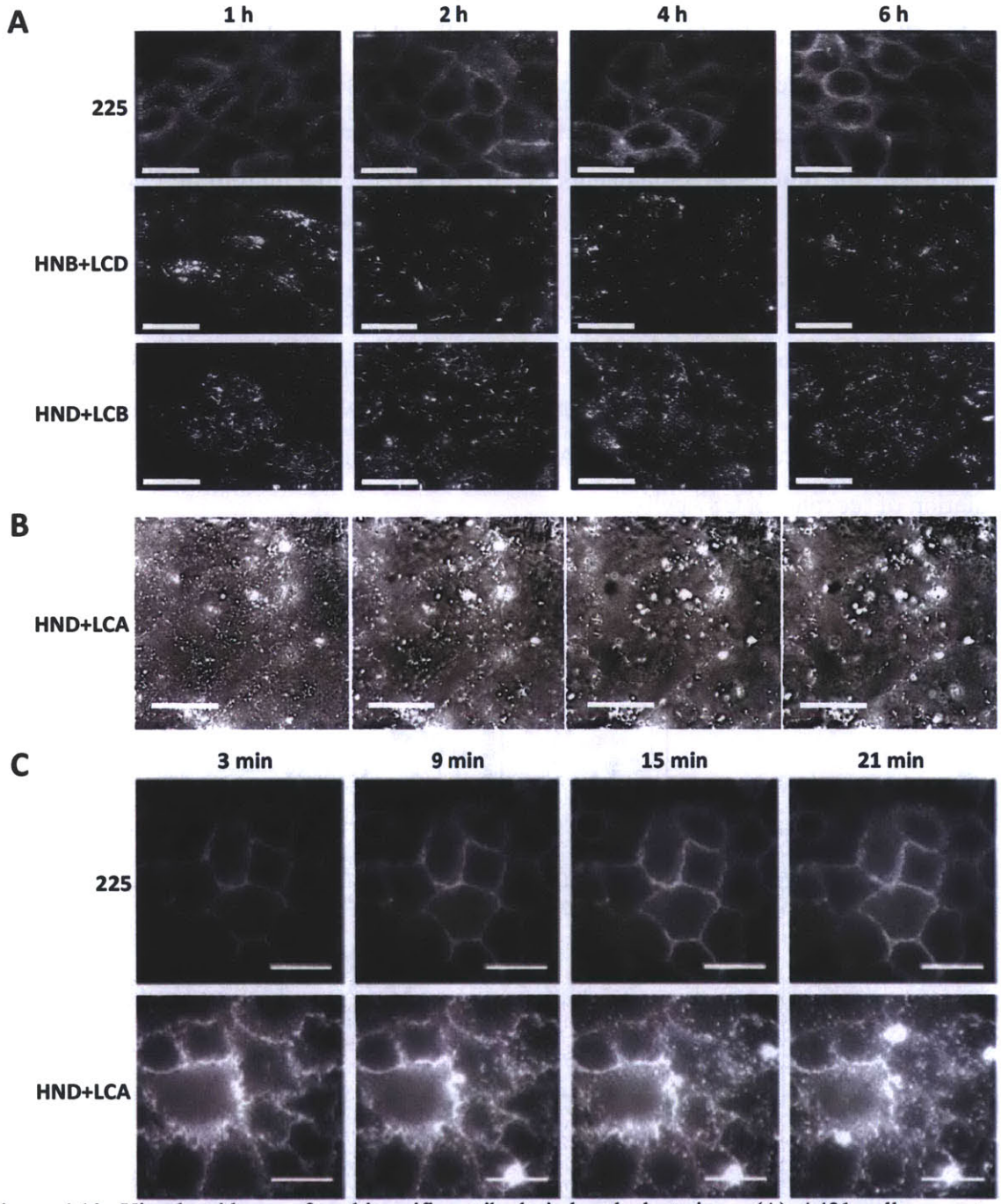

Figure 4.10. Visual evidence of multispecific antibody-induced clustering. (A) A431 cells were treated with fluorescently-labeled 225 or fluorescently-labeled trans-trispecific Ab-Fn3 fusion for the indicated time periods at 37°C. Cells were then washed to remove unbound antibody and imaged on a DeltaVision deconvolution microscope for comparison of EGFR localization. Images reflect projections of deconvolved 0.15 μm thick z-sections through the cell monolayer. Scale bars = 30 μm. (B) HT-29 cells were incubated with fluorescently-labeled HND+LCA for 6 h at 37°C. Cells were washed and imaged on a DeltaVision deconvolution microscope. Images represent deconvolved 0.15 μm thick sections ranging from the bottom (left) to the top (right) of the cell with 1.5 μm spacing between sections. Scale bars = 30 μm. (C) Fluorescently-labeled 225 or HND+LCA was added to live A549 cells and cells were imaged over a 30 minute timecourse to track cluster formation. Images reflect projections of deconvolved 0.15 μm thick z-sections through the cell monolayer. Scale bars = 30 μm.

Ab-Fn3 Fusion Treatment Increases the Rate of EGFR Internalization

As detailed in Chapter 2 and Appendix A, antibody-mediated downregulation can occur by one of three mechanisms: reduction of receptor synthesis rate; increase in receptor internalization rate; or reduction in recycled fraction. Recall that in the case of monoclonal antibody combination treatment, downregulation occurs as a result of recycling inhibition; Endocytosis rate is not affected.

In the case of bispecific Ab-Fn3 fusion treatment (HN-D construct), internalization is accelerated, as occurs upon the addition of EGF ligand (Figure 4.11A). The endocytosis rate enhancement increases for constructs of higher valency. As shown in Figure 4.11B-C, the trans-trispecific fusions HNB+LCD and HND+LCA, respectively, elicit robust and rapid downregulation of receptor in U87 cells.

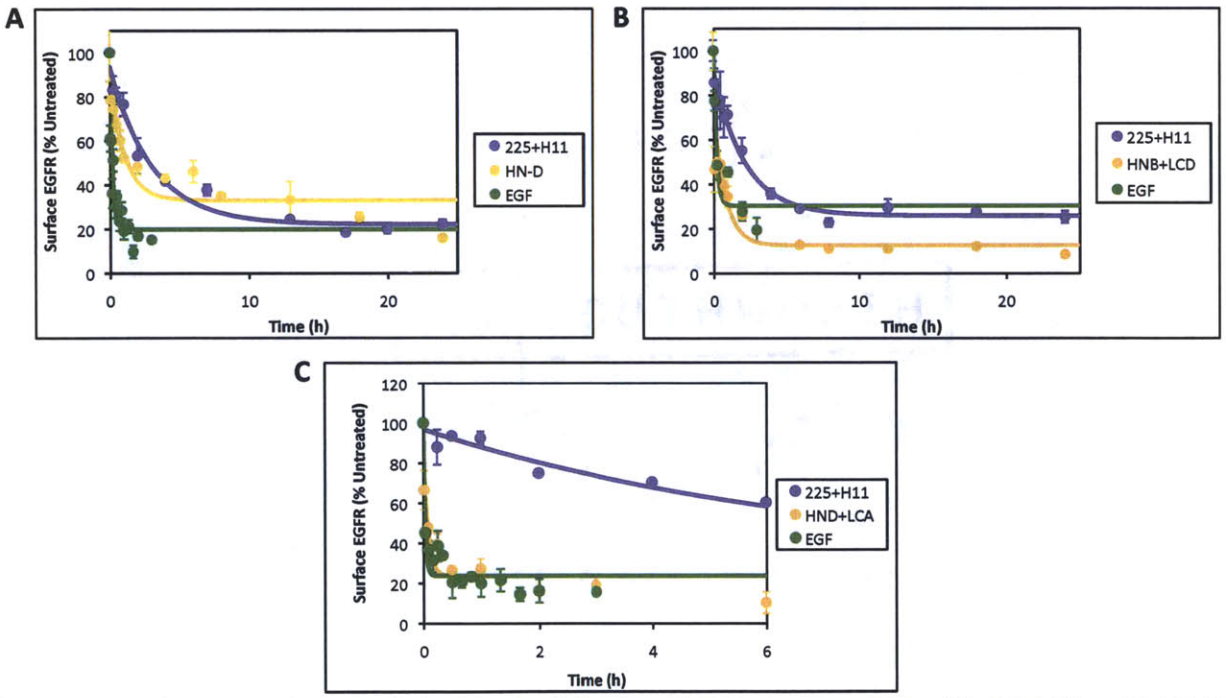

Figure 4.11. Surface EGFR downregulation kinetics following Ab-Fn3 treatment. HeLa (A), U87 (B), or HT-29 (C) cells were treated with the mAb combination 225+H11, the Ab-Fn3 fusion HN-D (A), HNB+LCD (B), HND+LCA (C), or EGF at 37°C for the indicated time periods. Cells were then detached and acid stripped. Surface EGFR was relabeled with murine 225 and quantified via flow cytometry. Percent surface receptor remaining relative to an untreated control is shown (±SD; n=3). Data was fit to first-order exponential curves using nonlinear least squares regression.

Thus, in contrast to combination antibody treatment, Ab-Fn3 fusion treatment increases the endocytic rate constant for EGFR. Notably, the acceleration of endocytosis for HN-D, HNB+LCD, and HND+LCA is still less dramatic than that induced by EGF treatment ($t_{1/2, EGF}$ = 0.13 h, $t_{1/2, HN\text{-}D}$ = 0.74 h, and $t_{1/2, 225+H11}$ = 2.12 h in HeLa cells; $t_{1/2, EGF}$ = 0.14 h, $t_{1/2, HNB+LCD}$ = 0.56 h, and $t_{1/2, 225+H11}$ = 1.52 h in U87 cells; and $t_{1/2, EGF}$ = 0.022 h, $t_{1/2, HND+LCA}$ = 0.054 h, and $t_{1/2, 225+H11}$ = 4.8 h in HT-29 cells). Note that in the case of both the HNB+LCD and the HND+LCA trans-trispecifics, treatment results in a lower steady-state surface receptor level than EGF or 225+H11 treatment, suggestive of the recruitment of additional downregulatory mechanisms, such as recycling inhibition.

Ab-Fn3 Fusion Treatment Inhibits Endosomal Recycling of EGFR

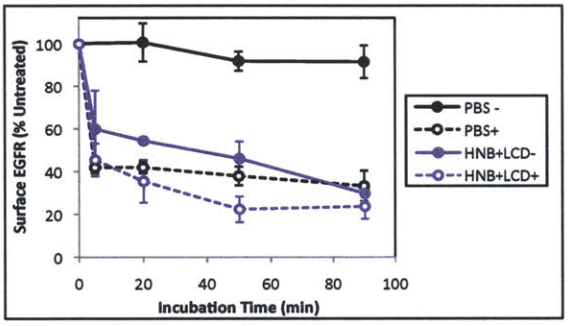

Figure 4.12. Trans-trispecific treatment inhibits EGFR recycling. U87 cells were incubated with PBS or 20 nM HNB+LCD in the presence or absence of 200 μM monensin (a non-specific inhibitor of receptor recycling) at 37°C for the indicated time periods. Cells were then detached and acid stripped to remove surface-bound Ab-Fn3. Surface EGFR was labeled with murine 225 and analyzed by flow cytometry. Percent surface receptor remaining relative to an untreated cells is plotted (±SD; n=3). "-" indicates the absence and "+" indicates the presence of monensin.

In addition to enhancing endocytic rate, treatment with Ab-Fn3 fusion constructs interferes with receptor recycling, consistent with the mechanism of mAb combination-induced downregulation. By adding the ionophore monensin to inhibit EGFR recycling, we show that HNB+LCD treatment in the presence or absence of monensin (25) elicits an equivalent response to monensin treatment alone. Thus, trans-trispecific fusions fully obstruct EGFR recycling within 90 minutes of treatment, shunting the receptor to lysosomal degradation (Figure 4.12).

Ab-Fn3 Fusions Exhibit Similar Distribution Kinetics to mAbs

Efficient penetration of antibody into solid tumors is critical for the efficacy of therapeutics targeting cell surface antigens (26, 27). We consequently addressed transport considerations for

our Ab-Fn3 fusion compounds compared to unconjugated IgG using tumor spheroid models (28).

Recent work by Thurber *et al* established a Thiele modulus to describe antibody penetration. This dimensionless parameter represents the ratio of antibody internalization rate to diffusion rate (29). The Thiele modulus (ϕ^2) can be expressed as:

$$\phi^2 = \frac{k_e R^2 [Ag]/\varepsilon}{D([Ab]_{surf} + K_d)} \qquad \text{(Equation 1)}$$

where k_e is the net endocytic uptake rate constant, R is the half-maximum intercapillary distance, [Ag] is the antigen concentration per tumor volume, ε is the drug-accessible tumor volume fraction, D is the drug diffusivity in tumor tissue, $[Ab]_{surf}$ is the antibody concentration at the capillary surface, and K_d is the equilibrium dissociation constant of the antibody. Antibody penetration depth can be determined by setting the Thiele modulus equal to 1, resulting in the following equation:

$$R = \sqrt{\frac{D([Ab]_{surf} + K_d)}{k_e R^2 [Ag]/\varepsilon}} \qquad \text{(Equation 2)}$$

If we assume that diffusivity and K_d of the IgG and Ab-Fn3 are approximately equivalent, the only parameters that differ between mAb treatment and Ab-Fn3 treatment are k_e and [Ag].

From our kinetic assays, we find that EGFR internalization is enhanced approximately threefold compared to constitutive internalization following Ab-Fn3 administration. However, Ab-Fn3 treatment concurrently introduces a new steady state in which surface receptor levels are reduced by 70-80% (three- to fivefold). As a result, the enhanced internalization rate precisely counterbalances the reduction in surface antigen expression, leading us to predict from our dimensional analysis that penetration of Ab-Fn3 fusions will be equivalent to that of mAbs.

To test this hypothesis, we formed hanging spheroids composed of A431 cells and visualized antibody perfusion via confocal microscopy. As shown in Figure 4.13, treatment with equivalent saturating concentrations of both mAb and Ab-Fn3 fusion (HN-D) resulted in a homogenous

distribution of these constructs throughout A431 tumor cell spheroids, confirming that conjugation of Fn3 domains to induce downregulation does not impair antibody delivery.

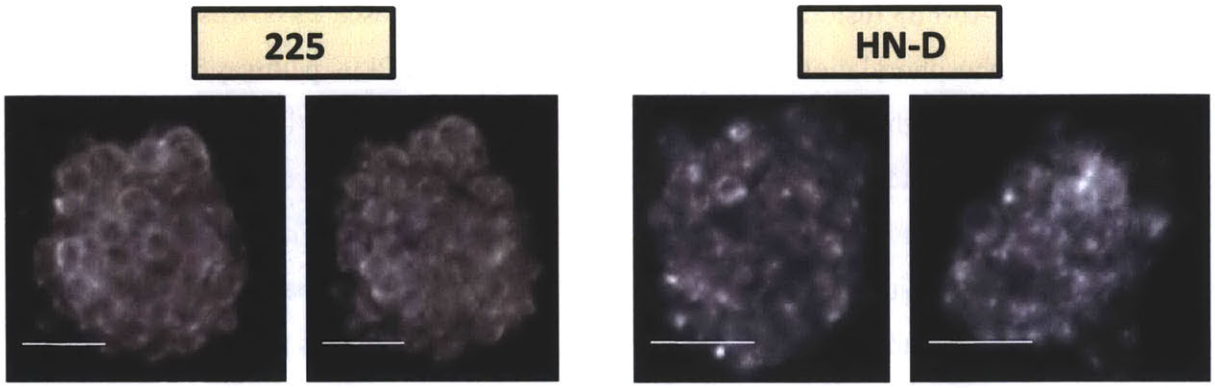

Figure 4.13. Ab-Fn3 fusions perfuse tumor cell spheroids at saturating concentrations. A431 spheroids were incubated with 20 nM fluorescently-labeled mAb 225 or bispecific Ab-Fn3 fusion HN-D. Spheroids were then washed and imaged on a Nikon confocal microscope to assess antibody penetration. All images were captured using equivalent intensity settings and brightness and contrast have been normalized using the ImageJ software package. Scale bars = 50 μm.

Ab-Fn3 Fusions Downregulate EGFR without Agonizing Receptor or Downstream Signaling

Due to the parallel trafficking effects of Ab-Fn3 fusions and EGF, we considered the possibility that our engineered molecules could be acting as receptor agonists and activating EGFR as ligand mimics. In the presence of EGF, receptor dimerization enables kinase activity in trans, so we sought to determine whether Ab-Fn3-induced receptor clustering elicits the same response. As noted in Chapter 2, combination mAb-mediated clustering is not agonistic (1), but Ab-Fn3 fusion-mediated clustering differs in that it accelerates receptor endocytosis in addition to obstructing receptor recycling, as does native ligand (30).

To test whether the most potently downregulating Ab-Fn3 fusions, the trans-trispecific constructs, activate EGFR, we treated A431 cells with these constructs and monitored receptor phosphorylation at eight known phosphosites in the EGFR intracellular domain including three major tyrosine autophosphorylation sites (Y1068, Y1148, and Y1173) (31), one minor autophosphorylation site (Y1086) (32), a Src tyrosine kinase target (Y845) (33), a Ca-calmodulin-dependent kinase II target (S1046) (34), a target of protein kinase C (T654) (35), and a MAPK phosphosite (T669) (36). As shown in Figure 4.14, all of these sites show some degree of phosphorylation in response to EGF stimulation, but none are activated by engineered fusion

treatment during the same 2 h timecourse. We conclude that despite its capacity to downregulate surface EGFR, Ab-Fn3-induced clustering is not sufficient to instigate EGFR activation.

To ensure that the Ab-Fn3 fusions were not agonizing signaling cascades downstream of EGFR, we examined the phosphorylation state of Akt, an effector in the PI3K pathway and ERK, an effector in the MAPK pathway. We focused specifically on the most actively downregulating trans-trispecific compound, HND+LCA, which we pursued in animal studies discussed in Chapter 5. As shown in Figure 4.15, in contrast to EGF treatment, Ab-Fn3 fusion treatment induces receptor downregulation without activating Akt or ERK above background levels. Taken together with the absence of EGFR agonism, this result motivates the therapeutic use of trans-trispecific constructs.

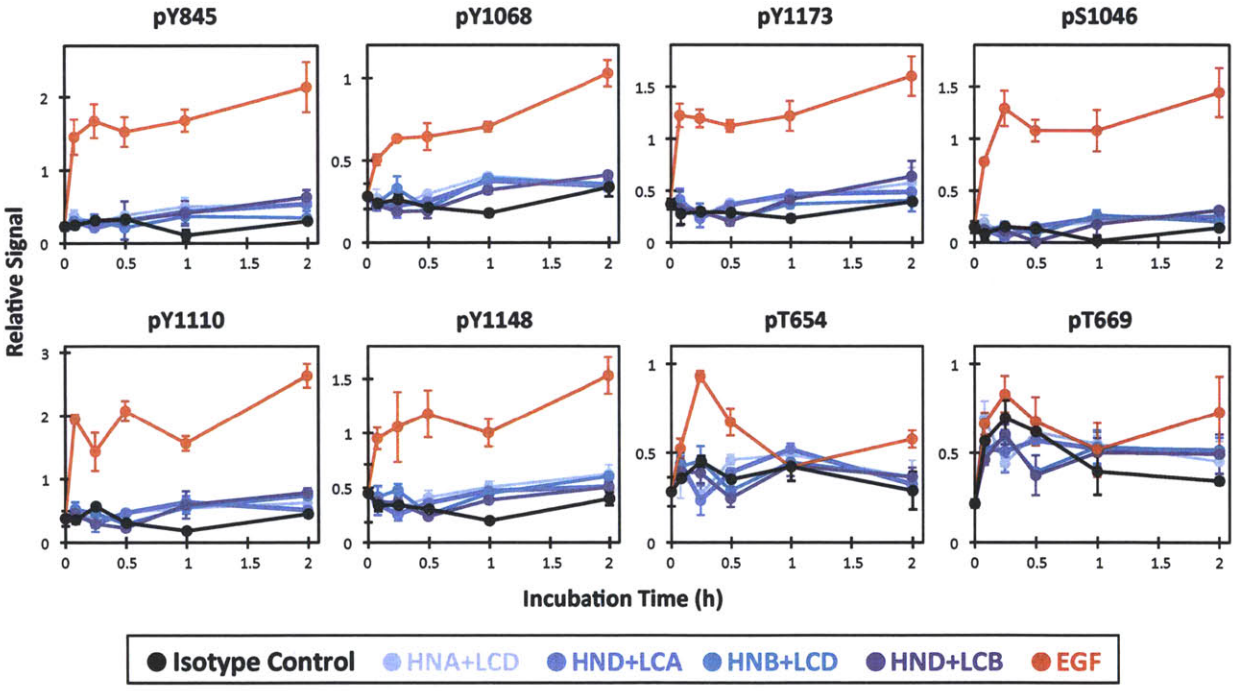

Figure 4.14. EGFR phosphorylation is not agonized by combination mAb treatment. In-cell western assays were performed on A431 cells for eight known EGFR tyrosine, serine, and threonine phosphosites. Activation profiles are shown for human IgG1 isotype control antibody (black), four trans-trispecific Ab-Fn3 fusions (shades of blue), and EGF (red). Phosphoprotein fluorescence was normalized by DNA fluorescence and signal relative to that in untreated cells is plotted versus time (±SD; n=3).

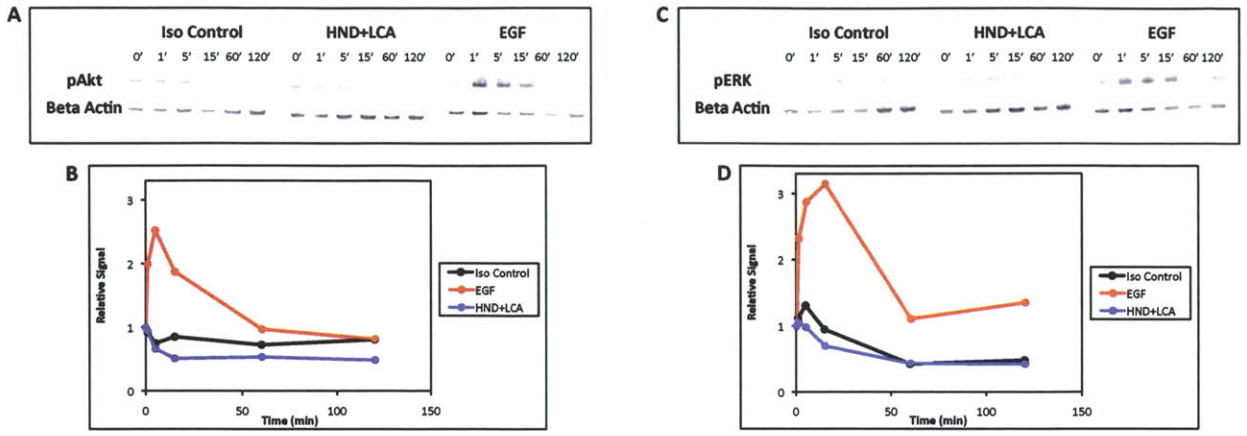

Figure 4.15. Ab-Fn3 fusions do not agonize PI3K or MAPK pathway signaling. Serum starved HT-29 cells were incubated with 20 nM isotype control antibody, the trans-trispecific construct HND+LCA, or EGF for the indicated time periods at 37°C. Cells were then lysed and phospho-Akt (A) or phospho-ERK (C) were quantified via immunoblot assay. Beta actin levels are shown as a loading control. (B) & (D) Quantification of immunoblot results presented in (A) & (C), respectively. Band intensities were normalized by beta actin levels and by the intensity of a control lysate included on each blot.

Multispecific Ab-Fn3 Fusions Inhibit Migration and Proliferation of Autocrine Ligand-Secreting Cell Lines

A major advantage of Ab-Fn3 fusions over current standard of care mAbs is their ability to exploit multiple mechanisms to inhibit EGFR activity. The 225 base antibody directly competes with EGF binding and antagonizes signaling by blocking ligand-mediated activation (21). In addition to competitively inhibiting EGF binding through their 225 variable domains, Ab-Fn3 fusions decrease the total amount of EGFR available for signaling through downregulation, compounding the antagonistic effects of 225.

The importance of recruiting multiple mechanisms to inhibit EGFR is highlighted in systems in which ligand is dysregulated. EGF and other native EGFR ligands facilitate tumor growth through a variety of autocrine and paracrine pathways (37-39). Specifically, activation of EGFR stimulates the synthesis of angiogenic growth factors, resulting in the development and expansion of vasculature to support tumor growth. Additionally, cancer cells often secrete EGF and other similar growth factors that may act directly on endothelial cells or on the tumor cells themselves. Secreted growth factors also act indirectly through modulation of protein expression in ancillary cells. For example, EGFR ligands induce expression of osteoclastogenic factors in bone marrow stromal cells that promote osteoclast maturation and activation, which ultimately results in bone degeneration and establishment of bone metastases (40, 41).

Autocrine expression or aberrant localization of receptor (42) can overwhelm exogenous therapeutics by increasing the apparent concentration of ligand, resulting in resistance to EGF-competitive mAbs. Consequently, the development of EGFR-targeted constructs that remain effective in autocrine-driven environments could be instrumental in overcoming the limitations of current clinically approved antibodies to increase the efficacy and applicability of anti-EGFR therapeutics.

To test whether Ab-Fn3 fusions repress signaling activity and modify cell behavior in autocrine-driven cells, we incubated the genotypically matched HMEC and TCT cell lines with various constructs and observed migration via wound healing assay. The transfected TCT cell line was engineered to express chimeric EGF at a rate of 0.6 h^{-1} per 10^6 cells, simulating the autocrine ligand burden often observed in tumor cells (18). As expected, monovalent Fn3 domains do not impact migration in normal HMEC or transformed TCT cells. The 225 mAb stifles HMEC motility, but does not significantly affect that of TCT cells, presumably due to the autocrine ligand challenge. Ab-Fn3 fusions showed no impact beyond the effects of 225 alone on the migration of healthy HMEC cells, but significantly ($P<0.05$ or $P<0.01$ for all constructs) restricted the movement of autocrine ligand-dependent TCT cells compared to 225 migration levels (Figure 4.16). Taken together, these results indicate that Ab-Fn3 fusions significantly inhibit motility of aberrantly activated cells without impacting healthy cells to a greater extent than the base antibody, which exhibits minimal off-target toxicity in the clinic (43, 44).

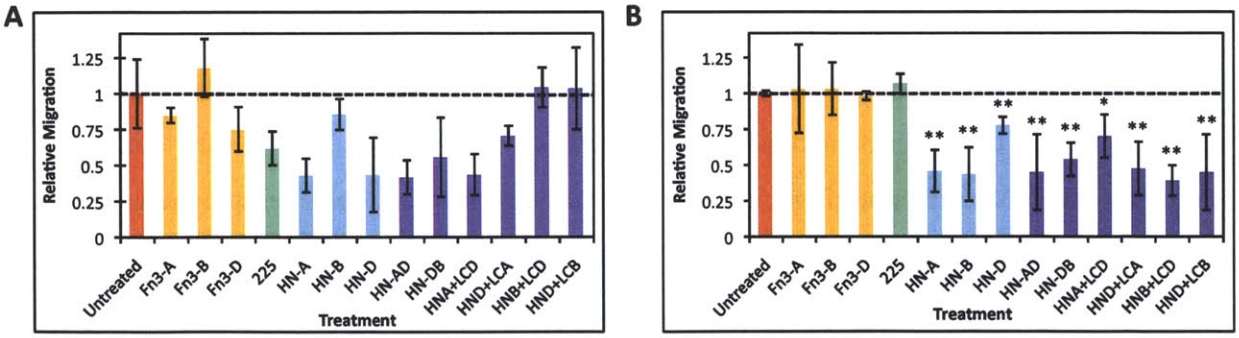

Figure 4.16. Autocrine ligand-secreting cell migration is reduced following Ab-Fn3 treatment. Migration of normal HMEC (A) and autocrine ligand-secreting TCT (B) cells was assessed following incubation with 20 nM of the indicated Fn3 domains (orange), mAbs (green), or Ab-Fn3 fusions (blue) using a scratch migration assay. Cell monolayers were wounded and subsequently incubated with the indicated constructs at 37°C for 24 h (HMEC) or 16 h (TCT). Relative migration is presented as fractional wound replenishment compared to that of an untreated control (±SD; n=3). The dashed lines indicate migration extent of untreated cells. *$P<0.05$ versus 225 cohort and **$P<0.01$ versus 225 cohort.

Based on our promising migration results, we performed proliferation assays on the HMEC and TCT cell lines, as well as on ECT cells (which express chimeric EGF at a rate of 0.3 h^{-1} per 10^6 cells) (18), HTGF-α cells (which express chimeric TGF-α at a rate of 1 ng per hour per 10^6 cells, 180-fold higher than endogenous levels), and HEPR cells (which express chimeric epiregulin at quantities 140-fold higher than endogenous levels). All cell lines are derived from normal mammary epithelial cells (HMEC) and simulate transformed cells that aberrantly express EGFR ligands.

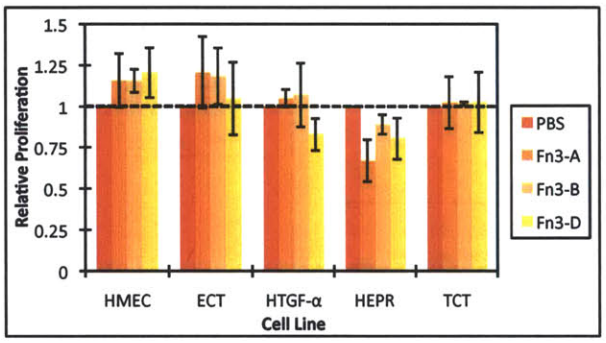

Figure 4.17. Cell proliferation is unaffected by monovalent Fn3 treatment. Proliferation of HMEC and four HMEC-derived autocrine ligand-secreting cell lines were assessed via Wst1 assay. Cells were treated with PBS or 20 nM of the indicated Fn3 clones 72 h at 37°C. Relative proliferation is presented as viable cell abundance compared to that of untreated cells (±SD; n=6). The dashed line demarks proliferation of untreated cells.

Proliferation of the parental HMEC line and the derived cell lines was not inhibited by monovalent Fn3 treatment, as expected (Figure 4.17). In HMEC cells, 225 moderately inhibited cell growth and the four tested trans-trispecific Ab-Fn3 fusions stifled growth to the same extent as the base mAb (Figure 4.18A, Table 4.6). In the ECT, TGF-α, and HNRG lines, 225 impaired cell growth to varying extents (Figures 4.18B-D). In the more aggressive TCT line, which expresses twice as much autocrine EGF as ECT, 225 was ineffective in inhibiting cell proliferation (Figure 4.18E, Table 4.6). In contrast, in all four autocrine lines tested, three of the four trans-trispecific Ab-Fn3 fusions substantially impaired cell proliferation at saturating concentrations (Figure 4.18B-E, Table 4.6). The effective fusions corresponded with those that downregulate the most actively (Figure 4.9). Specifically, the HND+LCB construct did not show potency on the TCT cell line. Note that IC_{50} values for the antibody fusions are predominantly in the range 3 to 30 nM, or ten- to 100-fold higher than the apparent K_d, indicating that saturating concentrations of antibody are required to inhibit proliferation. Due to their selective and efficient targeting of transformed cells, these constructs show strong promise as potential cancer therapeutics.

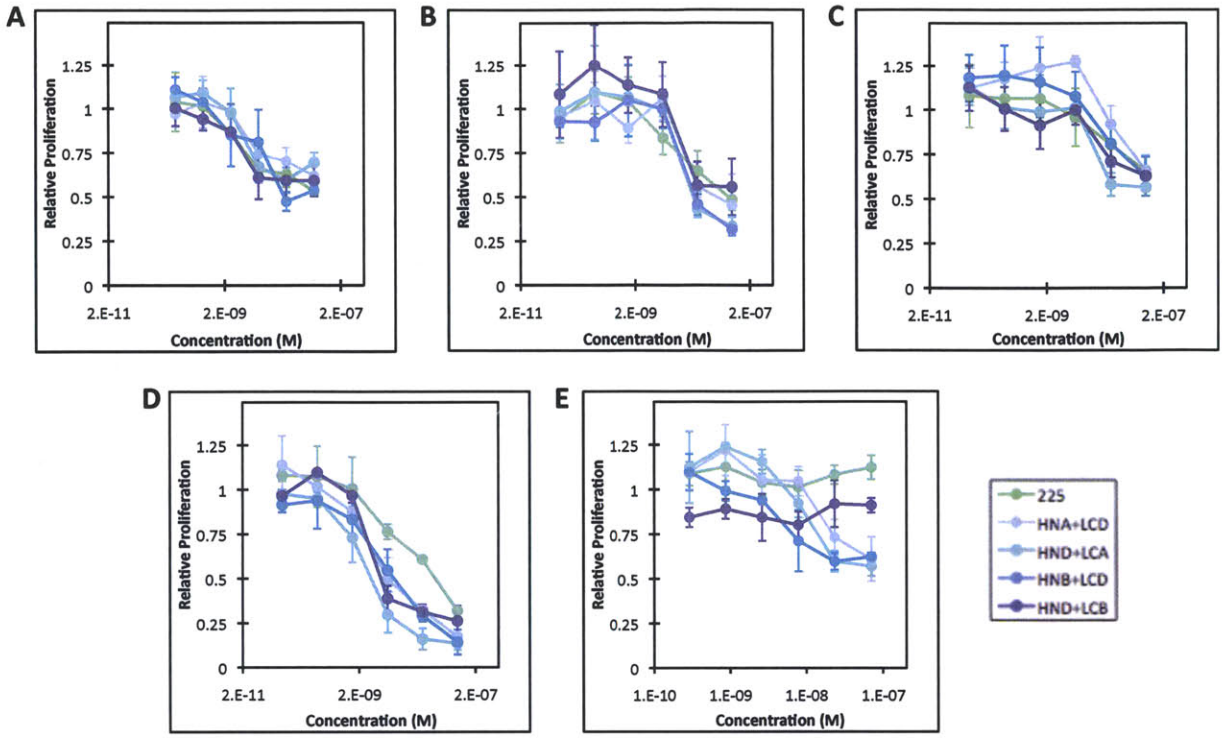

Figure 4.18. Autocrine ligand-secreting cell proliferation reduced following combination mAb treatment. Proliferation of HMEC and four HMEC-derived autocrine ligand-secreting cell lines: HMEC (A) ECT (B); HTGF-α (C); HEPR (D); and TCT (E) were assessed. Cells were treated with PBS or the indicated Fn3 clones for 72 h at 37°C. Proliferation by Wst1 assay is depicted as viable cell count compared to that of untreated cells (±SD; n=6).

Cell Line	225 IC_{50} (nM)	HNA+LCD IC_{50} (nM)	HND+LCA IC_{50} (nM)	HNB+LCD IC_{50} (nM)	HND+LCB IC_{50} (nM)
HMEC	3.5	8.2	3.5	5.3	2.9
ECT	16.7	31.0	20.9	30.9	15.7
HTGF-α	22.0	91.4	15.2	24.2	18.2
HEPR	14.3	3.7	2.6	7.9	3.8
TCT	*	24.6	12.6	3.6	*

Table 4.6. IC_{50} values for inhibition of proliferation by Ab-Fn3 fusions. The proliferation data from Figure 14.18 were fit to IC_{50} curves using nonlinear least squares regression. The computed IC_{50} values for each treatment condition on HMEC parental cells and the four HMEC-derived cell lines are presented. *225 and HND+LCB did not inhibit proliferation of the TCT cell line.

Discussion

We have developed antibody-fibronectin domain fusion compounds targeting multiple non-overlapping epitopes of a single receptor. These antibodies secrete stably from mammalian cells and bind EGFR with sub-nanomolar affinity at both physiological (7.4) and endosomal (6.0) pH (Tables 4.3, 4.4). These fusions benefit from avidity effects to improve upon the binding affinity

of the unconjugated base 225 antibody and, surprisingly, fusions with N-terminal Fn3 domains fused to the heavy chain secrete with higher yields than the 225 IgG (Figures 4.4, 4.7).

Ab-Fn3 fusions cluster and downregulate EGFR without agonizing the receptor or its downstream effectors (Figures 4.8-4.10, 4.14, 4.15), ultimately leading to inhibition of the growth and migration of transformed cells, as is true with combination mAb treatment (Figures 4.16, 4.18) (1). The key differences between the effects of combination mAb treatment and those of Ab-Fn3 fusions are: (1) combination mAb-induced downregulation extent is inversely correlated with receptor expression level, whereas trans-trispecific Ab-Fn3-induced downregulation is insensitive to receptor number up to 1.6×10^6 receptors/cell (Figure 4.9); (2) combination mAb treatment abrogates recycling but does not enhance endocytosis rate, whereas Ab-Fn3 fusion treatment blocks recycling and accelerates endocytosis (Figures 4.11, 4.12); and (3) Cluster formation occurs much more rapidly (within 9 min of administration) in the case of Ab-Fn3 fusion treatment (Figure 4.10C).

It is notable that we have achieved rapid receptor downregulation in the absence of agonism since rapid endocytosis occurs exclusively through clathrin-coated pits. However, recruitment to coated pits requires kinase activity, which suggests that the internalization we observe occurs through basal membrane turnover or through lipid rafts (45-47). We hypothesize that although the molecular rate of receptor internalization is not accelerated, clustered receptors are internalized synchronously, resulting in an apparent increase in the bulk endocytic rate constant following Ab-Fn3 administration.

The immediate application we anticipate for the Ab-Fn3 fusions we have designed is use as targeted EGFR-directed therapeutics in solid tumors. However, the modular format of the Ab-Fn3 fusion allows for the insertion of any Fn3 moiety with engineered specificity for an antigen of interest, providing a generalized scaffold for targeting multiple proteins with a single IgG-based compound. Furthermore, the successful secretion of tetraspecific Ab-Fn3 fusions with three Fn3 domain conjugates allows for dual targeting and, potentially, simultaneous clustering of two different receptors. This would be particularly significant for an EGFR-directed therapeutic since EGFR interacts with a vast network of receptors and intracellular proteins,

creating a vast array of potential multi-receptor cluster partners. Also, EGFR-targeted therapy resistance has been found to be mediated through upregulation of ErbB3 and c-Met signaling (48, 49). In particular, ErbB3 exhibits only transient responsiveness to tyrosine kinase inhibitors and is aberrantly active in cetuximab-resistant lung cancer (50, 51). EGFR-directed drug resistance through compensatory pathways directly motivates engagement of multiple receptors in an inactive clustered conformation to inhibit growth signaling and enhance therapeutic efficacy.

Like the IgG-scFv fusions presented in Chapter 3, a further application of Ab-Fn3 fusions could be as delivery vehicles for toxins, siRNA, or other cell disruption agents. By forming pools of clustered EGFR in the cytoplasm, these molecules could provide high local concentrations of toxic agents that would selectively destroy transformed cells. Furthermore, by conjugating the Ab-Fn3 fusions to fusogenic peptides, one could achieve high concentrations of receptors within endosomes which could facilitate disruption of the endosomal membrane and allow for diffusion of the toxic compound into the cytosol, enhancing therapeutic efficacy.

Finally, in addition to therapeutic potential, Ab-Fn3 fusions could prove useful in research and detection, with applications in such areas as molecular recognition, delivery of contrast agents, and diagnostics. With high affinity and specificity for EGFR, Ab-Fn3 fusions selectively and tightly bind EGFR, providing accurate detection for imaging and diagnostic applications.

Our *in vitro* migration and proliferation results (Figures 4.16-4.18) strongly suggest that our compound would inhibit tumor growth *in vivo*, based on previous findings with antibody combinations and multispecific constructs (10, 12, 13). The antibody backbone allows for superior retention in the bloodstream compared to small molecule drugs (19, 52) and the molecular specificity of our multi-epitopic fusions will minimize off-target toxicity. Also, the tumor penetration of our compound is not impaired by induced downregulation (Figure 4.13), indicating that it effectively saturates tumor cells at equivalent doses to IgG. Based on our promising *in vitro* results, the therapeutic efficacy of Ab-Fn3 fusions was extensively studied in mouse tumor xenograft models, which are described in Chapter 5.

Materials and Methods

Cell lines and antibodies

The transfected CHO-EG (53), U87-MGSH (54), and ECT (18) cell lines were established as described previously and all other lines were obtained from ATCC (Manassas, VA). Cells were maintained in their respective growth media (from ATCC unless otherwise indicated): DMEM for A431, U87-MG, U87-MGSH, BT-20, Hs578T, BT-549, MDA-MB-231, and CHO-EG cells, F-12K medium for A549 cells, McCoy's Modified 5A medium for HT-29 cells, EMEM for HeLa cells, and HuMEC Ready Medium (Invitrogen, Carlsbad, CA) for HMEC and ECT cells. U87-MG, U87-MGSH, and CHO-EG media were supplemented with 1 mM sodium pyruvate (Invitrogen) and 0.1 mM non-essential amino acids (Invitrogen) and transfected lines U87-MGSH and CHO-EG were selected with 0.3 mM Geneticin (Invitrogen). To prepare complete culture media, ATCC media were supplemented with 10% fetal bovine serum (FBS) and 1X penicillin-streptomycin solution. All cell lines were maintained at 37°C with 5% ambient CO_2. The 225 mAb was secreted from the commercially available hybridoma cell line (ATCC). H11 was purchased through Lab Vision (Fremont, CA).

Unless otherwise noted, all washes were conducted in PBS containing 0.1% BSA and all constructs were used at a concentration of 20 nM for single treatment and 10 nM each for combination treatment. EGF (Sigma, St. Louis, MO) was dosed at 20 nM. Trypsin-EDTA (Invitrogen) contains 0.05% trypsin and 0.5 mM EDTA.

Production of Ab-Fn3 fusions via HEK cell transfection

The human IgG1 heavy and light chains of each Ab-Fn3 fusion were inserted into the gWiz mammalian expression vector (Genlantis). Constructs were verified by sequence analysis. All plasmid sequences used for Ab-Fn3 constructs are provided in Appendix C. HEK 293F cells (Invitrogen) were grown to 1.2 million cells per mL and diluted to one million per mL. Miniprepped DNA and polyethyleneimine (Sigma) were independently diluted to 0.05 and 0.1 mg/mL in OptiPro medium and incubated at 22° for 15 min. Equal volumes of DNA and polyethyleneimine were mixed and incubated at 22° for 15 min. 500 mL of cells and 20 mL of DNA/polyethyleneimine mixture were added to a 2 L roller bottle and incubated at 37°, 5% CO_2

on a roller bottle adapter for seven days. The cell secretions were then centrifuged for 30 min at 15,000×g and the supernatant was filtered through a 0.22 μm bottle-top filter and purified via affinity column chromatography using protein A resin (Thermo Fisher Scientific, Waltham, MA). The eluted constructs were concentrated and transferred to PBS and then characterized by sodium dodecyl sulfate polyacrylamide gel electrophoresis (SDS-PAGE) analysis.

Affinity titrations

To characterize Ab-Fn3 binding affinities, A431 cells were trypsinized, washed in PBSA, and incubated with various concentrations of Ab-Fn3 in a 96-well plate on ice. The number of cells and sample volumes were selected to ensure at least tenfold excess Ab-Fn3 relative to EGFR. All samples were assayed in triplicate. Cells were incubated on ice for sufficient time to ensure that the approach to equilibrium was at least 99% complete. Cells were then washed and labeled with 66 nM PE-conjugated goat anti-human antibody (Rockland Immunochemicals, Gilbertsville, PA) for 20 min on ice. After a final wash, plates were analyzed on a FACS Calibur cytometer (BD Biosciences, San Jose, CA). The minimum and maximum fluorescence and the K_d value were determined by minimizing the sum of squared errors assuming a 1:1 binding interaction (% Bound = $[L]/([L]+K_d)$ where [L] is Ab-Fn3 concentration and K_d is the equilibrium dissociation constant of the Ab-Fn3 construct. Curve fitting was implemented in MATLAB (Mathworks, Natick, MA). Titrations were performed at both pH 6.0 (endosomal pH) and pH 7.4 (physiological pH).

Deconvolution Microscopy

mAb 225 and Ab-Fn3 fusion constructs were labeled with Alexa 488 using a fluorescent labeling kit (Invitrogen). A431, HT-29, or A549 cells were plated at 50,000 per well in 8-well microscopy chambers and allowed to settle overnight. They were then serum-starved for 8-12 h and incubated with the appropriate mAb or fusion construct for various time lengths at 37°, 5% CO_2. Cells were immediately washed and resuspended in phenol red-free medium (Invitrogen) for imaging on a Delta Vision inverted deconvolution microscope at 60X magnification (oil immersion lens). For A549 images, wells were not washed but rather dye was added and images were captured over a 30 minute time course. Deconvolution and projection of 0.15 μm z-slices

and image analysis were performed using the Softworx software package. All compared images were obtained using identical settings and brightness and contrast were normalized.

Receptor Downregulation Assays

Cells were seeded at 5×10^4 per well in 96-well plates, serum starved for 12-16 h, treated with the indicated mAbs or Ab-Fn3 fusions in serum-free medium, and incubated at 37°C. At each time point, cells were washed and treated with trypsin-EDTA for 20 min at 37°C. Trypsin was neutralized with medium (10% FBS) and cells were transferred to v-bottom plates on ice. They were then washed, acid stripped (0.2 M acetic acid, 0.5 M NaCl, pH 2.5), and washed again prior to incubation with 20 nM 225 for 1 h on ice to label surface EGFR. Cells were then washed and labeled with 66 nM PE-conjugated goat anti-mouse antibody (Invitrogen) for 20 min on ice. After a final wash, plates were analyzed on a FACS Calibur cytometer (BD Biosciences, San Jose, CA). Cell pelleting was conducted at 1000×g. Data was fit to a single exponential curve to determine downregulation halftime (% Surface Receptor Remaining = Min + (Max - Min)*e^{-kt}). Curve fitting was implemented in MATLAB (Mathworks).

Monensin Recycling Assays

U87 cells were seeded at 5×10^4 per well in 96-well plates and serum starved for 12-16 h. They were then incubated in basal medium with or without 200 μM monensin (Sigma, St. Louis, MO) at 37°C for 20 min. The indicated Ab-Fn3 trans-trispecific constructs were then added and incubation proceeded at 37°C. At each time point, cells were dissociated in trypsin, acid stripped, and labeled for surface EGFR through incubation with 20 nM 225 for 1 h on ice. Cells were then washed and labeled with 66 nM PE-conjugated goat anti-mouse antibody (Invitrogen) for 20 min at 4°C. Cells were washed a final time and analyzed on a FACS Calibur cytometer (BD Biosciences).

Confocal Microscopy

Spheroids were prepared by the hanging drop method (28, 55) in microwell trays (Nunc, Rochester, NY). Five hundred A431 wells were seeded per well in a tray and incubated upside-down for three days at 37°C and 5% CO_2 to allow for spheroid formation. The spheroids were then washed with PBS and transferred to 8-well microscopy chamber dishes and allowed to

attach overnight at 37°C. mAb or Ab-Fn3 fusions were labeled with Alexa 488 following the manufacturer's protocol (Invitrogen) and added was added to the wells at a concentration of 20 nM for 1 h at 37°C. Labeled construct was then removed and cells were washed with PBS and resuspended in phenol red-free DMEM. Images were acquired on a Nikon confocal microscope (Zeiss, Thornwood, NY) using a 20X objective and are presented as overlays of 2.0 μm-spaced z-sections through the 100-200 nm spheroid diameter. Exposure conditions were consistent across all images shown and z-stack projection and image analysis were performed in ImageJ.

In-Cell Western Assays

A431 cells were seeded at 4×10^4 per well in 96-well plates and allowed to adhere for 24 h. Following 12-16 h of serum starvation, cells were treated with the designated mAbs in serum-free medium at 37°C for the specified time length. All subsequent incubations were performed at room temperature. Cells were fixed for 20 min (PBS, 4% formaldehyde), permeabilized via four 5 min incubations (PBS, 0.1% triton), blocked for 1 h in blocking buffer (1:1 PBS:Odyssey Blocking Buffer (Licor Biosciences, Lincoln, NE)), and labeled overnight at 4°C with 15 nM anti-phosphosite antibodies (Genscript, Piscataway, NJ) in blocking buffer. Cells were then washed three times with PBST (PBS, 0.1% Tween-20) and labeled with 66 nM 800-conjugated goat anti-rabbit antibody (Rockland Immunochemicals) and 400 nM TO-PRO-3 DNA stain (Invitrogen) in blocking buffer for 30 min. After three final PBST washes, wells were aspirated dry for analysis on a Licor Odyssey infrared scanner (Licor Biosciences). Phospho-signal was normalized to cell abundance by dividing 800 (phosphoprotein) by 700 (TO-PRO-3) channel fluorescence.

Western Blots

HT-29 or HCT-116 cells were cultured to confluence in 6-well plates and serum starved for 12 h. Cells were subsequently incubated with 20 nM antibody or Ab-Fn3 fusion for the indicated length of time at 37°C.. Cells were then washed once with cold PBS and incubated with rotation for 5 min in lysis buffer (50 mM Tris•HCl, 2% SDS, 5% glycerol, 5 mM EDTA, 1 mM NaF, protease and phosphatase inhibitors (Thermo Fisher Scientific, Pittsburgh, PA), 10 mM β-GP, 1 mM PMSF and 1 mM Na_3VO_4). Total protein levels were quantified via BCA assay (Thermo Fisher Scientific) and lysates were normalized to a protein concentration of 3.5 mg/mL. Lysates

were clarified by passage through centrifugal filter plates for 8-12 h at 4000×g. The lysates were subsequently subjected to SDS-PAGE on 8% E-Page gels and blotted onto nitrocellulose via iBlot apparatus (Invitrogen). The blotted membrane was then blocked in 1:1 PBS:Odyssey Blocking Buffer (Licor Biosciences) for 1 h at room temperature. Blots were then incubated with 1:1000 dilutions of either anti-phosphoAkt S473 rabbit antibody or anti-phosphoERK1/2 Y202/Y204 rabbit antibody overnight at 4°C (Cell Signaling, Danvers, MA). A 1:15,000 dilution of mouse anti-beta actin antibody was added the next morning and incubation proceeded for 2 h. Following three washes, the membrane was incubated with goat anti-mouse (800 cw) and anti-rabbit (700 cw) near IR dye conjugate antibodies. After four additional washes, membranes were visualized on the Licor Odyssey infrared imaging system. Phospho-Akt and phospho-ERK signals were normalized by beta actin signal for each lysate and all samples were normalized to a control lysate to ensure consistent intensity between blots.

Migration Assays

HMEC and TCT cells were seeded at 5×10^4 per well in 96-well plates and grown to confluence. Monolayers were wounded with a pipet tip, washed with PBS, and incubated in complete medium with the indicated mAbs or Ab-Fn3 fusion constructs. Scratch area was measured immediately and after 24 h incubation (HMEC cells) or 16 h incubation (TCT cells) at 37°C using Image J software analysis of images from a Nikon confocal microscope (Nikon Instruments, Melville, NY). Percent migration was calculated as the fractional reduction in scratch area in the treated wells divided by that of untreated wells.

Cell Proliferation Assays

HMEC, ECT, TCT, HTGF-α, and HEPR cells were seeded at 3×10^3 per well in 96-well plates and allowed to adhere for 24 h. They were then treated with the indicated mAbs or Ab-Fn3 fusion constructs at the prescribed concentrations in complete medium and incubated at 37°C for 72 h. Cell viability (relative to an untreated control) was assessed using the Wst1 tetrazolium salt cleavage assay (Roche, Indianapolis, IN) (56, 57). Relative proliferation was calculated as the 450 nm absorbance of treated wells relative to that of untreated controls. Data was then fit to the equation: Relative Proliferation = $\text{Min}+(\text{Max}-\text{Min})(1-(x/(x+IC_{50})))$ where x is the concentration of Ab or Ab-Fn3 fusion and IC_{50} is the concentration required to achieve half-

maximal inhibition of growth. A nonlinear least squares regression algorithm was implemented in MATLAB (Mathworks).

Statistical Analysis

Heteroscedastic two-tailed student's t tests were performed on migration and proliferation assay results to compare 225, Fn3, and Ab-Fn3 treatments. P values of less than 0.05 were deigned significant.

References

1. Spangler JB, *et al.* (2010) Combination antibody treatment down-regulates epidermal growth factor receptor by inhibiting endosomal recycling. *Proc Natl Acad Sci U S A* 107(30):13252-13257.
2. Muller D & Kontermann RE (2010) Bispecific antibodies for cancer immunotherapy: Current perspectives. *BioDrugs* 24(2):89-98.
3. Gall JM, Davol PA, Grabert RC, Deaver M, & Lum LG (2005) T cells armed with anti-CD3 x anti-CD20 bispecific antibody enhance killing of CD20+ malignant B cells and bypass complement-mediated rituximab resistance in vitro. *Exp Hematol* 33(4):452-459.
4. Muller D & Kontermann RE (2007) Recombinant bispecific antibodies for cellular cancer immunotherapy. *Curr Opin Mol Ther* 9(4):319-326.
5. Dreier T, *et al.* (2003) T cell costimulus-independent and very efficacious inhibition of tumor growth in mice bearing subcutaneous or leukemic human B cell lymphoma xenografts by a CD19-/CD3- bispecific single-chain antibody construct. *J Immunol* 170(8):4397-4402.
6. Friedman M, *et al.* (2009) Engineering and characterization of a bispecific HER2 x EGFR-binding affibody molecule. *Biotechnol Appl Biochem* 54(2):121-131.
7. Fury MG, Lipton A, Smith KM, Winston CB, & Pfister DG (2008) A phase-I trial of the epidermal growth factor receptor directed bispecific antibody MDX-447 without and with recombinant human granulocyte-colony stimulating factor in patients with advanced solid tumors. *Cancer Immunol Immunother* 57(2):155-163.

8. Kiewe P & Thiel E (2008) Ertumaxomab: a trifunctional antibody for breast cancer treatment. *Expert Opin Investig Drugs* 17(10):1553-1558.
9. Cochran JR (2010) Engineered proteins pull double duty. *Sci Transl Med* 2(17):17ps15.
10. Ben-Kasus T, Schechter B, Lavi S, Yarden Y, & Sela M (2009) Persistent elimination of ErbB-2/HER2-overexpressing tumors using combinations of monoclonal antibodies: relevance of receptor endocytosis. *Proc Natl Acad Sci U S A* 106(9):3294-3299.
11. Dechant M, *et al.* (2008) Complement-dependent tumor cell lysis triggered by combinations of epidermal growth factor receptor antibodies. *Cancer Res* 68(13):4998-5003.
12. Roovers RC, *et al.* (2011) A bi-paratopic anti-EGFR nanobody efficiently inhibits solid tumour growth. *Int J Cancer*.
13. Friedman LM, *et al.* (2005) Synergistic down-regulation of receptor tyrosine kinases by combinations of mAbs: implications for cancer immunotherapy. *Proc Natl Acad Sci U S A* 102(6):1915-1920.
14. Hackel BJ, Neil JR, White FM, & Wittrup KD (Submitted) Epidermal growth factor receptor downregulation by small heterodimeric binding proteins.
15. Koide A & Koide S (2007) Monobodies: antibody mimics based on the scaffold of the fibronectin type III domain. *Methods Mol Biol* 352:95-109.
16. Cota E & Clarke J (2000) Folding of beta-sandwich proteins: three-state transition of a fibronectin type III module. *Protein Sci* 9(1):112-120.
17. Main AL, Harvey TS, Baron M, Boyd J, & Campbell ID (1992) The three-dimensional structure of the tenth type III module of fibronectin: an insight into RGD-mediated interactions. *Cell* 71(4):671-678.
18. Joslin EJ, Opresko LK, Wells A, Wiley HS, & Lauffenburger DA (2007) EGF-receptor-mediated mammary epithelial cell migration is driven by sustained ERK signaling from autocrine stimulation. *J Cell Sci* 120(Pt 20):3688-3699.
19. Simister NE & Mostov KE (1989) An Fc receptor structurally related to MHC class I antigens. *Nature* 337(6203):184-187.
20. Hackel BJ NJ, White FM, & Wittrup KD (Submitted) Epidermal growth factor receptor downregulation by small heterodimeric binding proteins.

21. Li S, *et al.* (2005) Structural basis for inhibition of the epidermal growth factor receptor by cetuximab. *Cancer Cell* 7(4):301-311.
22. Ettenberg SA, *et al.* (2010) Inhibition of tumorigenesis driven by different Wnt proteins requires blockade of distinct ligand-binding regions by LRP6 antibodies. *Proc Natl Acad Sci U S A* 107(35):15473-15478.
23. Ogiso H, *et al.* (2002) Crystal structure of the complex of human epidermal growth factor and receptor extracellular domains. *Cell* 110(6):775-787.
24. Ferguson KM, *et al.* (2003) EGF activates its receptor by removing interactions that autoinhibit ectodomain dimerization. *Mol Cell* 11(2):507-517.
25. Basu SK, Goldstein JL, Anderson RG, & Brown MS (1981) Monensin interrupts the recycling of low density lipoprotein receptors in human fibroblasts. *Cell* 24(2):493-502.
26. Adams GP, *et al.* (2001) High affinity restricts the localization and tumor penetration of single-chain fv antibody molecules. *Cancer Res* 61(12):4750-4755.
27. Saga T, *et al.* (1995) Targeting cancer micrometastases with monoclonal antibodies: a binding-site barrier. *Proc Natl Acad Sci U S A* 92(19):8999-9003.
28. Thurber GM & Wittrup KD (2008) Quantitative spatiotemporal analysis of antibody fragment diffusion and endocytic consumption in tumor spheroids. *Cancer Res* 68(9):3334-3341.
29. Thurber GM, Schmidt MM, & Wittrup KD (2008) Factors determining antibody distribution in tumors. *Trends Pharmacol Sci* 29(2):57-61.
30. Wiley HS (2003) Trafficking of the ErbB receptors and its influence on signaling. *Exp Cell Res* 284(1):78-88.
31. Downward J, Waterfield MD, & Parker PJ (1985) Autophosphorylation and protein kinase C phosphorylation of the epidermal growth factor receptor. Effect on tyrosine kinase activity and ligand binding affinity. *J Biol Chem* 260(27):14538-14546.
32. Margolis BL, *et al.* (1989) All autophosphorylation sites of epidermal growth factor (EGF) receptor and HER2/neu are located in their carboxyl-terminal tails. Identification of a novel site in EGF receptor. *J Biol Chem* 264(18):10667-10671.
33. Sato K, Sato A, Aoto M, & Fukami Y (1995) c-Src phosphorylates epidermal growth factor receptor on tyrosine 845. *Biochem Biophys Res Commun* 215(3):1078-1087.

34. Countaway JL, Nairn AC, & Davis RJ (1992) Mechanism of desensitization of the epidermal growth factor receptor protein-tyrosine kinase. *J Biol Chem* 267(2):1129-1140.
35. Takishima K, Griswold-Prenner I, Ingebritsen T, & Rosner MR (1991) Epidermal growth factor (EGF) receptor T669 peptide kinase from 3T3-L1 cells is an EGF-stimulated "MAP" kinase. *Proc Natl Acad Sci U S A* 88(6):2520-2524.
36. Hunter T, Ling N, & Cooper JA (1984) Protein kinase C phosphorylation of the EGF receptor at a threonine residue close to the cytoplasmic face of the plasma membrane. *Nature* 311(5985):480-483.
37. Salomon DS, Brandt R, Ciardiello F, & Normanno N (1995) Epidermal growth factor-related peptides and their receptors in human malignancies. *Crit Rev Oncol Hematol* 19(3):183-232.
38. Normanno N, Bianco C, De Luca A, Maiello MR, & Salomon DS (2003) Target-based agents against ErbB receptors and their ligands: a novel approach to cancer treatment. *Endocr Relat Cancer* 10(1):1-21.
39. Normanno N, *et al.* (2005) The ErbB receptors and their ligands in cancer: an overview. *Curr Drug Targets* 6(3):243-257.
40. Gupta D, *et al.* (2001) Adherence of multiple myeloma cells to bone marrow stromal cells upregulates vascular endothelial growth factor secretion: therapeutic applications. *Leukemia* 15(12):1950-1961.
41. De Luca A, *et al.* (2008) The role of the EGFR signaling in tumor microenvironment. *J Cell Physiol* 214(3):559-567.
42. Kuwada SK, *et al.* (1998) Differential signaling and regulation of apical vs. basolateral EGFR in polarized epithelial cells. *Am J Physiol* 275(6 Pt 1):C1419-1428.
43. Saltz LB, *et al.* (2004) Phase II trial of cetuximab in patients with refractory colorectal cancer that expresses the epidermal growth factor receptor. *J Clin Oncol* 22(7):1201-1208.
44. Cunningham D, *et al.* (2004) Cetuximab monotherapy and cetuximab plus irinotecan in irinotecan-refractory metastatic colorectal cancer. *N Engl J Med* 351(4):337-345.
45. Sorkin A & Goh LK (2009) Endocytosis and intracellular trafficking of ErbBs. *Exp Cell Res* 315(4):683-696.

46. Sigismund S, *et al.* (2005) Clathrin-independent endocytosis of ubiquitinated cargos. *Proc Natl Acad Sci U S A* 102(8):2760-2765.

47. Zhu JX, *et al.* (2005) Decorin evokes protracted internalization and degradation of the epidermal growth factor receptor via caveolar endocytosis. *J Biol Chem* 280(37):32468-32479.

48. Schoeberl B, *et al.* (2009) Therapeutically targeting ErbB3: a key node in ligand-induced activation of the ErbB receptor-PI3K axis. *Sci Signal* 2(77):ra31.

49. Schoeberl B, *et al.* (2010) An ErbB3 antibody, MM-121, is active in cancers with ligand-dependent activation. *Cancer Res* 70(6):2485-2494.

50. Sergina NV, *et al.* (2007) Escape from HER-family tyrosine kinase inhibitor therapy by the kinase-inactive HER3. *Nature* 445(7126):437-441.

51. Wheeler DL, *et al.* (2008) Mechanisms of acquired resistance to cetuximab: role of HER (ErbB) family members. *Oncogene* 27(28):3944-3956.

52. Roopenian DC & Akilesh S (2007) FcRn: the neonatal Fc receptor comes of age. *Nat Rev Immunol* 7(9):715-725.

53. Harms BD, Bassi GM, Horwitz AR, & Lauffenburger DA (2005) Directional persistence of EGF-induced cell migration is associated with stabilization of lamellipodial protrusions. *Biophys J* 88(2):1479-1488.

54. Huang PH, *et al.* (2007) Quantitative analysis of EGFRvIII cellular signaling networks reveals a combinatorial therapeutic strategy for glioblastoma. *Proc Natl Acad Sci U S A* 104(31):12867-12872.

55. Kelm JM, Timmins NE, Brown CJ, Fussenegger M, & Nielsen LK (2003) Method for generation of homogeneous multicellular tumor spheroids applicable to a wide variety of cell types. *Biotechnol Bioeng* 83(2):173-180.

56. Ishiyama M, *et al.* (1996) A combined assay of cell viability and in vitro cytotoxicity with a highly water-soluble tetrazolium salt, neutral red and crystal violet. *Biol Pharm Bull* 19(11):1518-1520.

57. Hamasaki K, Kogure K, & Ohwada K (1996) A biological method for the quantitative measurement of tetrodotoxin (TTX): tissue culture bioassay in combination with a water-soluble tetrazolium salt. *Toxicon* 34(4):490-495.

5. Therapeutic Evaluation of Engineered Multispecific Antibodies and Elucidation of the Mechanistic Basis for Tumor Inhibition

Introduction

The two current clinically approved anti-EGFR monoclonal antibody drugs (cetuximab and panitumumab) rely on ligand competition and are thus hindered by transport limitations, receptor mutation, and autocrine secretion of stimulatory ligands (1-3). The multi-epitopic targeting strategy we propose circumvents these issues by downregulating receptor to allow for further antibody penetration into tumors, by effectively clustering both wild-type and mutant receptors to permit efficacy in the presence of activating mutations, and by binding to sites on EGFR that are not competitive with native ligand to retain therapeutic potency in autocrine-driven environments. We thus sought to compare our multispecific EGFR-targeted antibody-based constructs to currently approved therapies in established mouse xenograft models.

A particular challenge for EGFR-targeted antibodies is mutation of the receptor. In particular, the EGFRvIII decouples signal activation from ligand stimulation, resulting in constitutive activity that is resistant to ligand competitive treatments (5). The 806 antibody specifically targets an epitope that is exposed in the mutant but not the wild-type form of EGFR (6) and has been shown to control tumor growth in combination therapy studies with 528, a monoclonal antibody that binds to extracellular domain 3 of the receptor (7).

Another major challenge in the use of EGFR therapeutics is that many tumors have mutations downstream of EGFR, often in the KRAS or BRAF genes, which encode the *ras* and *raf* proteins, respectively (8-11). *Ras* serves as a signal effector in both the mitogen-activated protein kinase (MAPK) and phosphoinositide 3 kinase (PI3K) pathways whereas *Raf* is an effector in only the MAPK pathway. Both clinically approved EGFR-targeted antibodies are ineffective against tumors with KRAS (12-17) or BRAF (18, 19) mutations, indicating that EGFR ligand competition is insufficient to block downstream activation. One means of overcoming this obstacle is enhancing immune effector function (20, 21), as has been achieved with bispecific T cell-engaging (BiTE) variants of cetuximab (22).

We hoped to address both the downstream signaling and mutational challenges with the novel mechanism of multispecific antibody-induced clustering. We thus examined the performance of our most active BS28 construct in a mouse tumor xenograft model of the EGFRvIII-transfected U87-SH glioblastoma line (23). We also assess the efficacy of our most promising Ab-Fn3 fusion in three tumor models that vary in KRAS and BRAF mutational status. Our results show strong efficacy of our engineered constructs and consistency between *in vitro* downregulation extent and *in vivo* inhibition of tumor growth.

Results

Bispecific antibodies incorporating the 225 and 806 variable domains inhibit tumor growth

Of the four bispecific antibody orientations used to fuse the 806 scFv to the full 225 IgG, the C-terminal fusion to the light chain (BS28-LC) downregulated surface EGFR levels the most potently across a range of wild type and mutant EGFR-expressing cell lines. We thus compared the ability of BS28-LC and its constituent antibodies (mAb 225, mAb 806, or both) to inhibit growth of U87-SH tumor xenografts. U87-SH cells express 1.9×10^5 copies of wild type EGFR and 1.4×10^6 copies of the mutant EGFRvIII (24). The *in vitro* surface EGFR downregulation induced by each antibody treatment is shown in Figure 5.1A.

U87-SH cells were injected subcutaneously into the left flank of 6-8 week old athymic mice and tumors were grown for eight days. Beginning on day 8, twice weekly antibody injections at a dosage of 5 mg/kg were commenced. As shown in Figure 5.1B, BS28-LC effectively controls tumor growth for more than 20 days. Individual mAb treatment and combination treatment slow tumor growth to a lesser extent, showing remarkable consistency with the extent of surface downregulation induced by each treatment (Figure 5.1A). Growth profiles of the individual mice in each cohort accentuate these trends (Figure 5.1C). At the termination of the experiment (day 23), tumor volume differed significantly ($P<0.05$) between the 225+806 combination and BS28-LC treatment groups.

When the treatment dose was augmented to 7.5 mg/kg, BS28-LC therapy similarly inhibited growth for 22 days (Figures 5.2A-B) compared to control tumors. Both the mean and individual

tumor growth curves are shown in Figure 5.2. Tumor sizes were significantly different ($P<0.05$) between the PBS and BS28-LC cohorts at the time of PBS group sacrifice (day 19).

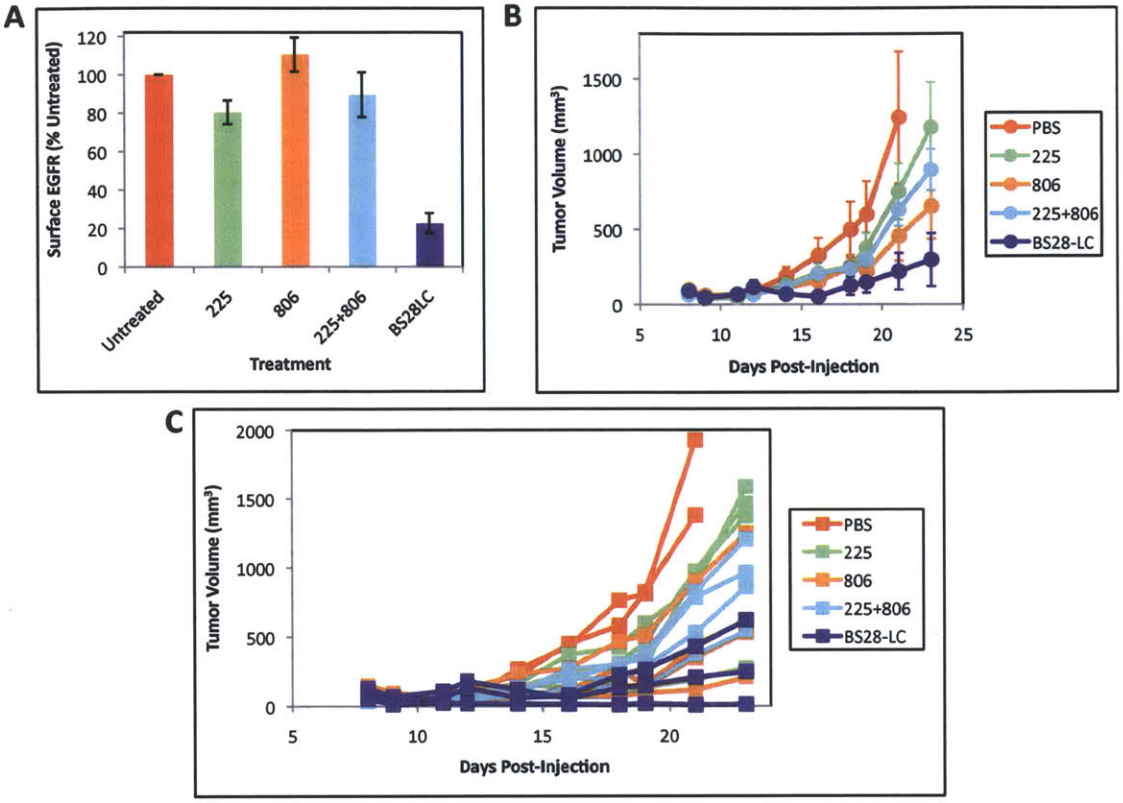

Figure 5.1. *In vitro* downregulation predicts *in vivo* performance of a bispecific antibody targeting wild type and mutant EGFR. (A) U87-SH cells were treated with the indicated antibodies for 13 h at 37°C. Antibody was then stripped and surface EGFR was relabeled and quantified via flow cytometry. Average surface EGFR levels remaining from three independent experiments are shown (± SD). (B) U87-SH cells were injected subcutaneously into the left flank of 6-8 week old female nude mice. Beginning on day 8 post-inoculation, mice were treated twice weekly with either PBS or 5 mg/kg of the specified antibody. Average tumor volumes over the 23-day experiment are shown (± SEM). On day 23, $P<0.05$ for the BS28-LC treatment group versus the 225+806 treatment group by student's t test. (C) Individual mouse growth curves from the experiment shown in (B).

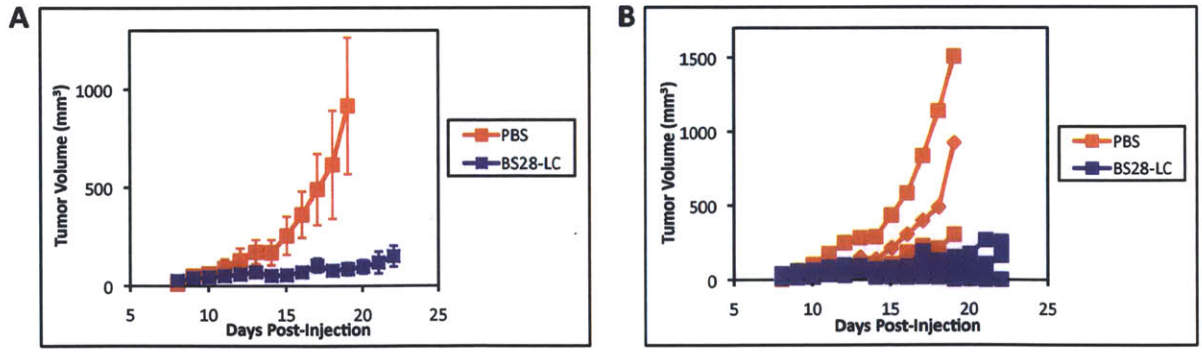

Figure 5.2. Engineered bispecific antibody controls xenografted tumor growth of U87-SH glioblastoma cells. (A) U87-SH cells were injected subcutaneously into the left flank of 6-8 week old female nude mice. Beginning on day 8 post-inoculation, mice were treated twice weekly with either PBS or 7.5 mg/kg of the BS28-LC bispecific antibody. Average tumor volumes over the 22-day experiment are shown (± SEM). On day 19 (termination of PBS cohort), $P<0.05$ for the PBS versus the BS28-LC treatment groups by student's t test. (B) Individual mouse growth curves from the experiment shown in (A).

Mice that were treated every three days with PBS or 7.5 mg/kg of either 225, 806, 225+806 in combination, or BS28-LC were sacrificed on day 22 (24 hours post-treatment). Tumors were dissected and immunofluorescently stained for antibody distribution. As shown in Figure 5.3, antibody was well perfused throughout the small BS28-LC-treated tumors. Background fluorescence is shown in the larger PBS-treated control tumor.

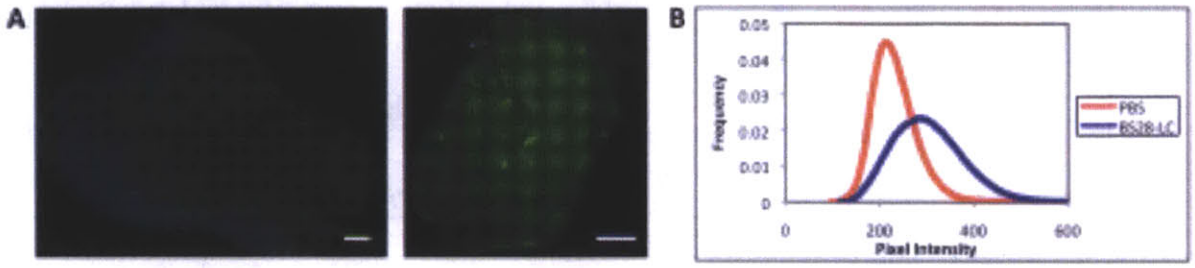

Figure 5.3. Antibody is well perfused in an inhibited tumor. (A) U87-SH cells were injected subcutaneously into the left flank of 6-8 week old female nude mice. Beginning on day 8 post-inoculation, mice were treated twice weekly with PBS (left) or 7.5 mg/kg BS28-LC (25). Mice were administered a final injection on day 21 and sacrificed 24 hours later. Tumors were then sectioned and immunofluorescently stained for both human IgG1 (green) and cell nuclei (blue). Tumors were imaged on the Delta Vision Spectris microscope and image intensities were normalized. Scale bars = 1 mm. (B) Histogram of antibody pixel intensities for PBS-treated tumor (red) and BS28-LC-treated tumor (blue).

The same tumor sections were then immunofluorescently stained for EGFR. Overall EGFR expression in the tumor was decreased following two weeks of BS28-LC treatment compared to saline-treated control tumors, presumably due to chronic downregulation (Figure 5.4).

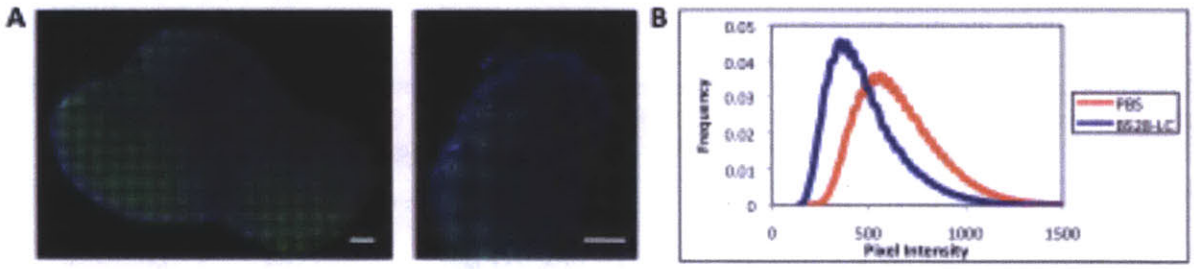

Figure 5.4. Tumor control correlates with downregulation of EGFR expression. U87-SH cells were injected subcutaneously into the left flank of 6-8 week old female nude mice. Beginning on day 8 post-inoculation, mice were treated twice weekly with PBS (left) or 7.5 mg/kg BS28-LC (25). Mice were administered a final injection on day 21 and sacrificed 24 hours later. Tumors were then sectioned and immunofluorescently stained for both human EGFR (green) and cell nuclei (blue). Tumors were imaged on the Delta Vision Spectris microscope and image intensities were normalized. Scale bars = 1 mm. (B) Histogram of EGFR (26) pixel intensities for PBS-treated tumor (red) and BS28-LC-treated tumor (blue).

Ab-Fn3 fusions exhibit equivalent pharmacokinetic properties to unconjugated antibody

Before evaluating the therapeutic efficacy of Ab-Fn3 fusions, we wished to determine their clearance properties to establish an appropriate dosing regimen for these novel constructs. We

injected cetuximab (225), the base antibody, or our most active trans-trispecific Ab-Fn3 fusion, HND+LCA, into 6-8 week old female athymic mice and measured blood plasma antibody concentration over a 48 h time course. As shown in Figure 5.5, the pharmacokinetics of the Ab-Fn3 fusion were identical to those of the unmodified antibody. Fitting our data to biphasic clearance curves of the equation:

$$Y = Ae^{-at} + Be^{-bt}$$

where Y is relative antibody signal and t is time post-injection, we find that approximately 50% of the antibody is cleared in the α phase with a halftime of 10 min and 50% is cleared in the β phase with a halftime of 9 h. The full list of parameters is provided in Table 5.1. Based on standard dosing regimens for IgG in mouse xenograft models, we chose to dose animals every 3 days.

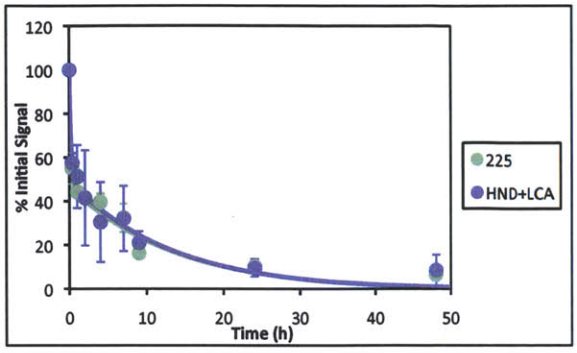

Figure 5.5. Ab-Fn3 fusion clears with same pharmacokinetic profile as monoclonal antibody. The base 225 antibody or the trans-trispecific fusion HND+LCA were injected into 6-8 week old female athymic mice and blood plasma antibody levels were measured for 48 h. The fraction of initial signal at each timepoint is displayed (±SD) with a fitted biphasic clearance curve overlaid (three mice per cohort).

Parameter	Description	225	HND+LCA
A	α clearance fraction	53	50
B	β clearance fraction	47	50
$t_{1/2,\alpha}$	α clearance halftime	0.13 h	0.14 h
$t_{1/2,\beta}$	β clearance halftime	9.1 h	8.9 h

Table 5.1. Clearance parameters for 225 and HND+LCA constructs in nude mice. Parameters were obtained from a least squares regression fit to the equation $Y = Ae^{-at} + Be^{-bt}$ where Y represents relative antibody signal and t represents time post-injection. The $t_{1/2}$ values were computed as $t_{1/2,\alpha}=\ln(2)/a$ and $t_{1/2,\beta}=\ln(2)/b$.

Ab-Fn3 fusions exhibit superior efficacy to clinically approved cetuximab and in vitro *downregulation is predictive of* in vivo *tumor inhibition*

To compare Ab-Fn3 efficacy to that of the base antibody, we performed tumor xenograft studies on four different cell lines: A431 epidermoid carcinoma cells (2.8×10^6 EGFR/cell), HT-29 colorectal carcinoma cells (1.0×10^5 EGFR/cell), HCT-116 colorectal carcinoma cells (2.4×10^5 EGFR/cell), and U87 glioblastoma cells (1.9×10^5 EGFR/cell). Based on our *in vitro* downregulation results and production considerations, we chose to characterize the cis-trispecific

fusion HN-AD and the trans-trispecific fusion HND+LCA in tumor models. For all xenografts, cells were injected into the flank of 6-8 week old female athymic mice. Tumors were grown for one week, at which point the treatment with either PBS, 225, or an engineered trispecific compound was initiated. Treatments continued every three days for three to five weeks, depending on the tumor growth rate of the cell line.

We established that EGFR downregulation is inversely correlated with receptor density of a cell line, making the A431 epidermoid carcinoma cell line the most challenging to target. Consequently, we first examined the efficacy of Ab-Fn3 fusions in this most challenging environment. Based on *in vitro* downregulation studies, 225 or the cis-trispecific fusion HN-AD only reduces surface EGFR levels by 10-15% after 13 hour incubation at 37°C (Figure 5.6A). Accordingly, in xenograft models, we observe no statistically significant tumor control via 225 or HN-AD treatment at a dose of 7.5 mg/kg (Figure 5.6B).

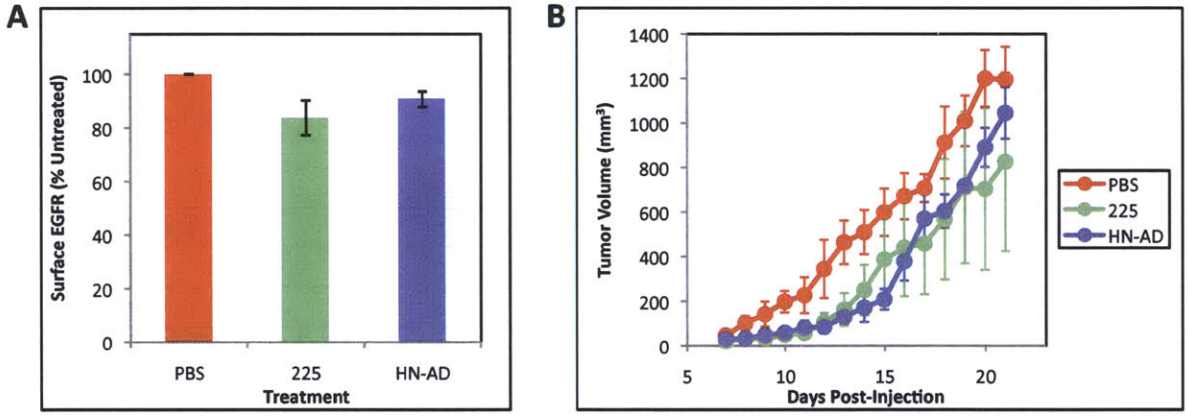

Figure 5.6. Monoclonal antibody 225 and a cis-trispecific Ab-Fn3 fusion fail to downregulate surface EGFR *in vitro* and fail to inhibit tumor growth *in vivo*. (A) Cultured A431 cells were treated with the indicated antibodies for 13 h at 37°C. Bound antibody was then stripped and surface EGFR was relabeled and quantified via flow cytometry. Average surface EGFR levels remaining from three independent experiments are shown (±SD; n=3). (B) A431 cells were injected subcutaneously into the left flank of 6-8 week old female nude mice. Beginning on day 7 post-inoculation, mice were treated twice weekly with either PBS or 7.5 mg/kg of the specified antibody. Average tumor volumes over the 21-day experiment are depicted (± SEM). No statistical significance was observed between the groups by student's t test.

We subsequently assessed the performance of the HN-AD cis-trispecific Ab-Fn3 fusion in a xenograft model of a less EGFR dense cell line, HT-29. *In vitro*, HT-29 cells were potently downregulated by HN-AD but not by 225 (Figure 5.7A). This trend was paralleled in HT-29 xenograft tumors, with HN-AD effectively inhibiting tumor growth for 40 days ($p<0.05$ on days 18 through 29 and $p<0.01$ for days 30 through 34 for HN-AD compared to all other treatment

groups by paired student's t test) while unmodified 225 did not significantly impact tumor volume compared to the saline control during this period (Figure 5.7B)

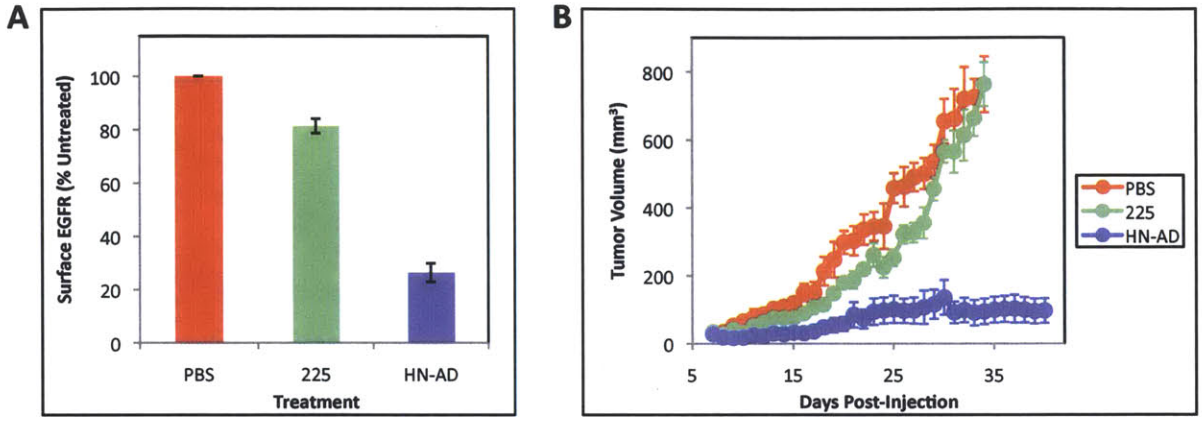

Figure 5.7. Cis-trispecific Ab-Fn3 fusion drastically downregulates surface EGFR *in vitro* and potently inhibits tumor growth *in vivo* whereas the base 225 antibody does not. (A) Cultured HT-29 cells were treated with the indicated antibodies for 13 h at 37°C. Bound antibody was stripped and surface EGFR was relabeled and quantified via flow cytometry. Average surface EGFR levels remaining from three independent experiments are shown (± SD; n=3). (B) HT-29 cells were injected subcutaneously into the left flank of 6-8 week old female nude mice. Beginning on day 7 post-inoculation, mice were treated twice weekly with either PBS or 7.5 mg/kg of the specified antibody. Average tumor volumes over the 40-day experiment are depicted (± SEM). From days 18 through 29, $p<0.05$ and from day 30 to the termination of the study, $p<0.01$ for the HN-AD treatment group compared to each of the other two cohorts by paired student's t test.

The HT-29 xenograft assay was recapitulated with the most potently downregulating trans-trispecific fusion, HND+LCA. As was true of the HN-AD construct, HND+LCA significantly reduced EGFR expression *in vitro* and tumor growth *in vivo*, whereas the unconjugated 225 antibody showed minimal efficacy using a 10 mg/kg dosing regimen. Similar results were observed for the HCT-116 and U87 cell lines (Figure 5.8). Using a one-way repeated measures ANOVA algorithm, we find that for HT-29 and U87 xenograft models, $p<0.01$ for the HND+LCA versus the PBS or 225 cohorts. For HCT-116 xenografts, $p<0.01$ for the HND+LCA versus the PBS cohort and $p<0.05$ for the HND+LCA versus the 225 cohort.

Both Ligand Blocking and Effector Function Contribute to Ab-Fn3-Mediated Tumor Inhibition

The HT-29 and HCT-116 cell lines carry genetic mutations that encode proteins downstream of EGFR in the MAPK and PI3K pathways. HT-29 carries the p.V600E BRAF mutation(27), leading to hyperactivation of the *raf* protein, which acts as an effector in the MAPK pathway. HCT-116 carries the p.G13D KRAS mutation (27), leading to dysregulated signaling by *ras*, an effector that mediates both the PI3K and MAPK pathways. Consequently, it is surprising that

our EGFR-targeted construct showed efficacy in these models. We examined three hypotheses that could potentially explain the efficacy of our construct, both in the absence and presence of BRAF or KRAS mutations.

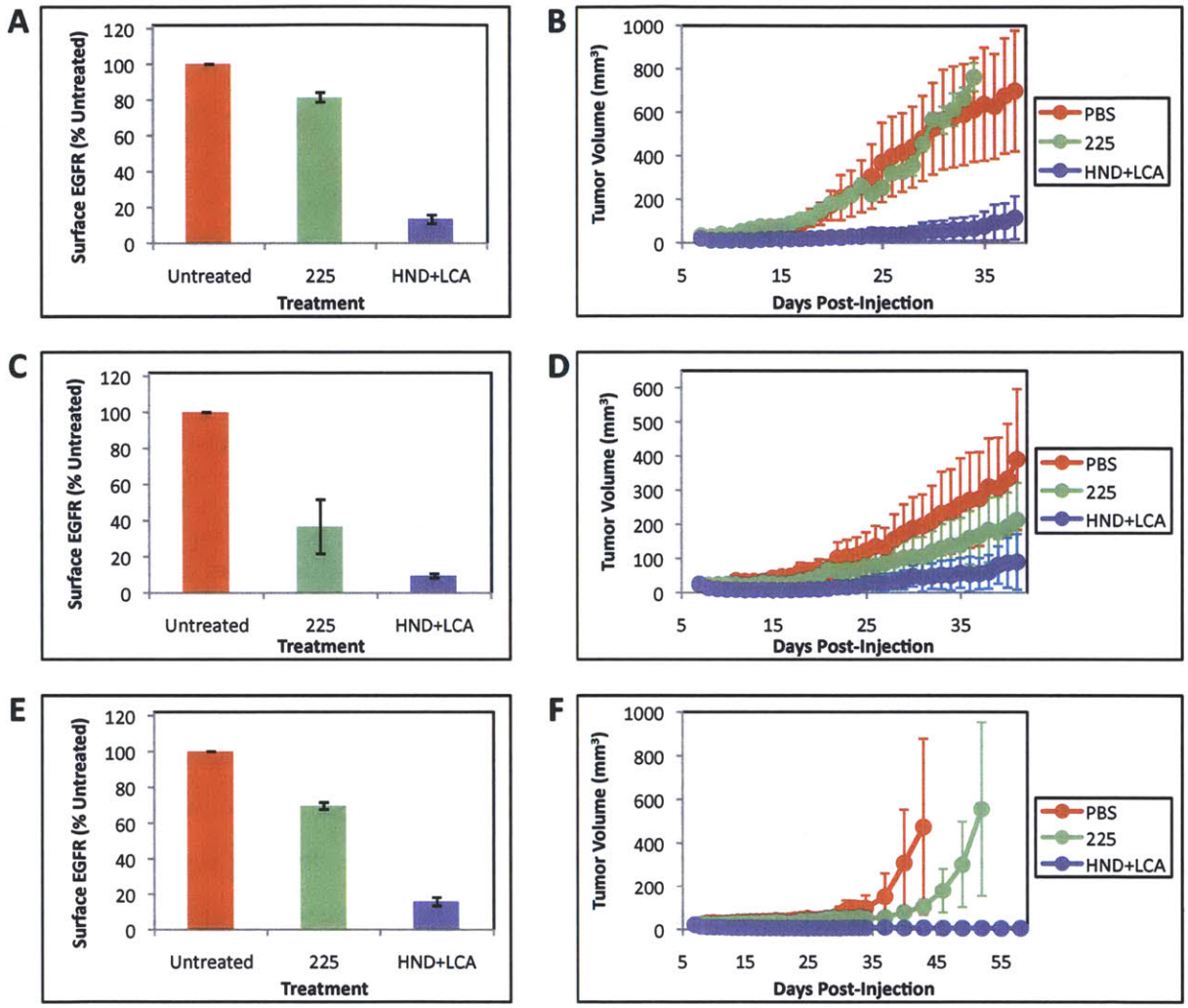

Figure 5.8. Trans-trispecific Ab-Fn3 fusion downregulates surface EGFR *in vitro* and inhibits tumor growth *in vivo* whereas the unconjugated 225 antibody does not. For downregulation assays, cultured HT-29 (A), HCT-116 (C), or U87 cells (E) were treated with the indicated antibodies for 13 h at 37°C. Bound antibody was stripped and surface EGFR was relabeled and quantified via flow cytometry. Average surface EGFR levels remaining from three independent experiments are shown (± SD; n=3). For xenograft models, HT-29 (B), HCT-116 (D) or U87 cells (F) were injected subcutaneously into the left flank of 6-8 week old female nude mice. Beginning on day 7 post-inoculation, mice were treated every three days with either PBS or 10 mg/kg of the specified antibody. Treatment spanned the duration of the experiment for HT-29 and HCT-116 xenografts whereas treatment was stopped on day 31 for U87 xenografts. Average tumor volumes from four mice are depicted (± SEM). For HT-29 and U87 xenografts, $P<0.01$ for the HND+LCA versus the PBS or 225 cohorts. For HCT-116 xenografts, $P<0.01$ for the HND+LCA versus the PBS cohort and $P<0.05$ for the HND+LCA versus the 225 cohort. Statistical analyses were performed using a one-way repeated measures ANOVA algorithm.

The first hypothesis involved a recently discovered mechanism through which EGFR binds to the SGLT1 glucose transporter to stabilize intracellular glucose levels, thereby preventing autophagic death (28-30). We theorized that the overall reduction of EGFR induced by Ab-Fn3 fusion-mediated clustering would lead to a reduction in basal glucose levels, thus sensitizing the cells to autophagy. To formally test this hypothesis, we performed a series of cell proliferation assays in HT-29 and HCT-116 cells in the absence and presence of glucose. Cells were incubated for 72 h at 37°C with 20 nM antibody or Ab-Fn3 fusion and subsequently assessed for viability via the Wst-1 proliferation assay. As shown in Figure 5.9, antibody treatment did not affect HT-29 or HCT-116 cell proliferation under high glucose (25 mM) or glucose starvation (0.5 mM) conditions. Insensitivity to the glucose environment precludes the possibility that Ab-Fn3 fusion-mediated tumor inhibition results from destabilization of intracellular glucose levels.

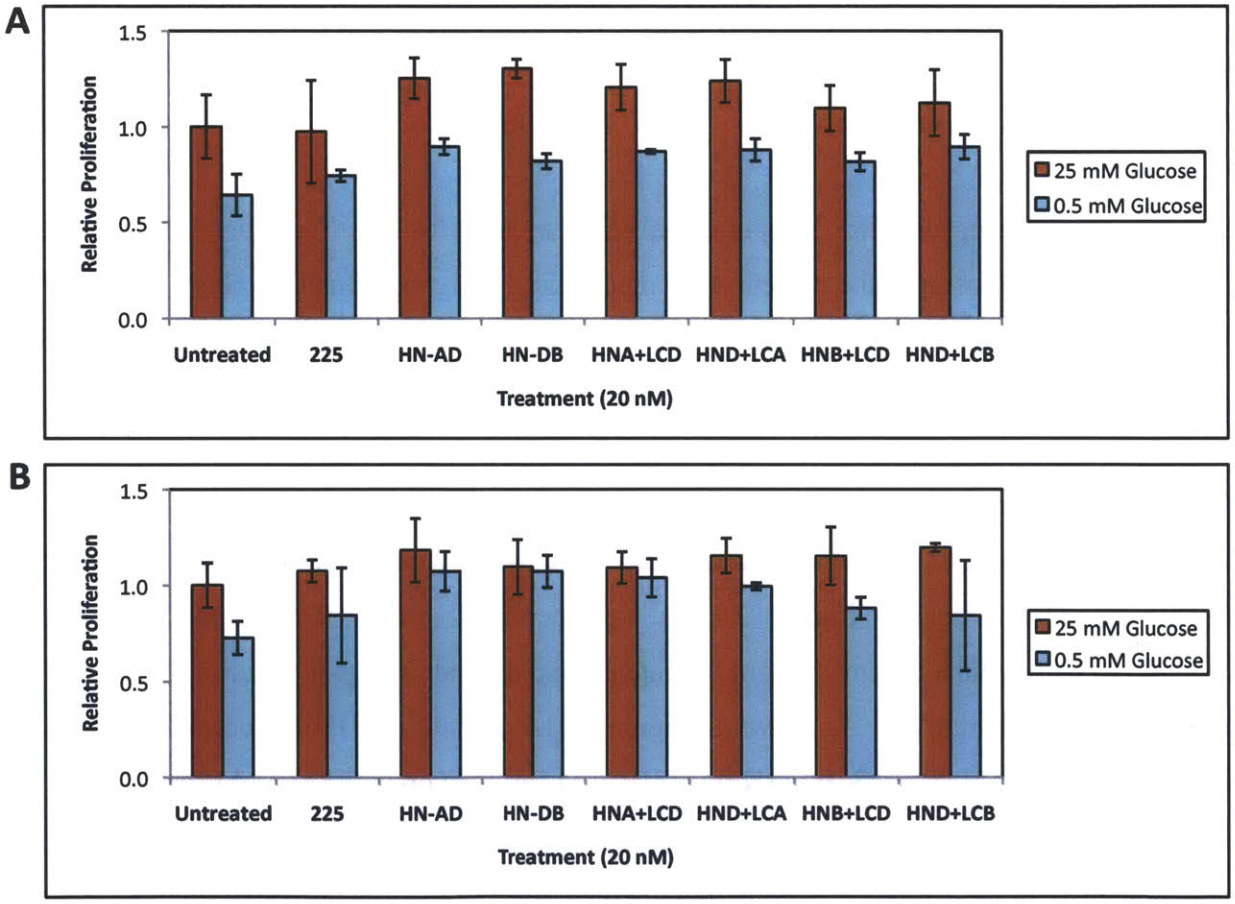

Figure 5.9. Glucose starvation does not affect survival of HT-29 or HCT-116 cells in presence of antibody treatment. HT-29 (A) or HCT-116 (B) cells were seeded on 96-well plates and allowed to attach for 24 h. Incubation in 20 nM antibody proceeded for 72 h at 37°C and cells were then assessed for proliferation via Wst-1 assay. Proliferation relative to untreated cells (±SD; n=3) is depicted under glucose-rich (25 mM) and glucose starvation (0.5 mM) conditions.

An alternative hypothetical mechanism for Ab-Fn3 fusion-mediated inhibition of tumor growth involves the obstruction EGFR signaling through the complementary strategies of ligand inhibition (via the 225 base) and receptor downregulation (via multi-epitopic targeting of the Fn3 domains). It was recently shown that the response of MAPK and PI3K signaling have extreme sensitivity to the abundance of phosphorylated EGFR (pErbB1) (4). As shown in Figure 5.10 from Chen *et al* (4), the difference between 99% and 99.9% inhibition of EGFR activity translates into an 80% reduction in activity of ERK (an effector in the MAPK pathway) and Akt (an effector in the PI3K pathway).

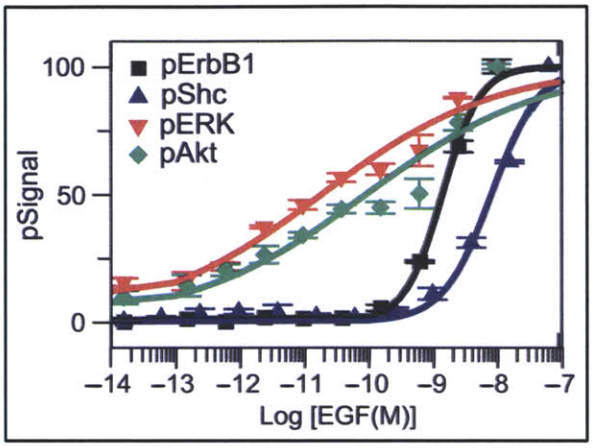

Figure 5.10. EGF dose response profile of ErbB1 and downstream effectors. The response of ErbB1, Shc, ERK, and Akt phosphorylation to a range of EGF concentrations was measured five minutes after treatment via in-cell western assay. This figure is reproduced with permission from (4).

This downstream amplification of input signal could account for the differential response to 225 versus the Ab-Fn3 fusion if the two-pronged mechanism of ligand inhibition plus downregulation incrementally reduces residual EGFR signaling that occurs when only ligand inhibition is employed (*i.e.* in the presence of unconjugated 225).

To examine whether or not ligand competition plays a role in the observed therapeutic effect, we designed a version of the HND+LCA trans-trispecific fusion with two mutations in the variable domain of the heavy chain to impair 225 binding. Specifically, residues Y102 and D103 of the 225 heavy chain, which are involved in hydrogen bond and salt bridge interactions with EGFR, were mutated to alanine (2). As shown in Figure 5.11A, mutation of D103 decreased the binding affinity of 225 by nearly thirty-fold (K_d=1.0×10^{-10} M for 225 versus 2.8×10^{-9} M for D103A), whereas mutation of Y102 had a minimal effect. The two variable domain mutations were used simultaneously in the HND+LCA construct to create the 225 binding defective mutant, HND+LCAx. The reduction in binding from the 225 mutated construct was mitigated by the presence of the two Fn3 domains, resulting in only about a tenfold difference in affinity between HND+LCA (K_d=7.1×10^{-11}M) and HND+LCAx (5.9×10^{-10} M) (Figure 5.11B).

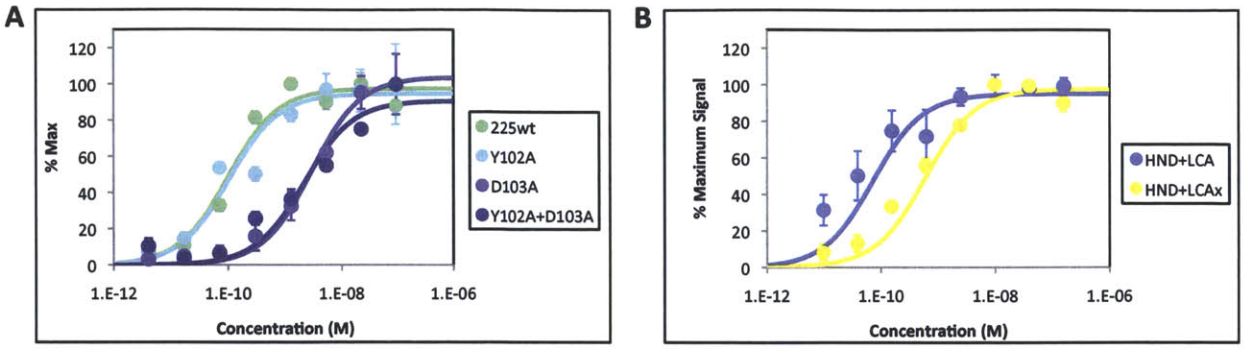

Figure 5.11. Introduction of two mutations in the variable domain of the 225 heavy chain impairs binding to EGFR. (A) The indicated 225 variants (either wild type 225 or 225 with the Y102A, D103A, or both mutations) were titrated on the surface of HMEC cells. The indicated concentrations of antibody were added to cell suspensions and incubated for 3 h at 4°C. EGFR-bound antibody was detected with fluorophore-conjugated anti-human secondary antibody. Signal relative to maximum fluorescence is plotted (±SD; n=3). (B) The indicated trans-trispecific constructs were titrated on the surface of A431 cells. The indicated concentrations were added to cell suspensions and incubated for 3 h at 4°C. Bound antibody was detected with fluorophore-conjugated anti-human secondary antibody. Relative signal normalized to maximum fluorescence is plotted (±SD; n=3).

To verify that the competition with EGF was impaired by the mutations introduced into the 225 variable domain, we performed competition assays on the surface of A431 cells. As shown in Figure 5.12, the mutated HND+LCAx construct competes 7-fold less efficiently with EGF than does the wild type HND+LCA (K_I=4.2×10^{-9} M for HND+LCAx versus K_I=5.9×10^{-10} M for HND+LCA).

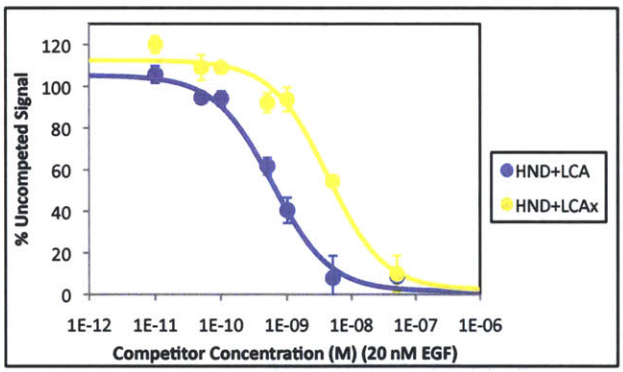

Figure 5.12. Introduction of two mutations in the variable domain of the 225 heavy chain impairs antibody competition with EGF. (A) A431 cells were incubated with the indicated concentration of competitor antibody (either wild type HND+LCA or 225-mutated HND+LCAx) for 1 hour at 4°C. Soluble fluorescently labeled EGF was then added to the cells and incubation proceeded for 30 min. Fluorescent signal was subsequently analyzed via flow cytometry. Signal relative to the uncompeted control is presented (±SD, n=3).

The third hypothetical mechanism for Ab-Fn3 fusion efficacy that we considered was the possibility that effector function was enhanced by fusion-induced clustering. The role of immune cell recruitment via Fcγ receptor interaction in antibody efficacy has long been appreciated (20) and the 225 antibody is known to evoke ADCC in non-small cell lung(31) and colorectal (32) cancers, mediated through natural killer (NK) cells or macrophages.

To parse the contribution of immune effector function to Ab-Fn3-mediated tumor inhibition, we designed a mutant version of the HND+LCA trans-trispecific fusion (hereafter referred to as HND+LCAf) with deficient Fc-γ receptor binding. Specifically, the D265A mutation was introduced into the constant region of the IgG heavy chain to drastically reduce immune cell interaction (33, 34) and, consequently, ADCC. As demonstrated in Figure 5.13, this point mutation inhibits Fc-γ receptor 4 (which engages macrophages and NK cells) binding by 96%. As expected, the presence of this constant domain mutation does not affect antibody affinity (K_d=7.1×10^{-11} M for HND+LCA and K_d=7.8×10^{-11} M for HND+LCAf) or EGF competition (K_I=5.9×10^{-10} M for HND+LCA and K_I=4.8×10^{-10} M for HND+LCAf).

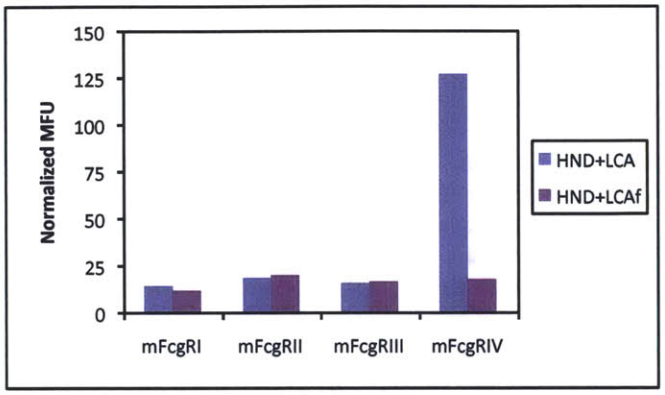

Figure 5.13. Introduction of an Fc domain mutation in the 225 IgG ablates binding to Fcγ receptor IV. Yeast displaying Fcγ receptor I, II, III, or IV were incubated with 20 nM either HND+LCA or HND+LCAf. Bound Ab-Fn3 fusion was detected via flow cytometry with a fluorophore-conjugated anti-human secondary antibody. The normalized fluorescent signal is plotted for each receptor. This work was performed by Tiffany Chen.

Based on deconvolution microscopy analysis, Ab-Fn3 fusion-induced receptor clustering iss not impacted by either the 225 variable domain or Fc region mutations. The punctate distribution of EGFR is evident as early as 1 h after exposure to Ab-Fn3 fusion and does not differ noticibly between HND+LCA, HND+LCAx, and HND+LCAf treatment (Figure 5.14).

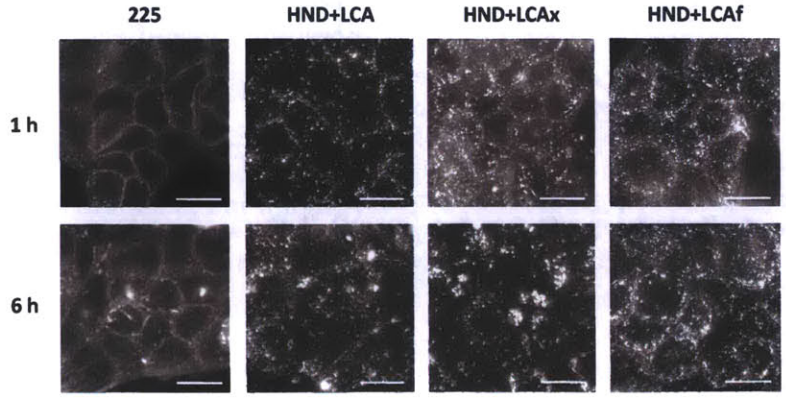

Figure 5.14. Mutations in the 225 IgG variable domain and Fc domain do not impact receptor clustering. The indicated constructs were labeled with fluorescent dye, incubated with HT-29 cells for 1 or 6 h at 37°C, and subsequently washed and visualized on a DeltaVision Spectris microscope. Images were deconvolved and normalized and represent projections of 0.15 μm slices through the full cell volume. Scale bars = 15 μm.

To ensure that the 225 variable domain and Fc-domain mutations did not abrogate Ab-Fn3-mediated EGFR downregulation, we compared the downregulation kinetics of HND+LCA, HND+LCAx, and HND+LCAf. As shown in Figure 5.15, the kinetics of downregulation were not significantly altered by either of the mutations relative to the wild type trans-trispecific ($t_{1/2}$=0.05 h for HND+LCA, $t_{1/2}$=0.11 h for HND+LCAx, and $t_{1/2}$=0.14 h for HND+LCAf). Also, as expected, the steady-state surface EGFR levels were identical following HND+LCA and HND+LCAf treatment. The steady-state level of surface EGFR in the HND+LCAx mutant was slightly higher than that of HND+LCA due to the loss of trispecificity as a result of the 225 variable domain mutation.

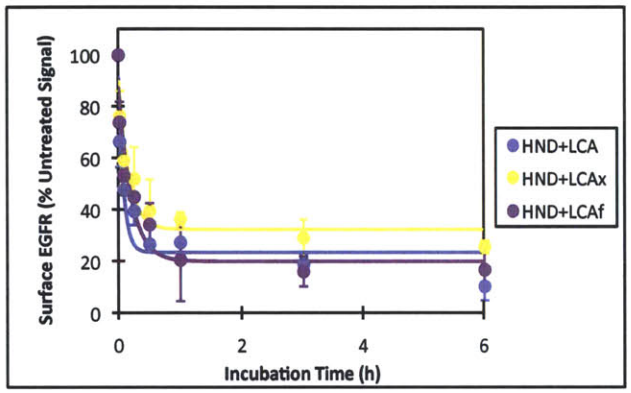

Figure 5.15. IgG variable domain and effector function point mutations do not alter downregulation kinetics and only slightly affect downregulation extent. HT-29 cells were treated with wild type HND+LCA trans-trispecific Ab-Fn3 or variants of this construct with a 225 variable domain mutation (HND+LCAx) or a CH2 domain mutation (HND+LCAf). Cells were dissociated at the indicated time, acid stripped to eliminate bound antibody, and relabeled with murine 225 to detect surface receptor. EGFR levels were quantified via flow cytometry and normalized to those of untreated cells.

To isolate the contributions of signal inhibition and effector function to *in vivo* tumor inhibition, we assessed the performance of the HND+LCAx and HND+LCAf mutants relative to the wild type HND+LCA in HT-29, HCT-116, and U87 xenograft models. As before, tumor cells were injected subcutaneously into the flank of 6-8 week old nude mice and tumors were allowed to grow for 7 days. Beginning on day 7 post-tumor inoculation, 10 mg/kg of the prescribed construct was injected every three days. From Figure 5.16, we find that the contributions of ligand inhibition and effector function vary for the three cell lines tested. In the BRAF mutant HT-29 cell line, both ligand inhibition and effector function are requisite for tumor control. However, in the KRAS mutant HCT-116 cell line and the BRAF/KRAS wild type cell line U87, ligand inhibition is sufficient for tumor control; although immune effector function may contribute, it is not strictly required for the observed therapeutic effect. Statistical analysis via one-way repeated measures ANOVA demonstrates significance ($P<0.01$) between the

HND+LCA and the PBS, HND+LCAx, and HND+LCAf cohorts for HT-29 xenografts and significance ($P<0.01$) between the HND+LCA and only the PBS and HND+LCAx cohorts for HCT-116 and U87 cells.

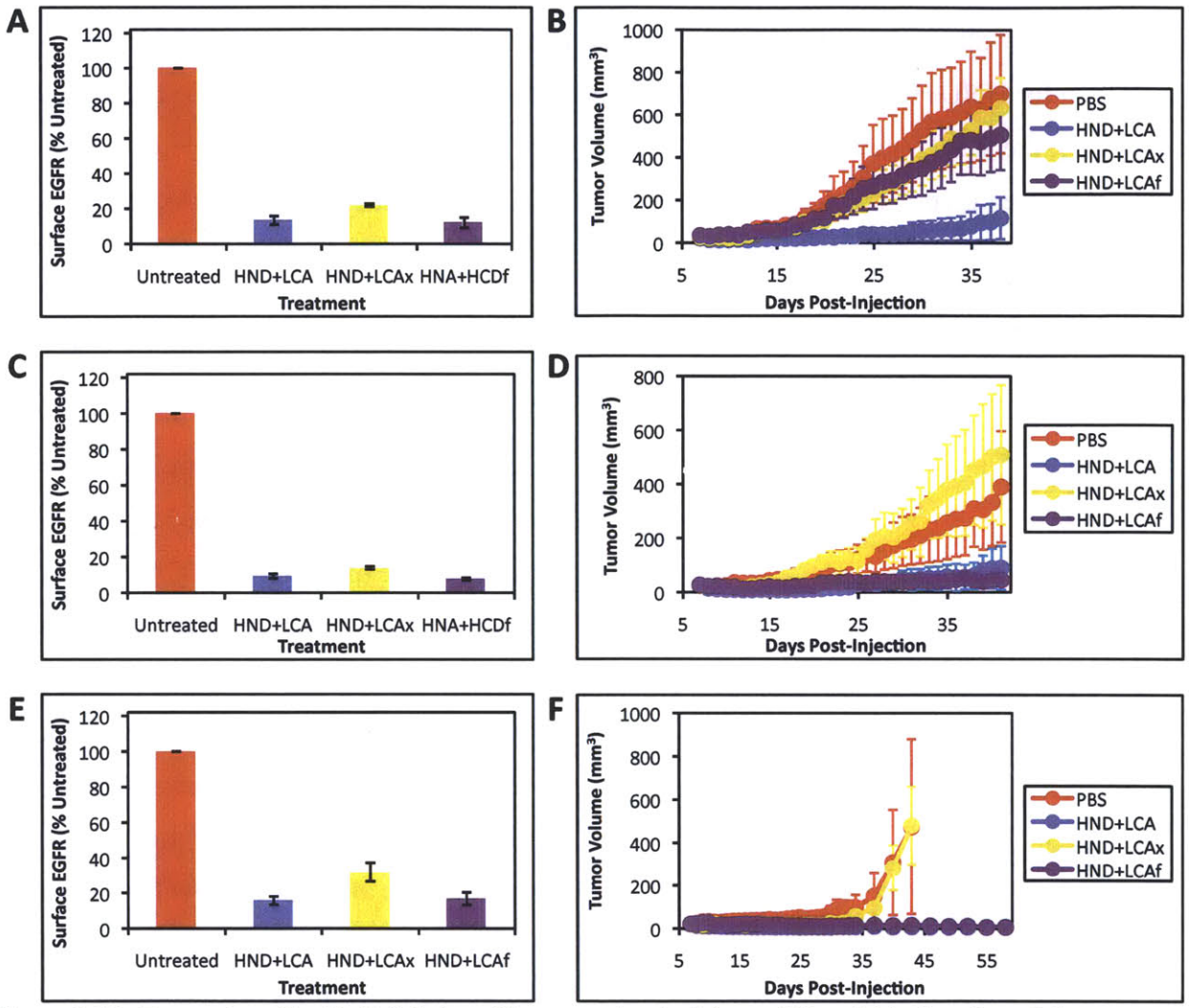

Figure 5.16. Trans-trispecific Ab-Fn3 fusion efficacy requires both intact 225 variable domain and, in some cases, intact Fc effector function. For downregulation assays, cultured HT-29 (A), HCT-116 (C), or U87 cells (E) were treated with the indicated antibodies for 13 h at 37°C. Following treatment, antibody was stripped and surface EGFR was relabeled and quantified via flow cytometry. Average surface EGFR levels remaining from three independent experiments are shown (± SD). For xenograft models, HT-29 (B), HCT-116 (D) or U87 cells (F) were injected subcutaneously into the left flank of 6-8 week old female nude mice. Beginning on day 7 post-inoculation, mice were treated every three days with PBS or 10 mg/kg of the specified antibody. Average tumor volumes from four mice are shown (± SEM). For HT-29 xenografts, $P<0.01$ for the HND+LCA versus the PBS, HND+LCAx, and HND+LCAf cohorts. For HCT-116 and U87 xenografts, $P<0.01$ for the HND+LCA versus the PBS and HND+LCAx cohorts. Statistical analyses were performed using a one-way repeated measures ANOVA algorithm.

As with the BS28-treated xenografts, HT-29 tumors were dissected and immunofluorescently stained for total EGFR content at the termination of the experiment (day 38). Consistent with

our findings from bispecific antibody-treated tumors, HND+LCA-treated tumors expressed significantly less EGFR than untreated tumors. Notably, the HND+LCAx- and HND+LCAf-treated tumors (which were not controlled by therapy) did not show evidence of EGFR downregulation (Figure 5.17).

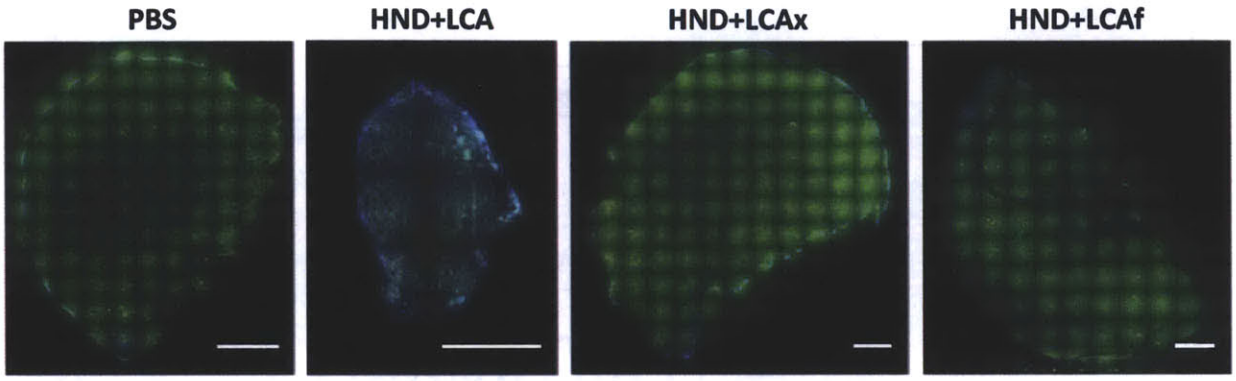

Figure 5.17. HT-29 tumor control coincides with downregulation of EGFR expression. HT-29 cells were injected subcutaneously into the left flank of 6-8 week old female nude mice. Beginning on day 7 post-inoculation, mice were treated twice weekly with PBS or 10 mg/kg of the indicated trans-trispecific Ab-Fn3 fusion. Mice were administered a final injection on day 37 and sacrificed 24 hours later. Tumors were then sectioned and immunofluorescently stained for both human EGFR (green) and cell nuclei (blue). Tumors were imaged on the Delta Vision Spectris microscope and image intensities were normalized. Scale bars = 1 mm.

To further probe the role of signal inhibition in retarding tumor growth, we used western blot analysis to determine the extent of Akt and ERK phosphorylation antagonism in HT-29 cells following treatment with saturating concentrations of 225, HND+LCA, HND+LCAx, and HND+LCAf. Note that ERK activity in these cells still responds to EGF stimulation despite the downstream mutation in the *raf* protein. Cells were incubated with antibody or fusion constructs for 13 h and subsequently pulsed with EGF, followed by cell lysis and phosphoprotein quantification.

We first assessed Akt antagonism by trans-trispecific constructs compared to the 225 mAb. In the BRAF mutant cell line HT-29, which has wild-type PI3K signaling, Akt showed a rapid and intense response to EGF stimulation, with peak stimulation at 1 min post-treatment (Figure 4.18). Isotype control antibody did not impact signaling dynamics. However, the 225 mAb delayed and attenuated the response to EGF, showing maximal activity 5 min post-treatment with a peak at two-thirds the intensity of PBS-treated cells. Remarkably, all the trans-trispecific construct HND+LCA and its ligand binding and effector function mutant counterparts completely blocked

Akt activation in HT-29 cells. Thus, ligand blockade combined with downregulation effectively inhibits signaling downstream of EGFR.

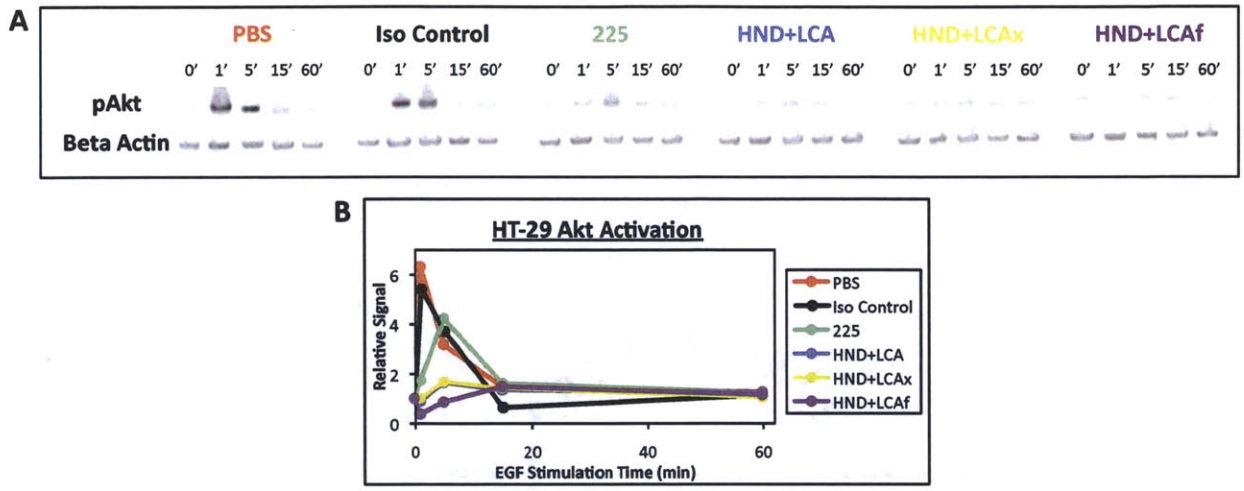

Figure 5.19. Ab-Fn3 fusions block signaling through PI3K pathway. (A) Serum starved HT-29 cells were treated for 13 h at 37°C with PBS, or 20 nM of an isotype control antibody, 225, HND+LCA, HND+LCAx, or HND+LCAf. They were then stimulated with 20 nM EGF for the indicated time intervals at 37°C. Cell lysis proceeded and pAkt and beta actin were quantified via immunoblot assay. (B) Quantification of immunoblot results presented in (A). Band intensities were normalized by beta actin levels and by the intensity of a control lysate included on each blot. The activation threshold is set at 1.7-fold background.

Even more striking than the Akt inhibition is the differential ERK antagonism effected by trans-trispecific constructs compared to 225. ERK phosphorylation is apparent within 1 min of EGF stimulation and declines back to basal levels by 60 min post-treatment in the presence of PBS or an isotype control antibody (Figure 5.19). Incubation with 225 delays ERK activation so that maximum pERK signal is observed at 5 min post-EGF treatment. However, peak activation levels still remain identical to those in untreated or isotype control-treated cells. Incubation with HND+LCA, HND+LCAx, and HND+LCAf completely ablate ERK activation in the presence of EGF. These results demonstrate that the combination of ligand inhibition and Ab-Fn3-induced receptor downregulation conspire to abrogate activity of the MAPK pathway although neither mechanism alone is sufficient. These findings are consistent with our *in vivo* observation that both downregulation capacity and intact ligand inhibition are vital for therapeutic efficacy.

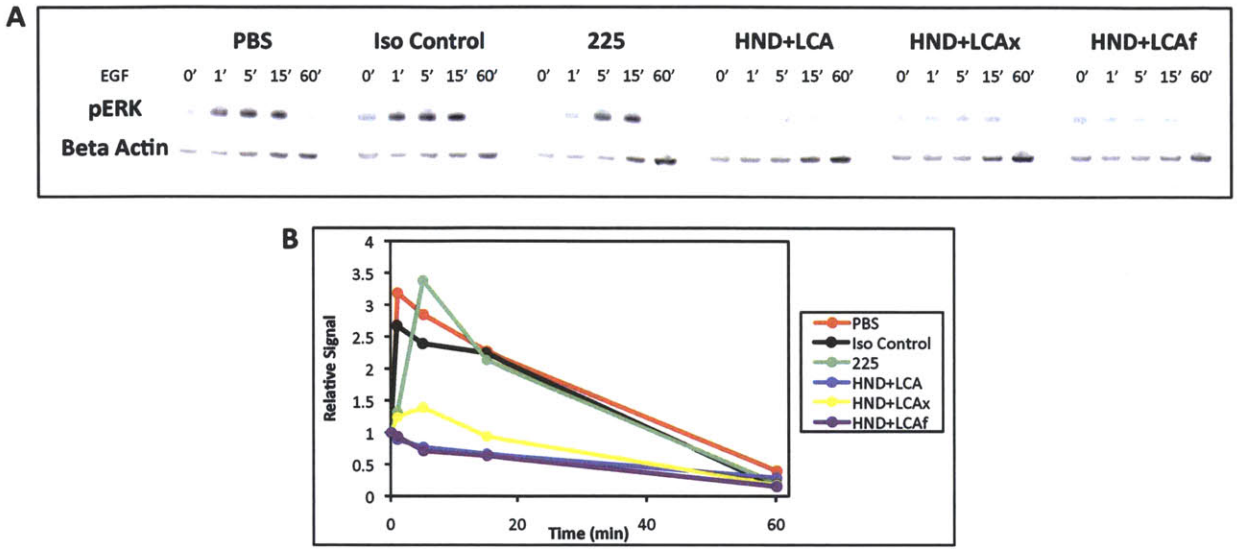

Figure 5.19. Ab-Fn3 fusions ablate signaling through MAPK pathway. (A) Serum starved HT-29 cells were incubated for 13 h at 37°C with PBS, or 20 nM of an isotype control antibody, 225, HND+LCA, HND+LCAx, or HND+LCAf. They were subsequently stimulated with 20 nM EGF for the indicated lengths of time at 37°C. Cells were then lysed and the abundance of pERK and beta actin were analyzed via immunoblot quantification. (B) Quantification of immunoblot results presented in (A). Band intensities were normalized by beta actin levels and by the intensity of a control lysate included on each blot. The activation threshold is set at 1.7-fold background.

Discussion

Based on previous observations using combinations of antibodies directed against multiple targets on EGFR (7, 35) or ErbB2 (36, 37), we predicted that our multi-epitopic antibodies would effectively control tumor growth in mouse xenograft models of EGFR-expressing cancer.

In the case of the 225/806 bispecific antibody (BS28-LC), we achieve tumor inhibition that is superior to that induced by combination therapy by enhancing avidity effects (Figures 5.1, 5.2). The *in vivo* tumor control in the U87-SH model is strongly correlated with the *in vitro* downregulation elicited by single, combination, or bispecific antibody treatment. Notably, the effective dose of our bispecific construct (5 mg/kg) is tenfold below that of the 225 monoclonal antibody (38). It is thus advantageous to re-format synergistic antibody combinations as bispecific constructs, particularly in situations where the binding of one of the antibodies is limited, as is the case for the 806 antibody (6, 39). Our immunofluorescent staining of the excised tumors indicates that BS28-LC is well perfused in the tumor 24 h post-treatment and that EGFR levels are reduced following two weeks of treatment with this construct (Figures 5.3, 5.4).

We also establish the therapeutic efficacy of Ab-Fn3 fusion constructs in three different xenograft tumor models (Figures 5.7, 5.8). These findings resonate with recent demonstration that a camelid-derived single domain antibody that simultaneously binds two epitopes of EGFR domain III retards the growth of solid tumors (40). Again, we observe that *in vitro* downregulation is predictive of *in vivo* efficacy.

Surprisingly, two of the xenograft models we studied (HT-29 and HCT-116) resist treatment with the base 225 antibody via downstream mutations yet show sensitivity to Ab-Fn3 fusions. While 225 induces significant inhibition of EGFR phosphorylation through ligand competition, the incremental inhibition of EGFR activation by the complementary mechanism of receptor clustering and downregulation results in potent obstruction of downstream signaling through the Akt and MAPK pathways (Figures 5.18, 5.19). Furthermore, our results suggest a role for ADCC in therapeutic efficacy in the HT-29 model (Figure 5.16). The rapid formation of receptor-antibody clusters on the surface of tumor cells could enhance immune effector cell recruitment, potentiating the immunological effects of 225 (31, 32). ADCC effects are known to be mediated through NK cells, but there is growing evidence that macrophages may play a key role in antibody-dependent tumor cell killing (41-44). Based on hematoxylin and eosin staining of dissected tumor sections, we saw little evidence of NK cell infiltration in controlled tumors, but we did observe an abundance of macrophages in these specimens. Although immune effector function appears to contribute to the Ab-Fn3 mechanism of action, it is important to note that immune effector function alone cannot account for the observed therapeutic effect as constructs that lack ligand inhibition capacity but possess intact immune effector function fail to substantively slow tumor growth.

Encouragingly, Ab-Fn3 fusion half-life parallels that of human IgG1 (Figure 5.5), suggesting that like monoclonal antibodies, our fusions benefit from neonatal Fc receptor recycling in the bloodstream (45). Thus, pharmacokinetic studies implicate a dosing schedule similar to that of clinically approved IgGs, and potency at 10 mg/kg suggests that our construct may be effective at lower doses than currently available monoclonal antibodies, which would reduce undesirable side effects and cut manufacturing costs.

The establishment of the strategy of multi-epitopic targeting holds exciting promise for development of drugs targeting other ErbB family members or receptor tyrosine kinases in general. By enhancing the avidity of antibody-based constructs and introducing the complementary mechanism of cluster-induced downregulation, we may recover or improve the efficacy of existing drugs as well as design novel therapeutics that benefit from a multi-epitopic strategy. With the addition of a third fibronectin clone to the IgG scaffold, one can envision the development of a tetraspecific Ab-Fn3 fusion that targets two receptors at two non-overlapping epitopes, resulting in the clustering and consequent downregulation of multiple receptors from a single construct. This would be particularly relevant for EGFR targeting, where cells often evade EGFR therapy through compensatory signaling via other ErbB receptors (notably ErbB3) or the c-MET receptor (46-50), as discussed in Chapter 4. Overall, the multi-epitopic strategy we present introduces an effective means of targeting, clustering, and downregulating a receptor to inhibit signaling and, ultimately, tumor growth.

Materials & Methods

Cell Culture

All cell lines and media were purchased from ATCC (Manassas, VA) unless otherwise specified. Cells were grown at 37°, 5% CO_2 in a humidified atmosphere. U87-SH cells (23) were cultured in DMEM containing 10% FBS, 1% sodium pyruvate, 1% non-essential amino acids, and 0.2 g/L G418 for selection. HT-29 and HCT-116 cells were cultured in McCoy's 5A medium supplemented with 10% FBS and 1X penicillin-streptomycin solution (PS). U87 cells were cultured in DMEM with 10% FBS, 1% sodium pyruvate, 1% non-essential amino acids, and 1X PS. HEK 293-F cells (Invitrogen, Carlsbad, CA) were maintained in suspension in FreeStyle Expression medium (Invitrogen). Adherent cells were detached for subculture or assay use with 0.25% trypsin and 1 mM EDTA. For serum starvation, medium was removed by aspiration, cells were washed with warm PBS, and fresh serum-free medium was added. Complete medium refers to serum-rich medium.

Unless otherwise noted, all washes were conducted in PBS containing 0.1% BSA and all constructs were used at a concentration of 20 nM for single treatment and 10 nM each for combination treatment. EGF (Sigma, St. Louis, MO) was dosed at 20 nM. Trypsin-EDTA (Invitrogen) contains 0.05% trypsin and 0.5 mM EDTA.

Downregulation Assays

Cells were subcultured into 96-well plates at a density of 30,000 per well, incubated for 12-18 h to allow attachment, and serum starved for 12 h. Subsequently, cells were treated with 20 nM of the indicated antibody or Ab-Fn3 fusion for 13 h at 37°C. Medium was removed by aspiration and cells were washed with PBS, detached with trypsin, and placed on ice for the remainder of the assay. Bound antibody constructs were removed by 5 min acid strip with 0.2 M acetic acid, 0.5 M NaCl. Cells were washed with PBSA and incubated in mouse 225 antibody, washed again, and labeled with R-phycoerythrin-conjugated anti-mouse secondary antibody (Invitrogen). Cells were washed and analyzed using a FACS Calibur flow cytometer (BD Biosciences, San Jose, CA). Mean fluorescence was normalized to PBS-treated control samples.

Production of Antibody-Fibronectin Fusions via HEK Cell Transfection

The human IgG1 heavy and light chains of each antibody-fibronectin fusion construct were inserted into the gWiz mammalian expression vector (Genlantis, San Diego, CA). Constructs were verified by sequence analysis. HEK 293-F cells were grown in suspension to a density of 1.2×10^6 per mL in 400 mL and diluted to 1×10^6 per mL prior to transfection. Miniprepped DNA and polyethyleneimine (Sigma, St. Louis, MO) were diluted separately to 0.05 and 0.1 mg/mL, respectively, in 10 mL OptiPro medium and incubated at 22°C for 15 min. Equal volumes of diluted DNA and polyethyleneimine were then mixed and incubated at 22°C for 15 min. Subsequently, 500 mL of cells and 20 mL of DNA/polyethyleneimine mixture were added to a 2 L roller bottle and incubated at 37°, 5% CO_2 on a roller bottle adapter for seven days. The cell secretions were then centrifuged for 30 min at 15,000×*g* and the supernatants were filtered through a 0.22 μm bottle-top filter and purified via affinity column chromatography using protein A resin (Thermo Fisher Scientific, Waltham, MA). The eluted antibodies were concentrated and transferred to PBS and then characterized by sodium dodecyl sulfate polyacrylamide gel electrophoresis (SDS-PAGE) analysis.

Mouse Xenograft Studies

U87-SH glioblastoma cells (2×10^6), HT29 colorectal carcinoma cells (3×10^6), HCT-116 colorectal carcinoma cells (2×10^6), or U87 glioblastoma cells (3×10^6) were injected subcutaneously into the right flanks of 6-8 week-old female Ncr *nu/nu* mice. By day 7 post-injection (or day 8 post-injection for the U87-SH cell line), tumors had grown to a minimum volume of 20 mm^3. Mice were randomized and a twice weekly or every three day retro-orbital injection regimen of PBS or either 225 human IgG1, 806 human IgG1, bispecific antibody, or Ab-Fn3 fusion was commenced (150 μg per treatment for 7.5 mg/kg dosing and 200 μg per treatment for 10 mg/kg dosing). Treatments continued for 3-5 weeks depending on tumor growth rate and tumor volume was monitored daily with a digital caliper using the formula Volume = $0.5\times(\text{Length})\times(\text{Width})^2$. Throughout the experiment, mice were monitored for overall health and activity in accordance with Massachusetts Institute of Technology Committee on Animal Care protocol number 0509-048-12. Heteroscedastic two-tailed student's *t* tests were performed to compare tumor growth between cohorts. Each cohort included three or four mice.

Tumor Immunofluorescence Studies

The xenografted U87-SH tumors were dissected on day 22, immersed in optimal cutting temperature freezing medium, and flash frozen with liquid nitrogen in a bath of 2-methylbutane (Sigma). Tumors were subsequently sectioned (7 μm slices) in a cryostat and affixed to slides. For immunofluorescent staining, slides were fixed with formalin for 10 min and then washed three times with PBS. Cells were subsequently permeabilized in PBS containing 0.1% Triton X-100 for 10 min and washed three additional times. Blocking with a 5% solution of goat serum (Invitrogen) proceeded for 1 h at room temperature, followed by overnight incubation with either polyclonal rabbit anti-EGFR antibody (Abcam, Cambridge, MA) or anti-human Fc antibody (Invitrogen) in 5% goat serum at 4°C. Slides were rinsed three times and incubated with goat anti-rabbit 488-conjugated antibody (Invitrogen) in PBS containing 0.1% Tween 20 for 1 h at room temperature. Following four final PBS washes, the slides were incubated with the DNA stain DAPI (Sigma) for one minute at room temperature, mounted with Vectashield (Vector Laboratories, Burlingame, CA), and sealed with clear nail polish. Imaging was performed on a DeltaVision Spectris microscope (Olympus, Center Valley, PA) at 10X magnification. Image

acquisition and processing were conducted using the Applied Precision software package. All images shown were acquired during a single session using identical intensity settings. The images have been stitched from a series of panels acquired in a single plane of focus.

Pharmacokinetic Studies

Antibody or Ab-Fn3 fusion was labeled with Licor 800cw near-infrared dye (Licor Biosciences, Lincoln, NE). A total of 200 μg per mouse (10 mg/kg) of labeled antibody or Ab-Fn3 fusion suspended in 100 μL PBS was retro-orbitally injected into 6-8 week-old female Ncr *nu/nu* mice (three mice per cohort). At each time point, 20 μL blood was collected from the tail vein and maintained in a capillary tube. The blood was then centrifuged for 5 min at 1500×*g* to remove red blood cells and the plasma layer was transferred to a fresh capillary tube for analysis. Near-infrared signal was detected using the Licor Odyssey infrared imaging system at a wavelength of 800 nm. Signal was normalized to the first collection time point (immediately post-injection).

Cell Proliferation Assays

HT-29 or HCT-116 cells were seeded at 3×10^3 per well in 96-well plates and allowed to adhere for 24 h. They were then treated with the indicated mAbs or Ab-Fn3 fusion constructs at the prescribed concentrations in DMEM containing either 5 or 25 mM glucose and incubated at 37°C for 72 h. Cell viability (relative to an untreated control) was assessed using the Wst1 tetrazolium salt cleavage assay (Roche, Indianapolis, IN) (51, 52). Relative proliferation was calculated as the 450 nm absorbance of treated wells relative to that of untreated control cells.

Affinity titrations

To characterize Ab-Fn3 binding affinities, HMEC or A431 cells were trypsinized, washed in PBSA, and incubated with various concentrations of Ab-Fn3 in a 96-well plate on ice. The number of cells and sample volumes were selected to ensure at least tenfold excess Ab-Fn3 relative to EGFR. All samples were assayed in triplicate. Cells were incubated on ice for sufficient time to ensure that the approach to equilibrium was at least 99% complete. Cells were then washed and labeled with 66 nM PE-conjugated goat anti-human antibody (Rockland Immunochemicals, Gilbertsville, PA) for 20 min on ice. After a final wash, plates were analyzed on a FACS Calibur cytometer (BD Biosciences, San Jose, CA). The minimum and maximum

fluorescence and the equilibrium dissociation constant (K_d) value were determined by minimizing the sum of squared errors assuming a 1:1 binding interaction (% Bound = $[L]/([L]+K_d)$ where [L] is Ab-Fn3 concentration and K_d is the equilibrium dissociation constant of the Ab-Fn3 construct. Curve fitting was implemented in MATLAB (Mathworks, Natick, MA). Titrations were performed at physiological pH (pH 7.4).

Live Cell EGFR Imaging

Cells were plated at 20,000 cells/well in 8-well microscopy chambers (Nunc, Rochester, NY) and allowed to attach overnight. Cells were then serum starved for 12 h and incubated with Alexa 488-labeled (Invitrogen) monoclonal antibody or Ab-Fn3 fusion for 1 or 6 h at 37°C. Wells were then washed to remove unbound constructs and cells were resuspended in phenol red-free DMEM (Invitrogen). Cell monolayers were visualized using a DeltaVision Spectris microscope (Olympus) at 60X magnification (oil immersion lens). During imaging, cells were maintained at 37°C and 5% CO_2. Image acquisition and processing were conducted using the Applied Precision and ImageJ software packages. All images shown were acquired during a single session using identical intensity settings and brightness and contrast settings have been normalized. These images represent projections from 0.15 μm sections spanning the full cell monolayer.

Yeast-Displayed Fcγ Receptor Binding Assay

Transformed yeast stably displaying the extracellular domain of Fcγ receptor I (residues 25-297), II (residues 30-207), III (residues 31-215), or IV (residues 21-203) followed by a cmyc tag were incubated with 100 nM Ab-Fn3 fusion for 30 min at 22°C. Chicken anti-cmyc antibody (Invitrogen) was also added to detect properly displayed receptor. Cells were then washed and goat anti-human 488-labeled secondary antibody (Invitrogen) was added to detect bound IgG fusion. Concurrently, goat anti-chicken 647-labeled secondary antibody (Invitrogen) was added to detect cmyc. Cells were incubated at 4°C for 15 min, washed, and then analyzed on a FACS Calibur flow cytometer (BD Biosciences) and mean Ab-Fn3 fluorescence is reported for functionally displaying yeast (gated based on cmyc detection).

Western Blots

HT-29 or HCT-116 cells were cultured to confluence in 6-well plates and serum starved for 12h. Cells were then incubated with 20 nM antibody or Ab-Fn3 fusion for 13 h at 37°C. Subsequently, 20 nM EGF was added and incubation proceeded at 37°C for the prescribed time length. Cells were then washed twice with cold PBS and incubated with rotation for 5 min in lysis buffer (50 mM Tris•HCl, 2% SDS, 5% glycerol, 5 mM EDTA, 1 mM NaF, protease and phosphatase inhibitors (Thermo Fisher Scientific, Pittsburgh, PA), 10 mM β-GP, 1 mM PMSF and 1 mM Na_3VO_4). Total protein levels were quantified via BCA assay (Thermo Fisher Scientific, Pittsburgh, PA) and lysates were normalized to a final concentration of 3.5 mg/mL. Lysates were clarified by passage through centrifugal filter plates for 8-12 h at 4000×g. The lysates were subsequently subjected to SDS-PAGE on 8% E-Page gels and blotted onto nitrocellulose via iBlot apparatus (Invitrogen). The blotted membrane was then blocked in 1:1 PBS:Odyssey Blocking Buffer (Licor Biosciences) for 1 h at room temperature. Blots were then incubated with 1:1000 dilutions of either anti-phosphoERK1/2 Y202/Y204 rabbit antibody or anti-phosphoAkt S473 rabbit antibody overnight at 4°C (Cell Signaling, Danvers, MA). A 1:15,000 dilution of mouse anti-beta actin antibody (Sigma) was added the next morning and incubation proceeded for 2 h at room temperature. Following three washes, the membrane was incubated with goat anti-mouse (800 cw) and anti-rabbit (700 cw) near IR dye conjugate antibodies. After four additional washes, membranes were visualized on the Licor Odyssey infrared imaging system. Phospho-ERK and phospho-Akt signals were normalized by beta actin signal for each lysate and all samples were normalized to a control lysate to ensure consistent intensity between blots. Images were normalized and quantified using ImageJ software (NIH).

Statistical Analysis

Heteroscedastic two-tailed student's t tests (for experiments shorter than 25 days) or one-way repeated measures ANOVA (for experiments longer than 25 days with the exception of the HT-29 HN-AD model for direct comparison to the A431 HN-AD model) were performed on mouse xenograft data to compare 225, Fn3, and Ab-Fn3 treatments. Both algorithms were implemented in MATLAB (Mathworks).

References

1. Grunwald V & Hidalgo M (2003) Developing inhibitors of the epidermal growth factor receptor for cancer treatment. *J Natl Cancer Inst* 95(12):851-867.
2. Li S, *et al.* (2005) Structural basis for inhibition of the epidermal growth factor receptor by cetuximab. *Cancer Cell* 7(4):301-311.
3. Cohenuram M & Saif MW (2007) Panitumumab the first fully human monoclonal antibody: from the bench to the clinic. *Anticancer Drugs* 18(1):7-15.
4. Chen WW, *et al.* (2009) Input-output behavior of ErbB signaling pathways as revealed by a mass action model trained against dynamic data. *Mol Syst Biol* 5:239.
5. Wong AJ, *et al.* (1992) Structural alterations of the epidermal growth factor receptor gene in human gliomas. *Proc Natl Acad Sci U S A* 89(7):2965-2969.
6. Johns TG, *et al.* (2002) Novel monoclonal antibody specific for the de2-7 epidermal growth factor receptor (EGFR) that also recognizes the EGFR expressed in cells containing amplification of the EGFR gene. *Int J Cancer* 98(3):398-408.
7. Perera RM, *et al.* (2005) Treatment of human tumor xenografts with monoclonal antibody 806 in combination with a prototypical epidermal growth factor receptor-specific antibody generates enhanced antitumor activity. *Clin Cancer Res* 11(17):6390-6399.
8. Bollag G & McCormick F (1991) Regulators and effectors of ras proteins. *Annu Rev Cell Biol* 7:601-632.
9. Macaluso M, *et al.* (2002) Ras family genes: an interesting link between cell cycle and cancer. *J Cell Physiol* 192(2):125-130.
10. McCormick F (1999) Signalling networks that cause cancer. *Trends Cell Biol* 9(12):M53-56.
11. Vakiani E & Solit DB (2011) KRAS and BRAF: drug targets and predictive biomarkers. *J Pathol* 223(2):219-229.
12. Khambata-Ford S, *et al.* (2007) Expression of epiregulin and amphiregulin and K-ras mutation status predict disease control in metastatic colorectal cancer patients treated with cetuximab. *J Clin Oncol* 25(22):3230-3237.
13. Lievre A, *et al.* (2006) KRAS mutation status is predictive of response to cetuximab therapy in colorectal cancer. *Cancer Res* 66(8):3992-3995.

14. Di Fiore F, *et al.* (2007) Clinical relevance of KRAS mutation detection in metastatic colorectal cancer treated by Cetuximab plus chemotherapy. *Br J Cancer* 96(8):1166-1169.

15. Amado RG, *et al.* (2008) Wild-type KRAS is required for panitumumab efficacy in patients with metastatic colorectal cancer. *J Clin Oncol* 26(10):1626-1634.

16. De Roock W, *et al.* (2008) KRAS wild-type state predicts survival and is associated to early radiological response in metastatic colorectal cancer treated with cetuximab. *Ann Oncol* 19(3):508-515.

17. Lievre A, *et al.* (2008) KRAS mutations as an independent prognostic factor in patients with advanced colorectal cancer treated with cetuximab. *J Clin Oncol* 26(3):374-379.

18. Di Nicolantonio F, *et al.* (2008) Wild-type BRAF is required for response to panitumumab or cetuximab in metastatic colorectal cancer. *J Clin Oncol* 26(35):5705-5712.

19. De Roock W, *et al.* (2010) Effects of KRAS, BRAF, NRAS, and PIK3CA mutations on the efficacy of cetuximab plus chemotherapy in chemotherapy-refractory metastatic colorectal cancer: a retrospective consortium analysis. *Lancet Oncol* 11(8):753-762.

20. Griggs J & Zinkewich-Peotti K (2009) The state of the art: immune-mediated mechanisms of monoclonal antibodies in cancer therapy. *Br J Cancer* 101(11):1807-1812.

21. Dechant M, *et al.* (2008) Complement-dependent tumor cell lysis triggered by combinations of epidermal growth factor receptor antibodies. *Cancer Res* 68(13):4998-5003.

22. Lutterbuese R, *et al.* (2010) T cell-engaging BiTE antibodies specific for EGFR potently eliminate KRAS- and BRAF-mutated colorectal cancer cells. *Proc Natl Acad Sci U S A* 107(28):12605-12610.

23. Huang PH, *et al.* (2007) Quantitative analysis of EGFRvIII cellular signaling networks reveals a combinatorial therapeutic strategy for glioblastoma. *Proc Natl Acad Sci U S A* 104(31):12867-12872.

24. Spangler JB, *et al.* (2010) Combination antibody treatment down-regulates epidermal growth factor receptor by inhibiting endosomal recycling. *Proc Natl Acad Sci U S A* 107(30):13252-13257.

25. Garrett TP, *et al.* (2009) Antibodies specifically targeting a locally misfolded region of tumor associated EGFR. *Proc Natl Acad Sci U S A* 106(13):5082-5087.
26. Ettenberg SA, *et al.* (2010) Inhibition of tumorigenesis driven by different Wnt proteins requires blockade of distinct ligand-binding regions by LRP6 antibodies. *Proc Natl Acad Sci U S A* 107(35):15473-15478.
27. Ikediobi ON, *et al.* (2006) Mutation analysis of 24 known cancer genes in the NCI-60 cell line set. *Mol Cancer Ther* 5(11):2606-2612.
28. Weihua Z, *et al.* (2008) Survival of cancer cells is maintained by EGFR independent of its kinase activity. *Cancer Cell* 13(5):385-393.
29. Yun J, *et al.* (2009) Glucose deprivation contributes to the development of KRAS pathway mutations in tumor cells. *Science* 325(5947):1555-1559.
30. Xu S & Weihua Z (2011) Loss of EGFR induced autophagy sensitizes hormone refractory prostate cancer cells to adriamycin. *Prostate*.
31. Kurai J, *et al.* (2007) Antibody-dependent cellular cytotoxicity mediated by cetuximab against lung cancer cell lines. *Clin Cancer Res* 13(5):1552-1561.
32. Zhang W, *et al.* (2007) FCGR2A and FCGR3A polymorphisms associated with clinical outcome of epidermal growth factor receptor expressing metastatic colorectal cancer patients treated with single-agent cetuximab. *J Clin Oncol* 25(24):3712-3718.
33. Baudino L, *et al.* (2008) Crucial role of aspartic acid at position 265 in the CH2 domain for murine IgG2a and IgG2b Fc-associated effector functions. *J Immunol* 181(9):6664-6669.
34. Shields RL, *et al.* (2001) High resolution mapping of the binding site on human IgG1 for Fc gamma RI, Fc gamma RII, Fc gamma RIII, and FcRn and design of IgG1 variants with improved binding to the Fc gamma R. *J Biol Chem* 276(9):6591-6604.
35. Pedersen MW, *et al.* (2010) Sym004: a novel synergistic anti-epidermal growth factor receptor antibody mixture with superior anticancer efficacy. *Cancer Res* 70(2):588-597.
36. Friedman LM, *et al.* (2005) Synergistic down-regulation of receptor tyrosine kinases by combinations of mAbs: implications for cancer immunotherapy. *Proc Natl Acad Sci U S A* 102(6):1915-1920.

37. Ben-Kasus T, Schechter B, Lavi S, Yarden Y, & Sela M (2009) Persistent elimination of ErbB-2/HER2-overexpressing tumors using combinations of monoclonal antibodies: relevance of receptor endocytosis. *Proc Natl Acad Sci U S A* 106(9):3294-3299.

38. Herbst RS, Kim ES, & Harari PM (2001) IMC-C225, an anti-epidermal growth factor receptor monoclonal antibody, for treatment of head and neck cancer. *Expert Opin Biol Ther* 1(4):719-732.

39. Johns TG, *et al.* (2004) Identification of the epitope for the epidermal growth factor receptor-specific monoclonal antibody 806 reveals that it preferentially recognizes an untethered form of the receptor. *J Biol Chem* 279(29):30375-30384.

40. Roovers RC, *et al.* (2011) A bi-paratopic anti-EGFR nanobody efficiently inhibits solid tumour growth. *Int J Cancer*.

41. Takai H, *et al.* (2009) Histopathological analyses of the antitumor activity of anti-glypican-3 antibody (GC33) in human liver cancer xenograft models: The contribution of macrophages. *Cancer Biol Ther* 8(10):930-938.

42. Li G, *et al.* (2010) Dual functional monoclonal antibody PF-04605412 targets integrin alpha5beta1 and elicits potent antibody-dependent cellular cytotoxicity. *Cancer Res* 70(24):10243-10254.

43. Oflazoglu E, *et al.* (2009) Macrophages and Fc-receptor interactions contribute to the antitumour activities of the anti-CD40 antibody SGN-40. *Br J Cancer* 100(1):113-117.

44. Beatty GL, *et al.* (2011) CD40 agonists alter tumor stroma and show efficacy against pancreatic carcinoma in mice and humans. *Science* 331(6024):1612-1616.

45. Simister NE & Mostov KE (1989) An Fc receptor structurally related to MHC class I antigens. *Nature* 337(6203):184-187.

46. Sergina NV, *et al.* (2007) Escape from HER-family tyrosine kinase inhibitor therapy by the kinase-inactive HER3. *Nature* 445(7126):437-441.

47. Wheeler DL, *et al.* (2008) Mechanisms of acquired resistance to cetuximab: role of HER (ErbB) family members. *Oncogene* 27(28):3944-3956.

48. Engelman JA, *et al.* (2007) MET amplification leads to gefitinib resistance in lung cancer by activating ERBB3 signaling. *Science* 316(5827):1039-1043.

49. Schoeberl B, *et al.* (2010) An ErbB3 antibody, MM-121, is active in cancers with ligand-dependent activation. *Cancer Res* 70(6):2485-2494.

50. Schoeberl B, *et al.* (2009) Therapeutically targeting ErbB3: a key node in ligand-induced activation of the ErbB receptor-PI3K axis. *Sci Signal* 2(77):ra31.
51. Ishiyama M, *et al.* (1996) A combined assay of cell viability and in vitro cytotoxicity with a highly water-soluble tetrazolium salt, neutral red and crystal violet. *Biol Pharm Bull* 19(11):1518-1520.
52. Hamasaki K, Kogure K, & Ohwada K (1996) A biological method for the quantitative measurement of tetrodotoxin (TTX): tissue culture bioassay in combination with a water-soluble tetrazolium salt. *Toxicon* 34(4):490-495.
53. Balak MN, *et al.* (2006) Novel D761Y and common secondary T790M mutations in epidermal growth factor receptor-mutant lung adenocarcinomas with acquired resistance to kinase inhibitors. *Clin Cancer Res* 12(21):6494-6501.
54. Kobayashi S, *et al.* (2005) EGFR mutation and resistance of non-small-cell lung cancer to gefitinib. *N Engl J Med* 352(8):786-792.
55. Kosaka T, *et al.* (2006) Analysis of epidermal growth factor receptor gene mutation in patients with non-small cell lung cancer and acquired resistance to gefitinib. *Clin Cancer Res* 12(19):5764-5769.
56. Pao W, *et al.* (2005) Acquired resistance of lung adenocarcinomas to gefitinib or erlotinib is associated with a second mutation in the EGFR kinase domain. *PLoS Med* 2(3):e73.
57. Regales L, *et al.* (2009) Dual targeting of EGFR can overcome a major drug resistance mutation in mouse models of EGFR mutant lung cancer. *J Clin Invest* 119(10):3000-3010.

6. Conclusions and Future Perspectives

Conclusions

We have taken the idea of antibody-induced characterization from conception and preliminary characterization to mechanistic elucidation and application to the development of two novel classes of cancer therapeutics. In the process, we have gained important insights into EGFR kinetics that could form the basis for development of new drugs that target and downregulate this receptor.

As discussed in Chapter 2, we establish that combinations of non-competitive EGFR-targeted antibodies can cluster and downregulate surface in a range of cell lines. Interestingly, we find that a combination of two mAbs targeting extracellular domain 3: (1) The murine form of the clinically approved cetuximab and (2) The N-terminal domain 3-targeted mAb H11 induce the greatest extent of downregulation. More generally, combinations of domain 3-targeted mAbs show more synergism than combinations targeting two different domains. Also, we find that unlike EGF-mediated downregulation, combination mAb-mediated downregulation exclusively obstructs recycling and does not accelerate endocytosis. In contrast to EGF, combination treatment does not activate the receptor or downstream signaling pathways. We establish that downregulation requires two bivalent mAbs and that it is coincident with dramatic receptor clustering. To motivate use of antibody combinations as a therapeutic strategy, we demonstrate that mAb-induced downregulation selectively and efficiently inhibits the migration and proliferation of cells that aberrantly secrete autocrine ligand, mimicking the dysregulated tumor environment.

We then apply these insights to the development of bispecific antibodies targeting both the wild type and the mutated or activated forms of EGFR. As detailed in Chapter 3, these bispecific constructs enhance the apparent affinity of antibody-receptor interaction and effectively downregulate receptor on both wild-type and mutant EGFR-expressing cell lines. This particular case illustrates the advantage of the bispecific format, which enables avidity-mediated synergy that is not observed with combination treatment.

Another approach we pursue in engineering antibodies that engage multiple epitopes on EGFR is the conjugation of Fn3 domains to the cetuximab IgG, creating the bispecific, trispecific, and even tetraspecific constructs described in Chapter 4. We determine that the optimal format in terms of both secretion and downregulation efficacy is the trans-trispecific fusion, which involves one heavy chain N-terminal and one light chain C-terminal Fn3 moiety. We establish that these constructs accelerate endocytosis and block recycling in the absence of receptor or downstream signaling activation. Like antibody combinations, trans-trispecific mutants selectively antagonize migration and growth of autocrine-driven cells.

Prompted by our promising *in vitro* results, we evaluated the therapeutic efficacy of our lead bispecific antibody and Ab-Fn3 fusion in mouse tumor xenograft models of EGFR-expressing cancer. As discussed in Chapter 5, we observe significant inhibtion of tumor growth following administration of multispecific therapeutics, which correlates well with our *in vitro* downregulation studies and coincides with an overall decrease in EGFR expression. Surprisingly, we achieve strong tumor control in cell lines that resist treatment with the base cetuximab antibody due to mutations in downstream effector proteins. Manipulation of our antibody fusions allows us to implicate ligand inhibition, downregulation, and effector function in the therapeutic mechanism of these constructs. In particular, the combined effects of multispecific antibody-mediated downregulation and ligand competition ablate signaling through both the PI3K and MAPK pathways in a cell line with a mutation downstream of EGFR in the MAPK cascade. The efficacy observed our pre-clinical studies provides motivation for further *in vivo* characterization and pre-clinical development of these multispecific molecules as potential therapeutic agents for cancer treatment.

Future Perspectives

The efficacy of our multispecific fusions may extend to other tumor cell lines representing cancers of diverse origins that overexpress EGFR. Evaluation of these fusions in a breadth of systems will characterize the robustness of response and will prove informative for the therapeutic indications of our constructs. Further studies in non-immune deficient mice will be essential in the pre-clinical development of our molecules to ensure the absence of immunogenicity. In addition, although the relatively low effective doses compared to the less

potent unconjugated IgG of our antibody could mollify off-target effects, rigorous characterization of the toxicity of our compounds must be performed. We predict based on our HMEC-derived autocrine cell line data that our constructs would exhibit similar toxicity behavior to the base cetuximab antibody, which has been well-tolerated in the clinic (1, 2). However, skin rashes are frequently observed in cetuximab-treated patients, with rash severity correlating strongly to drug response (3). In the downstream development of our engineered constructs, it will be important to determine whether conjugation of scFv and Fn3 domains to the cetuximab IgG exacerbates or mitigates toxic side effects.

In addition to realization of the exciting therapeutic potential for our constructs in the treatment of epithelial-based cancers, we envision the extension of our multi-epitopic clustering strategy to create novel more effective EGFR-targeted constructs. In particular, isolation of additional non-competitive domain 3-targeted antibodies could incrementally improve downregulation, based on the epitope bias discovered from our pairwise downregulation screen. It would be of particular utility to engineer antibodies that more efficiently downregulate receptor on A431 cells, as this cell line resists downregulation and, consequently, therapeutic intervention. Additionally, other topologies for a tetraspecific Ab-Fn3 fusion could be explored that extend the cis-trispecific by fusing an additional Fn3 domain at the HC or LC position for comparison with the HN+HC+LC format used in our downregulation panel. In addition to enhancing receptor clustering, the ability to target four epitopes introduces the possibility of engaging multiple receptors in clusters and thereby simultaneously preventing their active signaling. This would be particularly relevant for the EGFR system, as compensatory signaling via ErbB3 and c-Met have been shown to confer resistance to EGFR therapies via PI3K pathway activation (4-8). The frequent co-expression and colocalization of EGFR and interacting RTKs would facilitate multi-receptor clustering and allow for robust and widespread efficacy of engineered tetraspecific therapeutics.

We find that the multispecific antibody-induced downregulation mechanism is effective even in systems involving receptor mutation (EGFRvIII) and ligand dysregulation (HMEC-derived autocrine cell lines), making this strategy a promising candidate for drug synergism. In particular, targeting EGFR downregulation could be a useful tool for circumventing secondary resistance to existing therapies, for instance the T790M receptor mutation which appears in

>90% of patients who develop acquired resistance to the TKIs gefitinib or erlotinib (9-12). It will thus be useful to characterize how our drugs would complement existing therapies, for instance through sensitization to TKIs (13) or cell disruptive agents (13, 14). Also, it has recently been reported that EGFR promotes survival through signal-independent mechanisms (15, 16), motivating the use of our agents to decrease the overall EGFR burden through antibody-mediated downregulation.

In addition to its utility in systems involving EGFR mutation and ligand upregulation, multi-epitopic antibody action lends itself to multi-step targeting strategies and delivery applications due to its remarkable specificity and affinity for target antigen as well as its induction of rapid clustering and internalization of receptor in the absence of agonism. The high concentrations of clustered receptor-antibody complexes achieved by multispecific constructs could render them powerful vehicles for acute presentation of destructive agents or fusogenic peptides that facilitate endosomal escape. In addition, surface-localized clustered antibody-receptor complexes could serve as active immune effector cell recruitment sites, eliciting extensive ADCC or CDC (17). The enhancement of effector function via Fc engineering or introduction of T cell-engaging moieties could potentiate these immune effects (18, 19).

Finally, the modularity of multi-epitopic targeting design makes our strategy readily extensible to other receptor networks of therapeutic interest. Design of multispecific fusions directed to other RTKs and combination of two or more multi-epitopic therapies with distinct targets present exciting new directions in drug development.

In conclusion, we have gained extensive insight into the phenomenon of antibody-mediated receptor downregulation and used our findings to engineer therapeutics that employ this mechanism to inhibit tumor growth. The constructs we have developed hold powerful potential in cancer therapy and pave the way for a new wave of antibody-based drugs and combination treatments that exploit receptor clustering and downregulation to achieve therapeutic efficacy.

References

1. Saltz LB, *et al.* (2004) Phase II trial of cetuximab in patients with refractory colorectal cancer that expresses the epidermal growth factor receptor. *J Clin Oncol* 22(7):1201-1208.
2. Cunningham D, *et al.* (2004) Cetuximab monotherapy and cetuximab plus irinotecan in irinotecan-refractory metastatic colorectal cancer. *N Engl J Med* 351(4):337-345.
3. Lenz HJ, *et al.* (2006) Multicenter phase II and translational study of cetuximab in metastatic colorectal carcinoma refractory to irinotecan, oxaliplatin, and fluoropyrimidines. *J Clin Oncol* 24(30):4914-4921.
4. Sergina NV, *et al.* (2007) Escape from HER-family tyrosine kinase inhibitor therapy by the kinase-inactive HER3. *Nature* 445(7126):437-441.
5. Wheeler DL, *et al.* (2008) Mechanisms of acquired resistance to cetuximab: role of HER (ErbB) family members. *Oncogene* 27(28):3944-3956.
6. Engelman JA, *et al.* (2007) MET amplification leads to gefitinib resistance in lung cancer by activating ERBB3 signaling. *Science* 316(5827):1039-1043.
7. Schoeberl B, *et al.* (2010) An ErbB3 antibody, MM-121, is active in cancers with ligand-dependent activation. *Cancer Res* 70(6):2485-2494.
8. Schoeberl B, *et al.* (2009) Therapeutically targeting ErbB3: a key node in ligand-induced activation of the ErbB receptor-PI3K axis. *Sci Signal* 2(77):ra31.
9. Balak MN, *et al.* (2006) Novel D761Y and common secondary T790M mutations in epidermal growth factor receptor-mutant lung adenocarcinomas with acquired resistance to kinase inhibitors. *Clin Cancer Res* 12(21):6494-6501.
10. Kobayashi S, *et al.* (2005) EGFR mutation and resistance of non-small-cell lung cancer to gefitinib. *N Engl J Med* 352(8):786-792.
11. Kosaka T, *et al.* (2006) Analysis of epidermal growth factor receptor gene mutation in patients with non-small cell lung cancer and acquired resistance to gefitinib. *Clin Cancer Res* 12(19):5764-5769.
12. Pao W, *et al.* (2005) Acquired resistance of lung adenocarcinomas to gefitinib or erlotinib is associated with a second mutation in the EGFR kinase domain. *PLoS Med* 2(3):e73.

13. Regales L, *et al.* (2009) Dual targeting of EGFR can overcome a major drug resistance mutation in mouse models of EGFR mutant lung cancer. *J Clin Invest* 119(10):3000-3010.
14. Xu S & Weihua Z (2011) Loss of EGFR induced autophagy sensitizes hormone refractory prostate cancer cells to adriamycin. *Prostate*.
15. Weihua Z, *et al.* (2008) Survival of cancer cells is maintained by EGFR independent of its kinase activity. *Cancer Cell* 13(5):385-393.
16. Yao Y, *et al.* (Mitochondrially localized EGFR is independent of its endocytosis and associates with cell viability. *Acta Biochim Biophys Sin (Shanghai)* 42(11):763-770.
17. Dechant M, *et al.* (2008) Complement-dependent tumor cell lysis triggered by combinations of epidermal growth factor receptor antibodies. *Cancer Res* 68(13):4998-5003.
18. Strohl WR (2009) Optimization of Fc-mediated effector functions of monoclonal antibodies. *Curr Opin Biotechnol* 20(6):685-691.
19. Lutterbuese R, *et al.* (2010) T cell-engaging BiTE antibodies specific for EGFR potently eliminate KRAS- and BRAF-mutated colorectal cancer cells. *Proc Natl Acad Sci U S A* 107(28):12605-12610.

Appendix A: Basic Trafficking Model

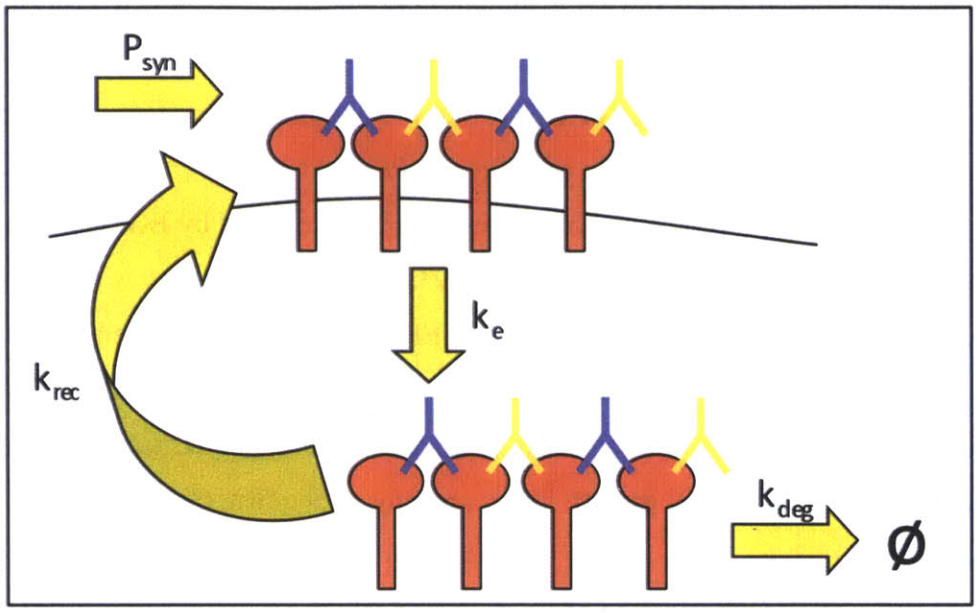

From the diagram:

$$\frac{dR_S}{dt} = P_{syn} - R_S k_e + R_I k_{rec}$$

$$\frac{dR_I}{dt} = R_S k_e - R_I k_{rec} - R_I k_{deg}$$

$$R_{Total} = R_S + R_I$$

$$\frac{dR_{Total}}{dt} = P_{syn} - R_I k_{deg}$$

Assume steady state.

$$\Rightarrow \frac{dR_{Total}}{dt} = \frac{dR_S}{dt} = 0$$

$$0 = P_{syn} - R_I k_{deg}$$

$$\boxed{R_I = \frac{P_{syn}}{k_{deg}}}$$

$$0 = P_{syn} - R_S k_e + R_I k_{rec}$$

$$R_S k_e = P_{syn} + R_I k_{rec} = P_{syn} + \frac{P_{syn}}{k_{deg}} k_{rec}$$

$$R_S = \frac{P_{syn} + \frac{P_{syn}}{k_{deg}} k_{rec}}{k_e}$$

Let t=treated and u=untreated.

Further assume that:

1) $k_{deg,t} = k_{deg,u} = k_{deg}$

2) $P_{syn,u} = P_{syn,u} = P_{syn}$

3) $k_{rec,t} = 0$

$$\%\ \text{Receptor Remaining} = \frac{R_{S,t}}{R_{S,u}} = \frac{\frac{P_{syn} + \frac{P_{syn}}{k_{deg}} k_{rec,t}}{k_{e,t}}}{\frac{P_{syn} + \frac{P_{syn}}{k_{deg}} k_{rec,u}}{k_{e,u}}} = \left(\frac{k_{e,u}}{k_{e,t}}\right)\left[\frac{1 + \frac{k_{rec,t}}{k_{deg}}}{1 + \frac{k_{rec,u}}{k_{deg}}}\right]$$

$$\%\ \text{Receptor Remaining} = \left(\frac{k_{e,u}}{k_{e,t}}\right)\left[\frac{1}{1 + \frac{k_{rec,u}}{k_{deg}}}\right]$$

From literature values (Lauffenburger & Linderman (1993). Receptors. New York: Oxford University Press):

$k_{rec,u} \approx 10^{-2} - 10^{-1}$ min^{-1} (5.8×10^{-2} min^{-1})

$k_{deg} \approx 10^{-3} - 10^{-2}$ min^{-1} (2.2×10^{-3} min^{-1})

Now consider $k_{rec,u}/k_{deg}$.

$$Max\left(\frac{k_{rec,u}}{k_{deg}}\right) = \frac{10^{-1}\ \text{min}^{-1}}{10^{-3}\ \text{min}^{-1}} = 100$$

$$Min\left(\frac{k_{rec,u}}{k_{deg}}\right) = \frac{10^{-2}\ \text{min}^{-1}}{10^{-2}\ \text{min}^{-1}} = 1$$

$$\Rightarrow 1 \le \frac{k_{rec,u}}{k_{deg}} \le 100$$

Using the exact values from Lauffenburger & Linderman: $k_{rec,u}/k_{deg} \approx 26.4$

Based on experimental results, endocytosis accelerates or stays constant following treatment, so:

$$\frac{k_{e,u}}{k_{e,t}} \le 1$$

Assume that endocytosis is unaffected by treatment, so $k_{e,u} = k_{e,t}$.

$$\%\ \text{Receptor Remaining} = \frac{R_{S,t}}{R_{S,u}} = \frac{1}{1 + \frac{k_{rec,u}}{k_{deg}}}$$

Using the exact parameter values:

$$\%\ \text{Receptor Remaining} = \frac{R_{S,t}}{R_{S,u}} = \frac{1}{1+26.4} \approx 3.6\%$$

The upper and lower bounds on downregulation are thus as follows:

$$\frac{1}{1+100} \le \%\ \text{Receptor Remaining} \le \frac{1}{1+1}$$

$$1.0\% \le \%\ \text{Receptor Remaining} \le 50\%$$

Dependence of downregulation extent on antibody clone used implies:

1) Variable $k_{e,t}$
2) Variable $k_{rec,t}$

OR BOTH

We can constrain $k_{e,t}$ based on our experimental results from Chapter 2:

Normal metabolic turnover $\approx$ 36 h $\Rightarrow$ $\ln(2)/k_{e,u}$ = 36 h $\Rightarrow$ $k_{e,u} = 3.2\times10^{-4}$ min^{-1}

Fastest downregulation halftime $\approx$ 2 h $\Rightarrow$ $\ln(2)/k_{e,t}$ = 4 h $\Rightarrow$ $k_{e,t}$ = 0.006 min^{-1}

Slowest downregulation halftime $\approx$ 11 h $\Rightarrow$ $\ln(2)/k_{e,t}$ = 11 h $\Rightarrow$ $k_{e,t}$ = 0.001 min^{-1}

Thus, assuming surface downregulation is a result of an endocytic rate change ONLY, the lower bound for $k_{e,u}/k_{e,t}$ is:

$$\frac{k_{e,u}}{k_{e,t}} \geq \frac{3.2\times10^{-4}\ \text{min}^{-1}}{0.006\ \text{min}^{-1}} = 0.055$$

The ratio of the endocytic rates is thus bounded by:

$$0.055 \leq \frac{k_{e,u}}{k_{e,t}} \leq 1$$

We may now estimate the limitations on downregulation extent:

$$\%\ \text{Receptor Remaining} = \frac{R_{S,t}}{R_{S,u}} = \left(\frac{k_{e,u}}{k_{e,t}}\right) \left[\frac{1}{1+\frac{k_{rec,u}}{k_{deg}}}\right]$$

$0.2 - 0.4$ $\quad$ $0.11 - 1$ $\quad$ $0.01 - 0.5$

$$0.1\% \leq \%\ \text{Receptor Remaining} \leq 50\%$$

Thus, steady-state downregulation level is bounded and depends on the acceleration of endocytosis as well as the endogenous rates of recycling and degradation in a given cell line.

Appendix B: Comprehensive Phosphotyrosine Mass Spectrometry Dataset

The full mass spectrometry dataset from our global phosphotyrosine screen described in Chapter 2 (Figure 2.15B) included 28 proteins from the 15' timepoint and 48 proteins from the 60' timepoint. Phosphoprotein activity in A431 cells treated with an isotype control antibody, 225, H11, 225+H11, or EGF is shown in Figure B.1. Proteins and the phosphopeptide sequences are identified in Table B.1.

Consistent with the Akt and ERK effectors shown in Figure 2.15B, EGF stimulates effector proteins to varying extents, but none of the single or combination treatments activates the detected proteins based on a threshold of 1.7-fold background.

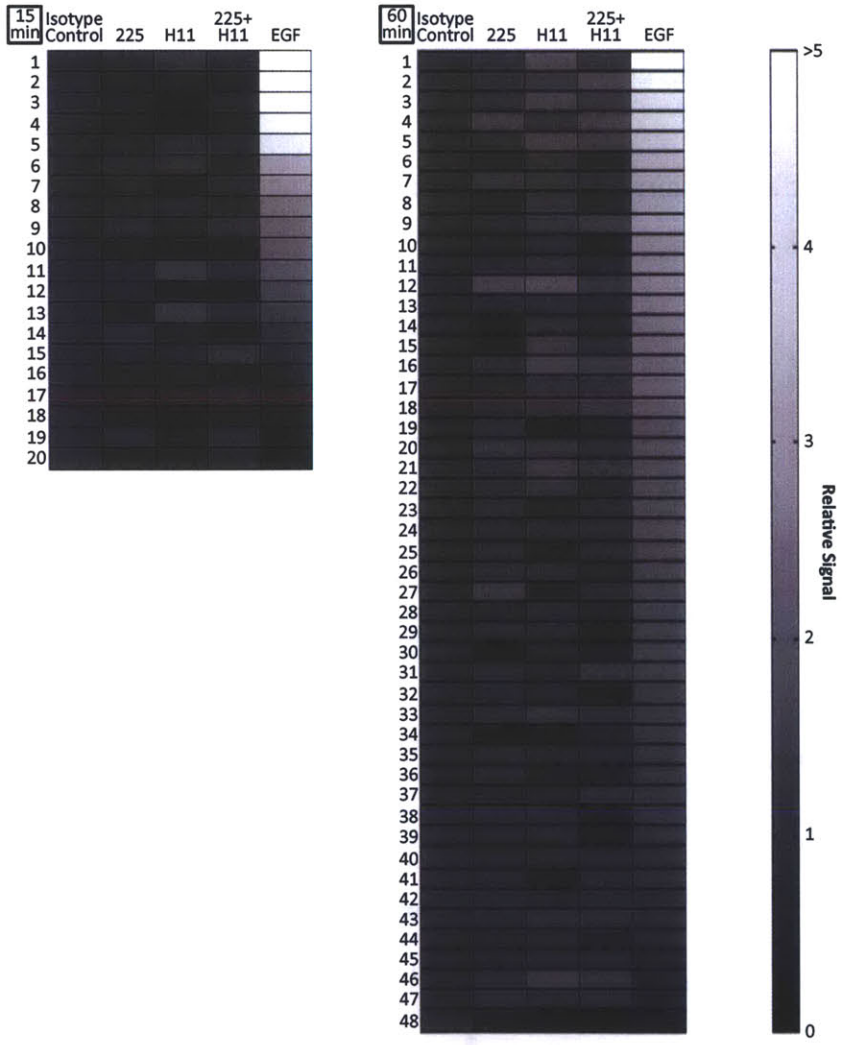

Figure B.1. Global mass spectrometry analysis of mAb-treated cells. Serum-starved A431 cells were incubated with single mAbs, the 225+H11 mAb combination, or EGF for 15 min (*left*) or 60 min (1) at 37°C. EGF stimulation was held constant at 15 min for both screens. Cells were then subjected to an iTraq-based mass spectrometry assay to identify and quantify phosphorylated peptides. Phosphoprotein signal was normalized to total protein concentration for each condition and relative phosphorylation levels (compared to an isotype control) are shown for all detected peptides. The 60 min screen was performed twice with strong agreement between phosphorylation levels for proteins observed in both biological replicates.

15'

Number	Abbreviation	Protein Name	Site	Sequence
1	EGFR	epidermal growth factor receptor isoform a	Y1173	K.GSTAENAEyLR.V
2	EGFR	epidermal growth factor receptor isoform a	Y1148	K.GSHQISLDNPDyQQDFFPK.E
3	PDLIM1	PDZ and LIM domain 1	Y321	R.VTPPEGyEVVTVFPK.-
4	AF6	myeloid/lymphoid or mixed-lineage leukemia (trithorax homolog, Drosophila); translocated to, 4 isoform 2	Y1214	R.EyFTFPASK.S
5	PTK6	PTK6 protein tyrosine kinase 6	Y447	R.LSSFTSyENPT.-
6	PKP3	plakophilin 3	Y175	R.ADyDTLSLR.S
7	Erbin	ERBB2 interacting protein isoform 2	Y1104	R.AQIPEGDyLSYR.E
8	ERK1	mitogen-activated protein kinase 3 isoform 2	Y204	R.IADPEHDHTGFLTEyVATR.W
9	Paxillin	paxillin	Y118	R.VGEEEHVySFPNK.Q
10	ERK2	mitogen-activated protein kinase 1	Y187	R.VADPDHDHTGFLTEyVATR.W
11	SHC1	SHC (Src homology 2 domain containing) transforming protein 1 isoform p52Shc	Y318	R.ELFDDPSyVNVQNLDK.A
12	PKP4	plakophilin 4 isoform a	Y1168	K.STTNyVDFYSTK.R
13	EphA2	ephrin receptor EphA2	Y575	R.QSPEDVyFSK.S
14	P3PBP3	phosphoinositol 3-phosphate-binding protein-3	Y492	R.SEDIyADPAAYVMR.R
15	DYRK1A	dual-specificity tyrosine-(Y)-phosphorylation regulated kinase 1A isoform 3	Y320	R.IYQyIQSR.F
16	PRP4K	serine/threonine-protein kinase PRP4K	Y849	K.LCDFGSASHVADNDITPyLVSR.F
17	CDK1	cell division cycle 2 protein isoform 1	Y14	K.IGEGTyGVVYK.G
18	EphA2	ephrin receptor EphA2	Y772	R.VLEDDPEATyTTSGGKIPIR.W
19	Na+/K+ -ATPase a1	Na+/K+ -ATPase alpha 1 subunit isoform a proprotein	Y260	R.GIVVyTGDR.T
20	GSK3b	glycogen synthase kinase 3 beta	Y216	R.GEPNVSyICSR.Y

60'

Number	Abbreviation	Protein Name	Site	Sequence
1	PLCg	phospholipase C gamma 1 isoform b	Y771	K.IGTAEPDyGALYEGR.N + Phospho (Y)
2	EGFR	epidermal growth factor receptor isoform a	Y1173	K.GSTAENAEyLR.V + Phospho (Y)
3	EGFR	epidermal growth factor receptor isoform a	Y1148	K.GSHQISLDNPDyQQDFFPK.E + Phospho (Y)
4	PKP3	plakophilin 3	Y175	R.ADYDTLSLR.S + Phospho (Y)
5	SHC1	SHC (Src homology 2 domain containing) transforming protein 1 isoform p52Shc	Y318	R.ELFDDPSyVNVQNLDK.A + Phospho (ST)
6	ERK1	mitogen-activated protein kinase 3 isoform 2	Y204	R.IADPEHDHTGFLTEyVATR.W + Phospho (Y)
7	Cortactin a	cortactin isoform a	Y421	R.LPSSPVyEDAASFK.A + Phospho (Y)
8	ERK2	mitogen-activated protein kinase 1	Y187	R.VADPDHDHTGFLTEyVATR.W + Phospho (Y)
9	ANX2	annexin A2 isoform 2	Y30	K.AyTNFDAER.D + Phospho (Y)
10	SHP2	protein tyrosine phosphatase, non-receptor type 11	Y580	R.VyENVGLMQQQK.S + Phospho (Y)
11	BCAR1	breast cancer anti-estrogen resistance 1	Y249	R.HLLAPGPQDIyDVPPVR.G + Phospho (Y)
12	HSP90b	heat shock 90kDa protein 1, beta	Y276	K.yIDQEELNK.T + Phospho (Y)
13	TYK2	tyrosine kinase 2	Y292	R.LLAQAEGEPCyIR.D + Phospho (Y)
14	TIM	rho guanine nucleotide exchange factor 5	Y665	R.DySTVSASPTALSTLK.Q + Phospho (Y)
15	LISCH3	LISCH protein isoform 3	Y518	R.SGDLPyDGRLLEEAVR.K + Phospho (Y)
16	Integrin b1	integrin beta 1 isoform 1A precursor	Y783	K.WDTGENPIyK.S + Phospho (Y)
17	CAV1	caveolin 1	Y14	K.YVDSEGHLyTVPIR.E + Phospho (Y)
18	MPP5	membrane protein, palmitoylated 5	Y242	R.VyESIGQYGGETVK.I + Phospho (Y)
19	Syntaxin 4	syntaxin 4	Y251	K.NILSSADyVER.G + Phospho (Y)
20	EphB3	ephrin receptor EphB3 precursor	Y792	R.FLEDDPSDPTyTSSLGGK.I + Phospho (Y)
21	Cofilin 1	cofilin 1 (non-muscle)	Y89	R.YALYDATyETK.E + Phospho (Y)
22	SHP2	protein tyrosine phosphatase, non-receptor type 11	Y62	K.IQNTGDyYDLYGGEK.F + Phospho (Y)
23	Cortactin a	cortactin isoform a	Y446	R.GPVSGTEPEPVySMEAADYR.E + Phospho (Y)
24	EphA2	ephrin receptor EphA2	Y772	R.VLEDDPEATyTTSGGKIPIR.W + Phospho (Y)

25	p38 MAPK	mitogen-activated protein kinase 14 isoform 1	Y182	R.HTDDEMTGyVATR.W + Phospho (Y)
26	PI3K p85	phosphoinositide-3-kinase, regulatory subunit 2 (beta)	Y464	R.EYDQLYEEYTR.T + Phospho (Y)
27	PYK2	PTK2B protein tyrosine kinase 2 beta isoform a	Y819	K.QMVEDyQWLR.Q + Phospho (Y)
28	EphB2	ephrin receptor EphB2 isoform 2 precursor	Y781	R.FLEDDTSDPTyTSALGGK.I + Phospho (Y)
29	ANX1	annexin I	Y216	K.QAWFIENEEQEyVQTVK.S + Phospho (Y)
30	ErbB3	erbB-3 isoform 1 precursor	Y1328	R.SLEATDSAFDNPDyWHSR.L + Phospho (Y)
31	Erbin	ERBB2 interacting protein isoform 2	Y1104	R.AQIPEGDyLSYR.E + Phospho (Y)
32	PKP4	plakophilin 4 isoform a	Y1168	K.STTNYVDFYSTK.R + Phospho (ST)
33	DYRK1A	dual-specificity tyrosine-(Y)-phosphorylation regulated kinase 1B isoform a	Y320	R.IYQyIQSR.F + Phospho (Y)
34	RAK	fyn-related kinase	Y46	R.HGHyFVALFDYQAR.T + Phospho (Y)
35	PZR	myelin protein zero-like 1 isoform a	Y263	K.SESVVyADIR.K + Phospho (Y)
36	P3PBP3	phosphoinositol 3-phosphate-binding protein-3	Y492	R.SEDIyADPAAYVMR.R + Phospho (Y)
37	a-Catenin	catenin, alpha 1	Y619	R.LVYDGIR.D + Phospho (Y)
38	EphA1	ephrin receptor EphA1	Y281	R.LLDDFDGTyETQGGKIPIR.W + Phospho (Y)
39	PRPK4	serine/threonine-protein kinase PRP4K	Y849	K.LCDFGSASHVADNDITPyLVSR.F + Phospho (Y)
40	CDK1	cell division cycle 2 protein isoform 1	Y14	K.IGEGTYGVVyK.G + Phospho (Y)
41	Yes	Yamaguchi sarcoma viral (v-yes-1) oncogene homolog isoform A	Y316	R.EEPIyIITEYMAK.G + Phospho (Y)
42	GSK3b	glycogen synthase kinase 3 beta	Y216	R.GEPNVSyICSR.Y + Phospho (Y)
43	XB130	kin of IRRE like	Y560	R.TPYEAyDPIGK.Y + Phospho (Y)
44	Src/Fyn/Yes	protein-tyrosine kinase fyn isoform a	Y420	R.LIEDNEYTAR.Q + Phospho (Y)
45	Paxillin	paxillin	Y118	R.VGEEEHVySFPNK.Q + Phospho (Y)
46	Na+/K+ - ATPase a1	Na+/K+ -ATPase alpha 1 subunit isoform a proprotein	Y260	R.GIVVyTGDR.T + Phospho (Y)
47	RPTPa	protein tyrosine phosphatase, receptor type, A isoform 1 precursor	Y791	K.VVQEYIDAFSDYANFK.- + Phospho (Y)
48	FYB-120/130	FYN binding protein (FYB-120/130) isoform 2	Y561	K.TTAVEIDyDSLK.L + Phospho (Y)

Table B.1. Peptide sequences and corresponding proteins detected in 15 and 60 min A431 phosphotyrosine mass spectrometry screens. Lowercase residues in the sequences denote phosphorylated amino acids (either Y, S, or T).

Appendix C: DNA Sequences

All secreted constructs were based on the gWiz backbone (Genlantis, San Diego, CA) with the heavy and light chain of each antibody fusion. For the first construct (gWiz 225 HC), the full vector is shown. For subsequent constructs, only the engineered region from the Pst1 to the Sal1 sites from the gWiz polylinker region are shown.

The 225 and 806 variable sequences were obtained from the information contained in their respective patents.

The constructs described herein are:

1) Unconjugated Antibodies
2) Bispecific 225/806-Containing Antibodies (BS28)
3) Antibody-Fibronectin Fusions (Ab-Fn3 Fusions)

Abbreviations
HC=Heavy Chain
LC=Light Chain
VH=Heavy Chain Variable Domain
VL=Light Chain Variable Domain

1) Unconjugated Antibodies

gWiz 225 HC (225 variable domain on human IgG1 Scaffold)

PstI--Kozak--Leader—MluI—225 VH—NheI---C1,2,3--Stop—SalI

TCGCGCGTTTCGGTGATGACGGTGAAAACCTCTGACACATGCAGCTCCCGGAGACGGTCACAGCTTGTCTGTAAGCGGATGCCGG
GAGCAGACAAGCCCGTCAGGGCGCGTCAGCGGGTGTTGGCGGGTGTCGGGGCTGGCTTAACTATGCGGCATCAGAGCAGATTGT
ACTGAGAGTGCACCATATGCGGTGTGAAATACCGCACAGATGCGTAAGGAGAAAATACCGCATCAGATTGGCTATTGGCCATTGC
ATACGTTGTATCCATATCATAATATGTACATTTATATTGGCTCATGTCCAACATTACCGCCATGTTGACATTGATTATTGACTAGTT
ATTAATAGTAATCAATTACGGGGTCATTAGTTCATAGCCCATATATGGAGTTCCGCGTTACATAACTTACGGTAAATGGCCCGCCT
GGCTGACCGCCCAACGACCCCCGCCCATTGACGTCAATAATGACGTATGTTCCCATAGTAACGCCAATAGGGACTTTCCATTGAC
GTCAATGGGTGGAGTATTTACGGTAAACTGCCCACTTGGCAGTACATCAAGTGTATCATATGCCAAGTACGCCCCCTATTGACGTC
AATGACGGTAAATGGCCCGCCTGGCATTATGCCCAGTACATGACCTTATGGGACTTTCCTACTTGGCAGTACATCTACGTATTAGT
CATCGCTATTACCATGGTGATGCGGTTTTGGCAGTACATCAATGGGCGTGGATAGCGGTTTGACTCACGGGGATTTCCAAGTCTCC
ACCCCATTGACGTCAATGGGAGTTTGTTTTGGCACCAAAATCAACGGGACTTTCCAAAATGTCGTAACAACTCCGCCCCATTGACG
CAAATGGGCGGTAGGCGTGTACGGTGGGAGGTCTATATAAGCAGAGCTCGTTTAGTGAACCGTCAGATCGCCTGGAGACGCCATC
CACGCTGTTTTGACCTCCATAGAAGACACCGGGACCGATCCAGCCTCCGCGGCCGGGAACGGTGCATTGGAACGCGGATTCCCCG
TGCCAAGAGTGACGTAAGTACCGCCTATAGACTCTATAGGCACACCCCTTTGGCTCTTATGCATGCTATACTGTTTTTGGCTTGGG
GCCTATACACCCCCGCTTCCTTATGCTATAGGTGATGGTATAGCTTAGCCTATAGGTGTGGGTTATTGACCATTATTGACCACTCCC
CTATTGGTGACGATACTTTCCATTACTAATCCATAACATGGCTCTTTGCCACAACTATCTCTATTGGCTATATGCCAATACTCTGTC
CTTCAGAGACTGACACGGACTCTGTATTTTTACAGGATGGGGTCCCATTTATTATTTACAAATTCACATATACAACAACGCCGTCC
CCCGTGCCCGCAGTTTTTATTAAACATAGCGTGGGATCTCCACGCGAATCTCGGGTACGTGTTCCGGACATGGGCTCTTCTCCGGT
AGCGGCGGAGCTTCCACATCCGAGCCCTGGTCCCATGCCTCCAGCGGCTCATGGTCGCTCGGCAGCTCCTTGCTCCTAACAGTGGA
GGCCAGACTTAGGCACAGCACAATGCCCACCACCACCAGTGTGCCGCACAAGGCCGTGGCGGTAGGGTATGTGTCTGAAAATGA
GCGTGGAGATTGGGCTCGCACGGCTGACGCAGATGGAAGACTTAAGGCAGCGGCAGAAGAAGATGCAGGCAGCTGAGTTGTTGT
ATTCTGATAAGAGTCAGAGGTAACTCCCGTTGCGGTGCTGTTAACGGTGGAGGGCAGTGTAGTCTGAGCAGTACTCGTTGCTGCC

GCGCGCGCCACCAGACATAATAGCTGACAGACTAACAGACTGTTCCTTTCCATGGGTCTTTTCTGCAGGCCGCCACC
ATGGGTTGGAGCCTCATCTTGCTCTTCCTTGTCGCTGTTGCTACGCGTCAGGTACAAC
TGAAGCAGTCAGGACCTGGCCTAGTGCAGCCCTCACAGAGCCTGTCCATCACCTGCA
CAGTCTCTGGTTTCTCATTAACTAACTATGGTGTACACTGGGTTCGCCAGTCTCCAGG
AAAGGGTCTGGAGTGGCTGGGAGTGATATGGAGTGGTGGAAACACAGACTATAATA
CACCTTTCACATCCAGACTGAGCATCAACAAGGACAATTCCAAGAGCCAAGTTTTCT
TTAAAATGAACAGTCTGCAATCTAATGACACAGCCATATATTACTGTGCCAGAGCCC
TCACCTACTATGATTACGAGTTTGCTTACTGGGGCCAAGGGACCCTGGTCACCGTTT
CCGCTGCTAGCACCAAGGGCCCATCGGTCTTCCCCCTGGCACCCTCCTCCAAGAGCA
CCTCTGGGGGCACAGCGGCCCTGGGCTGCCTGGTCAAGGACTACTTCCCCGAACCG
GTGACGGTGTCGTGGAACTCAGGCGCCCTGACCAGCGGCGTGCACACCTTCCCGGCT
GTCCTACAGTCCTCAGGACTCTACTCCCTCAGCAGCGTGGTGACCGTGCCCTCCAGC
AGCTTGGGCACCCAGACCTACATCTGCAACGTGAATCACAAGCCCAGCAACACCAA
GGTGGACAAGAAAGTTGAGCCCAAATCTTGTGACAAAACTCACACATGCCCACCGT
GCCCAGCACCTGAACTCCTGGGGGGACCGTCAGTCTTCCTCTTCCCCCCAAAACCCA
AGGACACCCTCATGATCTCCCGGACCCCTGAGGTCACATGCGTGGTGGTGGACGTG
AGCCACGAAGACCCTGAGGTCAAGTTCAACTGGTACGTGGACGGCGTGGAGGTGCA
TAATGCCAAGACAAAGCCGCGGGAGGAGCAGTACAACAGCACGTACCGTGTGGTCA
GCGTCCTCACCGTCCTGCACCAGGACTGGCTGAATGGCAAGGAGTACAAGTGCAAG
GTCTCCAACAAAGCCCTCCCAGCCCCCATCGAGAAAACCATCTCCAAAGCCAAAGG
GCAGCCCCGAGAACCACAGGTGTACACCCTGCCCCCATCCCGGGATGAGCTGACCA
AGAACCAGGTCAGCCTGACCTGCCTGGTCAAAGGCTTCTATCCCAGCGACATCGCCG
TGGAGTGGGAGAGCAATGGGCAGCCGGAGAACAACTACAAGACCACGCCTCCCGTG
CTGGACTCCGACGGCTCCTTCTTCCTCTACAGCAAGCTCACCGTGGACAAGAGCAGG
TGGCAGCAGGGGAACGTCTTCTCATGCTCCGTGATGCATGAGGCTCTGCACAACCAC
TACACGCAGAAGAGCCTCTCCCTGTCTCCGGGTAAATGATAAGTCGACACGTGTGATCAGA
TATCGCGGCCGCTCTAGACCAGGCGCCTGGATCCAGATCACTTCTGGCTAATAAAAGATCAGAGCTCTAGAGATCTGTGTGTTGGT

TTTTTGTGGATCTGCTGTGCCTTCTAGTTGCCAGCCATCTGTTGTTTGCCCCTCCCCCGTGCCTTCCTTGACCCTGGAAGGTGCCACT
CCCACTGTCCTTTCCTAATAAAATGAGGAAATTGCATCGCATTGTCTGAGTAGGTGTCATTCTATTCTGGGGGGTGGGGTGGGGCA
GCACAGCAAGGGGGAGGATTGGGAAGACAATAGCAGGCATGCTGGGGATGCGGTGGGCTCTATGGGTACCTCTCTCTCTCTCTCT
CTCTCTCTCTCTCTCTCTCTCTCTCGGTACCTCTCTCTCTCTCTCTCTCTCTCTCTCTCTCTCTCTCTCGGTACCAGGTGCTGAAGA
ATTGACCCGGTTCCTCCTGGGCCAGAAAGAAGCAGGCACATCCCCTTCTCTGTGACACACCCTGTCCACGCCCCTGGTTCTTAGTT
CCAGCCCCACTCATAGGACACTCATAGCTCAGGAGGGCTCCGCCTTCAATCCCACCCGCTAAAGTACTTGGAGCGGTCTCTCCCTC
CCTCATCAGCCCACCAAACCAAACCTAGCCTCCAAGAGTGGGAAGAAATTAAAGCAAGATAGGCTATTAAGTGCAGAGGGAGAG
AAAATGCCTCCAACATGTGAGGAAGTAATGAGAGAAATCATAGAATTTCTTCCGCTTCCTCGCTCACTGACTCGCTGCGCTCGGTC
GTTCGGCTGCGGCGAGCGGTATCAGCTCACTCAAAGGCGGTAATACGGTTATCCACAGAATCAGGGGATAACGCAGGAAAGAAC
ATGTGAGCAAAAGGCCAGCAAAAGGCCAGGAACCGTAAAAAGGCCGCGTTGCTGGCGTTTTTCCATAGGCTCCGCCCCCCTGACG
AGCATCACAAAAATCGACGCTCAAGTCAGAGGTGGCGAAACCCGACAGGACTATAAAGATACCAGGCGTTTCCCCCTGGAAGCT
CCCTCGTGCGCTCTCCTGTTCCGACCCTGCCGCTTACCGGATACCTGTCCGCCTTTCTCCCTTCGGGAAGCGTGGCGCTTTCTCAAT
GCTCACGCTGTAGGTATCTCAGTTCGGTGTAGGTCGTTCGCTCCAAGCTGGGCTGTGTGCACGAACCCCCCGTTCAGCCCGACCGC
TGCGCCTTATCCGGTAACTATCGTCTTGAGTCCAACCCGGTAAGACACGACTTATCGCCACTGGCAGCAGCCACTGGTAACAGGA
TTAGCAGAGCGAGGTATGTAGGCGGTGCTACAGAGTTCTTGAAGTGGTGGCCTAACTACGGCTACACTAGAAGGACAGTATTTGG
TATCTGCGCTCTGCTGAAGCCAGTTACCTTCGGAAAAAGAGTTGGTAGCTCTTGATCCGGCAAACAAACCACCGCTGGTAGCGGT
GGTTTTTTTGTTTGCAAGCAGCAGATTACGCGCAGAAAAAAAGGATCTCAAGAAGATCCTTTGATCTTTTCTACGGGGTCTGACGC
TCAGTGGAACGAAAACTCACGTTAAGGGATTTTGGTCATGAGATTATCAAAAAGGATCTTCACCTAGATCCTTTTAAATTAAAAAT
GAAGTTTTAAATCAATCTAAAGTATATATGAGTAAACTTGGTCTGACAGTTACCAATGCTTAATCAGTGAGGCACCTATCTCAGCG
ATCTGTCTATTTCGTTCATCCATAGTTGCCTGACTCCGGGGGGGGGGGGCGCTGAGGTCTGCCTCGTGAAGAAGGTGTTGCTGACT
CATACCAGGCCTGAATCGCCCCATCATCCAGCCAGAAAGTGAGGGAGCCACGGTTGATGAGAGCTTTGTTGTAGGTGGACCAGTT
GGTGATTTTGAACTTTTGCTTTGCCACGGAACGGTCTGCGTTGTCGGGAAGATGCGTGATCTGATCCTTCAACTCAGCAAAAGTTC
GATTTATTCAACAAAGCCGCCGTCCCGTCAAGTCAGCGTAATGCTCTGCCAGTGTTACAACCAATTAACCAATTCTGATTAGAAAA
ACTCATCGAGCATCAAATGAAACTGCAATTTATTCATATCAGGATTATCAATACCATATTTTTGAAAAAGCCGTTTCTGTAATGAA
GGAGAAAACTCACCGAGGCAGTTCCATAGGATGGCAAGATCCTGGTATCGGTCTGCGATTCCGACTCGTCCAACATCAATACAAC
CTATTAATTTCCCCTCGTCAAAAATAAGGTTATCAAGTGAGAAATCACCATGAGTGACGACTGAATCCGGTGAGAATGGCAAAAG
CTTATGCATTTCTTTCCAGACTTGTTCAACAGGCCAGCCATTACGCTCGTCATCAAAATCACTCGCATCAACCAAACCGTTATTCAT
TCGTGATTGCGCCTGAGCGAGACGAAATACGCGATCGCTGTTAAAAGGACAATTACAAACAGGAATCGAATGCAACCGGCGCAG
GAACACTGCCAGCGCATCAACAATATTTTCACCTGAATCAGGATATTCTTCTAATACCTGGAATGCTGTTTTCCCGGGGATCGCAG
TGGTGAGTAACCATGCATCATCAGGAGTACGGATAAAATGCTTGATGGTCGGAAGAGGCATAAATTCCGTCAGCCAGTTTAGTCT
GACCATCTCATCTGTAACATCATTGGCAACGCTACCTTTGCCATGTTTCAGAAACAACTCTGGCGCATCGGGCTTCCCATACAATC
GATAGATTGTCGCACCTGATTGCCCGACATTATCGCGAGCCCATTTATACCCATATAAATCAGCATCCATGTTGGAATTTAATCGC
GGCCTCGAGCAAGACGTTTCCCGTTGAATATGGCTCATAACACCCCTTGTATTACTGTTTATGTAAGCAGACAGTTTTATTGTTCAT
GATGATATATTTTTATCTTGTGCAATGTAACATCAGAGATTTTGAGACACAACGTGGCTTTCCCCCCCCCCCCATTATTGAAGCATT
TATCAGGGTTATTGTCTCATGAGCGGATACATATTTGAATGTATTTAGAAAAATAAACAAATAGGGGTTCCGCGCACATTTCCCCG
AAAAGTGCCACCTGACGTCTAAGAAACCATTATTATCATGACATTAACCTATAAAAATAGGCGTATCACGAGGCCCTTTCGTC

gWiz 225 LC (225 variable domain on human IgG1 Scaffold)

PstI-- Kozak--Leader -- DraIII—225 VH—BsiWI---Ckappa—Stop—SalI

CTGCAGGCCGCCACCATGAGGGTCCCCGCTCAGCTCCTGGGGCTCCTGCTGCTCTGG
CTCCCAGGTGCACGATGTGACATCCTGCTGACCCAGTCTCCAGTCATCCTGTCTGTG
AGTCCAGGAGAAAGAGTCAGTTTCTCCTGCAGGGCCAGTCAGAGTATTGGCACAAA
CATACACTGGTATCAGCAAAGAACAAATGGTTCTCCAAGGCTTCTCATAAAGTATGC
TTCTGAGTCTATCTCTGGCATCCCTTCCAGGTTTAGTGGCAGTGGATCAGGGACAGA
TTTTACTCTTAGCATCAACAGTGTGGAGTCTGAAGATATTGCAGATTATTACTGTCA
ACAAAATAATAACTGGCCAACCACGTTCGGTGCTGGGACCAAGCTGGAGCTCAAAC
GTACGGTGGCTGCACCATCTGTCTTCATCTTCCCGCCATCTGATGAGCAGTTGAAAT
CTGGAACTGCCTCTGTTGTGTGCCTGCTGAATAACTTCTATCCCAGAGAGGCCAAAG
TACAGTGGAAGGTGGATAACGCCCTCCAATCGGGTAACTCCCAGGAGAGTGTCACA
GAGCAGGACAGCAAGGACAGCACCTACAGCCTCAGCAGCACCCTGACGCTGAGCAA
AGCAGACTACGAGAAACACAAAGTCTACGCCTGCGAAGTCACCCATCAGGGCCTGA
GCTCGCCCGTCACAAAGAGCTTCAACAGGGGAGAGTGTTAATAGGTCGAC

gWiz 806 HC (806 variable domain on human IgG1 Scaffold)

PstI-- Kozak--Leader—MluI—806 VH—NheI---C1,2,3--Stop—SalI

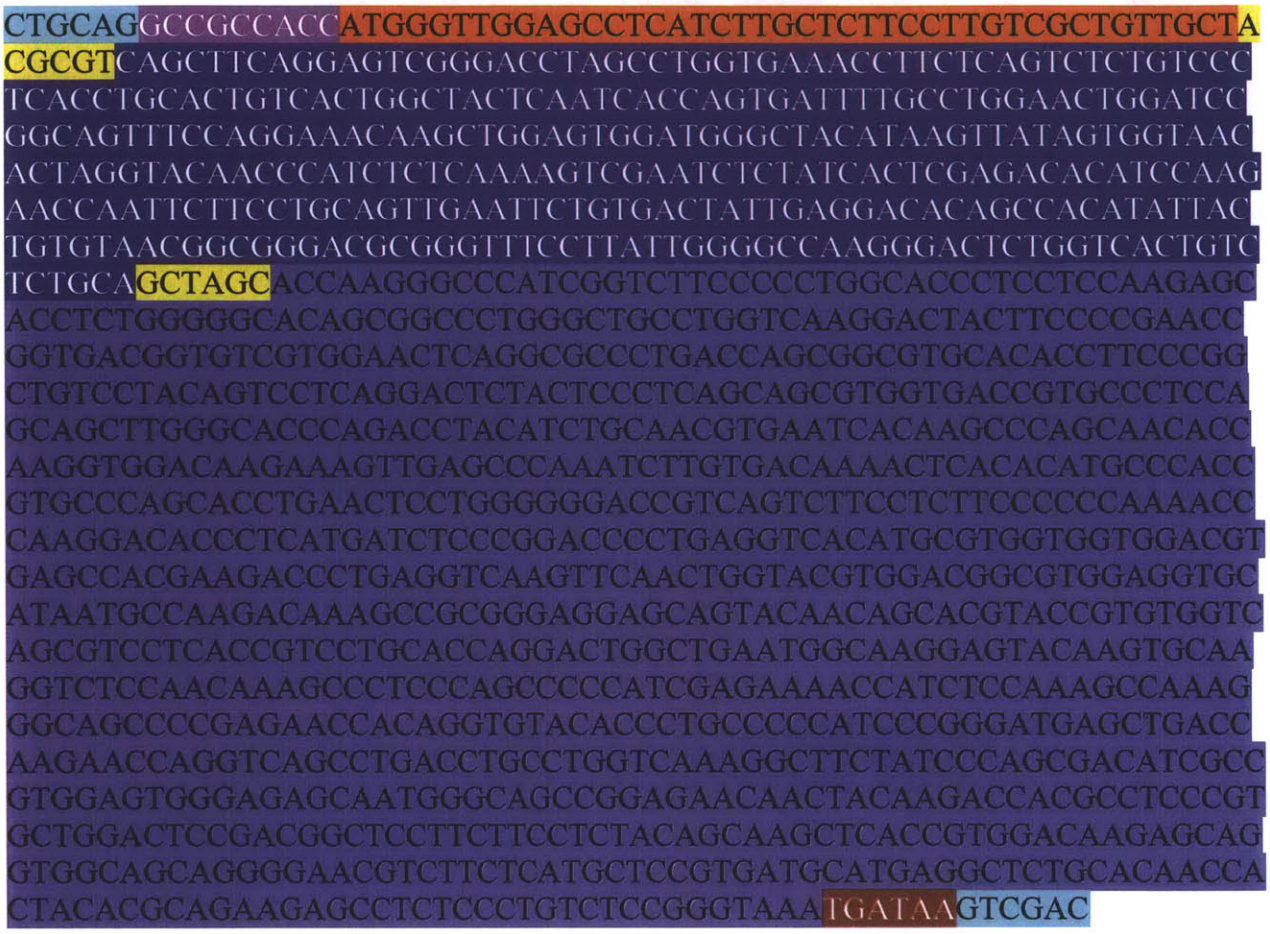

gWiz 806 LC (806 variable domain on human IgG1 Scaffold)

PstI-- Kozak--Leader -- DraIII—806 VL—BsiWI---Ckappa—Stop—SalI

CTGCAGGCCGCCACCATGAGGGTCCCCGCTCAGCTCCTGGGGCTCCTGCTGCTCTGG
CTCCCAGGTGCACGATGTGACATCCTGATGACCCAATCTCCATCCTCCATGTCTGTA
TCTCTGGGAGACACAGTCAGCATCACTTGCCATTCAAGTCAGGACATTAACAGTAAT
ATAGGGTGGTTGCAGCAGAGACCAGGGAAATCATTTAAGGGCCTGATCTATCATGG
AACCAACTTGGACGATGAAGTTCCATCAAGGTTCAGTGGCAGTGGATCTGGAGCCG
ATTATTCTCTCACCATCAGCAGCCTGGAATCTGAAGATTTTGCAGACTATTACTGTGT
ACAGTATGCTCAGTTTCCGTGGACGTTCGGTGGAGGCACCAAGCTGGAAATCAAAC
GTCGTACGGTGGCTGCACCATCTGTCTTCATCTTCCCGCCATCTGATGAGCAGTTGA
AATCTGGAACTGCCTCTGTTGTGTGCCTGCTGAATAACTTCTATCCCAGAGAGGCCA
AAGTACAGTGGAAGGTGGATAACGCCCTCCAATCGGGTAACTCCCAGGAGAGTGTC
ACAGAGCAGGACAGCAAGGACAGCACCTACAGCCTCAGCAGCACCCTGACGCTGAG
CAAAGCAGACTACGAGAAACACAAAGTCTACGCCTGCGAAGTCACCCATCAGGGCC
TGAGCTCGCCCGTCACAAAGAGCTTCAACAGGGGAGAGTGTTAATAGGTCGAC

2) Bispecific 225/806-Containing Antibodies (BS28)

gWiz BS28-HN (Secreted with gWiz 225 LC)

PstI -- Kozak Sequence -- Leader -- 806 VH -- $(Gly_4Ser)_3$ linker -- 806 VL -- $(Gly_4Ser)_2$ -- MluI—225 VH -- NheI -- CH1,2,3 -- Stop -- SalI

CTGCAGGCCGCCACCATGGGTTGGAGCCTCATCTTGCTCTTCCTTGTCGCTGTTGCTC
AGCTTCAGGAGTCGGGACCTAGCCTGGTGAAACCTTCTCAGTCTCTGTCCCTCACCT
GCACTGTCACTGGCTACTCAATCACCAGTGATTTTGCCTGGAACTGGATCCGGCAGT
TTCCAGGAAACAAGCTGGAGTGGATGGGCTACATAAGTTATAGTGGTAACACTAGG
TACAACCCATCTCTCAAAAGTCGAATCTCTATCACTCGAGACACATCCAAGAACCAA
TTCTTCCTGCAGTTGAATTCTGTGACTATTGAGGACACAGCCACATATTACTGTGTAA
CGGCGGGACGCGGGTTTCCTTATTGGGGCCAAGGGACTCTGGTCACTGTCTCTGCAG
GAGGCGGCGGATCTGGCGGTGGAGGTTCTGGCGGCGGCGGATCTGACATCCTGATG
ACCCAATCTCCATCCTCCATGTCTGTATCTCTGGGAGACACAGTCAGCATCACTTGC
CATTCAAGTCAGGACATTAACAGTAATATAGGGTGGTTGCAGCAGAGACCAGGGAA
ATCATTTAAGGGCCTGATCTATCATGGAACCAACTTGGACGATGAAGTTCCATCAAG
GTTCAGTGGCAGTGGATCTGGAGCCGATTATTCTCTCACCATCAGCAGCCTGGAATC
TGAAGATTTTGCAGACTATTACTGTGTACAGTATGCTCAGTTTCCGTGGACGTTCGGT
GGAGGCACCAAGCTGGAAATCAAACGTGGAGGCGGCGGATCTGGCGGTGGAGGTTC
TACGCGTCAGGTACAACTGAAGCAGTCAGGACCTGGCCTAGTGCAGCCCTCACAGA
GCCTGTCCATCACCTGCACAGTCTCTGGTTTCTCATTAACTAACTATGGTGTACACTG
GGTTCGCCAGTCTCCAGGAAAGGGTCTGGAGTGGCTGGGAGTGATATGGAGTGGTG
GAAACACAGACTATAATACACCTTTCACATCCAGACTGAGCATCAACAAGGACAATT
TCCAAGAGCCAAGTTTTCTTTAAAATGAACAGTCTGCAATCTAATGACACAGCCATA
TATTACTGTGCCAGAGCCCTCACCTACTATGATTACGAGTTTGCTTACTGGGGCCAA
GGGACCCTGGTCACCGTTTCCGCTGCTAGCACCAAGGGCCCATCGGTCTTCCCCCTG
GCACCCTCCTCCAAGAGCACCTCTGGGGGCACAGCGGCCCTGGGCTGCCTGGTCAA
GGACTACTTCCCCGAACCGGTGACGGTGTCGTGGAACTCAGGCGCCCTGACCAGCG
GCGTGCACACCTTCCCGGCTGTCCTACAGTCCTCAGGACTCTACTCCCTCAGCAGCG
TGGTGACCGTGCCCTCCAGCAGCTTGGGCACCCAGACCTACATCTGCAACGTGAATC
ACAAGCCCAGCAACACCAAGGTGGACAAGAAAGTTGAGCCCAAATCTTGTGACAAA
ACTCACACATGCCCACCGTGCCCAGCACCTGAACTCCTGGGGGGACCGTCAGTCTTC
CTCTTCCCCCCAAAACCCAAGGACACCCTCATGATCTCCCGGACCCCTGAGGTCACA
TGCGTGGTGGTGGACGTGAGCCACGAAGACCCTGAGGTCAAGTTCAACTGGTACGT
GGACGGCGTGGAGGTGCATAATGCCAAGACAAAGCCGCGGGAGGAGCAGTACAAC
AGCACGTACCGTGTGGTCAGCGTCCTCACCGTCCTGCACCAGGACTGGCTGAATGGC
AAGGAGTACAAGTGCAAGGTCTCCAACAAAGCCCTCCCAGCCCCCATCGAGAAAAC
CATCTCCAAAGCCAAAGGGCAGCCCCGAGAACCACAGGTGTACACCCTGCCCCCAT
CCCGGGATGAGCTGACCAAGAACCAGGTCAGCCTGACCTGCCTGGTCAAAGGCTTC
TATCCCAGCGACATCGCCGTGGAGTGGGAGAGCAATGGGCAGCCGGAGAACAACTA
CAAGACCACGCCTCCCGTGCTGGACTCCGACGGCTCCTTCTTCCTCTACAGCAAGCT
CACCGTGGACAAGAGCAGGTGGCAGCAGGGGAACGTCTTCTCATGCTCCGTGATGC
ATGAGGCTCTGCACAACCACTACACGCAGAAGAGCCTCTCCCTGTCTCCGGGTAAAT
GATAAGTCGAC

gWiz BS28-HC (Secreted with gWiz 225 LC)

PstI -- Kozak Sequence -- Leader -- MluI—225 VH -- NheI -- CH1,2,3 -- MluI -- $(Gly_4Ser)_2$ -- NheI -- 806 VH -- $(Gly_4Ser)_3$ linker -- 806 VL -- Stop -- SalI

CTGCAGGCCGCCACCATGGGTTGGAGCCTCATCTTGCTCTTCCTTGTCGCTGTTGCTA
CGCGTCAGGTACAACTGAAGCAGTCAGGACCTGGCCTAGTGCAGCCCTCACAGAGC
CTGTCCATCACCTGCACAGTCTCTGGTTTCTCATTAACTAACTATGGTGTACACTGGG
TTCGCCAGTCTCCAGGAAAGGGTCTGGAGTGGCTGGGAGTGATATGGAGTGGTGGA
AACACAGACTATAATACACCTTTCACATCCAGACTGAGCATCAACAAGGACAATTC
CAAGAGCCAAGTTTTCTTTAAAATGAACAGTCTGCAATCTAATGACACAGCCATATA
TTACTGTGCCAGAGCCCTCACCTACTATGATTACGAGTTTGCTTACTGGGGCCAAGG
GACCCTGGTCACCGTTTCCGCTGCTAGCACCAAGGGCCCATCGGTCTTCCCCCTGGC
ACCCTCCTCCAAGAGCACCTCTGGGGGCACAGCGGCCCTGGGCTGCCTGGTCAAGG
ACTACTTCCCCGAACCGGTGACGGTGTCGTGGAACTCAGGCGCCCTGACCAGCGGC
GTGCACACCTTCCCGGCTGTCCTACAGTCCTCAGGACTCTACTCCCTCAGCAGCGTG
GTGACCGTGCCCTCCAGCAGCTTGGGCACCCAGACCTACATCTGCAACGTGAATCAC
AAGCCCAGCAACACCAAGGTGGACAAGAAAGTTGAGCCCAAATCTTGTGACAAAAC
TCACACATGCCCACCGTGCCCAGCACCTGAACTCCTGGGGGGACCGTCAGTCTTCCT
CTTCCCCCCAAAACCCAAGGACACCCTCATGATCTCCCGGACCCCTGAGGTCACATG
CGTGGTGGTGGACGTGAGCCACGAAGACCCTGAGGTCAAGTTCAACTGGTACGTGG
ACGGCGTGGAGGTGCATAATGCCAAGACAAAGCCGCGGGAGGAGCAGTACAACAG
CACGTACCGTGTGGTCAGCGTCCTCACCGTCCTGCACCAGGACTGGCTGAATGGCAA
GGAGTACAAGTGCAAGGTCTCCAACAAAGCCCTCCCAGCCCCCATCGAGAAAACCA
TCTCCAAAGCCAAAGGGCAGCCCCGAGAACCACAGGTGTACACCCTGCCCCCATCC
CGGGATGAGCTGACCAAGAACCAGGTCAGCCTGACCTGCCTGGTCAAAGGCTTCTA
TCCCAGCGACATCGCCGTGGAGTGGGAGAGCAATGGGCAGCCGGAGAACAACTACA
AGACCACGCCTCCCGTGCTGGACTCCGACGGCTCCTTCTTCCTCTACAGCAAGCTCA
CCGTGGACAAGAGCAGGTGGCAGCAGGGGAACGTCTTCTCATGCTCCGTGATGCAT
GAGGCTCTGCACAACCACTACACGCAGAAGAGCCTCTCCCTGTCTCCGGGTAAAAC
GCGTGGAGGTGGCGGTAGTGGCGGAGGTGGTTCTGCTAGCCAGCTTCAGGAGTCGG
GACCTAGCCTGGTGAAACCTTCTCAGTCTCTGTCCCTCACCTGCACTGTCACTGGCTA
CTCAATCACCAGTGATTTTGCCTGGAACTGGATCCGGCAGTTTCCAGGAAACAAGCT
GGAGTGGATGGGCTACATAAGTTATAGTGGTAACACTAGGTACAACCCATCTCTCAA
AAGTCGAATCTCTATCACTCGAGACACATCCAAGAACCAATTCTTCCTGCAGTTGAA
TTCTGTGACTATTGAGGACACAGCCACATATTACTGTGTAACGGCGGGACGCGGGTT
TCCTTATTGGGGCCAAGGGACTCTGGTCACTGTCTCTGCAGGAGGCGGCGGATCTGG
CGGTGGAGGTTCTGGCGGCGGCGGATCTGACATCCTGATGACCCAATCTCCATCCTC
CATGTCTGTATCTCTGGGAGACACAGTCAGCATCACTTGCCATTCAAGTCAGGACAT
TAACAGTAATATAGGGTGGTTGCAGCAGAGACCAGGGAAATCATTTAAGGGCCTGA
TCTATCATGGAACCAACTTGGACGATGAAGTTCCATCAAGGTTCAGTGGCAGTGGAT
CTGGAGCCGATTATTCTCTCACCATCAGCAGCCTGGAATCTGAAGATTTTGCAGACT
ATTACTGTGTACAGTATGCTCAGTTTCCGTGGACGTTCGGTGGAGGCACCAAGCTGG
AAATCAAACGTTGATAAGTCGAC

gWiz BS28-LN (Secreted with gWiz 225 HC)

PstI-- Kozak--Leader --NdeI -- NheI -- 806 VH -- $(Gly_4Ser)_3$ linker -- 806 VL -- BamHI—
$(Gly_4Ser)_2$—DraIII—225 VL—BsiWI---Ckappa—Stop—SalI

CTGCAGGCCGCCACCATGAGGGTCCCCGCTCAGCTCCTGGGGCTCCTGCTGCTCTGG
CTCCCAGGTGCACATATGGCTAGCCAGCTTCAGGAGTCGGGACCTAGCCTGGTGAA
ACCTTCTCAGTCTCTGTCCCTCACCTGCACTGTCACTGGCTACTCAATCACCAGTGAT
TTTGCCTGGAACTGGATCCGGCAGTTTCCAGGAAACAAGCTGGAGTGGATGGGCTA
CATAAGTTATAGTGGTAACACTAGGTACAACCCATCTCTCAAAAGTCGAATCTCTAT
CACTCGAGACACATCCAAGAACCAATTCTTCCTGCAGTTGAATTCTGTGACTATTGA
GGACACAGCCACATATTACTGTGTAACGGCGGGACGCGGGTTTCCTTATTGGGGCCA
AGGGACTCTGGTCACTGTCTCTGCAGGAGGCGGCGGATCTGGCGGTGGAGGTTCTG
GCGGCGGCGGATCTGACATCCTGATGACCCAATCTCCATCCTCCATGTCTGTATCTC
TGGGAGACACAGTCAGCATCACTTGCCATTCAAGTCAGGACATTAACAGTAATATA
GGGTGGTTGCAGCAGAGACCAGGGAAATCATTTAAGGGCCTGATCTATCATGGAAC
CAACTTGGACGATGAAGTTCCATCAAGGTTCAGTGGCAGTGGATCTGGAGCCGATTA
TTCTCTCACCATCAGCAGCCTGGAATCTGAAGATTTTGCAGACTATTACTGTGTACA
GTATGCTCAGTTTCCGTGGACGTTCGGTGGAGGCACCAAGCTGGAAATCAAACGTG
GATCCGGAGGTGGCGGTAGTGGCGGAGGTGGTTCTTCACGATGTGACATCCTGCTGA
CCCAGTCTCCAGTCATCCTGTCTGTGAGTCCAGGAGAAAGAGTCAGTTTCTCCTGCA
GGGCCAGTCAGAGTATTGGCACAAACATACACTGGTATCAGCAAAGAACAAATGGT
TCTCCAAGGCTTCTCATAAAGTATGCTTCTGAGTCTATCTCTGGCATCCCTTCCAGGT
TTAGTGGCAGTGGATCAGGGACAGATTTTACTCTTAGCATCAACAGTGTGGAGTCTG
AAGATATTGCAGATTATTACTGTCAACAAAATAATAACTGGCCAACCACGTTCGGTG
CTGGGACCAAGCTGGAGCTCAAACGTACGGTGGCTGCACCATCTGTCTTCATCTTCC
CGCCATCTGATGAGCAGTTGAAATCTGGAACTGCCTCTGTTGTGTGCCTGCTGAATA
ACTTCTATCCCAGAGAGGCCAAAGTACAGTGGAAGGTGGATAACGCCCTCCAATCG
GGTAACTCCCAGGAGAGTGTCACAGAGCAGGACAGCAAGGACAGCACCTACAGCCT
CAGCAGCACCCTGACGCTGAGCAAAGCAGACTACGAGAAACACAAAGTCTACGCCT
GCGAAGTCACCCATCAGGGCCTGAGCTCGCCCGTCACAAAGAGCTTCAACAGGGGA
GAGTGTTAATAGGTCGAC

gWiz BS28-LC (Secreted with gWiz 225 HC)

PstI -- Kozak Sequence -- Leader -- DraIII -- 225 VL -- BsiWI -- Ckappa -- $(Gly_4Ser)_2$ Linker -- 806VH -- $(Gly4Ser)_3$ linker -- 806VL -- GS Spacer -- Cmyc Epitope Tag -- Stop -- SalI

CTGCAGGCCGCCACCATGAGGGTCCCCGCTCAGCTCCTGGGGCTCCTGCTGCTCTGG
CTCCCAGGTGCACACGATGTGACATCCTGCTGACCCAGTCTCCAGTCATCCTGTCTG
TGAGTCCAGGAGAAAGAGTCAGTTTCTCCTGCAGGGCCAGTCAGAGTATTGGCACA
AACATACACTGGTATCAGCAAAGAACAAATGGTTCTCCAAGGCTTCTCATAAAGTAT
GCTTCTGAGTCTATCTCTGGCATCCCTTCCAGGTTTAGTGGCAGTGGATCAGGGACA
GATTTTACTCTTAGCATCAACAGTGTGGAGTCTGAAGATATTGCAGATTATTACTGT
CAACAAAATAATAACTGGCCAACCACGTTCGGTGCTGGGACCAAGCTGGAGCTCAA
ACGTACGGTGGCTGCACCATCTGTCTTCATCTTCCCGCCATCTGATGAGCAGTTGAA
ATCTGGAACTGCCTCTGTTGTGTGCCTGCTGAATAACTTCTATCCCAGAGAGGCCAA
AGTACAGTGGAAGGTGGATAACGCCCTCCAATCGGGTAACTCCCAGGAGAGTGTCA
CAGAGCAGGACAGCAAGGACAGCACCTACAGCCTCAGCAGCACCCTGACGCTGAGC
AAAGCAGACTACGAGAAACACAAAGTCTACGCCTGCGAAGTCACCCATCAGGGCCT
GAGCTCGCCCGTCACAAAGAGCTTCAACAGGGGAGAGTGTGGAGGTGGCGGTAGTG
GCGGAGGTGGTTCTCAGCTTCAGGAGTCGGGACCTAGCCTGGTGAAACCTTCTCAGT
CTCTGTCCCTCACCTGCACTGTCACTGGCTACTCAATCACCAGTGATTTTGCCTGGAA
CTGGATCCGGCAGTTTCCAGGAAACAAGCTGGAGTGGATGGGCTACATAAGTTATA
GTGGTAACACTAGGTACAACCCATCTCTCAAAAGTCGAATCTCTATCACTCGAGACA
CATCCAAGAACCAATTCTTCCTGCAGTTGAATTCTGTGACTATTGAGGACACAGCCA
CATATTACTGTGTAACGGCGGGACGCGGGTTTCCTTATTGGGGCCAAGGGACTCTGG
TCACTGTCTCTGCAGGAGGCGGCGGATCTGGCGGTGGAGGTTCTGGCGGCGGCGGA
TCTGACATCCTGATGACCCAATCTCCATCCTCCATGTCTGTATCTCTGGGAGACACA
GTCAGCATCACTTGCCATTCAAGTCAGGACATTAACAGTAATATAGGGTGGTTGCAG
CAGAGACCAGGGAAATCATTTAAGGGCCTGATCTATCATGGAACCAACTTGGACGA
TGAAGTTCCATCAAGGTTCAGTGGCAGTGGATCTGGAGCCGATTATTCTCTCACCAT
CAGCAGCCTGGAATCTGAAGATTTTGCAGACTATTACTGTGTACAGTATGCTCAGTT
TCCGTGGACGTTCGGTGGAGGCACCAAGCTGGAAATCAAACGTGGATCAGAACAAA
AGCTTATTTCTGAAGAGGACTTGTAATAGGTCGAC

3) Antibody-Fibronectin Fusions (Ab-Fn3 Fusions)

The three EGFR-targeted Fn3 domain clones used in engineered fusions have the following sequences (from Hackel BJ Neil JR, White FM, & Wittrup KD (Submitted) Epidermal growth factor receptor downregulation by small heterodimeric binding proteins):

Fn3 Clone A

GTTTCCGATGTTCCGAGGGACCTGGAGGTTGTTGCTGCGACCCCCACCAGCCTACTG
ATCAGCTGGTTCGACTACGCTGTGACTTATTACAGGATCACTTACGGAGAAACAGGA
GGAAATAGCCCTGTCCAGGAGTTCACTGTGCCTGGTTGGATCTCCACTGCTACCATC
AGCGGCCTTAAACCTGGAGTTGATTATACCATCACTGTGTATGCTGTCACTGACAAC
TCTCGTTGGCCTTTTCGCTCTACTCCAATTTCCACTAATTACCGAACAGAAATTGACA
AACCACCCCAG

Fn3 Clone B

GTTTCTGATGTTCCGAGGGACCTGGAAGTTGTTGCTGCGACCCCCACCAGCCTACTG
ATCAGCTGGTACGGTTTTTCGCTTGCGAGCTCTTACAGGATCACTTACGGAGAAACA
GGAGGAAATAGCCCTGTCCAGGAGTTCACTGTGCCTCGTTCGCCCTGGTTTGCTACC
ATCAGCGGCCTTAAACCTGGAGTTGATTATACCATCACTGTGTATGCTGTCACTTCTA
ACGACTTTTCTAATCGTTACTCTGGTCCAATTTCCATTAATTACCGAACAGAAATTGA
CAAACCATCCCAG

Fn3 Clone D

GTTTCTGATGTTCCGAGGGACCTGGAAGTTGTTGCTGCGACCCCCACCAGCCTACTG
ATCAGCTGGCTTCACCATCGCTCTGACGTGCGCTCTTACAGGATCACTTACGGAGAA
ACAGGAGGAAATAGCCCTGTCCAGAAGTTCACTGTGCCTGGGTCGCGCTCCCTGGCT
ACCATCAGCGGCCTTAAACCTGGAGTTGATTATACCATCACTGTGTATGCTGTCACT
TGGGGGTCTTACTGTTGCTCTAATCCAATTTCCATTAATTACCGAACAGAAATTGAC
AAACCATCCCAG

gWiz HN-A (N-terminal heavy chain fusion)

PstI--Kozak--Leader --NdeI -- NheI -- Fn3 1-101 (2) – BamHI—$(Gly_4Ser)_2$—MluI—225 VH—
NheI---CH1,2,3—Stop—SalI

CTGCAGGCCGCCACCATGGGTTGGAGCCTCATCTTGCTCTTCCTTGTCGCTGTTGCTC
ATATGGCTAGCGTTTCCGATGTTCCGAGGGACCTGGAGGTTGTTGCTGCGACCCCCA
CCAGCCTACTGATCAGCTGGTTCGACTACGCTGTGACTTATTACAGGATCACTTACG
GAGAAACAGGAGGAAATAGCCCTGTCCAGGAGTTCACTGTGCCTGGTTGGATCTCC
ACTGCTACCATCAGCGGCCTTAAACCTGGAGTTGATTATACCATCACTGTGTATGCT
GTCACTGACAACTCTCGTTGGCCTTTTCGCTCTACTCCAATTTCCACTAATTACCGAA
CAGAAATTGACAAACCACCCCAGGGATCCGGAGGTGGCGGTAGTGGCGGAGGTGGT
TCTACGCGTCAGGTACAACTGAAGCAGTCAGGACCTGGCCTAGTGCAGCCCTCACA
GAGCCTGTCCATCACCTGCACAGTCTCTGGTTTCTCATTAACTAACTATGGTGTACAC
TGGGTTCGCCAGTCTCCAGGAAAGGGTCTGGAGTGGCTGGGAGTGATATGGAGTGG
TGGAAACACAGACTATAATACACCTTTCACATCCAGACTGAGCATCAACAAGGACA
ATTCCAAGAGCCAAGTTTTCTTTAAAATGAACAGTCTGCAATCTAATGACACAGCCA
TATATTACTGTGCCAGAGCCCTCACCTACTATGATTACGAGTTTGCTTACTGGGGCC
AAGGGACCCTGGTCACCGTTTCCGCTGCTAGCACCAAGGGCCCATCGGTCTTCCCCC
TGGCACCCTCCTCCAAGAGCACCTCTGGGGGCACAGCGGCCCTGGGCTGCCTGGTCA
AGGACTACTTCCCCGAACCGGTGACGGTGTCGTGGAACTCAGGCGCCCTGACCAGC
GGCGTGCACACCTTCCCGGCTGTCCTACAGTCCTCAGGACTCTACTCCCTCAGCAGC
GTGGTGACCGTGCCCTCCAGCAGCTTGGGCACCCAGACCTACATCTGCAACGTGAAT
CACAAGCCCAGCAACACCAAGGTGGACAAGAAAGTTGAGCCCAAATCTTGTGACAA
AACTCACACATGCCCACCGTGCCCAGCACCTGAACTCCTGGGGGGACCGTCAGTCTT
CCTCTTCCCCCCAAAACCCAAGGACACCCTCATGATCTCCCGGACCCCTGAGGTCAC
ATGCGTGGTGGTGGACGTGAGCCACGAAGACCCTGAGGTCAAGTTCAACTGGTACG
TGGACGGCGTGGAGGTGCATAATGCCAAGACAAAGCCGCGGGAGGAGCAGTACAA
CAGCACGTACCGTGTGGTCAGCGTCCTCACCGTCCTGCACCAGGACTGGCTGAATGG
CAAGGAGTACAAGTGCAAGGTCTCCAACAAAGCCCTCCCAGCCCCCATCGAGAAAA
CCATCTCCAAAGCCAAAGGGCAGCCCCGAGAACCACAGGTGTACACCCTGCCCCCA
TCCCGGGATGAGCTGACCAAGAACCAGGTCAGCCTGACCTGCCTGGTCAAAGGCTT
CTATCCCAGCGACATCGCCGTGGAGTGGGAGAGCAATGGGCAGCCGGAGAACAACT
ACAAGACCACGCCTCCCGTGCTGGACTCCGACGGCTCCTTCTTCCTCTACAGCAAGC
TCACCGTGGACAAGAGCAGGTGGCAGCAGGGGAACGTCTTCTCATGCTCCGTGATG
CATGAGGCTCTGCACAACCACTACACGCAGAAGAGCCTCTCCCTGTCTCCGGGTAAA
TGATAAGTCGAC

gWiz HC-A (C-terminal heavy chain fusion)

PstI-- Kozak--Leader—MluI—225 VH—NheI---C1,2,3—$(Gly_4Ser)_2$-- NdeI -- NheI -- Fn3 1-101 (Clone A = E6.2.6) – BamHI --Stop—SalI

CTGCAGGCCGCCACCATGGGTTGGAGCCTCATCTTGCTCTTCCTTGTCGCTGTTGCTA
CGCGTCAGGTACAACTGAAGCAGTCAGGACCTGGCCTAGTGCAGCCCTCACAGAGC
CTGTCCATCACCTGCACAGTCTCTGGTTTCTCATTAACTAACTATGGTGTACACTGGG
TTCGCCAGTCTCCAGGAAAGGGTCTGGAGTGGCTGGGAGTGATATGGAGTGGTGGA
AACACAGACTATAATACACCTTTCACATCCAGACTGAGCATCAACAAGGACAATTC
CAAGAGCCAAGTTTTCTTTAAAATGAACAGTCTGCAATCTAATGACACAGCCATATA
TTACTGTGCCAGAGCCCTCACCTACTATGATTACGAGTTTGCTTACTGGGGCCAAGG
GACCCTGGTCACCGTTTCCGCTGCTAGCACCAAGGGCCCATCGGTCTTCCCCCTGGC
ACCCTCCTCCAAGAGCACCTCTGGGGGCACAGCGGCCCTGGGCTGCCTGGTCAAGG
ACTACTTCCCCGAACCGGTGACGGTGTCGTGGAACTCAGGCGCCCTGACCAGCGGC
GTGCACACCTTCCCGGCTGTCCTACAGTCCTCAGGACTCTACTCCCTCAGCAGCGTG
GTGACCGTGCCCTCCAGCAGCTTGGGCACCCAGACCTACATCTGCAACGTGAATCAC
AAGCCCAGCAACACCAAGGTGGACAAGAAAGTTGAGCCCAAATCTTGTGACAAAAC
TCACACATGCCCACCGTGCCCAGCACCTGAACTCCTGGGGGGACCGTCAGTCTTCCT
CTTCCCCCCAAAACCCAAGGACACCCTCATGATCTCCCGGACCCCTGAGGTCACATG
CGTGGTGGTGGACGTGAGCCACGAAGACCCTGAGGTCAAGTTCAACTGGTACGTGG
ACGGCGTGGAGGTGCATAATGCCAAGACAAAGCCGCGGGAGGAGCAGTACAACAG
CACGTACCGTGTGGTCAGCGTCCTCACCGTCCTGCACCAGGACTGGCTGAATGGCAA
GGAGTACAAGTGCAAGGTCTCCAACAAAGCCCTCCCAGCCCCCATCGAGAAAACCA
TCTCCAAAGCCAAAGGGCAGCCCCGAGAACCACAGGTGTACACCCTGCCCCCATCC
CGGGATGAGCTGACCAAGAACCAGGTCAGCCTGACCTGCCTGGTCAAAGGCTTCTA
TCCCAGCGACATCGCCGTGGAGTGGGAGAGCAATGGGCAGCCGGAGAACAACTACA
AGACCACGCCTCCCGTGCTGGACTCCGACGGCTCCTTCTTCCTCTACAGCAAGCTCA
CCGTGGACAAGAGCAGGTGGCAGCAGGGGAACGTCTTCTCATGCTCCGTGATGCAT
GAGGCTCTGCACAACCACTACACGCAGAAGAGCCTCTCCCTGTCTCCGGGTAAAGG
AGGTGGCGGTAGTGGCGGAGGTGGTTCTCATATGGCTAGCGTTTCCGATGTTCCGAG
GGACCTGGAGGTTGTTGCTGCGACCCCCACCAGCCTACTGATCAGCTGGTTCGACTA
CGCTGTGACTTATTACAGGATCACTTACGGAGAAACAGGAGGAAATAGCCCTGTCC
AGGAGTTCACTGTGCCTGGTTGGATCTCCACTGCTACCATCAGCGGCCTTAAACCTG
GAGTTGATTATACCATCACTGTGTATGCTGTCACTGACAACTCTCGTTGGCCTTTTCG
CTCTACTCCAATTTCCACTAATTACCGAACAGAAATTGACAAACCACCCCAGGGATC
CTGATAAGTCGAC

gWiz LN-A (N-terminal light chain fusion)

PstI--Leader --NdeI -- NheI -- Fn3 1-101 (Clone D = EI3.4.3) – BamHI—$(Gly_4Ser)_2$—DraIII—
225 VL—BsiWI---Ckappa—Stop—SalI

CTGCAGGCCGCCACCATGAGGGTCCCCGCTCAGCTCCTGGGGCTCCTGCTGCTCTGG
CTCCCAGGTGCACATATGGCTAGCGTTTCCGATGTTCCGAGGGACCTGGAGGTTGTT
GCTGCGACCCCCACCAGCCTACTGATCAGCTGGTTCGACTACGCTGTGACTTATTAC
AGGATCACTTACGGAGAAACAGGAGGAAATAGCCCTGTCCAGGAGTTCACTGTGCC
TGGTTGGATCTCCACTGCTACCATCAGCGGCCTTAAACCTGGAGTTGATTATACCAT
CACTGTGTATGCTGTCACTGACAACTCTCGTTGGCCTTTTCGCTCTACTCCAATTTCC
ACTAATTACCGAACAGAAATTGACAAACCACCCCAGGGATCCGGAGGTGGCGGTAG
TGGCGGAGGTGGTTCTTCACGATGTGACATCCTGCTGACCCAGTCTCCAGTCATCCT
GTCTGTGAGTCCAGGAGAAAGAGTCAGTTTCTCCTGCAGGGCCAGTCAGAGTATTGG
CACAAACATACACTGGTATCAGCAAAGAACAAATGGTTCTCCAAGGCTTCTCATAA
AGTATGCTTCTGAGTCTATCTCTGGCATCCCTTCCAGGTTTAGTGGCAGTGGATCAG
GGACAGATTTTACTCTTAGCATCAACAGTGTGGAGTCTGAAGATATTGCAGATTATT
ACTGTCAACAAAATAATAACTGGCCAACCACGTTCGGTGCTGGGACCAAGCTGGAG
CTCAAACGTACGGTGGCTGCACCATCTGTCTTCATCTTCCCGCCATCTGATGAGCAG
TTGAAATCTGGAACTGCCTCTGTTGTGTGCCTGCTGAATAACTTCTATCCCAGAGAG
GCCAAAGTACAGTGGAAGGTGGATAACGCCCTCCAATCGGGTAACTCCCAGGAGAG
TGTCACAGAGCAGGACAGCAAGGACAGCACCTACAGCCTCAGCAGCACCCTGACGC
TGAGCAAAGCAGACTACGAGAAACACAAAGTCTACGCCTGCGAAGTCACCCATCAG
GGCCTGAGCTCGCCCGTCACAAAGAGCTTCAACAGGGGAGAGTGTTAATAGGTCGA
C

gWiz LC-A (C-terminal light chain fusion)

PstI--Leader -- DraIII -- 225 VL -- BsiWI -- Ckappa -- $(Gly_4Ser)_2$ -- NdeI -- NheI -- Fn3 1-101 (Clone D = EI3.4.3) -- BamHI -- Stop -- SalI

CTGCAGGCCGCCACCATGAGGGTCCCCGCTCAGCTCCTGGGGCTCCTGCTGCTCTGG
CTCCCAGGTGCACGATGTGACATCCTGCTGACCCAGTCTCCAGTCATCCTGTCTGTG
AGTCCAGGAGAAAGAGTCAGTTTCTCCTGCAGGGCCAGTCAGAGTATTGGCACAAA
CATACACTGGTATCAGCAAAGAACAAATGGTTCTCCAAGGCTTCTCATAAAGTATGC
TTCTGAGTCTATCTCTGGCATCCCTTCCAGGTTTAGTGGCAGTGGATCAGGGACAGA
TTTTACTCTTAGCATCAACAGTGTGGAGTCTGAAGATATTGCAGATTATTACTGTCA
ACAAAATAATAACTGGCCAACCACGTTCGGTGCTGGGACCAAGCTGGAG
CTCAAACGTACGGTGGCTGCACCATCTGTCTTCATCTTCCCGCCATCTGATGAGCAG
TTGAAATCTGGAACTGCCTCTGTTGTGTGCCTGCTGAATAACTTCTATCCCAGAGAG
GCCAAAGTACAGTGGAAGGTGGATAACGCCCTCCAATCGGGTAACTCCCAGGAGAG
TGTCACAGAGCAGGACAGCAAGGACAGCACCTACAGCCTCAGCAGCACCCTGACGC
TGAGCAAAGCAGACTACGAGAAACACAAAGTCTACGCCTGCGAAGTCACCCATCAG
GGCCTGAGCTCGCCCGTCACAAAGAGCTTCAACAGGGGAGAGTGTGGAGGTGGCGG
TAGTGGCGGAGGTGGTTCTCATATGGCTAGCGTTTCCGATGTTCCGAGGGACCTGGA
GGTTGTTGCTGCGACCCCCACCAGCCTACTGATCAGCTGGTTCGACTACGCTGTGAC
TTATTACAGGATCACTTACGGAGAAACAGGAGGAAATAGCCCTGTCCAGGAGTTCA
CTGTGCCTGGTTGGATCTCCACTGCTACCATCAGCGGCCTTAAACCTGGAGTTGATT
ATACCATCACTGTGTATGCTGTCACTGACAACTCTCGTTGGCCTTTTCGCTCTACTCC
AATTTCCACTAATTACCGAACAGAAATTGACAAACCACCCCAGGGATCCTAATAGGT
CGAC

gWiz HN-AD (Representative cis trispecific fusion chain)

PstI--Leader --NdeI -- NheI -- Fn3 1-101 (Clone A) – BamHI—$(Gly_4Ser)_3$—KpnI -- Fn3 1-101 (Clone D) – BamHI -- $(Gly_4Ser)_3$— MluI—225 VH—NheI---CH1,2,3—Stop—SalI

CTGCAGATGGGTTGGAGCCTCATCTTGCTCTTCCTTGTCGCTGTTGCTCATATGGCTA
GCGTTTCCGATGTTCCGAGGGACCTGGAGGTTGTTGCTGCGACCCCCACCAGCCTAC
TGATCAGCTGGTTCGACTACGCTGTGACTTATTACAGGATCACTTACGGAGAAACAG
GAGGAAATAGCCCTGTCCAGGAGTTCACTGTGCCTGGTTGGATCTCCACTGCTACCA
TCAGCGGCCTTAAACCTGGAGTTGATTATACCATCACTGTGTATGCTGTCACTGACA
ACTCTCGTTGGCCTTTTCGCTCTACTCCAATTTCCACTAATTACCGAACAGAAATTGA
CAAACCACCCCAGGGATCCGGAGGCGGTTCAGGCGGAGGTAAAGGTGGCGGAGGT
ACCGTTTCTGATGTTCCGAGGGACCTGGAAGTTGTTGCTGCGACCCCCACCAGCCTA
CTGATCAGCTGGCTTCACCATCGCTCTGACGTGCGCTCTTACAGGATCACTTACGGA
GAAACAGGAGGAAATAGCCCTGTCCAGAAGTTCACTGTGCCTGGGTCGCGCTCCCT
GGCTACCATCAGCGGCCTTAAACCTGGAGTTGATTATACCATCACTGTGTATGCTGT
CACTTGGGGGTCTTACTGTTGCTCTAATCCAATTTCCATTAATTACCGAACAGAAATT
GACAAACCATCCCAGGGATCCGGAGGTGGCGGTAGTGGCGGAGGTGGTTCTACGCG
TCAGGTACAACTGAAGCAGTCAGGACCTGGCCTAGTGCAGCCCTCACAGAGCCTGT
CCATCACCTGCACAGTCTCTGGTTTCTCATTAACTAACTATGGTGTACACTGGGTTCG
CCAGTCTCCAGGAAAGGGTCTGGAGTGGCTGGGAGTGATATGGAGTGGTGGAAACA
CAGACTATAATACACCTTTCACATCCAGACTGAGCATCAACAAGGACAATTCCAAG
AGCCAAGTTTTCTTTAAAATGAACAGTCTGCAATCTAATGACACAGCCATATATTAC
TGTGCCAGAGCCCTCACCTACTATGATTACGAGTTTGCTTACTGGGGCCAAGGGACC
CTGGTCACCGTTTCCGCTGCTAGCACCAAGGGCCCATCGGTCTTCCCCCTGGCACCC
TCCTCCAAGAGCACCTCTGGGGGCACAGCGGCCCTGGGCTGCCTGGTCAAGGACTA
CTTCCCCGAACCGGTGACGGTGTCGTGGAACTCAGGCGCCCTGACCAGCGGCGTGC
ACACCTTCCCGGCTGTCCTACAGTCCTCAGGACTCTACTCCCTCAGCAGCGTGGTGA
CCGTGCCCTCCAGCAGCTTGGGCACCCAGACCTACATCTGCAACGTGAATCACAAGC
CCAGCAACACCAAGGTGGACAAGAAAGTTGAGCCCAAATCTTGTGACAAAACTCAC
ACATGCCCACCGTGCCCAGCACCTGAACTCCTGGGGGGACCGTCAGTCTTCCTCTTC
CCCCCAAAACCCAAGGACACCCTCATGATCTCCCGGACCCCTGAGGTCACATGCGTG
GTGGTGGACGTGAGCCACGAAGACCCTGAGGTCAAGTTCAACTGGTACGTGGACGG
CGTGGAGGTGCATAATGCCAAGACAAAGCCGCGGGAGGAGCAGTACAACAGCACG
TACCGTGTGGTCAGCGTCCTCACCGTCCTGCACCAGGACTGGCTGAATGGCAAGGA
GTACAAGTGCAAGGTCTCCAACAAAGCCCTCCCAGCCCCCATCGAGAAAACCATCT
CCAAAGCCAAAGGGCAGCCCCGAGAACCACAGGTGTACACCCTGCCCCCATCCCGG
GATGAGCTGACCAAGAACCAGGTCAGCCTGACCTGCCTGGTCAAAGGCTTCTATCCC
AGCGACATCGCCGTGGAGTGGGAGAGCAATGGGCAGCCGGAGAACAACTACAAGA
CCACGCCTCCCGTGCTGGACTCCGACGGCTCCTTCTTCCTCTACAGCAAGCTCACCG
TGGACAAGAGCAGGTGGCAGCAGGGGAACGTCTTCTCATGCTCCGTGATGCATGAG
GCTCTGCACAACCACTACACGCAGAAGAGCCTCTCCCTGTCTCCGGGTAAATGATAA
GTCGAC

gWiz HNA+HCB (Representative double HC fusion chain)

PstI-- Kozak--Leader --NdeI -- NheI -- Fn3 1-101 (Clone A) – BamHI—$(Gly_4Ser)_2$—MluI—225 VH—NheI---CH1,2,3——$(Gly_4Ser)_2$ -- NdeI -- NheI -- Fn3 1-101 (Clone B) – BamHI—Stop—SalI

CTGCAGGCCGCCACCATGGGTTGGAGCCTCATCTTGCTCTTCCTTGTCGCTGTTGCTC
ATATGGCTAGCGTTTCCGATGTTCCGAGGGACCTGGAGGTTGTTGCTGCGACCCCCA
CCAGCCTACTGATCAGCTGGTTCGACTACGCTGTGACTTATTACAGGATCACTTACG
GAGAAACAGGAGGAAATAGCCCTGTCCAGGAGTTCACTGTGCCTGGTTGGATCTCC
ACTGCTACCATCAGCGGCCTTAAACCTGGAGTTGATTATACCATCACTGTGTATGCT
GTCACTGACAACTCTCGTTGGCCTTTTCGCTCTACTCCAATTTCCACTAATTACCGAA
CAGAAATTGACAAACCACCCCAGGGATCCGGAGGTGGCGGTAGTGGCGGAGGTGGT
TCTACGCGTCAGGTACAACTGAAGCAGTCAGGACCTGGCCTAGTGCAGCCCTCACA
GAGCCTGTCCATCACCTGCACAGTCTCTGGTTTCTCATTAACTAACTATGGTGTACAC
TGGGTTCGCCAGTCTCCAGGAAAGGGTCTGGAGTGGCTGGGAGTGATATGGAGTGG
TGGAAACACAGACTATAATACACCTTTCACATCCAGACTGAGCATCAACAAGGACA
ATTCCAAGAGCCAAGTTTTCTTTAAAATGAACAGTCTGCAATCTAATGACACAGCCA
TATATTACTGTGCCAGAGCCCTCACCTACTATGATTACGAGTTTGCTTACTGGGGCC
AAGGGACCCTGGTCACCGTTTCCGCTGCTAGCACCAAGGGCCCATCGGTCTTCCCCC
TGGCACCCTCCTCCAAGAGCACCTCTGGGGGCACAGCGGCCCTGGGCTGCCTGGTCA
AGGACTACTTCCCCGAACCGGTGACGGTGTCGTGGAACTCAGGCGCCCTGACCAGC
GGCGTGCACACCTTCCCGGCTGTCCTACAGTCCTCAGGACTCTACTCCCTCAGCAGC
GTGGTGACCGTGCCCTCCAGCAGCTTGGGCACCCAGACCTACATCTGCAACGTGAAT
CACAAGCCCAGCAACACCAAGGTGGACAAGAAAGTTGAGCCCAAATCTTGTGACAA
AACTCACACATGCCCACCGTGCCCAGCACCTGAACTCCTGGGGGGACCGTCAGTCTT
CCTCTTCCCCCCAAAACCCAAGGACACCCTCATGATCTCCCGGACCCCTGAGGTCAC
ATGCGTGGTGGTGGACGTGAGCCACGAAGACCCTGAGGTCAAGTTCAACTGGTACG
TGGACGGCGTGGAGGTGCATAATGCCAAGACAAAGCCGCGGGAGGAGCAGTACAA
CAGCACGTACCGTGTGGTCAGCGTCCTCACCGTCCTGCACCAGGACTGGCTGAATGG
CAAGGAGTACAAGTGCAAGGTCTCCAACAAAGCCCTCCCAGCCCCCATCGAGAAAA
CCATCTCCAAAGCCAAAGGGCAGCCCCGAGAACCACAGGTGTACACCCTGCCCCCA
TCCCGGGATGAGCTGACCAAGAACCAGGTCAGCCTGACCTGCCTGGTCAAAGGCTT
CTATCCCAGCGACATCGCCGTGGAGTGGGAGAGCAATGGGCAGCCGGAGAACAACT
ACAAGACCACGCCTCCCGTGCTGGACTCCGACGGCTCCTTCTTCCTCTACAGCAAGC
TCACCGTGGACAAGAGCAGGTGGCAGCAGGGGAACGTCTTCTCATGCTCCGTGATG
CATGAGGCTCTGCACAACCACTACACGCAGAAGAGCCTCTCCCTGTCTCCGGGTAAA
GGAGGTGGCGGTAGTGGCGGAGGTGGTTCTCATATGGCTAGCGTTTCTGATGTTCCG
AGGGACCTGGAAGTTGTTGCTGCGACCCCCACCAGCCTACTGATCAGCTGGTACGGT
TTTTCGCTTGCGAGCTCTTACAGGATCACTTACGGAGAAACAGGAGGAAATAGCCCT
GTCCAGGAGTTCACTGTGCCTCGTTCGCCCTGGTTTGCTACCATCAGCGGCCTTAAA
CCTGGAGTTGATTATACCATCACTGTGTATGCTGTCACTTCTAACGACTTTTCTAATC
GTTACTCTGGTCCAATTTCCATTAATTACCGAACAGAAATTGACAAACCATCCCAGG
GATCCTGATAAGTCGAC